Design and fabrication of organic electronic devices for in vitro diagnostics : from petri dish to multiparametric systems

Aimie Pavia

N°d'ordre NNT : 2021LYSEM018

THESE de DOCTORAT DE L'UNIVERSITE DE LYON

opérée au sein de
l'Ecole des Mines de Saint-Etienne

Ecole Doctorale N° 488
Sciences, Ingénierie, Santé

Spécialité de doctorat : Microélectronique
Discipline : Bioélectronique

Soutenue publiquement le 02/06/2021, par :
Aimie Pavia

Design and fabrication of organic electronic devices for in vitro diagnostics: from petri dish to multiparametric systems

Devant le jury composé de :

O'Connor, Rodney	**Professeur**	**École des Mines de Saint-Etienne**	**Président du Jury et examinateur**
Hadziioannou, Georges	**Directeur de recherche**	**Université de Bordeaux**	**Rapporteur**
Malliaras, George	**Professeur**	**Cambridge University**	**Rapporteur**
Ismailova, Esma	**Maître de conférences**	**École des Mines de Saint-Etienne**	**Examinatrice**
Owens, Róisín.M	**Professeure**	**Cambridge University**	**Directrice de thèse**
Djenizian, Thierry	**Professeur**	**École des Mines de Saint-Etienne**	**Directeur de thèse**
Kergoat, Loïg	**Docteur**	**Panaxium**	**CO-encadrant de thèse**

Spécialités doctorales	Responsables :	Spécialités doctorales	Responsables
SCIENCES ET GENIE DES MATERIAUX	K. Wolski Directeur de recherche	MATHEMATIQUES APPLIQUEES	M. Batton-Hubert
MECANIQUE ET INGENIERIE	S. Drapier, professeur	INFORMATIQUE	O. Boissier, Professeur
GENIE DES PROCEDES	F. Gruy, Maître de recherche	SCIENCES DES IMAGES ET DES FORMES	JC. Pinoli, Professeur
SCIENCES DE LA TERRE	B. Guy, Directeur de recherche	GENIE INDUSTRIEL	N. Absi, Maitre de recherche
SCIENCES ET GENIE DE L'ENVIRONNEMENT	V.Laforest, Directeur de recherche	MICROELECTRONIQUE	Ph. Lalevée, Professeur

EMSE : Enseignants-chercheurs et chercheurs autorisés à diriger des thèses de doctorat (titulaires d'un doctorat d'État ou d'une HDR)

ABSI	Nabil	MR	Génie industriel	CMP
AUGUSTO	Vincent	MR	Génie industriel	CIS
AVRIL	Stéphane	PR	Mécanique et ingénierie	CIS
BADEL	Pierre	PR	Mécanique et ingénierie	CIS
BALBO	Flavien	PR	Informatique	FAYOL
BASSEREAU	Jean-François	PR	Sciences et génie des matériaux	SMS
BATTON-HUBERT	Mireille	PR	Mathématiques appliquées	FAYOL
BEIGBEDER	Michel	MA	Informatique	FAYOL
BILAL	Blayac	DR	Sciences et génie de l'environnement	SPIN
BLAYAC	Sylvain	PR	Microélectronique	CMP
BOISSIER	Olivier	PR	Informatique	FAYOL
BONNEFOY	Olivier	PR	Génie des Procédés	SPIN
BORBELY	Andras	DR	Sciences et génie des matériaux	SMS
BOUCHER	Xavier	PR	Génie Industriel	FAYOL
BRUCHON	Julien	PR	Mécanique et ingénierie	SMS
CAMEIRAO	Ana	PR	Génie des Procédés	SPIN
CHRISTIEN	Frédéric	PR	Science et génie des matériaux	SMS
DAUZERE-PERES	Stéphane	PR	Génie Industriel	CMP
DEBAYLE	Johan	MR	Sciences des Images et des Formes	SPIN
DEGEORGE	Jean-Michel	MA	Génie industriel	Fayol
DELAFOSSE	David	PR	Sciences et génie des matériaux	SMS
DELORME	Xavier	PR	Génie industriel	FAYOL
DESRAYAUD	Christophe	PR	Mécanique et ingénierie	SMS
DJENIZIAN	Thierry	PR	Science et génie des matériaux	CMP
BERGER-DOUCE	Sandrine	PR	Sciences de gestion	FAYOL
DRAPIER	Sylvain	PR	Mécanique et ingénierie	SMS
DUTERTRE	Jean-Max	PR	Microélectronique	CMP
EL MRABET	Nadia	MA	Microélectronique	CMP
FAUCHEU	Jenny	MA	Sciences et génie des matériaux	SMS
FAVERGEON	Loïc	MR	Génie des Procédés	SPIN
FEILLET	Dominique	PR	Génie Industriel	CMP
FOREST	Valérie	PR	Génie des Procédés	CIS
FRACZKIEWICZ	Anna	DR	Sciences et génie des matériaux	SMS
GAVET	Yann	MA	Sciences des Images et des Formes	SPIN
GERINGER	Jean	MA	Sciences et génie des matériaux	CIS
GONDRAN	Natacha	MA	Sciences et génie de l'environnement	FAYOL
GONZALEZ FELIU	Jesus	MA	Sciences économiques	FAYOL
GRAILLOT	Didier	DR	Sciences et génie de l'environnement	SPIN
GRIMAUD	Frederic	EC	Génie mathématiques et industriel	FAYOL
GROSSEAU	Philippe	DR	Génie des Procédés	SPIN
GRUY	Frédéric	PR	Génie des Procédés	SPIN
HAN	Woo-Suck	MR	Mécanique et ingénierie	SMS
HERRI	Jean Michel	PR	Génie des Procédés	SPIN
ISMAILOVA	Esma	MC	Microélectronique	CMP
KERMOUCHE	Guillaume	PR	Mécanique et Ingénierie	SMS
KLOCKER	Helmut	DR	Sciences et génie des matériaux	SMS
LAFOREST	Valérie	DR	Sciences et génie de l'environnement	FAYOL
LERICHE	Rodolphe	DR	Mécanique et ingénierie	FAYOL
LIOTIER	Pierre-Jacques	MA	Mécanique et ingénierie	SMS
MEDINI	Khaled	EC	Sciences et génie de l'environnement	FAYOL
MOLIMARD	Jérôme	PR	Mécanique et ingénierie	CIS
MOULIN	Nicolas	MA	Mécanique et ingénierie	SMS
MOUTTE	Jacques	MR	Génie des Procédés	SPIN
NAVARRO	Laurent	MR	Mécanique et ingénierie	CIS
NEUBERT	Gilles	PR	Génie industriel	FAYOL
NIKOLOVSKI	Jean-Pierre	Ingénieur de recherche	Mécanique et ingénierie	CMP
O CONNOR	Rodney Philip	PR	Microélectronique	CMP
PICARD	Gauthier	PR	Informatique	FAYOL
PINOLI	Jean Charles	PR	Sciences des Images et des Formes	SPIN
POURCHEZ	Jérémy	DR	Génie des Procédés	CIS
ROUSSY	Agnès	MA	Microélectronique	CMP
SANAUR	Sébastien	MA	Microélectronique	CMP
SERRIS	Eric	IRD	Génie des Procédés	FAYOL
STOLARZ	Jacques	CR	Sciences et génie des matériaux	SMS
VALDIVIESO	François	PR	Sciences et génie des matériaux	SMS
VIRICELLE	Jean Paul	DR	Génie des Procédés	SPIN
WOLSKI	Krzystof	DR	Sciences et génie des matériaux	SMS
XIE	Xiaolan	PR	Génie industriel	CIS
YUGMA	Gallian	MR	Génie industriel	CMP

Mise à jour : 04/02/2021

à $[\varepsilon l]_{S,}$

Abstract

Drug and toxicity assays are necessary to develop advanced treatments, as a way of improving medical diagnostics and testing the potential toxicity of new chemicals. *In vitro* testing is a powerful pre-clinical method used not only to initiate the drug development but also to iterate on the molecule to improve its safety and efficiency before the clinical trial. The actual *in vitro* models are currently not on par regarding the *in vivo* system they attempt to mimic. A great deal of information is missing from the basic *in vitro* assays, because the *in vitro* models are overly simplified and mainly monitored via visual criteria. Two research direction can be invested in to overcome this issue: a) elaboration of more complex *in vitro* biological model directed towards complete autonomous organ-on-chip systems and b) improvement of the monitoring of these complex biological models. To do so, we propose a multi parametric system approach, by integrating bioelectronic devices. Electrophysiological monitoring offers a complementary approach to optical techniques. It allows label-free detection of multiple, simultaneous biomarkers occurring in the *in vitro* model. To merge the electronic and biological assays protocols, we integrate Organic Microelectrode Arrays (OMEA) into standard biological experiment protocols. This approach, from the petri dish to a multi-parametric device, is the core of this work, presented in this thesis.

A review on Organic Microelectrodes introduces the field of organic material, their fabrication, and applications in microelectrode arrays devices. Specific properties of conjugated polymers such as PEDOT:PSS are of interest to interface with biology. . This organic material can be transparent, conformable, easy to fabricate, and mechanically matched to soft biological tissues. More importantly, the conducting polymers are excellent transducers of biological signals: they can be ion-to-electron transducers or vice-versa. Bioelectronic devices create a bridge between the electronic and the biological worlds. For instance, electrophysiology performed using organic microelectrodes arrays delivers extremely valuable data for drug or toxicity assays. Different methods are implemented to process the organic materials into microelectronic fabrication protocols such as patterning and encapsulation steps. In the introduction section, a number of applications are detailed for *in vitro* studies.

To include electrophysiology monitoring steps into usual biological experiments, the planar bioelectronic chips are assembled in the form of a standard cell biology tool: the 12-well plate. The OMEAs are arranged in a multiparametric format enabling simultaneous visual and electrical monitoring. Furthermore, this “smart well plate” fits most of the biological protocols for *in vitro* assays. A specific design adapted from the 12-well plate done using computer-aided design software. In addition, a supplementary supported holder and wire system is integrated into the design concept. It enables the smart well-plate to fit inside generic biological equipment such as microscopes, hoods and incubator and simultaneously performs continuous electrophysiological monitoring.

In electronic setup and architecture, one of the main restrictions is the number of channels that are available for both input and output data. A way to reduce the channel number and to maintain the same number of electronic components is studied, namely matrix design architecture. Organic electrochemical transistor (OECT) design has an arranged matrix structure. First, OECTs fabrication steps were optimized. From metal deposition to encapsulation technique, the chapter 3 describes the methodology of the OECT matrix microfabrication protocols. Then, a second process is developed to perform multi-stacking of conductive tracks over encapsulation layers to design a matrix architecture. Electrical and structural characterizations are then performed on the matrix device.

Furthermore, the bioelectronic device’s ability to monitor biological experiments *in vitro* is tested. First, an OMEA is used to monitor the viability of lipid bilayer viability in Chapter 4. Then, they are used to measure the formation of the epithelial barrier, and finally to detect electrogenic cell activity in Chapter 5. In the first experiment, transmembrane proteins (TMP) embedded in a lipid bilayer are deposited on an OMEA using PEDOT:PSS. The organic material created a soft interface with the lipids and provided a negatively hydrated charged cushion to support the proteins. By doing so, the organic polymer mimics the inner cell polarity and softness and enables the correct positioning of the TMPs inside the lipid bilayer. Electrophysiological assays were performed to study the behavior of proteins using the organic electrode. Then, two *in vitro* experiments are achieved using the OECTs matrix devices. The first experiment aims to monitor the epithelial barrier formation of MDCK cells seeded directly on the device’s surface. The measurement of the cut-off frequencies of the transistors gives information on the barrier integrity and density area upon the channel. The

second experiment integrates the OECTs matrix devices in a 3D *in vitro* model of electrophysiological cells. Motor neurons and Schwann cells are mixed into a spheroid, then seeded into a specific PDMS mold to develop into a peripheral nerve. The OECT matrix device used as the biological model substrate is used to detect action potential from the nerve fibers.

In conclusion, we have shown that including bioelectronic devices into generic tools from the biological experiment is possible. The matrix multi-stack devices were successfully performing electrophysiological monitoring *in vitro.* The etching fabrication method to pattern organic material is a promising technique to industrialize OMEAs This study opens new avenues for further *in vivo* testing, especially for long-term experiment.

Résumé

Les études pharmacologiques sont primordiales dans le développement des traitements de pointe. Elles permettent d'améliorer les diagnostics médicaux et de tester la toxicité potentielle de nouveaux produits chimiques. Les tests *in vitro* font partie intégrante des méthodes précliniques utilisées pour initier le développement d'un médicament, et pour itérer sur la formulation moléculaire afin de s'assurer de son innocuité et de son efficacité avant les essais cliniques. Malheureusement, les modèles biologiques actuels *in vitro* font défaut et ne sont pas prédictifs du système *in vivo* qu'ils tentent d'imiter. Beaucoup d'éléments ne sont pas inclus dans les tests *in vitro* basiques. En effet, les modèles biologiques sont ultra simplifiés, et de façon générale, contrôlés sur des critères visuels. Deux axes de recherche sont investis pour répondre à cette problématique : 1) Élaborer un modèle biologique *in vitro* plus complexe, tels que des systèmes complets et autonomes appelés organ-on-chip. 2) Améliorer les méthodes de contrôle de ces modèles biologiques complexes. Aussi, nous proposons un système de suivi multiparamétrique *in vitro* intégrant des dispositifs bioélectroniques. La surveillance électrophysiologique offre une approche complémentaire aux techniques de contrôles optiques. Elle permet la détection simultanée de plusieurs biomarqueurs se produisant aléatoirement dans le modèle *in vitro*. Pour fusionner les protocoles d'analyses électroniques et biologiques, nous intégrons des réseaux de microélectrodes organiques (OMEA) dans des protocoles d'expérimentations biologiques usuels. Cette approche, allant de la boîte de Petri à un dispositif multiparamétrique, est au cœur du travail présenté dans ce manuscrit.

En premier lieu, une revue portant sur les microélectrodes organiques introduit le domaine des matériaux organiques, de leur fabrication et leurs applications. Les propriétés spécifiques des polymères conjugués tels que PEDOT:PSS sont adaptées pour interfacer avec la biologie. Ces derniers peuvent être transparents, conformables, faciles à fabriquer et s'accordent mécaniquement avec les tissus biologiques mous. Plus important encore, les polymères conducteurs sont d'excellents transducteurs de signaux biologiques : ils peuvent être des transducteurs ion-électron ou vice-versa. Les dispositifs bioélectroniques créent un pont entre le monde de l'électronique et celui de la biologie. Par exemple, l'électrophysiologie

réalisée à l'aide de OMEA fournit des précieuses données pour la pharmacologie. Différentes méthodes sont évaluées pour intégrer les matériaux organiques dans des protocoles de fabrication microélectroniques tels que les étapes de modelage et d'encapsulation. Pour terminer, quelques applications *in vitro* des dispositifs sont détaillées.

Pour intégrer le suivi électrophysiologique dans des expériences biologiques usuelles, les puces bioélectroniques sont assemblées sous la forme d'un outil standard utilisé en biologie cellulaire : la plaque 12-puits. Les OMEA sont disposées dans un format multiparamétrique permettant une observation visuelle et électrique simultanée. De plus, cette « plaque intelligente » s'intègre dans la plupart des protocoles biologiques de test *in vitro*. Une conception spécifique adaptée de la plaque 12-puits est réalisée à l'aide d'un logiciel de conception assistée par ordinateur. Un ensemble connectique permettant à la plaque de s'intégrer dans des équipements biologiques (microscopes, hottes, incubateurs…) permet d'effectuer une surveillance électrophysiologique continue.

Dans l'architectures des systèmes électroniques, l'une des principales restrictions est le nombre de canaux adressables pour les données d'entrée et de sortie. À cet égard, un moyen de réduire le nombre de canaux et de conserver le même nombre de composants électroniques est élaborer : l'agencement matriciel. La conception du transistor électrochimique organique (OECT) est adaptée pour une lecture matricielle. Tout d'abord, les étapes de fabrication des OECT ont été optimisées. Cette section décrit la méthodologie des protocoles de micro-fabrication de matrice OECT : du dépôt de métal à la technique d'encapsulation. Puis, un second processus est développé pour créer un réseau de pistes conductrices sur des couches d'encapsulation afin de concevoir une architecture matricielle. Des caractérisations électriques et structurelles sont par la suite effectuées sur le dispositif matriciel.

Enfin, la capacité du dispositif bioélectronique à monitorer des expériences biologiques *in vitro* est évaluée. Premièrement, un OMEA est utilisé pour contrôler la viabilité d'une bicouche lipidique. Ensuite, ils sont utilisés pour mesurer la formation d'une barrière cellulaire épithéliale, et pour détecter l'activité des cellules électrogéniques. Dans la première expérience, les protéines transmembranaires (TMP) intégrées dans une bicouche lipidique sont déposées sur un OMEA. Le matériau organique crée une interface souple pour les lipides, et forme un coussin hydraté chargé négativement soutenant les protéines. Ce faisant, le

polymère organique imite la polarité et la souplesse interne du corps cellulaire, et permet le positionnement correct des TMP à l'intérieur de la bicouche lipidique. Des mesures électrophysiologiques sont réalisées pour étudier le comportement des protéines à l'aide d'électrode organique. Par la suite, deux expériences *in vitro* sont réalisées en utilisant les dispositifs matriciels d'OECT. La première expérience vise à surveiller la formation de la barrière épithéliale des cellules ensemencées directement à la surface du dispositif. La mesure des fréquences de coupure des transistors donne des informations sur l'intégrité et la densité de la barrière cellulaire formée sur le canal. La deuxième expérience intègre les dispositifs matriciels OECT dans un modèle 3D *in vitro* de cellules électrophysiologiques. Des neurones moteurs et des cellules de Schwann sont mélangés pour former un sphéroïde, qui est ensemencés dans un moule PDMS. Sa forme spécifique permet aux cellules de se développer en un nerf périphérique myélinisé. Le dispositif est utilisé comme substrat sur lequel repose le modèle biologique, et est utilisé pour détecter le potentiel d'action des fibres nerveuses.

En conclusion, nous avons montré qu'il était possible d'intégrer des dispositifs bioélectroniques dans des équipements standards utilisé en biologie cellulaire. Les dispositifs matriciels multicouche ont effectué avec succès un monitoring électrophysiologique *in vitro*. La méthode de fabrication par gravure pour modeler la matière organique est une technique prometteuse pour l'industrialisation des OMEA. Cependant, des tests *in vitro* supplémentaires sont nécessaires pour valider leur utilisation dans une expérience à long terme.

Acknowledgement

I would like to first to my thesis Directors Pr Roisin Owens and Pr Therry Djenizian for advising this PhD, their support and interest, availability, and guidance. I am grateful to my mentors that gave me the opportunity to join their department, Flexible electronics (FEL) and Bioelectronic (BEL). I am especially thankful to Roisin Owens, that kept pushing me forward from internship to PhD, no matter how difficult the distance made this PhD organization. I felt privilege to have been able to join her new Bioelectronic system laboratory (BEST) periodically, meet and learn from new colleagues. You taught me to be independent and confident, and I will look up to you as a model of Professor.

I would also express my infinite gratitude to Dr Bradley Schmidt and Dr Pierre Leleux, that have trusted me from the very beginning of this journey and offered me a place in their company PANAXIUM. Not only have they been supportive in many aspects, but they also opened doors of great science, project, and perspective that expended the scope this PhD. I would like to thank Dr Loïg Kergoat, that also supervised my thesis and helped me during the hard time of redaction and defense, providing wise advice and guidance. To Mrs Carolyn Aubry, that has been a pillar throughout these years in the company, thank you for your patience, and carrying support. And a big thanks to my Panaxium colleagues that I look up to, and helped me growth within the company: Jolien, Isabel, Marcel, Aaron, Olivier, Karima, SiMing, Marie, Bahar Alwin and Jean.

I felt grateful to Pr Rodney Oconnor, that, more than allowing me to stay and work in the BEL department, included me in his wonderful team/family that I have been honored to be a part of. Thank you Rod for your support. David Moreau, Martin Baca, thank you for helping me daily, you are essential to this lab and support student to overcome their struggles. Rémy, you are an amazing PhD student. Be more confident of your work and capabilities. You have already become an excellent microfabrication expert in a few months, and the devices

you nicely gave me worked perfectly and saved my last experiment. Thank you for your kindness and generosity. Gerwin, special thanks to my office buddy. It has been a pleasure to be able to exchange not only scientifically, but also chit chat on more general ideas and values. I value our discussions and will follow your new journey starting after your PhD. Lionel, thank you for working with me in the clean room, you have been a real support during those harsh time when I was struggling on technical issues. Also thank you for being this straight honest colleague, that do not hesitate to speak for others when we needed it. Mary, you've been a mentor I've tried to follow the tracks. You are a reference in science to me and I will always remember how you made science easy and accessible to beginners. Magali, it has been a chance to meet you when I arrived at the CMP. I felt lucky to have started my PhD with you, and I would like to thank you for all the knowledge you shared with me about biology. We became friends and I saw you overcoming the struggles of PhD with harsh work, and it showed me what was strong and powerful dedication to research. To my BEL colleagues, Ian, Hajar, Marina, Attila, Charles, Esma, Romanos, and Rita, thank you for your presence, support and scientific knowledge that you kindly shared with me.

Many people from different teams and groups also greatly contributed to this PhD. I would like to thank Chris Martin, and the whole Cornell Nanofacility team for introducing me to microfabrication, and for their exceptional warm welcome to Ithaca. Also, a huge thanks to the clean room team of the CMP, Gaëlle, Jean and Frederic, as well as the CMP IT team: Michelle, Anaïs, Veronique, Gracien and Thierry. You've been life savior many times during these three years.

To my lovely "special team", that saw me at my best and worst for four years, without whom this thesis would have been a much more difficult exercise: Marie, in all objectivity, you are one of the best scientist/researchers I had the privilege to work with. You make miracles in the biological field and are skilled in many other fields. As a friend, I wish you the best for your future project. Thank you for teaming up with me, even if it did not fit into your own PhD projects. You gave me your time and energy, and I could not thank you enough to have enlighten my last and favourite PhD project. Severine, thank you for your kindness and

patience. Having gone through similar struggles during your PhD, I valued a lot your wise advice that helped me overcome many difficulties. I am looking forward to your future path as a strong and inspiring scientific researcher. Bastien, you are way more thoughtful than I would ever be by moving a step backwards and see the totality of the aspects of challenges and difficulties. More than once, you were able to take me out of stuck situations and find a way out / solutions to my PhD struggles. I am excited to join Panaxium and work with you more as a colleague. SBAM, thank you for your daily support. It was a relief and pleasure to wake up and get to work with you every day. I hope to be able to return the favor to you somehow someday. Many thanks and you have my forever gratitude.

To my dear parents, you gave me the most valuable gifts a child could hope for: the strength to challenge any obstacles in life, as harsh and unexpected they could be. The opportunity to growth and freely support my own convictions, despite being different from yours. And your unconditional love and support, specifically during this PhD adventure. Thank you

Quentin, last but not least, my foremost thanks for keeping up with me in these particular years of PhD. You've provided me support, love, and confidence I needed in the harsh moments. Thank you for keeping me company in my sleepless night of insomnia, wiping away tears of stress, discouragement, and frustrations. Thanks, my love, for overcoming this endeavour with me, and giving me bright and joyful days.

Table of contents

ABBREVATION LISTE

ACP	Adhesive Conductive Paste
BEL	Bioelectronic Laboratory
CE	Counter Electrode
CMOS	Complementary Metal Oxide Semi-conductor
CP	Conductive Polymer
CT	Conductive Track
CV	Cyclic Voltammetry
CVD	Chemical Vapor Deposition
DMM	Digital Multimeter
DNA	Deoxyribonucleic acid
E-STIM	Electrical Stimulation
ECG	Electrocardiogram
EEG	Electroencephalogram
EIS	Electrical Impedance Spectroscopy
EMG	Electromyogram
FDA	Food and Drug Administration
HEK	Human Embryonic Kidney
ITO	Indium Tin Oxide
MDCK	Madin Darby Canine Kidney
MEA	Microelectrode Array
OECT	Organic Electrochemical Transistor
OLED	Organic Light Emitting Diode
OM	Organic Material
OMC	Organic Mixed Conductor
OMEA	Organic Micro Electrodes Array
PaC	Parylene C
PCB	Printed Circuit Board
PCI	Peripheral Component Interconnect
PDMS	Polydimethylsiloxane
PEDOT:PSS	Poly (3,4-ethylenedioxythiophene):poly(styrene sulfonate)
PNS	Peripheral Nervous System
PPy	Polypyrrole
PVA	Polyvinyl Alcohol
RE	Reference Electrode
SLB	Supported Lipid Bilayer
TEER	Trans-Epithelial Electrical Resistance
TJ	Tight Junction
TMP	Trans Membrane Protein
UV	Ultraviolet
WE	Working Electrode

Chapter 1
Organic microelectrode arrays for biomedical applications

This chapter is an ongoing works and will be part of a future publication in collaboration with Zixuan lu and Róisín M. Owens

A MEA is a platform gathering multiple microscopic electrodes in a small area. They are made with biocompatible materials interfacing biology to record electrophysiological signals. Made upon rigid or flexible substrates, they allow extracellular recordings of biological events alongside optical monitorings, if the substrate is transparent. They are used both for *in vitro* and *in vivo* applications.

In industry, rigid MEAs used for *in-vitro* experimentation are built on two types of substrates: silicon and glass/quartz. The latter enables applications where high optical transmission, high thermal conductivity and strong chemical stability are required. They are typically preferred for optical monitoring using microscopes. As will be described in section 3 below, the micro electrodes, their conducting lines and connecting pads are mostly patterned using lithography, which is the most common technique used in the microelectronics industry. In the last decade, industrial processes have begun to implement organic materials into MEAs, where gold, platinum, and silicon nitride where the main material used in their composition.

In this review, we will focus on the Organic Micro Electrodes Arrays (OMEAs). First, we discuss why organic materials are used and what their useful properties are. Then, we explain the device physics of OMEAs, and highlight the properties of different organic conducting

materials. We describe OMEA fabrication protocols, and finally list the advantages of OMEAs in different *in vitro / in vivo* applications.

1.1 Why Conducting Polymers?

Inorganic materials used as active sensing materials limits the signal detection and amplification between biotic/abiotic interfaces[1]. Intercellular activity and interactions usually rely on ionic transport, thus traditional electronics based on metal, metal oxide, and other semiconducting materials have advantages for processing electronic signals but not ionic ones. Single crystal semiconductors (such as Si, Figure 1 (b)), the most common materials for electronics, consist of a rigid lattice of covalent bonds. In order to have mobile charges in the silicon lattice, elements are often added into the lattice as dopants by either direct addition during single-crystal-formation or post addition during device fabrication[2,3]. Group III and group V elements can accept holes (positive mobile charge) and electrons contributing to the conduction in the lattice, respectively[1]. Often, the charge carriers in the silicon lattice have very high mobility (around 10^3 $cm^2/V{\cdot}s$ electron mobility with 10^{22} m^{-3} dopant concentration at 300 K)[4], but they hardly have any ionic conductivity. Since the ionic current is one of the major signals existing in biological systems, the inorganic semiconducting material cannot support the communication at biological-electronic interfaces. Also, dangling bonds on the inorganic crystal surface can easily form a layer of oxide, which acts as an insulator blocking electrons and ions, further hindering signal transduction.

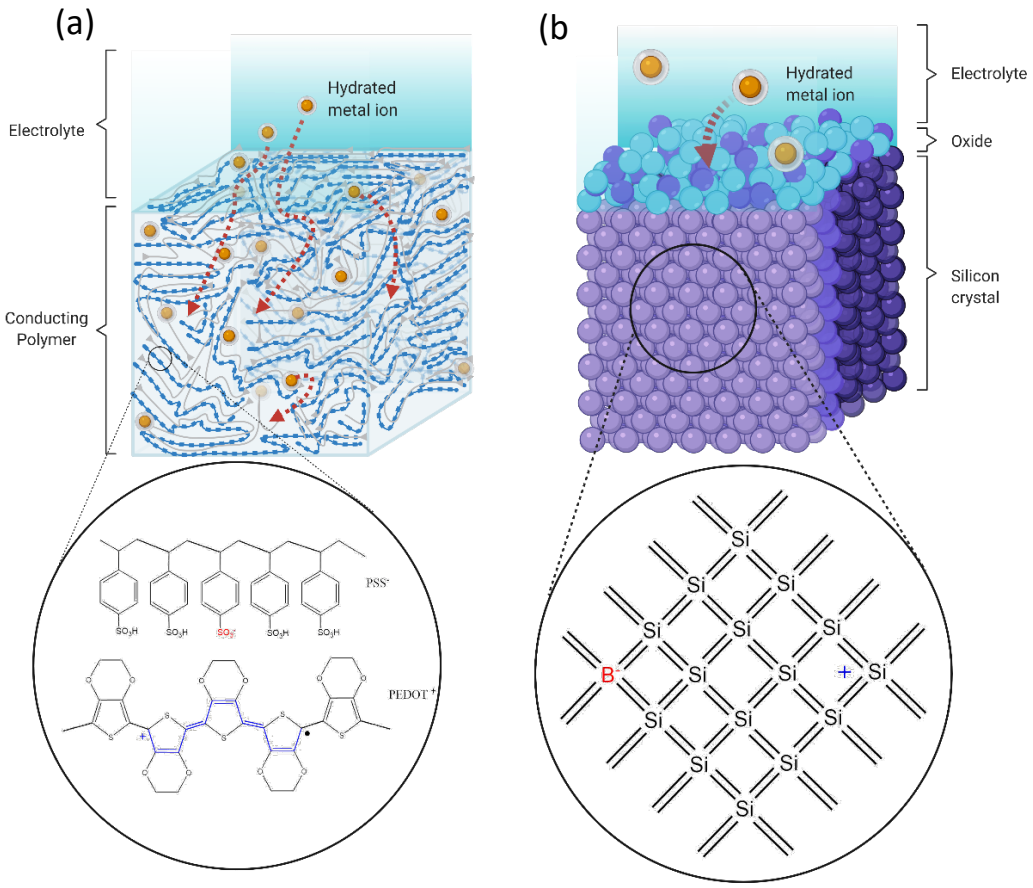

Figure 1: The structural differences between inorganic semiconductor materials and organic mixed conductors for bioelectronics: (a) scheme and structure of disordered PEDOT:PSS film in the biological environment; (b) scheme and structure of the rigid lattice of boron (p-type) doped single crystal silicon with silicon dioxide layer (modified from Rivany, et al, Chemistr of Materials, 2014)[1].

Conducting polymers (CP), a new class of organic electronic materials with both electrical and ionic conductivity, have emerged showing great promise for biological applications. The most commonly used conducting polymer in the field of bioelectronics, poly(3,4 - ethylenedioxythiophene) doped with poly(styrene sulfonate) (PEDOT:PSS) is shown in Figure 1(a). The p-type PEDOT has π-conjugation throughout the backbone, through which the mobile charge can transport freely[5,6]. With the presence of the negative dopant poly(styrene sulfonate) (PSS), the holes are stabilised on the backbone of poly(3,4 - ethylenedioxythiophene) (PEDOT), so that holes become mobile with an applied-voltage potential. In addition, since the mixture of PEDOT and PSS has a loose and disordered structure, the hydrated metal ions in the aqueous environment can move into the PEDOT:PSS bulk and change its conductivity[5,6]. This type of polymeric material, also known as organic

mixed conductors (OMCs)[7,8], that can support mixed ionic and electronic conduction, exhibits many advantages for interfacing with biological systems. First of all, the modification of π-conjugation and side-chain groups can be used to engineer the properties of the polymer[6]. For example, for a bithiophene-thienothiophene backbone (2T-TT), when the side chain is switched from alkoxy side chain to glycol side chain, the ionic injection into the film is facilitated without decreasing electric motilities[9]. Nielsen *et al.* have shown that the molecular design of the backbone of a series of conducting polymers can be tuned in many aspects, such as ion and hole transport, electrochromic properties, operational voltage, and material stability[10]. Second, the organic conducting polymer used as the active material for bioelectronics can be deposited with wide-range of methods avoiding high-temperature processing[6]. The polymer can be positioned at the desired area with a solvent process, such as spin-coating[11], inkjet-printing[12,13], screen-printing[14], and in-situ electrochemical polymerization[15,16]. Third, the OMC provides an oxide-free interface between a biological system and the devices[1,5]. Unlike silicon, OMC has no dangling bonds, so it has no active sites to form oxides[6]. Fourth, the conducting polymers provide great ionic transport at room temperature[6]. Relatively large distances and weak van der Waals forces between the organic molecule chains allow water molecules and hydrated ions to move into the material[6,8,17]. Lastly, the injection of the ions into the organic materials can modulate the doping states, and directly influence the electric carrier population[5]. Because of this, the OMC is able to transduce ionic signals from biological systems into electronic signals.

Alongside these key features of common OMCs, PEDOT:PSS, as the all-around champion material also has shown many more great properties. Biocompatibility[5], tissue-like mechanical properties[18], transparency[19], long-term stability in cell culture[20], resistance to physical deformation[21], autoclavabilty[22], and commercially availability are highlighted advantages that have been proved and confirmed in the literature. Thanks to these features, PEDOT:PSS based bioelectronic devices can be introduced to diverse applications, such as electroactive cell recording[23], barrier-tissue integrity monitoring[24], metabolite sensing[25], drug delivery[26], bioimaging[19], and many other fields of applications.

1.2 Organic Microelectrodes

1.2.1 Device physics and Characteristics of OMEs

Organic microelectrodes (OME) are one of the common devices applied across a wide range of biological sensing applications and studies. Since the invension of conducting polymer, researchers started to develop organic microelectrodes (OMEs) by coating traditional metal microelectrode with conducting polymers as the active-functional material[27,28].

Working Principle of OMEs

To describe their working principle, the energetic diagram of an organic electrode is demonstrated in Figure 2(a) to illustrate the charge transport in 5 phases. From the working electrode, a hole is injected into the highest occupied molecular orbitals (HOMO) (Phase 1)[29]. The holes can be transported through the delocalized HOMO throughout the polymer chain (Phase 2)[29]. Meanwhile, the anions are drifted by the potential applied by the counter electrode toward the polymer film (Phase 3)[29]. Then, the anions can travel within the free volume between the polymer crystals and chains (Phase 4)[29]. Lastly, the hole and the anion electrostatically compensate each other at a combination site (Phase 5)[29].

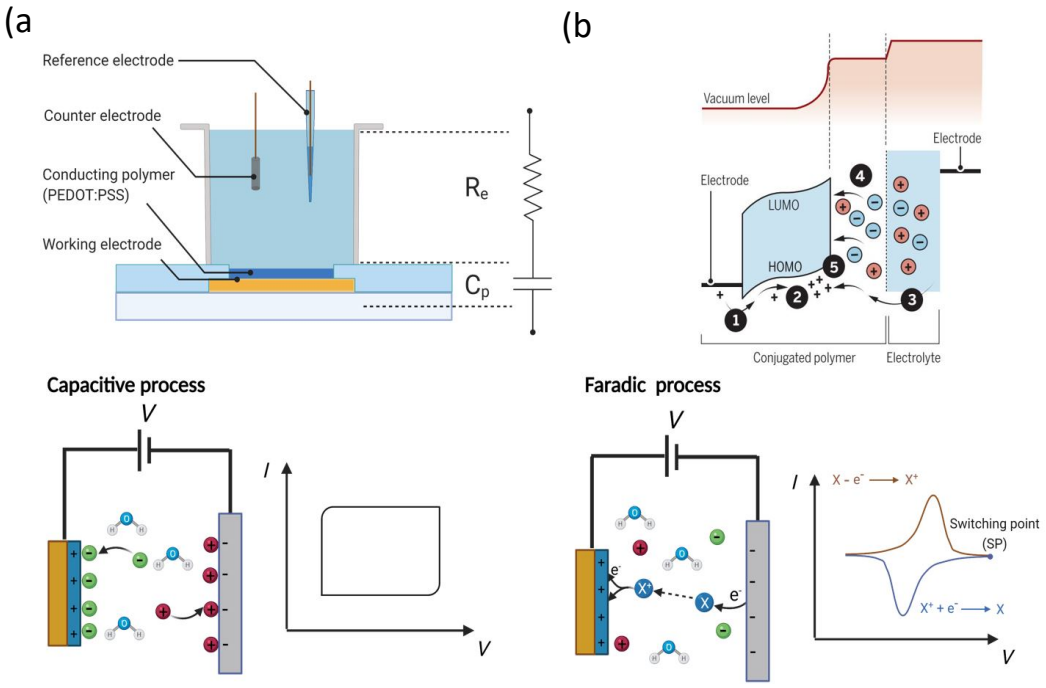

Figure 2 : (a) The scheme of organic microelectrode three-electrodes measurement set up with equivalent circuit (R_e is electrolyte resistance, and C_e is the conducting polymer capacitance); (b) the energy-level diagram of a microelectrode operation in the electrolyte with five phases: **(1)** a hole is injected from the metal electrode into the HOMO level of the polymer (HOMO and LUMO refer to highest occupied and lowest unoccupied molecular orbitals, respectively); **(2)** the hole is transported in the delocalized HOMO level in the polymer; **(3)** the anion is driven into the polymer by the potential; **(4)** anion travel within the free volume between the polymer chains and crystals; **(5)** electrostatic compensation of holes and anions at the combination site in the bulk; (c) and (d) cyclic voltomary and I-V plots for capacitive and Faradic process of conducting polymer coated electrodes (modified from Berggren and Malliaras, Science, 2019)[29].

For the traditional metal (such as Au) electrode, the anions directly compensate with the accumulated positive charges at the metal-electrolyte interface forming electric-double layer, which can be considered as a capacitor. Likewise, the OMC film possesses an ion-storage feature also behaving like a capacitor. Also, the OMEs have much free volume within the OMC film, so they have more surface area to electrostatically stabilise the injected anions. Thus, in the aspect of capacitance, the OMEs have much higher capacitance than the metal electrodes. As a result of this, the organic electrode with a larger effective area for ionic-electronic transduction lowers impedance compared to bare gold electrodes with the same size (Figure

2 (b))[11,20]. This relates to the charge-storage capacity of OMC, and this property can be depicted with its **volumetric capacitance (C^*)**[30,31]. Moreover, the impedance of a the overall capacitances can be expressed by equation 1:

$$Z_c = 1/(j2\pi fC) \quad (1)$$

where *f* is the frequency; C is the capacitance; j is the imaginary number unit. Therefore, the impedance of OMC is inversely proportional to its capacity. The OMC is a highly-capacitive (high C^*) material[30,31], so the OMC coating causes the decrease of the impedance when measured via electrochemical impedance spectroscopy[16].

Steady-State Characteristics Explored by Cyclic Voltammetry

The ion injection/ejection and ionic impedance behaviors are the intrinsic device properties of OMEs, which can be categorized with steady-state and transient characteristics, respectively. The ion injection and ejection into the OMC film can be explored by voltage sweep with a constant scan rate, whereas the ionic impedance can be investigated by sinusoidal voltage wave with frequency variations. To analyze these properties, the three-electrode configuration is usually established. As Figure 2(a) demonstrated, OME is the working electrode (WE) carrying out the measurement of interest. The current is applied by the counter electrode (CE) to sustain the ionic interaction within the conducting polymer of the WE. The reference electrode (RE) essential to control the potential and avoid potential fluctuation causing by large current changes[32]. The RE is usually made out of Ag/AgCl because it is a material operating under reduction-oxidation reaction. This eliminates the double-layer-capacitance effect to maintain applied voltage throughout the electrolyte before reaching the WE surface. Ag/AgCl RE is usually kept in KCl solution, and in order not to contaminate the measured biological solution, a salt bridge is used to avoid diffusion of KCl solution.

For the steady-state characteristics, the cyclic voltammetry (CV) is the common analysis technique. CV is a traditional method to observe rapid redox reaction over a large range of voltage potential[32]. Since the nature of redox reaction is gaining and losing of electrons, the characteristic curve describes the current response induced by reduction and oxidation reaction over a range of voltage. With the present of redox molecule (***X***), when the forward voltage scan induces a oxidation reaction, the anodic current rises and reaches a peak as the oxidation species ***X*** start to deplete while X^+ accumulate at the surface of the electrode [32].

Soon, the anodic current decline to the switching point (SP) where the species X^+ is zero at the electrode surface[32]. Then, the reverse scan initiates the oxidation reaction converts X^+ back to ***X*** and the cathodic (reduction) current behave with the same fashion to the anodic (oxidation) current curve[32]***.*** Due to its unique shape, the current-voltage curve is denoted as "duck-shape curve", and this redox reaction dominate behavior is called a **Faradaic process** (Figure 2(d)). Also, without redox molecules, some conducting polymer, such as Polyaniline (PANI) undergoes this Faradaic process as well. Its Faradaic process is related the conversion between its two redox-couples.

For the case of PEDOT:PSS and non-faradaic OMC coated microelectrodes, their operation involves ion injection and ejection instead of a redox reaction, and CV is used to monitor the electrostatic interaction ion charge within the OMC. When the forward voltage is applied, a large amount of previously diffused cations (ex. Na^+) are extracted and a great number of anions (e.g. Cl^-) are injected[17]. Then, this doping process comes to saturation with a small increase of cathodic current[17,33]. When, the reverse scan start, the de-doping process quickly begins with cation injection and anion extraction[17]. Because of the shape of this CV curve, the PEDOT:PSS (usually scan voltage range from 0 - 0.5V) represent a common behavior called "box-shape curve". These OMC coated electrode operation involves charge compensation, so this phenomenon is also named as the **capacitive process** (Figure 2 (b))[29].

Researchers recently obtained a deeper understanding of the properties of OMEs based on their steady-state measurements. Ganji. et al proved that PEDOT:PSS coated microelectrodes enhance up to 9.5 times of charge injection capacity compared to bare metal (Au) electrodes, and the maximum injected current increases with scaling up the OME size[34]. Also, PEDOT:PSS/Au OMEs demonstrated the excellent capability of convert available stored charge into injected electrical pulse (high *charge injection capacity/charge storage capacity* ratio)[34]. By combining the measurements of CV and quartz crystal microbalance (QCM), Savva. et al. showed that the thickness of the film contributes to the de-doping efficiency[17]. The thicker PEDOT:PSS film (~300 nm) can receive much more cations than the compensation sites and trap more cation and water molecules within the film even when the driving potential is paused[17]. If a sensitive ionic current detection or delivery is needed, the thickness of the film is a direct factor to be considered.

Frequency-dependent Characteristics Explored by Electrochemical Impedance Spectroscopy

For analyzing the transient characteristics of OMEs, electrochemical impedance spectroscopy (EIS) is a typically used technique. It also adopts a three-electrode configuration (Figure 2 (a)). Besides the working (WE) and reference electrode (RE) which control and measure the potential difference, a sinusoidal current is applied across the WE[35]. With this setup, the impedance spectra can be recorded for the analysis and study of the impedance characteristics of the OMEs with/without the biological system. According to Ohm's law, the impedance under an applied alternating voltage is determined by the division of the applied alternating voltage with the recorded alternating current signal[35]. The Impedance magnitude and phase can be plotted against the corresponding voltage frequency, which is usually called the Bode plot (Figure 3 (a)). In the ideal case, because the impedance of a resistor is independent of the frequency, it is shown almost like a horizontal straight line[35]. The capacitive component can be expressed by equation 1, so when both the y-axis (impedance) and x-axis (frequency) is plotted on a logarithmic scale, a capacitor's behaviors is shown as a straight line with a slope of -1[35]. The OMC-coated microelectrode has both resistive (electrolyte resistance (R_e)) and capacitive (OMC capacitance (C_p)) behaviors and the equivalent circuit is shown in Figure 3 (b)[16]. Therefore, at higher frequencies (10^2 – 10^5 Hz), the electrode is in the resistive domain, which behaves almost like a horizontal segment (Figure 2 (d))[16]. At low frequencies (10^{-1} – 10^2 Hz), the same electrode operates in the capacitive domain[16]. Furthermore, the voltage is often applied as a sinusoidal waveform, so the current response could have a time shift caused by characteristics of the circuit elements. This time shift is often expressed as an angular phase difference between the voltage and current waves[35]. This phase shift is plotted against each frequency on a phase diagram (Figure 3 (a)). A resistor's current response is immediate, so the phase is located around 0°. As a result of capacitance inducing current lagging 90° from the voltage input, a horizontal flat line

appears along the 90° mark. Therefore, for an OME, at the resistive domain, the phase remains around 0°, and once reaching the capacitive domain, the phase stays at 90° [35].

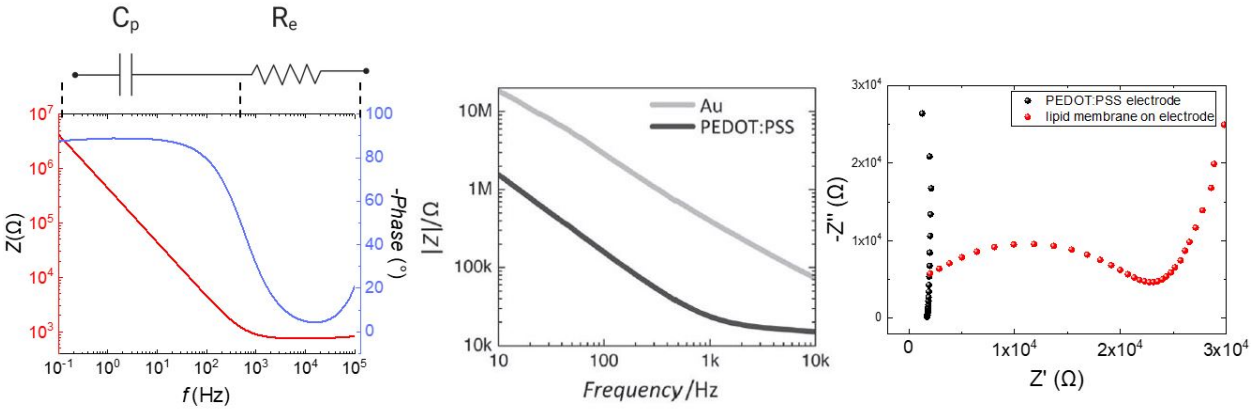

Figure 3: The electrochemical impedance spectroscopy of conducting polymer coated electrode: (a) the impedance (red) and phase (blue) versus frequency (Bode plot) plot of typical PEDOT:PSS coated electrode with resistive and capacitive regimes labelled by the electrode circuit; (c) The impedance lowering effect of PEDOT:PSS coated electrode comparing to gold electrode (adapted form Sessolo, et al. 2013)[11]; (c) The semicircle characteristics of a biobarrier (lipid membrane, red dots) presented in Nyquist plot (bare electrode is presented in black dots).

Independent of whether the electrodes are bare metal or coated with any conducting polymers, the impedance spectra always demonstrate the "universal curve" in electrochemistry with a 45°-slope-plateau shape. Owning to the impedance of the capacitive component being very high at high frequencies and the resistive component dominating the whole circuit at low frequencies, the pure resistance and capacitance behaviors are always isolated in an impedance spectrum. Even if the equivalent circuit is complicated by integrating biological systems, the resistance and capacitance of both electrode and bio-substances can be discerned. This components impedance spectrum is tightly related to equivalent circuit modelling, which will be discussed in a later section. Furthermore, a Nyquist plot in EIS is another way to illustrate impedance characteristics, which plots the imaginary part versus the real part of the impedance. It displays the real and imaginary parts, so it is easy to note the impedance contribution due to each equivalent circuit component. For example, since a biological barrier has both resistive and capacitive features, they can be expressed separately as the real part and imaginary part of the impedance, respectively. Hence, it is a complementary graph to the impedance information for the Bode plot. However, the Nyquist

plot does not explicitly plot the frequency, so the frequency of each point has to be traced back to the raw data[35].

1.2.2 Material Choice

Recently, many organic mixed conductors have been heavily developed to promote the performance of organic electrochemical transistor (OECT), which consists of OMC layer as the channel linking the source and drain electrodes, and a gate electrode injecting ions into the OMC to dope or dedope the channel. Some of these novels and highly performing materials have not much been evaluated on MEAs for certain biological applications. However, the electronic and ionic conductivity properties of these materials from OECTs can also be the figures of merit to direct OMEA applications. For example, Electronic mobility (μ) and volumetric capacitance (*C) are the crucial properties for OECT performance, and these two properties combining with other OMEA properties, such as redox activities (from CV) of some promising and popular OMCs from OECT characterization are summarized in Table 1.

Besides PEDOT:PSS, some other conducting polymer materials have been coated onto microelectrodes and OECTs. These conducting polymers have reported conductivity ranges from a single digits to hundreds of S cm^{-1}, and band-gaps are around 1-3 eV. First of all, polyaniline (PANI), p-type semiconductor, shows conductivity when present in acidic environments (pH < 3)[36]. When the nitrogen atoms on the PANI backbone are protonated, bipolarons are formed, and the cation radicals work as holes. The hole continuous can form on the backbond by successive transforming of bipolaron into polarons. The attractive property of PANI is its two redox-couple: leucoemeraldine (LE) can be oxidised to emeraidine (ED) form, and then ED is oxidised to Pernigraniline (PG) as the fully oxidized state[36]. The two-redox couple of PANI can facilitate the electron transfer between polymer and enzyme without extra charge-transfer mediators, so it provides a simplified metabolite sensing system[37]. However, the presence of oxygen induce ageing problem of PANI when the potential is around 0.5 mV, and the PANI has a dramatic loss of conductivity after a few CV cycles[36]. Moreover, polypyrrole (PPy) as one of the earliest CP used in the field of organic bioelectronics, It intrinsically has very high volumetric capacitance (400-500 F cm^{-3})[38]. However, the dense arrangement within the bulk block the dopant ion access to the interior sites, so a thicker PPy does not have a high capacitance per mass[39]. PPy also shows conductivity degradation once the voltage potential is applied above 0.3-0.4 mV[40,41].

In the case of polythiophene (PT), it has very high conductivity around 300 – 400 S cm^{-1}, and it is very stable in air and moisture at its p-doped and undoped forms[42]. However, It has very low n-doped potential (lower than -0.2 V) and loses conductivity due to oxidation at n-doping state, so the Pt-based devices do not have the desired life-time[42]. To overcome these problems, researchers have found that once phenyl, ethyl, or alkoxy groups substitute into the position 3 carbon on the thiophene ring (Table 1), the electric properties are greatly preserved for longer term[42,43]. The well-known PEDOT-based materials with excellent stability at n- and p-doping conditions are typical examples of this modification[43]. However, if just by PEDOT itself, it has low specific capacitance (92 F g^{-1}) [44], because its highly-packed interchain structure caused by high molecular weight[45]. When PEDOT is doped with poly(styrene sulfonate) (PSS), PSS can function as an ion conductor, which can greatly improve the ion transport and capacitance within the film[46]. Nevertheless, one of the drawbacks of PSS addition is that bulky PSS chains can lower the PEDOT volume faction, so the sulfonate anion/hole pair within the material is limited and hence the volumetric capacitance[31]. One way to increase volumetric capacitance is to increase the anion/hole sites by doping PEDOT with smaller anionic molecules[31]. Once PEDOT is doped with small molecules, such as tosylate (TOS, the pendant group in PSS, Figure 5 (f)), much anion/hole sites are created and the C* is improved with a neglected change of electronic mobility[5,47]. A large range of PEDOT-based materials are created by mixing with different additives and polymerizing with diverse methods to achieve versatile properties, and these materials have been summarized in a recent review[48].

Among these polymers, p(g2T-TT) is currently holding the record of highest μ and *C values since 2016[9,10]. Researchers have shown that the strategy of increasing the glycol side chain on p(gNDI-g2T) increase the ionic capacitance[49]. When NDI-T2 copolymer with alkyl chains demonstrate high electric mobility, but it has a great loss of mobility when 25% of the alkyl chains are replaced by glycol chains[50]. Therefore, side-chain engineering is a new route to modify the electric and ionic properties of OMCs. Furthermore, to the best of our knowledge, different biological conditions have not been systematically studied or tested for the for these new materials, so the characterization of them under various biological-relevant environments should be one of the future focuses of investigation, and the knowledge will help us to expand the library of OMC for bioelectronics.

Table 1: Summary of Common Conducting Polymers

Summary of Common Conducting Polymers					
poly(3,4 -ethylenedioxythiophene) doped with poly(styrene sulfonate) (PEDOT:PSS**)**	**Poly(3,4 - ethylenedioxythiophene) (**PEDOT**)**	**Polythiophene (**PT**)**	**Polypyrrole (**PPy**)**	**Polyaniline (**PANI**)**	**Names and Abbreviations**
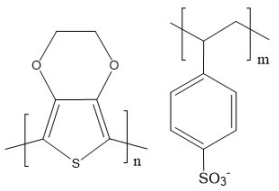	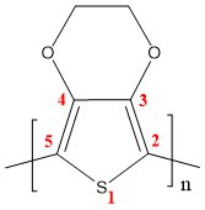	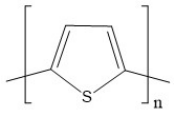	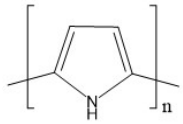	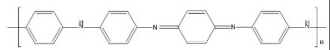	**Moleculalor Structure**
Transparency, high electronic conductivity, volumetric capacity, long-term stability, biocompatibility, and commercial-availability	High stability at p-doping and n-doping; high conductivity (300-500 S cm^{-1})	High conductivity (300 – 400 S cm^{-1})	high volumetric capacitance (400-500 F cm^{-3})	Two redox couples; High specific capacitance (530 F g^{-1})	**Highlighted Properties**
Bulky structure of PSS dilutes PEDOT content (lower volume fraction); higher Young' s modulus (few hundred MPa) than most of the biological tissues (few KPa).	Lower specific capacitance (92 F g^{-1})	Not stable during n-doping (inject cation).	Less stable (voltage > 0.3 V)	Low conductivity (0.1 -5 S cm^{-1}) and ageing process induced by O_2	**Drawbacks**
19,20,31,51,52	42,43	42	40–42	36	**References**

Summary of Common Conducting Polymers			
poly((ethoxy)ethyl 2-(2-(2-methoxyethoxy)ethoxy)acetate)-naphthalene-1,4,5,8-tetracarboxylic- diimide- co-3,3'-bis(2-(2-(2-methoxyethoxy)ethoxy)ethoxy)- (bithiophene)) (p(gNDI-g2T))	**NDI-T2 copolymer with 90 % glycol-based side chain** (N-90)	**poly(3-methyl-thiophene), polyaniline, poly(2-(3,3' -bis(2-(2-(2-methoxyethoxy)ethoxy)ethoxy)-[2,2' -bithiophen]-5-yl)thieno[3,2-b]thiophene)**	**poly(3,4-ethylenedioxythiophene) doped with tosylate** (PEDOT:TOS)
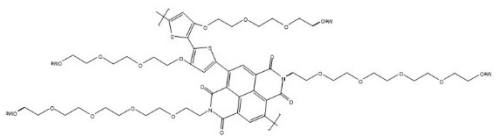	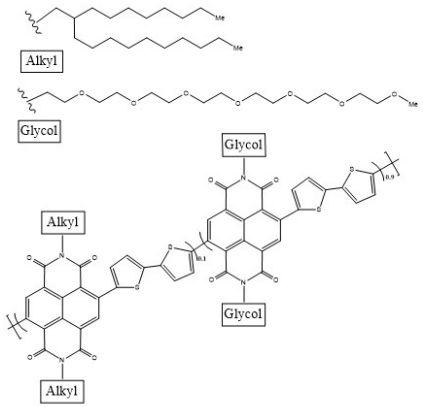	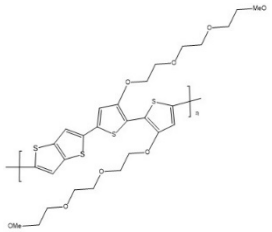	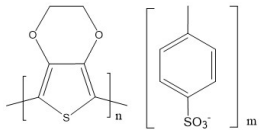
High C* value (397 F cm^{-3}) ; tunable ionic capacitance by glycol side chain	Capacitance and electron mobility are modified by side-chain engineering	High µC* value (228 F $cm^{-1}V^{-1}s^{-1}$) with high mobility (0.9 $cm^2 V^{-1}s^{-1}$) and high volumetric capacity (241 F cm^{-1}). Performance can be modified	High in µC* (126 F $cm^{-1}V^{-1}s^{-1}$) and C* (~136 F cm^{-3}) values; Deposition by vapour-phase polymerization; Conductivity improved by adding PEG.
low mobility ($3 \times 10^{-4} cm^2 V^{-1}s^{-1}$)	Lack of more systematic studies for biological applications.	Lack of more systematic studies for biological applications.	Lack of more systematic studies for biological applications.
54	50	9,47	47,53

1.3 Organic Microelectrode arrays: fabrication and micro manufacturing

In this section, we will describe conventional microfabrication of MEAs, and then discuss the adaptation and options available when integrating organic materials into standard microfabrication processes.

MEAs are dependent on fabrication within specialized laboratories. Microfabrication[55] takes place in the specific environment of a cleanroom. The cleanroom provides a "clean" environment that ensures the quality of the product fabrication steps. Submicron to micron sized particles are maintained at low levels during the multiple steps of the process thanks to High Efficiency Particles Air (HEPA) filters that prevent the particles from landing on the substrate and affecting the MEA fabrication. The cleanliness of each room is labelled "class °" (or "ISO °"), where ° indicates the number of particles per cubic meter. Humidity and temperature are also maintained constant for the chemical stability of different materials used during microfabrication. Specific lighting may also be required, for example no UV lights, to ensure integrity of photosensitive materials.

A microelectrode array is made of 4 distinctive parts:

1. Substrate: Platform on which every element of the MEAs is built during microfabrication steps. The material chosen, and its surface characteristics must guarantee a good thermal and chemical stability. Adequate surface topology should be optimized where adhesion of material layers is required.
2. Conductive tracks (CT): Lines, usually made of a material with an excellent electrical conductivity, carrying electrical signals obtained from the electrophysiological recording. They end at a contact pad connecting to the hardware systems.
3. Insulation layers: Coating made from electrical insulating material beneath and top to the CT. They prevent cross talking in between tracks and protect the MEA circuitry from the external environment (humidity, oxidation, mechanical stress etc...).
4. Interface: Areas in contact with the biological system studied. It is not covered by the insulation layers as they record electrophysiological activity from the model. Made of biocompatible materials, usually metals (Gold, platinum, ITO…), they form the electrode sensing/effective area.

Each of these four MEAs component influence the fabrication process, hence, the material used. As described in the previous sections, organic materials are quite often sensitive to temperature, harsh chemicals and sometimes light. In the following section, we describe

typical processes for fabrication of inorganic MEAs, and go on to describe the adaptations required to adjust a fabrication protocol for use with organic materials.

1.4 What are the constraints and limitations when integrating organic materials in the devices?

Substrate:

The most common materials substrates used in fabrication of MEAs for *in vitro* use are quartz and glass. Specific applications such as *in vivo* MEA types require characteristic matching with biological tissues and the *in vivo* environment: mechanical, chemical, conformability and flexibility. Therefore, substrates used in their fabrication are different (polydimethylsiloxane (PDMS), PaC, Silk etc…). It is worth noticing that even if the final substrate is altered, the substrate remains the same (wafer or glass slide) throughout the microfabrication steps. This new material must provide identical, or better, thermal, chemical and mechanical characteristics to the original substrate to endure the different fabrication steps. Therefore, substrate choice is important whether adhesion of the organic layer is required or not. Its surface topology and roughness mechanically impact the binding of the materials. Plus, the substrate material in contact with the organic layer should have a chemical structure inert to the organic material (OM).

Conductive tracks:

The second category of material answers the requirements of carrying the electrical information recorded, to the contact pads. Conductive tracks (CT) are usually made of material with low impedance and high signal to noise ratio properties, to ensure a good quality of the signal recorded. Furthermore, if encapsulation cannot be achieved at 100%, biocompatible materials are preferred during elaboration of the MEA to reduce toxicity risks. In that sense, gold, platinum, titanium and iridium titanium oxide are widely present as conductive track materials. Where gold is more ductile and conductive, ITO[56] offers transparency and platinum a higher Youngs modulus, providing a better resistance to mechanical deformation that could occur during the fabrication process or on flexible device. Any material chosen to convey the electrophysiological information from the biological model to the hardware is to be in contact

with the interface material: in our case, the OCM. The first characteristic and limitation to consider is the contact resistivity at the interface between the organic material and CT material. The thickness of the materials over layers impacts the behavior and quality of the recording as well.

Insulation/encapsulation

The encapsulation layer has to perform its purpose while remaining innocuous to the sensitive OM. Some microfabrication techniques and materials described below have shown their ability to match OM properties.

In industry[57], MEAs are mainly encapsulated with Silicon Nitride (Si_3N_4). This material, used as passive insulator, provides low thermal conductivity, and can perform at high temperatures, fitting the fabrication process of MEAs. Standard methods used to deposit SiN_4 encapsulation layers require plasma or high temperature processes (250°C-400°C)[58], which are not suitable for OMs and would degrade the MEA performance. Specific photosensitive resists have been developed to fit substrate and/or encapsulation purposes. As an example, SU8 from Microchem[59], and DE1 from Orthogonal[60] have dielectric properties fitting the expectation of biocompatibility or flexibility. To pattern and encapsulate OMC, parylene combined with peel-off techniques provides a stable option to encapsulate OMC[11]. The parylene layer is formed via chemical vapor deposition and patterned through dry etching technic[61]. This material provides good chemical stability, excellent conformability over rough surfaces, transparency and hydrophobicity[11]. Finally, PDMS has proven its mechanical and thermal stability, as well as a relatively acceptable performance as an encapsulation layer[62] in aqueous environments.

1.4.1 Deposition techniques for OMC

Spin Coating: As depicted in Figure 4 (a), the substrate is centered on a plate above a rotation axis in a bowl dedicated to spin-coated processes. This technique is used for OCM in liquid form, which are drop-cast at the center of the substrate. A homogeneous coverage of the

material is obtained thanks to the high rotation movement of the substrate, spreading the OMC all over the surface. Micrometer to millimeter scaled thickness can be obtained depending on the viscosity and the amount of material dispensed, and the rotation speed of the platform. The geometry of the substrate influences the edge effect appearing during spinning, making film thickness inhomogeneous on the extremities of the substrate or on non-planar surfaces[63].

Spray coating: droplets of the OMC are sprayed on top of the device (Figure 4 (d)), forming a layer by accumulation. The micrometer-sized drops coat the surface homogeneously and it is theoretically uses less material than the spin-coating technique. This also offers a better homogeneity of coverage on edges and textured surfaces than achievable via spin coating. The solvent evaporation rate during flight is the first parameter to consider, as is the viscosity of the resist chosen. Droplet propulsion speed, temperature and solvent concentration in the atmosphere are the three other parameters to consider when elaborating the fabrication protocol[63].

Thermal deposition: Deposition of organic polymers in their solid form can be achieved through thermal heating. The substrates are placed on a plateau facing the material source, in a thermal /electron beam metal evaporator vacuum chamber[64]. The surfaces face the metal targets crucible at the bottom of the machine, while undergoing rotation to ensure homogeneous deposition. An electrical current, or a laser beam, is applied on the crucible containing the OMC performing sublimation phase. A crystal placed inside the machine measures the thickness and deposition rate. Depending on the material, a faster deposition will result in bigger aggregate of particles than a slow evaporation rate, slightly changing he mechanical and electric properties of the material.

Chemical vapor deposition (CVD): The chemical vapor deposition technique allows formation of a thin film, and uniform coating over patterned surface. A thin film is formed via a thermal induced chemical reaction at the substrate surface. Reagents present in their gaseous form in

the environment will dissociate or chemically react upon heating, plasma or light activation. Some applications targeting PEDOT CVD deposition[65,66] have been elaborated.

Electrodeposition: This process schemed Figure 4 (c) revolves around deposition of materials on conductive substrates[67,68]. The electrodeposition technique can be divided in two different categories:

- Electroplating[69]: inducing a potential between a substrate (cathode) and an electrode made of the desired material (anode) to coat the substrate, dipped in an electrolyte containing the ions corresponding to the material. An oxide reduction reaction occurs in electrolyte, the cathode being the substrate to receive the coating, and the anode an electrode made of the same material.
- Electrochemical[70]: the CP coating onto the surface of a conductor substrate is done by electrolysis. Ions of the CP are in suspension in a solution in which the substrate is dipped and electrolysis is performed. Two subtypes are available : constant voltage and constant current deposition.

Electrospinning. This new process produces long fibers of polymer[7172], hydrogels[73], metal[74] and even composites[73], with a diameter ranging from the micrometer to the nanometer scale[75]. Easy to process, the electrospinning method requires a solvent in which nanoparticles of the OMC are dispersed[76]. A simple set up detailed Figure 4(a) involves a syringe containing the mixture, and a voltage applied at its needle. The parameters defining the diameter size and density of the fibers are: the intensity of the electric field applied, the viscosity of the mixture and the concentration of nanoparticles, the humidity in atmosphere, distance between needle and target substrate.

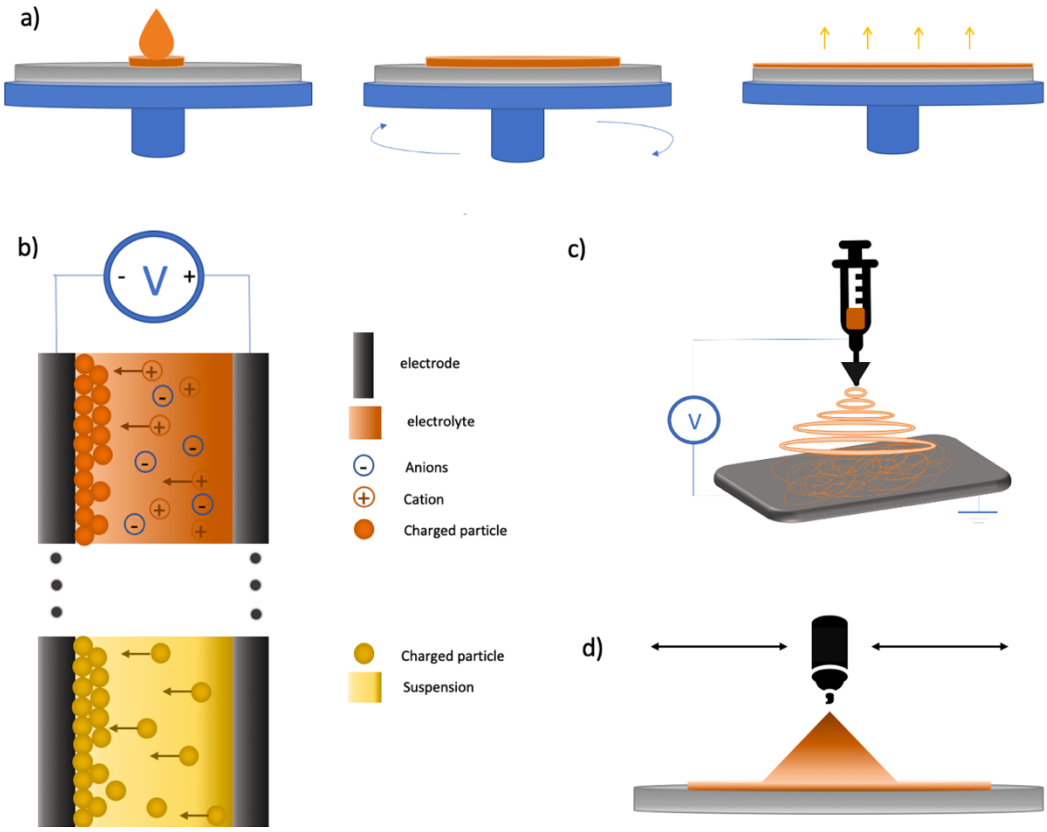

Figure 4 : Organic material deposition techniques. a) Spin-coating b) electrodeposition c) electrospinning and spray deposition are widely used in the research field when OM are disperse in a liquid phase.

Bar coating and doctor blading: Bar coating and doctor blading are similar techniques. Excess amount of material is deposited on the substrate. While the first one involves running a blade over the substrate, the second one uses a bar, and spreads the material on the surface. The gap between the tools and the substrate define the thickness of the material deposition. These methods require a certain viscosity of the material, and thickness under 10 micrometers cannot be achieved[77]. Nevertheless, these methods are inexpensive and easy to process, and are often used in research and industry.

Additive materials for improving adhesion and biocompatibility

Conductive polymers are interfacing biology and its harsh environment: humidity, proteins, serums and cells themselves can be damaging to the sensitive material and its device. One common issue regarding fabrication and longevity of the bioelectronic structure is delamination and foreign body response. In this regard, studies have been made to improve adhesion of the CP to the device, and its contact to the cells. These can be categoriesed into three types: . Mechanical, chemical and biological.

For delamination of OMC, surface topology of the material withstanding the OMC can be tuned to improve adhesion. Creating roughness impacts the surface tension properties[70], and can degrade or enhance adhesion, depending on the scale. Additives can be added on the substrate to answer the issue of delamination. For example, Polyurethane[78] allows strong adhesion of wet type of CPs such as PEDOT:PSS, PAni, or PPy on glass, PDMS, kapton, ITO or gold. Addition of Protein[79], or polymers like[80] help reduce the foreign body response (FBR) and improve the cell adhesion to the surface of the device.

Table 2: Summary of OMC deposition techniques:

	Material (structure)	Advantages	Limitations	Thickness min max
Spin coating	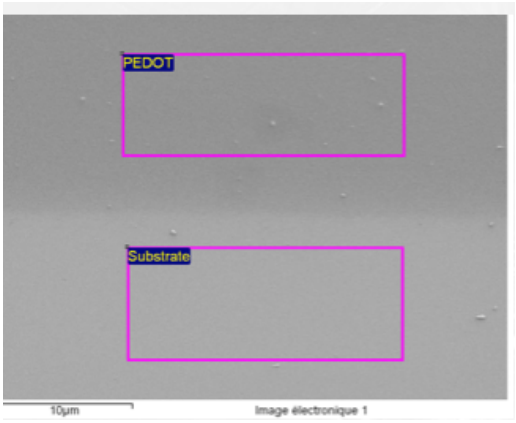 PEDOT:PSS spin over silicium wafer	• Ease of use for any wet type polymer • Covers large substrate area • Reproducible • Uniform thickness over planar substrates • Performs ultra-thin layer coating	• Non-uniform coating over non-planar, irregulate surfaces of the substrate • Substrate sizes limited • Large amount of material required	20nm>100um
Spray coating	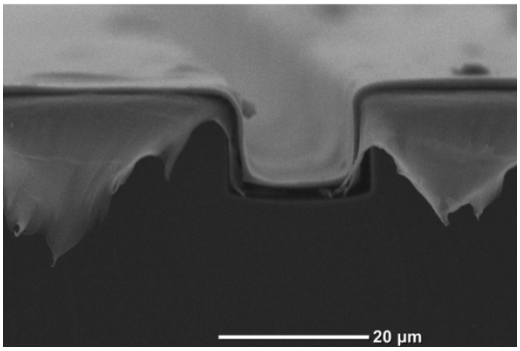 Pedot:pss mixture sprayed over patterned resist	• Uniform coatings over non-planar surfaces • sidewalls coating • low cost	• Sidewalls are coated: non-effective for lift off • Material homogeneity required in solvent to obtain uniform coating	20nm>500um

Chemical vapor deposition[65]	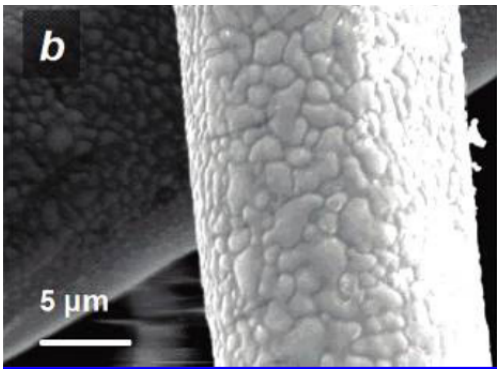	• Higher conductivity and better conformity of thin conducting polymer films • Low porosity level	• Requires chemical bonding on the substrate • Process in vacuum chamber • Process requires high temperature that can be damaging depending on the substrate • Some Monomers used are toxic and must be processed in controlled environment	100nm
Electrode position[69]	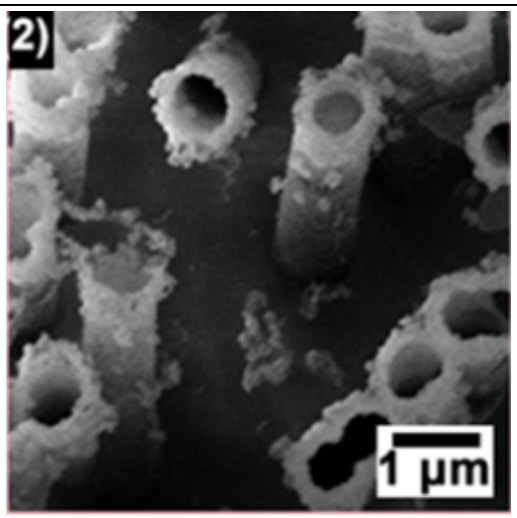 PEDOT:PSS coated nanostrawed	• Excellent bonding to substrate material • Coating of 3D structures • Cost effective	• Requires conducing substrates • Time consuming process •	20nm to hundreds of um

Electrospinning[76]	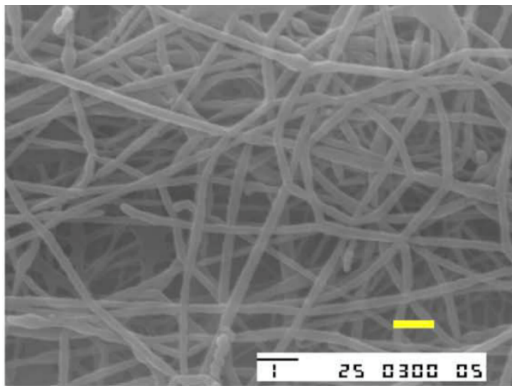 PEO over PPy nano fibers	• Flexibility and streatchability of the layer • Tunable porosity of the fibers network	• Patterning is difficult for light meshing layers • non-uniformity of the meshing layer: random & non-repeatable meshing structures	2nm to tens of um diameter of fibers
Doctor blading[81]	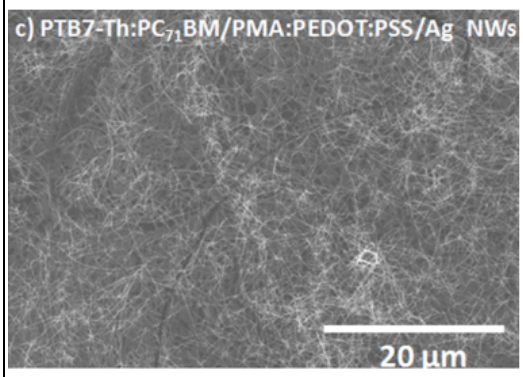 Picture of a drop of Ag nanowire ink on the top of the pristine PTB7-Th:PC71BM/ PMA:PEDOT:PSS	• Scalable process • Easy and fast to elaborate • Less material loss • Doesn't lose uniformity of the deposition over large substrate • Cost effective	• Creates relatively thick layers (minimum tens of micrometers) • Particles contaminating the dispersion of the material will creates defect and streaks drag alongside the film • Thickness deposition less precise and controlled than other deposition techniques	10 to 500um (depends on the viscosity of the material)

1.4.2 Patterning techniques for organic materials

Lithographic based techniques

Photolithography is a fabrication technique widely used in microelectronics, allowing to transfer patterns onto a substrate via shadow mask and several electron or light exposures. Those operations are based on chemical and physical properties of materials and resists, labelled electron sensitive and photosensitive respectively. Their main property changes the chemical structure when electrons or a certain UV wavelength is applied to the material. For photosensitive resists, it modifies the dissolution rate of its areas exposed. For OMC, chemical bonds structure are changed[82]. For photosensitive resists, the non-cross-linked parts are removed when the carrier is dipped into the appropriate developer, displaying the electronic circuit in a negative or positive tone, depending on the type of resist. Two step options are following in order to achieve the micro patterning by removing the excess material: etching or lift-off.Based upon photolithographic techniques, patterning of OMCs can be achieved directly or indirectly.

Etching techniques

Etching techniques require that the OMC has been deposited before the photosensitive resist. For the specific application of patterning resist over such sensitive materials, three requirements have to be fulfilled:

- The resist, solvent and developer used through photolithography steps should be chemically inert to the OMC.
- The UV range applied over the device during exposition should not interfere with the OM electrical and chemical properties.
- Thermal baking of the resist should be at a temperature that the OMC can withstand.

The etching step is divided in two categories (

(a)): Dry (plasma) and wet (chemical) etch. The first requires a plasma generator and gas delivering system inside a chamber under vacuum. The second is a quartz tank filled with liquid etchant that can be heated. In both cases, three main mechanisms are necessary to achieve

material removal. The flow of etchant over the substrate, the surface treatment (chemical and physical reaction) and the material removal.

1. **Wet:** Based on redox reactions, four steps are generated when materials are wet etched: Oxidation, dissolution, diffusion and convection. The parameters are: type of liquid and time of the bath and temperature. The etching rate is determined by either a slow chemical reaction, whether the bath time is the determining factor, or a fast reaction where the amount of etchant is the limiting factor. The disadvantages of the technique are under etching and lift off of small structures.
2. **Dry:** This technique involves removing of material by ionic bombardment inside a reactive ion etcher. Patterned are achieved by using a hard mask leaving areas exposed to the ions. Different parameters can improve the etching: speed, power, directionality (anisotropic or isotropic) Parameters to be optimized include: temperature, RF power, pressure, and time of etching. It is possible to obtain isotropic and anisotropic effects by customizing the parameters. The dry etch technique applied to OMCs such as PEDOT:PSS has been developed firstly using a PaC protective layer[83], then replacing it with specific resists[60]. The latest processing steps involve chemically inert solvent and developer to the OMC.

Reactive Ion etching machine[84]*:* Compared to wet etching, the material is not submerged in a liquid containing etchants. This technique revolves around chemically reactive plasma etching. The material is eroded, combining two effects, mechanical and chemical reaction with the ionized gas in the chamber.

*ION BEAM etching Milling machine***:** A specific type of dry etch. Compared to other methods, the process doesn't require high pressures. A larger variety of materials can be etched. Indeed, one key aspect of this tool is that it can remove material solely by physical bombarding, hence giving the tool a broad spectrum of material etch ability. The substrate is fixed on a rotating stage/platform, slightly tilted in front of the plasma source, at a certain distance, hence, the substrate is not surrounded by the plasma, and no radiation damage is received. Onto this plasma created inside the chamber, a direct beam is applied to control ion trajectory and energy toward the substrate.

Lift-off techniques

In opposition to the etching technique, where the material to pattern is deposited before the resist, the lift-off technique creates the patterning of the resist before the deposition of the material. When dipped in the appropriate solvent, the resist is removed alongside the OMC deposited over it. This process schemed Figure 5 (b) will mainly fit anisotropic types of material deposition, since the sidewalls of the resist pattern mustn't be covered in order to ensure a good lift of the material. Furthermore, from the thermal deposition, the resist used could undergo strong cross linking due to long exposure of the substrate to high temperatures in the chamber, hence making the lift-off difficult. This process technique is used if the resist employed for etching (dry or wet) have poor adhesion properties to the material that need to be patterned.

In the case of organic patterning via lift-off technique, two options are available[11,83]:

- Use of resist patterned via photolithography as a lift-off material. The OMC is deposited over the patterned layer, and once stabilized, the resist is removed in the appropriate solvent.
- Resist is patterned over third type of material as a hard mask for etching step. Once patterned, OMC is deposited over the layers. Then, the material is peeled-off manually leaving only the OMC on the surface.

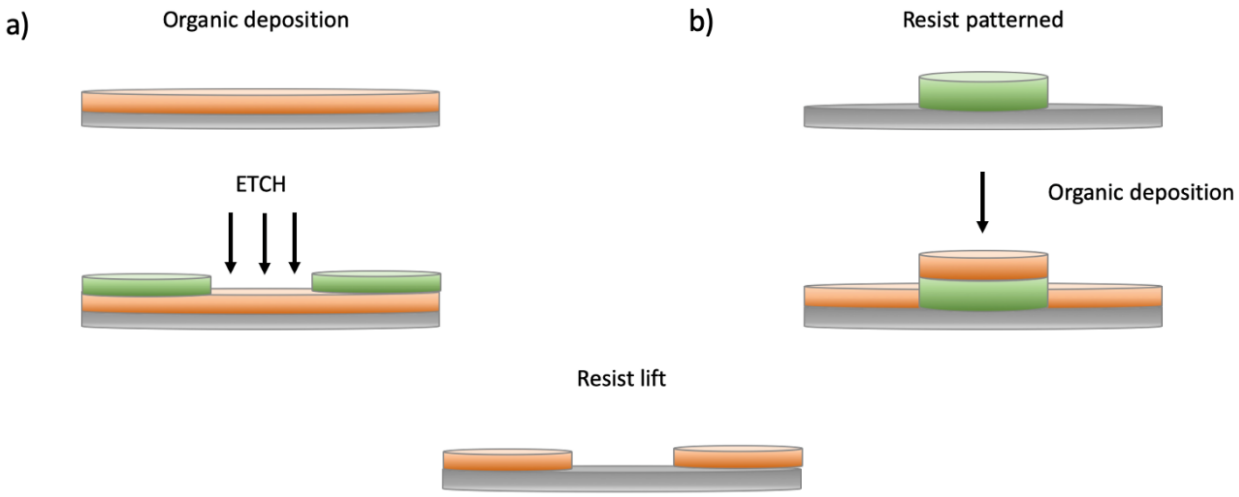

Figure 5 : Etching OM VS Peeling off OM technique

UV / laser patterning

An alternative option to pattern an organic film sensitive to light is via UV patterning[82]. It has been shown that under proper wavelength exposure, PEDOT:PSS thin layers increase in resistivity[85]. By doing so, the OM loses conductivity on the area exposed to UV (Figure 6 (b)). This process allows patterning of the material conductivity, which is different from material removal patterning. It is free from any etching step and resist patterning, thus preserving the PEDOT:PSS film chemical integrity. Laser ablation of OM has been used to create porous organic membrane[86].

.

Soft lithography patterning / Stamping

To pattern OM, soft lithography is a technique based on printing/stamping with a soft elastomer (usually PDMS) pre-patterned through photolithography[87]. This low-cost technique (Figure 6 (a)) can be divided into 3 subsections: micro-contact, replica and solvent assisted micro-molding.

Table 3: Patterning techniques for OMCs

Patterning techniques	Material structure	Pros	cons	Resolution Max min
Lithography based				
Etching	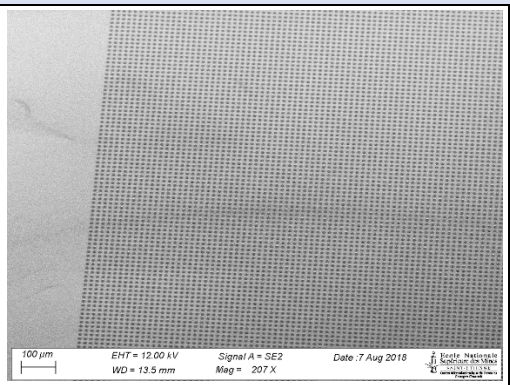	• High density and high resolution obtained • Industrial process	• Lift of resist difficult • Resist process has to be thermally and chemically inert to the polymer	microns
Lift-off[88]	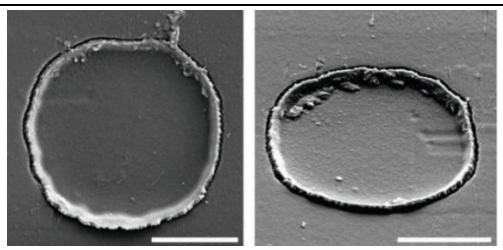	• Polymer guarded from any chemical or thermal impact from process	• Manual process • Requires sacrificial layer	microns
UV/Laser[82]	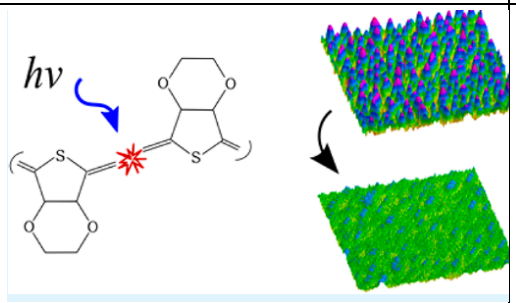	• Precise patterning • Chemical deactivation of polymers • Lithographic technique free	• Residuals polymers remains on the substrate	nanometer
stamping[89] **Soft lithography**	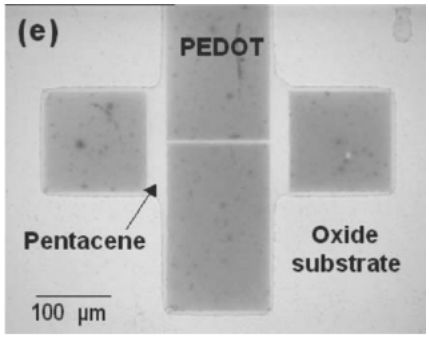	• Ease to process • Reproducible templates from device to device	• Polymers needs to have a better adherence to the substrate than the stamp • Resolution low	micrometers

Hybrid deposition + patterning				
Printing/additive[90]	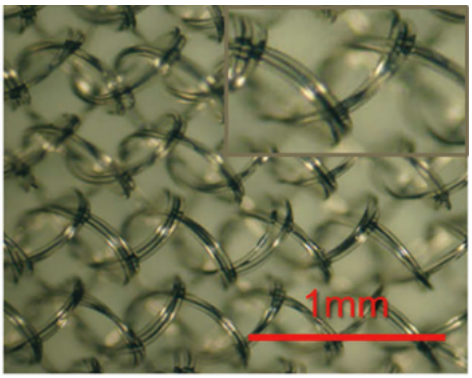	• Low cost technique / manufacturing • Fast processing method • Compatible with flexible substrates	• Large area deposition difficult for organic material[91] • Requires additives to the organic material to make it processable in inkjet tools	Micrometer features
Scanning probe/dip pen[92]	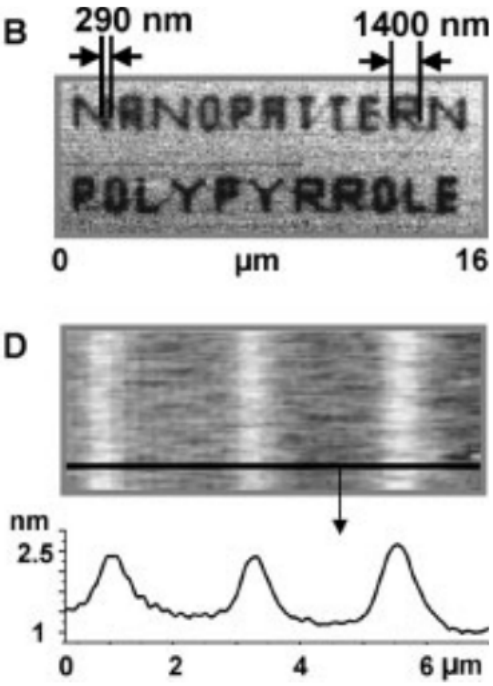	• Very high resolution	• Small area can be patterned • Time consuming technique • Tooling and machining are expensive	Nanometer sized

Sponges/scaffold[93]	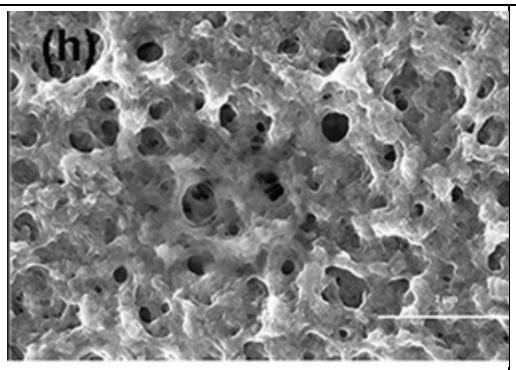	• Easy to fabricate • Porosity tunable	• Micrometer scale size	Millimeter sized scaffold with tunable porodity

1.4.3 Hybrid deposition and direct patterning of organic materials

Printing /additive processes

As additive manufacturing rises as a reliable and widely used process in many different industries, its translation to the microelectronic field is recent[94,95]. Indeed, precision and critical dimension of resolution were restricting parameters for their used in microelectrode fabrication[96]. Technical limitations have been overcome and new opportunities and capabilities are available in fabrication processes for microelectrodes; stretchability, bioresorbability and conformability is now feasible through printing techniques for biosensors[97]. Printing on fragile scaffold, such as bioresorbable materials, is conceivable[98,99]. Inkjet printing techniques are enlarging their formulations to enable new material deposition such as ITO [100] or organic inks[101].

Dip-pen / Nano lithography and Scanning-probe-based lithography

Dip-pen nanolithography is a direct printing-based technique using AFM. Similar to nanoimprint, this patterning technique uses probes and tips of the AFM to deposit ink materials at a nanoscale precision[92,102] Similarly, scanning probe lithography patterns materials using scanning probes, and can reach 10nm features precision. In contrast to the dip-pen technique, the scanning probe created an electrochemical reaction at the surface of the OM to change its structure: It locally crosslinks the polymer over the substrate.

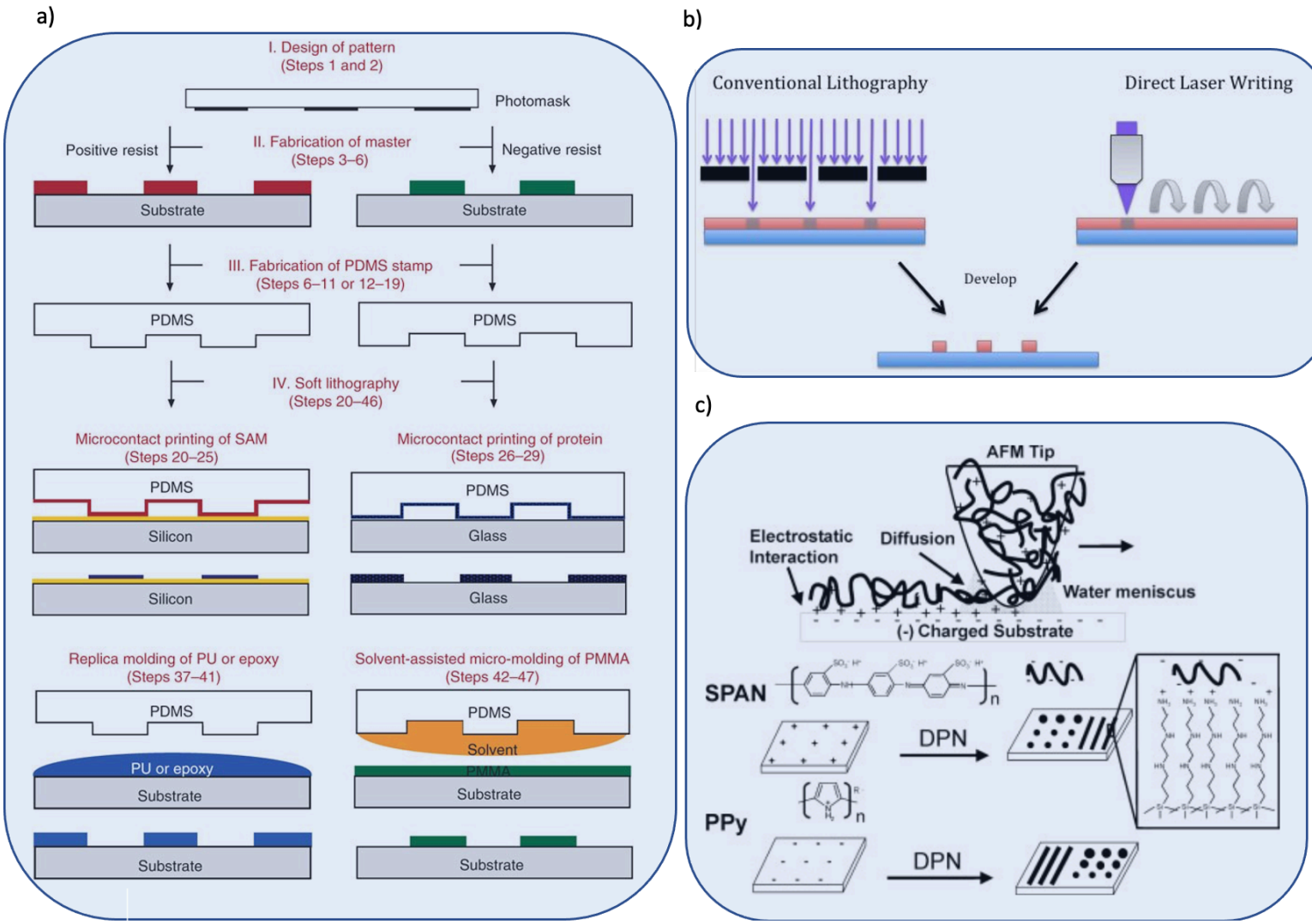

Figure 6 : Patterning techniques for OM : a) stamping method using a PDMS patterned stamp. B) Laser direct writing used on UV sensitive technique. Applied on OM such as PEDOT:PSS, the laser pattern the conductivity of the material. c) Did-pen nanolithographic technique used on conducting polymers.

1.5 Applications of OMEAs

OMEA have been widely used for the biological studies and medical research. Here, we generally categorise mainstream MEA related applications either as in vivo or *in vitro*, and within these two categories, the overview of each subcategorises are based on the device configurations, such as surface conformable OMEAs, deep-insertion OMEA probe, and rigid planar OMEAs, as illustrated in Figure 6.

(a) *In Vivo*

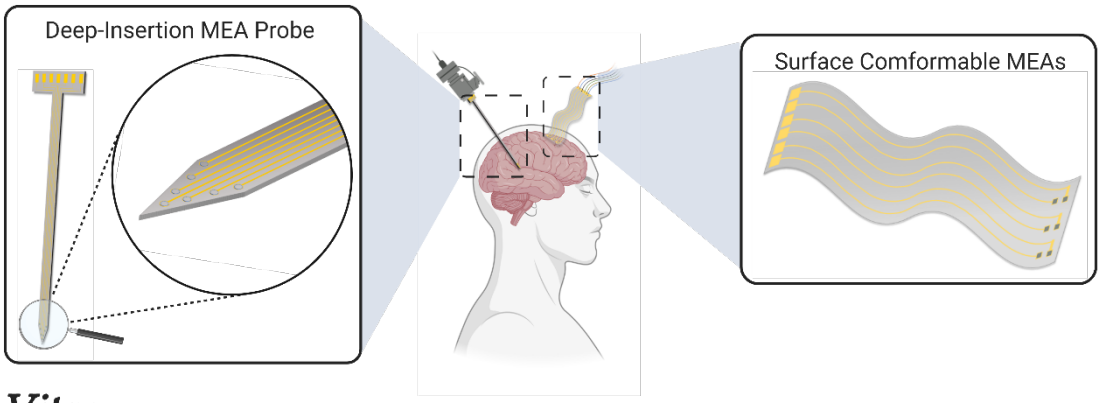

(b) *In Vitro*

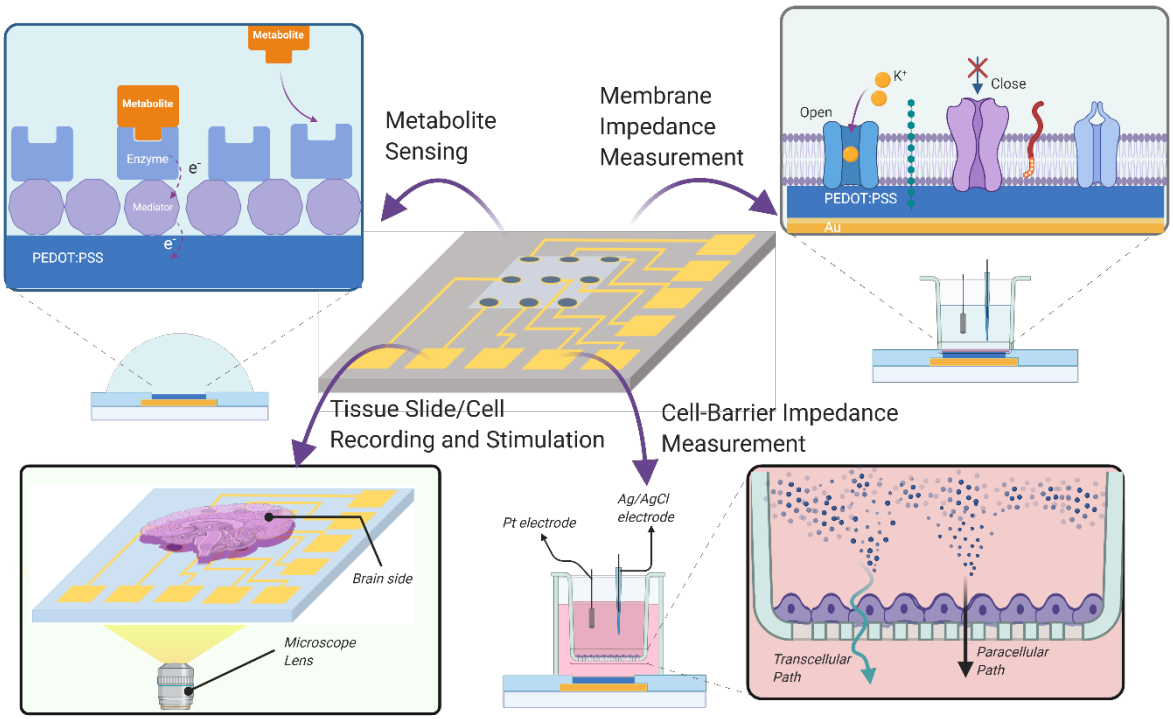

Figure 7 : The OMEA applications are categorised based on their configurations: (a) in vivo applications: deep-insertion OMEA probe and surface conformable OMEAs; (b) *in vitro* applications based on rigid planar OMEAs.

1.5.1 Deep-insertion MEA probe

Neurological disorders, such as Alzheimer's, Parkinson's, and epilepsy continuously burden the attention of the global health, and in vivo application with OMEA probes advance the neurosurgical community from the traditional brain probing systems (Figure 7 (a)). Michigan-style probe[103] and Utah arrays[104] are commercially available silicon-based probes with iridium and platinum active recording sites. Silicon based insertion probe has inconsistent performance in long-term recordings because of foreign body responses, such as impedance increase by immunocells and neuron loss. Compared to these inorganic probes, OMEA probes are showing excellent properties in recording and stimulation, reduction of recording impedance, high signal-to-noise ratio (SNR), high stimulation capacity, and lower inflammatory responses are the top advances contributing to the conducting polymer coating.

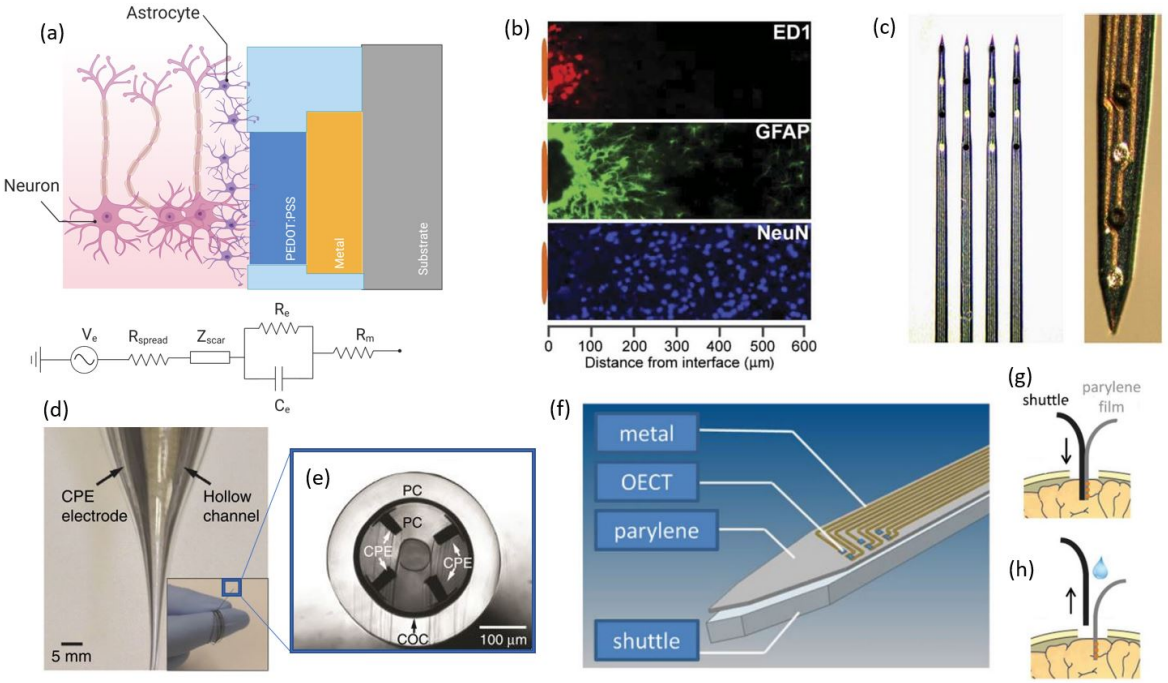

Figure 8: cellular immunoactivity between brain tissue and microelectrode: (a) astrocytes populating between neuron and electrode after probe insertion with an equivalent circuit model of between brain tissue the recording systems (V_e: biological voltage; R_{spread}: spreading resistance; Z_{scar}: scar impedance; Re: electrode resistance; C_e: electrode capacitance; Rm: metal resistance) parallel to the physical structure[105,106]; (b) inflammatory scar tissue labelled by cell-specific-markers: inflammatory cells (ED1), astrocyte (GFAP), and Neuron (NeuN) (adapted from Biran R. et al., *Exp. Neurol.*, 2005)[107]. (c) 16-site and 4 shank machigan style probe with PEDOT film coated electrodes (darken) and iridium (shiny) electrodes (Ludwig, K. A. *et al*., *J. Neural Eng.*, 2006)[88]; (d) and (e) thermal-drawn fiberic probe: (d) The diagmiter change during thermal draw process; (e) the crossesstional area of the multifunctional fibric probe with conductive polyethlene (CPE) electrodes and hollow core for chemical delivery (COC: cyclicolefin copolymer; CP: polycarbonate) (adapted from Canales, A. *et al.*, *Nat. Biotechnol.*, 2015)[108]; (e)-(h) The layout and insertion process of substrate-delamiating probe: (e) layout of microelectrodes and OECTs; (f) The insertion step; (h) delamination and remove of shuttle part (Williamson, A. *et al. Adv. Mater.*,2015)[109].

Generally, the OMEA probe-brain recording systems are modelled with the equivalent circuit in Figure 8 (a). V_e usually is the biological voltage source, and R_{spread} is the resistance of the extracellular space (media) between the active cell and electrode[105,106]. R_e and C_e are electrode resistance and capacitance, which are related to the intrinsic properties of the polymer coating, and R_m is the resistance of metallic connections[105,106]. In the case of neuron stimulation, the same circuit applies. On one hand, a large electrode area can reduce the R_{spread} and increase C_e having advantages to detect local field potential (LFP) for a population of neurons[106]. On the other hand, a smaller electrode has larger R_{spread} and areal reduction of C_e. For smaller size electrode for tissue implatation, a the high capacitance and low resistance OMC coating can still sustain high injection limit and avoiding voltage drop at the interface, so such microelectrodes are excellent at recording a small number of cells[106].

However, the circuit of recording/stimulation (Figure 5 (b)) is an ideal situation of the recording circuit. Once the probe is inserted into the brain tissue, an inflammatory response can quick effect the recording sites by releasing proinflammatory factor and astrogliosis (forming scar around the probe)[110]. The microglia and astrocyts inflamation response and populate around the recording sites increasing recording and stimulation impedance. During this process, the resistance induced by these scar and dead/injured neurons forms an extra impedance layer frustrates the voltage propagation to the recording electrodes. Accompany with this, neuron population loses around the inserted probe, so the recording signal can also be weaken by the distance[107]. Martin's group have demonstrated that the probe with PEDOT coated electrodes showed a drastic decline of impedance at the recording site and increase the amplitude of the signal comparing to the uncoated iridium electrode[88]. The PEDOT electrodes sustained longer-term (40 days) through the whole immune response periods: initial trauma, early reactive response, and sustained immune response, especially after around 20 days, the PEDOT coated electrodes provide much high SNR compared to uncoated ones[88].

From the device-design perspective, minimizing the probe size and matching Young's modulus of probe material with the tissue's are the two direct paths to reduce inflammatory responses[106]. Anikeeva's group applys thermal-drawn method produce filberic neuronal probe with diameter of crossesional area around a few hundred micrometer (Figure 8(d)). By

selective etch of the cadding of the fiber, the fiber stiffness is greatly reduced to 5 N/m[108]. The brain implantation experiments show that the forgeign body responses, such as glial response and blood-brain-barrier (BBB) breach, is minimized, so two-month consistent recodings were achieved[108]. The thermal-drawn method can also be multifunctional by building in optical waveguides for optical stimulation and fluidic channels for drug delivery[108]. To bring the Young's modulus of probe close to tissues, Malliaras group frabricate PEDOT devices on 4 μm parylene flexible substrate and implant into rat cortex with SU-8 shuttle. The shuttle can be delaminated from parlene substrate after implantation and there is no noticeable gial scar even after 1 month implatation[109]. Based on this work, they recently also developed "NeuroRoots", which consists of multiple separated flexible electrodes[111]. The NeuroRoots are guided by microwire during implatation, and they can delaminate from the microwire and remain in the brain for long-term measurements with high desinty recording sites[111]. Besides reducing probe size and matching material flexibility, coating the electrode with bioactive molecules, such as extracellular matrix (ECM), is also applied to reduce inflammatory response[110]. ECM can greatly promote neuron attachment on to the recording site and enhance the signal from the source[110]. Even though OMC coated electrode probe can significantly reduce the forgein body response and measure the brain activity with high signal quality, but the demages from probing process can still be a unignoriable side effect.

1.5.2 Surface Conformable OMEAs

To minimize the inflammatory response that happens during deep-insertion recording, electrocorticography (ECoG), as a less invasive method, with conformable OMEAs increasingly applied to monitoring the surface brain activities without damaging any tissue and providing real-time information before brain surgeries[112]. Besides the advantages of the conducting polymer coating described above, they are lightweight, can be easily adapted on substrates of different shape and bendability. The features of these OMEAs rely on their thin (1-10 μm) and flexible organic substrate (ie. parylene). They potentially capable to conform to the curvilinear surface of the brain, and even fit and attach to the brain sulci. Khodagholy et al. demonstrated PEDOT:PSS microelectrode array on parylene substrate (total thickness 4 μm) was capable to record epileptiform sharp-waves, and the activities they picked up match the silicon probe depth-recorded spectra[113]. Also, the array of PEDOT:PSS electrodes detected the same events and mapped out them with time-frequency analysis with high spacial resolution[113].

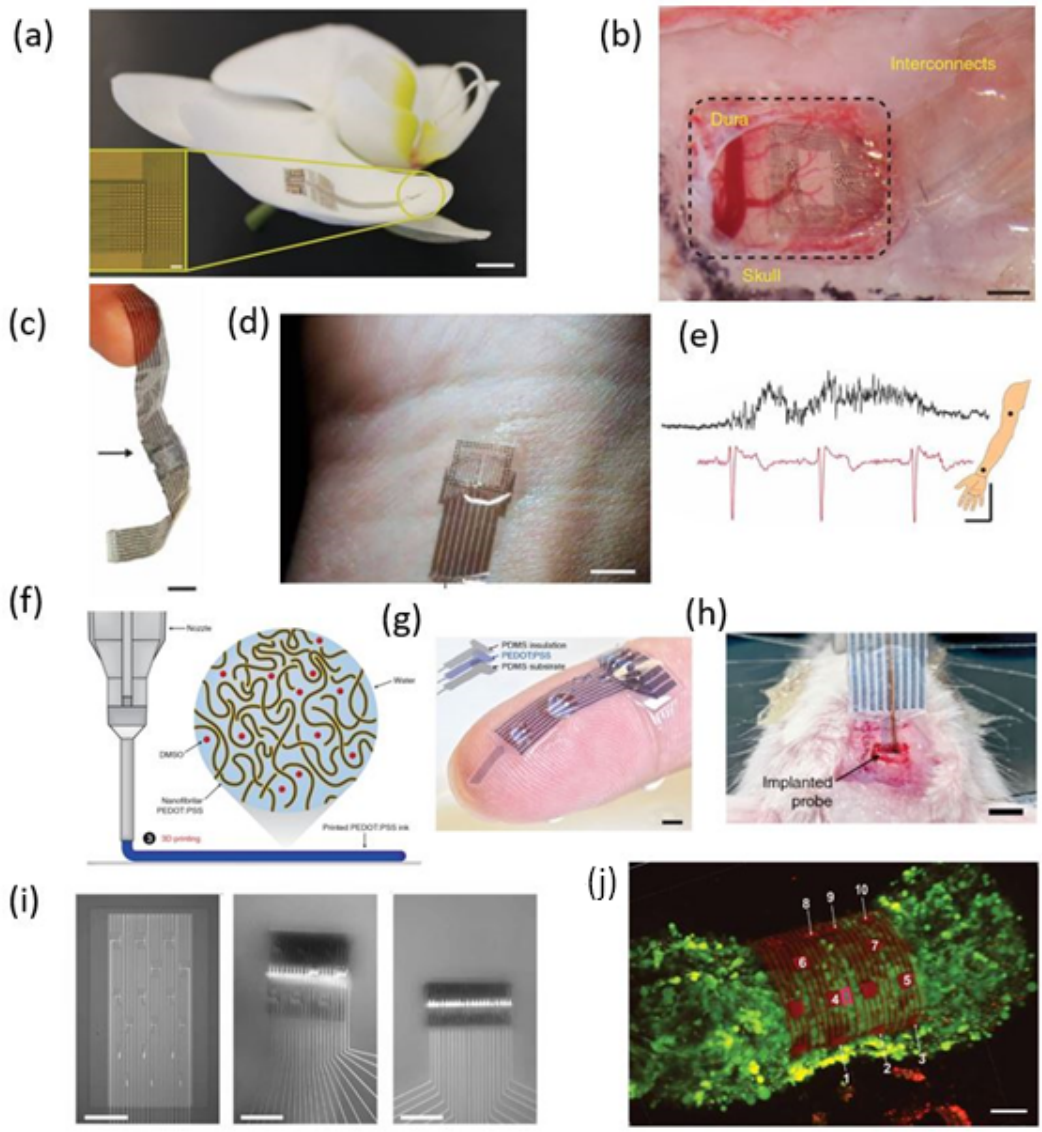

Figure 9 : the conformable OMEA applications: (a)-(b) NeuroGrid: NeuroGrid structure conform on an orchid petal surface (scale bar, 100 mm); the insert shows the electrode array (scale bar, 100 µm); (b) NeuroGrid conforms on the surface of a rat somatosensory cortex (scale bar, 1mm) (adapted from Khodagholy, D. et al., Nat. Neurosci., 2015)[114]. (c)-(e) anisotropic PEDOT composite coated soft electrodes: (a) image of two arrays bonded by PEDOT composite material; (b) high-density array adhered on human wrist for recording; (d) The electromyography (EMG) and electrocardiography(ECG) signal recorded grom wrist and biceps (Jastrzebska-Perfect, P. et al. Sci. Adv., 2020)[115]; (f)-(h) conformable brain probe prined by 3D printing techniques: (f) the schematic of printable PEDOT:PSS ink produced by lyoppilization and rediposion in water-dimethyl sulfoxide (DMSO); (g) the whole structure of printed PEDOT:PSS array with PDMS printed as insolation layer; (h) 3D printed neuron probe for rat brain recordings (Yuk, H. et al. Nat. Commun., 2020)[116]; (i)-(j) self-roll 3D-recording OMEA array: (a) the self-roll mechanism; (b) confocal image of OMEA array wrapping around cardiac spheroid recording (scale bar: 50 um) (Kalmykov, A. et al., Sci. Adv., 2019)[117].

Then, Khodagholy and colleagues further reported another system of conformable OMEA, called “NeuroGird”, to record LFPs and action potentials from surfaces of hippocampal and cortex[114]. The organic electrode dimensions and density (10 μm X 10 μm electrodes with 30 μm spacing) specifically matches the neural cell body size and density so that the action potentials from an individual neuron were stably recorded over 10 days[114]. Also, the LFP has monitored over a wide range of frequency implied to the mouse’s daily movements and activities (ie. Non-rapid eye movement sleep)[114]. Despite clean room microfabrication of flexible OMEAs is still dominating in the field, researchers achieved high quality devices by 3D printing approach. Yuk *et al*. is able to 3D print PEDOT:PSS flexible electrodes for in vivo rate brain recording, and they successfully pick up LFP, continous action potential, and single unit potnetials[116]. This 3D printing technique is promising for mass production and commercalise these OMC based probes in the future.

Beside *in vivo* recording, flexible property of OMEA array is also capable for wearable health monitoring and 3D recording from tissue surface. Recently, Jastrzebsk-pefect *et al.* developed flexible MEA from PEDOT:PSS particles and chitosan polymer composite with anisotropic electric resistance[115]. These devices can interface with human skin and conduct electrocadriogphray (ECG) and electromyography (EMG) with high spatiotemporal resolution[115]. Moreover, take the advantage of flexible substrate, the comformable OMEA can also used to monitor single cardiac spheoids. Kalmykov et al. fabriacated self-rolled MEAs by mismatch the residual stress bewtween the bottom and top layer of SU-8; these devices can capsulate a single human cardiac spheroid and maintian their viability[117]. The self-rolling-capsulation process even provides a 3D mapping of single field opential propagation across the spheroid[117]. Hence, recent various studies, such as long-term brain-health monitoring, point-of-care monitnoring, and even *in vitro* electrogenic tissue 3D mapping, not only have opened up our vision of conformable OMEAs , but also brought and guided our interests toward the further development their potentials in many more biomedical applications.

1.5.3 Planar OMEAs for *In Vitro* Applications

Planar OMEAs are the most common configuration found, and are used for many *in vitro* applications, such as metabolite detection, electroactive tissue and cell recording, and barrier cell and native cell membrane impedance sensing. Among these applications, OMC coatings show great versatility in sensing ion current, lowing signal impedance, and ease to functionalization, so the planar OMEAs catch increasingly amounts of attention in the field of bioelectronics.

Enzyme-Base Metabolite Sensing

Enzyme-based detection of metabolites and biomolecules from body fluid or gas is one of the most common applications of planar OMEAs. Generally, the detection mechanism is based on sensing the products of redox reaction or redox current generated by the metabolite-enzyme (redox) reaction. Usually, cathode or anode peaks of cyclic voltammograms are used to quantitatively measure the concentration of metabolite of interest. Glucose detection still dominates the market and research fields of metabolite biosensing[25,118]. Here, the development of glucose sensing with OMEA can be illustrated as a model. In many cases, glucose oxidase (GOx) is a specific recognition glucose enzyme, and it contains two molecules of cofactor, flavine adenine dinucleotide (FAD), which can oxidise glucose into gluconolactone meanwhile it accepts two electrons and yield hydrogen peroxide (Figure 9 (a))[119]. Therefore, GOx-base sensors are designed by detecting either hydrogen peroxide or redox current. Owing to the outstanding electric conductive of conducting polymer, OMEAs have been used to sense glucose concentrations through redox current (Figure 7 (a)-(c)). Furthermore, the layer formed from the enzyme might inhere an electron shielding effect, which frustrates the electron transport towards the electrode surface,[25] so a mediator is used to promote the electron transfer between enzyme and electrode surface[25]. Thanks to excellent electron transport properties of the conducting polymer, and once they can be intimately incorporated with the enzyme, they are qualified to be an excellent mediator to conduct redox current. Kros and coworkers showed that once GOx is directly incorporated with PEDOT-based surface, the redox current can be directly transported to PEDOT layer[119]. Later, Wang et al. demonstrated that ferrocene bound to a mixture of polyethyleimine nanobead (BPEI-Fc) and GOx and coated on PEDOT:PSS-carbon electrode, had very high glucose sensitivity (66 $\mu A\ mM^{-1}\ cm^{-2}$) comparing to many other types of sensors(Figure 9 (b))[120]. In addition, enzyme-based

organic-electrode sensors are promising candidates as low-cost, disposable, and eco-friendly point-to-care devices. Many academic research demonstrate the sensing chemistry with a single electrode, but the capability of producing replicates and statistical analysis can be enhance by electrode arrays. Bihar et al. fabricated glucose-sensing electrodes with completely inkjet-printed method onto a paper substrate (Figure 9 (c))[121]. This device provided a high sensitivity of glucose concentration for differentiating non-diabetic to diabetic saliva[121]. Besides glucose, other metabolites, such as creatinine[122], ascorbic acid[123], dopamine[123], uric acid[123], and many more can also be sensed based on their unique redox activities (sensed by CV or Differential pulse voltammogram), which attracting great interest within the field of enzyme-based OMEA sensing. Overall, the high-electronic transport, intimate incorporation with enzymes, and low fabrication cost are all crucial factors making enzyme-based OMEAs sensors powerful and promising tools for future point-to-care technologies.

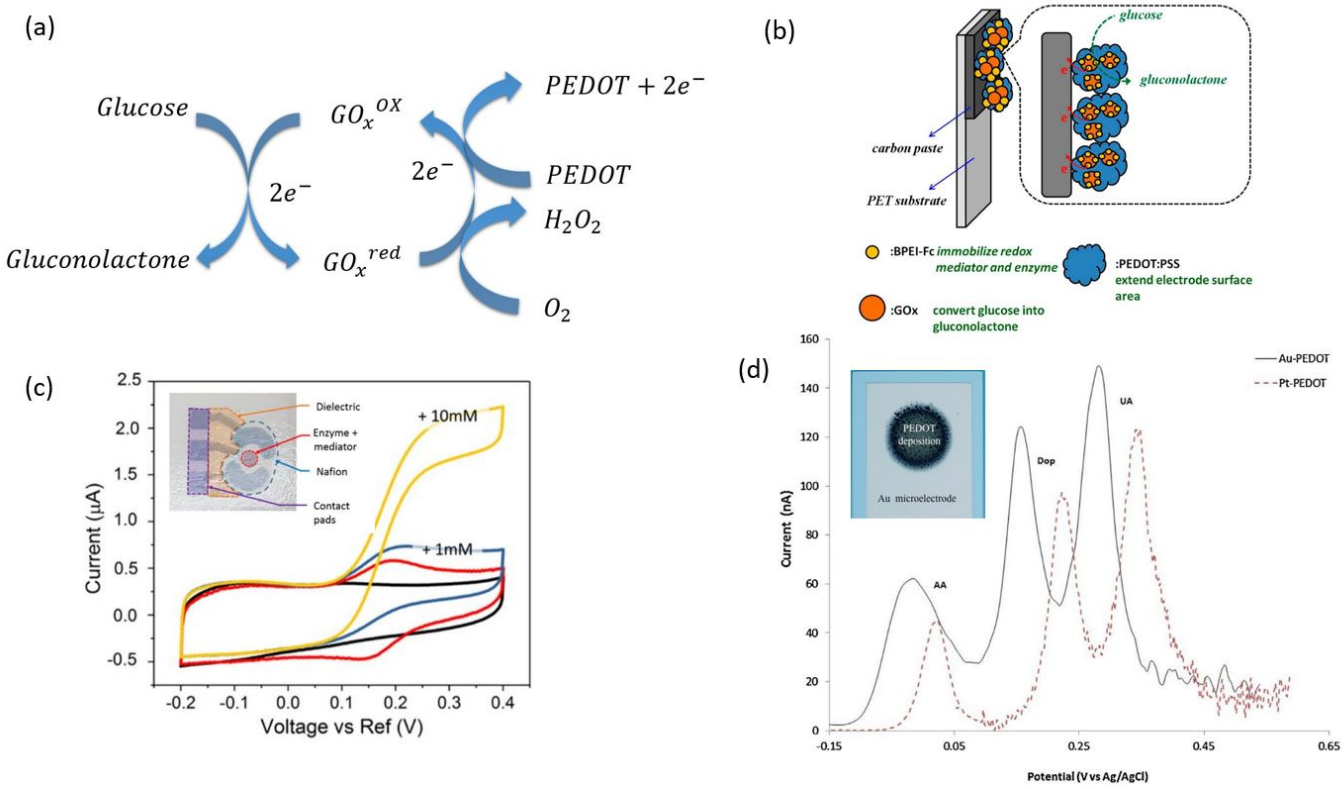

Figure 7: Biosensing with OMEA: (a) The redox reaction series of the sensing mechanism; (b) the structure of PEDOT:PSS-carbon electrode with mixture of polyethyleimine nanobead (BPEI-Fc) and GOx; (c) glucose-sensing CV curves with ink-jet-printed PEDOT:PSS electrode under four different measurement conditions (black line: before PEDOT:PSS deposition; red line: PEDOT:PSS electrode measured in PBS; blue and yellow lines are measuring with 1mM and 10mM glucose present; the insert is the electrode structure)(Bihar et al., *npj Flex. Electron.*, 2018); (d) Differential pulse voltammogram of ascorbic acid (AA), dopamine (Dop), and uric acid (UA) shows high selective at -40, 150 and 280 mV with electropolymerized PEDOT microelectrodes.

Electroactive Cell and Tissue Monitoring and Barrier Cell Impedance Recording

Similar to in vivo recording from brains, electroactive cell or tissue slides can be recorded by rigid planar OMEAs in a standard culture environment. Rigid OMEA as *in vitro* tool has been much investigated for pathology and medication to fight against the diseases related to electroactive cell/organ dysfunctions. Sessolo et al. fabricated OMEA with "parylene liftoff" method and successfully detected LFP and action potentials from slices of rat hippocampus with low noise (± 10 μV peak-to-peak)[11]. Taking advantage of the glass substrate, the recording site of each electrode was positioned with an optical microscope (Figure 8 (h))[11].This proved to be a powerful tool to spot the origin of the abnormal firing (i.e., epilepsy). However, there are two limitations of tissue slice recording. The first is that the presence of a layer of dead or injured cell acting as an insulator reduces the recording signals[11]. The other problem is that slice only can stay active for a short time period (several hours), so long-term study could not be carried out. Therefore, culturing electroactive cells on MEA is a more sustainable, simplified, low-cost, ethical-issue-free approach.

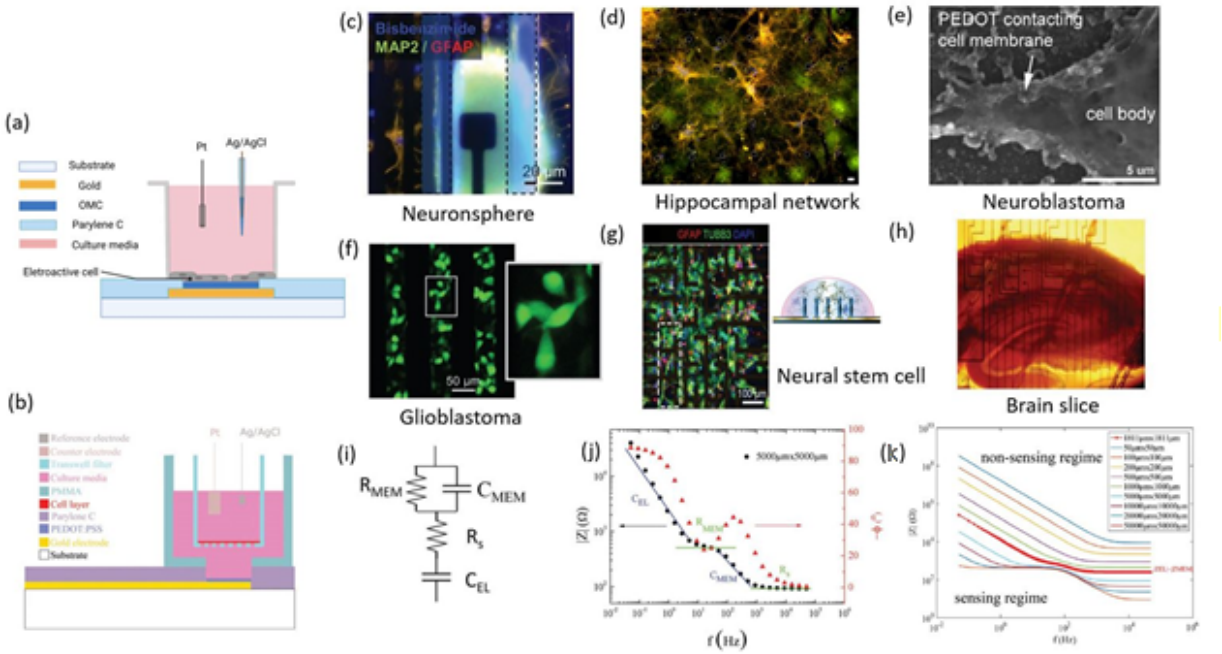

Figure 10 : Comparison of direct culture and transwell culture configuration of planar OMEAs: (a) Scheme of electroactive cells directly cultured on planar device for recording and stimulation; (b) scheme of seeding barrier cell layer onto transwell MEAs for impedance characterisation; (c)-(h) various type of electroactive cell or tissue system on chip: (c) neurosphere recording (PEGDA (blue dashed band) patterns with showing neuron (MAP2, green), astrocytes (GFAP, orange), cell nuclei (bisbenzimide, blue)); (d) cortico-hippocampal network recording (adapted from Blau, A. *et al. Biomaterials*, 2011)[124]; (e) PEDOT encapsulation SH-SY5Y neuroblastoma; (f) glioblastoma stimulation; (g) neural stem cell 3D stimulation with pillar electrode array; (h) brain slice recording planar MEA; (i)-(h) the barrier effect of cell monolayer with EIS measurements: (i) the equivalent circuit model of cell monolayer on transwell membrane of MEAs; (j) the impedance regimes of each equivalent circuit element represented in Bode plot; (k) sensing regime and non-sensing regime separated with impedance spectra of specific electrode area (red curve) where $|Z_{electrode}|$ is equal to the $|Z_{cell}|$(adapted from Koutsouras *et al. Adv. Healthc. Mater.*, 2019)[125].

The first neuronal culture recording and stimulating with planar Pt MEAs was reported by Pine in 1980[126]. Now, with the improved recording performance by CP coating, OMEAs neuron recording has a higher signal-to-noise ratio. To have a high-quality recording, a few challenges need to consider. The first one is the cell viability on OMEA in the cell-culture environment. Richardson-Burns et al. managed to record SH-SY5Y neuroblastoma cell with PEDOT:PSS microelectrodes[127]. The electrochemical polymerization was applied to coat PEDOT:PSS film onto the metal electrodes with the present of SH-SY5Y cells, and the cells wrapped fully or partially with PEDOT:PSS were able to maintain 82 % viability over 72 hours (Figure 10(e))[127]. This further confirmed the excellent biocompatibility of PEDOT:PSS for cell culture. In the same work, CV and EIS were used to sense the attachment of cells onto the electrodes by identifying decreased anode/cathode current and detecting higher impedance, respectively[127]. The second challenge is the maintenance of mature neurons since they do not undergo cell division. Pas et al. successfully co-cultured neuron and astrocytes on polypeptide (poly-D-lysine) and extracellular matrix (laminin) coated OMEAs and found that high cell density on the PEDOT:PSS MEAs drastically improved the recorded voltage amplitude due to the more neurons being closer to the electrode sites (Figure 10 (c))[128]. They improved the single-unit recording by culturing 3D neurospheres formed from rat primary cortical cells, which gave much higher local cell density[128]. The third challenge for recording neural cell is to place patterns according to the cell size and electrode dimensions and arrangement so that the cells could be placed on top of the electrode site and grow to the neighboring cells with controlled manner. Pas et al. then further patterned the OMEA with polyethylene glycol diacrylate (PEGDA, a cell-attachment inhibitor) with a laser writing technique and achieved to measure multi-neuron recording with a single electrode from neurospheres for the first time[128]. Besides neurons recording, researchers also stimulate cells with planar OMEAs. Dijk and colleagues stimulate glioblastoma cells with PEDOT:PSS electrodes, and concluded that the thicker PEDOT:PSS coating can reduce impedance and increase charge injection, and the optimal thickness (650nm) can provide much longer electrode life-time, which can be beneficial for long-term stimulation[33]. To mimic and stimulate neuron growth in native condition, Tomaskovic et al. cultures human neuronal stem cell (NSC) within biogel to imitate native 3D cell growth condition[129]. They direct-write print the PEDOT:PSS into pillar electrode, so this 3D-pillar electrodes can improve the stimulation by closer coupling with cells[129]. The NSC stimulated by 3D-electrode shows higher density of mature neuronal network compared

with the counterpart without stimulation[129]. Nowadays, these planar OMEAs have already shown stable and long-term recording and stimulation abilities, and soon, their advantages of versatility and biocompatibility can play a crucial role in the field of cell culture, differentiation, and tissue regeneration.

Furthermore, OMEA is not only a device of electroactive cell measurements, but also a powerful tool to sense barrier effect of cell layers. Usually, epithelial and endothelial cells form selective layers to maintain a stable chemical environments within organisms[130]. Connected by tight junctions (TJ), these barrier cells are capable of controlling molecules (including ions) that pass through the barrier[130]. These barrier monolayers are common but crucial due to their physiological function, so the integrity of their barrier monolayer is an indicator of disease. The barrier effect of these monolayers can be evaluated by electrochemical impedance spectroscopy (EIS). Monolayers formed by Caco-2 cells [131] and Madin Darby canine kidney (MDCK) cells[132] are typically used cell models for the EIS analysis within the field. The barrier monolayer can be cultured on the filter of a transwell above the OMEA, which mimic the lumen and basolateral domains by the top and bottom media chambers (Figure 10(b)). Once cells are confluent on the filter, the TJ can form intercellularly, so the cell layer creates a barrier to inhibit the ionic flow and influence the impedance spectra[125,133,134]

When AC voltage sweeps through mid-frequencies, the cell monolayer characteristics can be measured. Taking Caco-2 monolayers as an example, the frequency from 1 to 10^2 Hz explores the resistance effect of the paracellular pathway (between the cells), whereas at the higher frequency (10^2 – 10^3 Hz), the current provides the capacitance characteristics of the transcellular pathway (through the cells) (Figure 10 (j))[24,125,130]. Furthermore, the cell monolayer and transwell OMEAs are commonly modelled with the equivalent circuit shown in Figure 10(i). R_{MEM} is the tight junction resistance between cells, and C_{MEM} is the capacitance element contributed to the cell. R_s and C_{EL} are electrolyte impedance and the electrode capacitance, respectively[125]. Through this equivalent circuit model, the impedance (capacitive and resistive) properties of the cell monolayer can be extracted through the fitting of the impedance spectra.

However, according to the work from Koursouras et al., the barrier cell-impedance characteristic can only be sensed by relatively large electrodes (5000 μm X 5000 μm and 10000

µm X 10000 µm). Essentially, the sensitivity is due to the ratio of impedance modulus of the cell barrier ($|Z_{cell}|$) to the impedance modulus ($|Z_{electrode}|$) of the electrode (

Figure 10 (k))[125]. On one hand, when the $|Z_{electrode}|$ is greater than the $|Z_{cell}|$, the system is in the non-sensing regime, so the electrode cannot pick up any impedance signals from the cells. On the other hand, when the $|Z_{cell}|$ is greater than $|Z_{electrode}|$, the electrode can sense the cell-barrier impedance, which is noticeable both in the Bode plot and phase diagram (Figure 10 (c)). Therefore, the size of the electrode is a very crucial parameter for designing sensitive microelectrodes for various biological applications.

Native Cell Membrane Impedance Monitoring

The cell membrane, as the outermost barrier of individual cells, functions as first defensive screen, nutrient selector, and supplier, which maintains a stable intracellular environment. Cell-membrane-on-chip is recently becoming a popular topic on bioelectronics. Researchers have investigated Impedance properties of the native cell membrane with OMEAs. Pappa et al. demonstrated that human embryonic kidney (HEK) cell membranes were reconstructed on the PEDOT:PSS electrode which in turn sense the impedance increase compare to the bare electrodes, using EIS measurements [135]. The native membrane fused microelectrode can be simulated with an equivalent circuit shown in Figure 11 (a). The C_m and R_m in parallel represent the membrane resistance and capacitance, respectively, and the R_s is the electrolyte resistance above the microelectrode, and C_p is the capacitance of PEDOT:PSS coating[135]. With this equivalent circuit model, the membrane impedance characteristics C_m and R_m can be extracted[135,136].

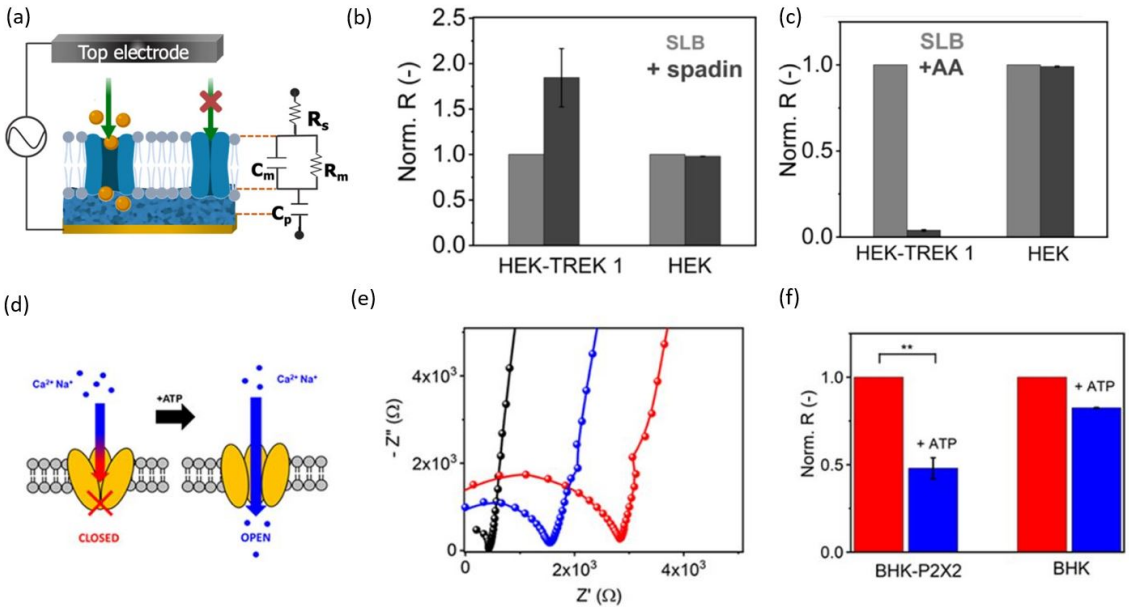

Figure 11 : : The EIS measurement of ion channel activity on membrane integrated with OMEAs: (a) a scheme of HEK-TREK-1 membrane on PEDOT:PSS coated microelectrode with equivalent circuit model, and each circuit element representing the physical element in the system (separated with red dashed lines); (b) a scheme of opening and closing the TREK-1 ion channel with AA and spadin, respectively; (d) spadin (10 µM) addition suppressing the TREK1 activity inducing an increase of membrane resistance; (e) AA activating TREK1 causing a decrease of normalized membrane resistance (Pappa, A.-M. *et al*. *ACS Nano* acsnano., 2020)[135]: (d) schematic of PX2X ATP-gated ion channel; (e) Nyquist plot of bare electrode (black), P2X2-rich membrane, and membrane treated with ATP (blue); (f) Membrane impedance of baby hamster kidney (BHK) membrane expressing P2X2-ion have more significate decrease when it is treated with ATP channel comparing with normal BHK membrane (Liu, H. Y. *et al.*, *Langmuir*, 2020)[136].

With this integration native cell membrane and OMEA, the ion channel activation and deactivation can be monitored with EIS measurements. On the HEK membrane, the TREK-1 potassium ion channel was overexpressed throughout the membrane, so when arachidonic acid (AA, a TREK-1 activation molecule) was added, it induced the ion flow through the membrane and the membrane impedance had a large drop (97% decrease)[135]. Spadin, a TREK-1 blocker, suppressed the ion current and caused the rising of membrane impedance[135]. Besides the ligand-gated ion channel, Liu and colleagues also managed to read out the impedance reduction caused by open the ATP-gated PX2P-ion channel on baby hamster kidney (BHK) membrane with the same membrane-microelectrode system[136]. This innovative membrane impedance sensing with OMEA breakthroughs the limitation of both low

throughput of ion-channel activity monitoring and cell viability maintaining from traditional ion channel monitoring methods (i.e., patch clamp), which is opening a new window for ion channel protein-related research and its drug screen studies.

1.6 Outlook

The recent rapid advances in the field of OMEAs truly demonstrates its capacity as implantable health monitoring devices, *in vitro* diagnostic sensors, tissue-on-chip models and many more. It will keep catching more attention in the field of medical care and lab research in the future. For further advancements in the field, there are few points of view worth considering. Firstly, to reduce the wiring resistance and fabrication difficulties, most of the wire design needs to keep a reasonable width and proper arrangement around the working electrode areas within the same plane. Thus, the wires occupancy may limit the packing density and deduction of the electrode sizes. The ideal separation of wiring and functional electrode into two (multi-) planes adapted from matrix technology might give more room to arrange a denser array-packing[137,138]. In the area of tissue or cell recordings, culture on the planar device is not representative of the native environment. Recently, researchers co-cultured multiple cells within conducting polymer scaffolds and monitored cell growth with impedance recordings[139]. The conducting scaffold not only maintained the needs of cell growth but also create a 3D and more biologically relevant environment. The combination of the spacial recognition of an array and the scaffold culture could enhance the sensing resolution and improve cell growth environments. Furthermore, in the field of biosensing, “sponge-like” surface of conducting polymer is a great advantage of incorporation of the enzyme and conducting polymer, but the balance of enzyme coverage and charge transport is important to maintain proper sensitivities, which needs much investigation and experience in the field. Last but not least, the ongoing and increasing amount of collaborations among material chemists, device engineers, and biological/medical researchers all over the world should be highly encouraged to make OMEAs more powerful and promising tools to study biological events and fight against diseases.

Bibliography

1. Rivnay, J., Owens, R. M. & Malliaras, G. G. The rise of organic bioelectronics. *Chemistry of Materials* **26**, 679–685 (2014).
2. Dornberger, E. *et al.* Influence of boron concentration on the oxidation-induced stacking fault ring in czochralski silicon crystals. *J. Cryst. Growth* **180**, 343–352 (1997).
3. Schubert, E. F. *Doping in III-V Semiconductors - E. Fred Schubert*. (1993).
4. Callister, William; Rethwisch, D. *Materials science and Engineering: An Introduction 9th Edition*. (Wiley, 2013).
5. Rivnay, J. *et al.* Organic electrochemical transistors. *Nature Reviews Materials* **3**, (2018).
6. Rivnay, J., Owens, R. M. & Malliaras, G. G. The rise of organic bioelectronics. *Chemistry of Materials* **26**, 679–685 (2014).
7. Savva, A. *et al.* Influence of Water on the Performance of Organic Electrochemical Transistors. *Chem. Mater.* **31**, 927–937 (2019).
8. Cendra, C. *et al.* Role of the Anion on the Transport and Structure of Organic Mixed Conductors. *Adv. Funct. Mater.* **29**, 1–11 (2019).
9. Giovannitti, A. *et al.* Controlling the mode of operation of organic transistors through side-chain engineering. *Proc. Natl. Acad. Sci. U. S. A.* **113**, 12017–12022 (2016).
10. Nielsen, C. B. *et al.* Molecular Design of Semiconducting Polymers for High-Performance Organic Electrochemical Transistors. *J. Am. Chem. Soc.* **138**, 10252–10259 (2016).
11. Sessolo, M. *et al.* Easy-to-fabricate conducting polymer microelectrode arrays. *Adv. Mater.* **25**, 2135–2139 (2013).
12. Mattana, G. *et al.* Inkjet-Printing: A New Fabrication Technology for Organic Transistors. *Adv. Mater. Technol.* **2**, 1700063 (2017).
13. Brooke, R. *et al.* Inkjet printing and vapor phase polymerization: Patterned conductive PEDOT for electronic applications. *J. Mater. Chem. C* **1**, 3353–3358 (2013).
14. Scheiblin, G. *et al.* Screen-printed organic electrochemical transistors for metabolite sensing. *MRS Commun.* **5**, 507–511 (2015).
15. Sukeerthi, S. & Contractor, A. Q. Molecular sensors and sensor arrays based on polyaniline microtubules. *Anal. Chem.* **71**, 2231–2236 (1999).
16. Koutsouras, D. A. *et al.* Impedance Spectroscopy of Spin-Cast and Electrochemically Deposited PEDOT:PSS Films on Microfabricated Electrodes with Various Areas. *ChemElectroChem* **4**, 2321–2327 (2017).
17. Savva, A., Wustoni, S. & Inal, S. Ionic-to-electronic coupling efficiency in PEDOT:PSS films operated in aqueous electrolytes. *J. Mater. Chem. C* **6**, 12023–12030 (2018).
18. Feron, K. *et al.* Organic bioelectronics: Materials and biocompatibility. *International*

Journal of Molecular Sciences **19**, (2018).

19. Ramuz, M. *et al.* Combined Optical and Electronic Sensing of Epithelial Cells Using Planar Organic Transistors. *Adv. Mater.* **26**, 7083–7090 (2014).

20. Dijk, G., Rutz, A. L. & Malliaras, G. G. Stability of PEDOT:PSS-Coated Gold Electrodes in Cell Culture Conditions. *Adv. Mater. Technol.* **5**, (2020).

21. Khodagholy, D. *et al.* High transconductance organic electrochemical transistors. *Nat. Commun.* **4**, (2013).

22. Uguz, I. *et al.* Autoclave Sterilization of PEDOT:PSS Electrophysiology Devices. *Adv. Healthc. Mater.* **5**, 3094–3098 (2016).

23. Yao, C., Li, Q., Guo, J., Yan, F. & Hsing, I. M. Rigid and flexible organic electrochemical transistor arrays for monitoring action potentials from electrogenic cells. *Adv. Healthc. Mater.* **4**, 528–533 (2015).

24. Rivnay, J. *et al.* Organic electrochemical transistors for cell-based impedance sensing. *Appl. Phys. Lett.* **106**, (2015).

25. Pappa, A. M. *et al.* Organic Electronics for Point-of-Care Metabolite Monitoring. *Trends in Biotechnology* **36**, 45–59 (2018).

26. Simon, D. T. *et al.* Organic electronics for precise delivery of neurotransmitters to modulate mammalian sensory function. *Nat. Mater.* **8**, 742–746 (2009).

27. Press, A. *et al.* Conducting Polymer Hydrogels as 3D Electrodes : Applications for Supercapacitors ** By Soumyadeb Ghosh * and Olle Inganäs. *Adv. Mater.* **11**, 1214–1218 (1999).

28. Cui, X. *et al.* Surface modification of neural recording electrodes with conducting polymer/biomolecule blends. *J. Biomed. Mater. Res.* **56**, 261–272 (2001).

29. Berggren, M. & Malliaras, G. G. How conducting polymer electrodes operate. *Science (80-.).* **364**, 233–234 (2019).

30. Rivnay, J. *et al.* High-performance transistors for bioelectronics through tuning of channel thickness. *Sci. Adv.* **1**, 1–6 (2015).

31. Proctor, C. M., Rivnay, J. & Malliaras, G. G. Understanding volumetric capacitance in conducting polymers. *J. Polym. Sci. Part B Polym. Phys.* **54**, 1433–1436 (2016).

32. Kissinger, P. T. & Heineman, W. R. Cyclic voltammetry. *Journal of Chemical Education* **60**, 702–706 (1983).

33. Dijk, G., Ruigrok, H. J. & O'Connor, R. P. Influence of PEDOT:PSS Coating Thickness on the Performance of Stimulation Electrodes. *Adv. Mater. Interfaces* **2000675**, 1–9 (2020).

34. Ganji, M., Tanaka, A., Gilja, V., Halgren, E. & Dayeh, S. A. Scaling Effects on the Electrochemical Stimulation Performance of Au, Pt, and PEDOT:PSS Electrocorticography Arrays. *Adv. Funct. Mater.* **27**, 1–14 (2017).

35. Loveday, D., Peterson, P. & Rodgers, B. Evaluation of organic coatings with electrochemical impedance spectroscopy: Part 1: Fundamentals of electrochemical impedance spectroscopy. *CoatingsTech* **1**, 46–52 (2004).

36. Dhand, C., Das, M., Datta, M. & Malhotra, B. D. Recent advances in polyaniline based biosensors. *Biosensors and Bioelectronics* **26**, 2811–2821 (2011).

37. Karyakin, A. A. *et al.* Processible polyaniline as an advanced potentiometric pH transducer. Application to biosensors. *Anal. Chem.* **71**, 2534–2540 (1999).

38. Naoi, K., Oura, Y. & Tsujimoto, H. Conducting Polymer With Favored Structure As a Possible Ultracapacitor Material. in *Proceedings of the Symposium on Electrochemical Capacitors II* (eds. Delnick, F. M., Ingersoll, D., Andrieu, X. & Naoi, K.) 120–126 (The Electrochemical Society, 1997).

39. Snook, G. A., Peng, C., Fray, D. J. & Chen, G. Z. Achieving high electrode specific capacitance with materials of low mass specific capacitance: Potentiostatically grown thick micro-nanoporous PEDOT films. *Electrochem. commun.* **9**, 83–88 (2007).

40. Kros, A., Sommerdijk, N. A. J. M. & Nolte, R. J. M. Poly(pyrrole) versus poly(3,4-ethylenedioxythiophene): Implications for biosensor applications. in *Sensors and Actuators, B: Chemical* **106**, 289–295 (Elsevier, 2005).

41. Yamato, H., Ohwa, M. & Wernet, W. Stability of polypyrrole and poly(3,4-ethylenedioxythiophene) for biosensor application. *J. Electroanal. Chem.* **397**, 163–170 (1995).

42. Snook, G. A., Kao, P. & Best, A. S. Conducting-polymer-based supercapacitor devices and electrodes. *Journal of Power Sources* **196**, 1–12 (2011).

43. Villers, D. *et al.* The Influence of the Range of Electroactivity and Capacitance of Conducting Polymers on the Performance of Carbon Conducting Polymer Hybrid Supercapacitor. *J. Electrochem. Soc.* **150**, A747 (2003).

44. Snook, G. A. & Chen, G. Z. The measurement of specific capacitances of conducting polymers using the quartz crystal microbalance. *J. Electroanal. Chem.* **612**, 140–146 (2008).

45. Ouyang, L., Musumeci, C., Jafari, M. J., Ederth, T. & Inganäs, O. Imaging the Phase Separation between PEDOT and Polyelectrolytes during Processing of Highly Conductive PEDOT:PSS Films. *ACS Appl. Mater. Interfaces* **7**, 19764–19773 (2015).

46. Yamamoto, S. & Malliaras, G. G. Controlling the Neuromorphic Behavior of Organic Electrochemical Transistors by Blending Mixed and Ion Conductors. *ACS Appl. Electron. Mater.* (2020). doi:10.1021/acsaelm.0c00203

47. Inal, S., Malliaras, G. G. & Rivnay, J. Benchmarking organic mixed conductors for transistors. *Nat. Commun.* **8**, 1–6 (2017).

48. Donahue, M. J. *et al.* Tailoring PEDOT properties for applications in bioelectronics. *Mater. Sci. Eng. R Reports* **140**, 100546 (2020).

49. Paterson, A. F. *et al.* Water stable molecular n-doping produces organic electrochemical transistors with high transconductance and record stability. *Nat. Commun.* **11**, 3004 (2020).

50. Giovannitti, A. *et al.* The Role of the Side Chain on the Performance of N-type Conjugated Polymers in Aqueous Electrolytes. *Chem. Mater.* **30**, 2945–2953 (2018).

51. Elschner, A., Kirchmeyer, S., Lovenich, W., Merker, U. & Reuter, K. *PEDOT: Principles and Applications of an Intrinsically Conductive Polymer*. (CRC Press, 2010).

52. ElMahmoudy, M. *et al.* Tailoring the Electrochemical and Mechanical Properties of PEDOT:PSS Films for Bioelectronics. *Macromol. Mater. Eng.* **302**, 1–8 (2017).

53. Winther-Jensen, B. & West, K. Vapor-phase polymerization of 3,4-ethylenedioxythiophene: A route to highly conducting polymer surface layers. *Macromolecules* **37**, 4538–4543 (2004).

54. Giovannitti, A. *et al.* N-type organic electrochemical transistors with stability in water. *Nat. Commun.* **7**, (2016).

55. Macromanu- Facturing .

56. Rodger, D. C. *et al.* Flexible parylene-based multielectrode array technology for high-density neural stimulation and recording. *Sensors Actuators, B Chem.* **132**, 449–460 (2008).

57. James, K. J. & Normann, R. A. Low-stress silicon nitride for insulating multielectrode arrays. *Annu. Int. Conf. IEEE Eng. Med. Biol. - Proc.* **16**, 836–837 (1994).

58. Meng, X. *et al.* Atomic layer deposition of silicon nitride thin films: A review of recent progress, challenges, and outlooks. *Materials (Basel).* **9**, (2016).

59. Seidel, D. *et al.* Impedimetric real-time monitoring of neural pluripotent stem cell differentiation process on microelectrode arrays. *Biosens. Bioelectron.* **86**, 277–286 (2016).

60. Braendlein, M. *et al.* Lactate Detection in Tumor Cell Cultures Using Organic Transistor Circuits. *Adv. Mater.* **29**, (2017).

61. De La Oliva, N., Mueller, M., Stieglitz, T., Navarro, X. & Del Valle, J. On the use of Parylene C polymer as substrate for peripheral nerve electrodes. *Sci. Rep.* **8**, 1–12 (2018).

62. Slavík, J., Skopalík, J., Provazník, I. & Hubálek, J. Multi-electrode array with a planar surface for cell patterning by microprinting. *Sensors (Switzerland)* **19**, 1–11 (2019).

63. Tait, J. G. *et al.* Spray coated high-conductivity PEDOT:PSS transparent electrodes for stretchable and mechanically-robust organic solar cells. *Sol. Energy Mater. Sol. Cells* **110**, 98–106 (2013).

64. Ryynänen, T. *et al.* Transparent microelectrode arrays fabricated by ion beam assisted deposition for neuronal cell *in vitro* recordings. *Micromachines* **11**, 1–11 (2020).

65. Lock, J. P., Im, S. G. & Gleason, K. K. Oxidative chemical vapor deposition of electrically conducting poly(3,4-ethylenedioxythiophene) films. *Macromolecules* **39**, 5326–5329 (2006).

66. Dominguez-Alfaro, A. *et al.* Tailored Methodology Based on Vapor Phase Polymerization to Manufacture PEDOT/CNT Scaffolds for Tissue Engineering. *ACS Biomater. Sci. Eng.* **6**, 1269–1278 (2020).

67. Murbach, J. M. *et al.* In situ electrochemical polymerization of poly(3,4-ethylenedioxythiophene) (PEDOT) for peripheral nerve interfaces. *MRS Commun.* **8**, 1043–1049 (2018).

68. Carli, S. *et al.* Electrodeposited PEDOT:Nafion Composite for Neural Recording and Stimulation. *Adv. Healthc. Mater.* **8**, 1–10 (2019).

69. Wen, R. *et al.* Intracellular Delivery and Sensing System Based on Electroplated Conductive Nanostraw Arrays. *ACS Appl. Mater. Interfaces* (2019). doi:10.1021/acsami.9b15619

70. Cui, X. & Martin, D. C. <Electrochemical-deposition-and-characterization-of-poly-3-4-ethylenedioxythiophene-on-neural-microelectrode-arrays_2003_Sensors-and-Actuators-B-Chemic.pdf>. *Sensors and Actuators* **89**, 92–102 (2003).

71. Hou, Y. *et al.* Repairing Transected Peripheral Nerve Using a Biomimetic Nerve Guidance Conduit Containing Intraluminal Sponge Fillers. *Adv. Healthc. Mater.* **8**, (2019).

72. Buchko, C. J., Chen, L. C., Shen, Y. & Martin, D. C. Processing and microstructural characterization of porous biocompatible protein polymer thin films. *Polymer (Guildf).* **40**, 7397–7407 (1999).

73. Creighton, R. L., Phan, J. & Woodrow, K. A. In situs 3D-patterning of electrospun fibers using two-layer composite materials. *Sci. Rep.* **10**, 1–14 (2020).

74. Miyamoto, A. *et al.* Inflammation-free, gas-permeable, lightweight, stretchable on-skin electronics with nanomeshes. *Nat. Nanotechnol.* **12**, 907–913 (2017).

75. Kim, S. jun, Phung, T. H., Kim, S., Rahman, M. K. & Kwon, K. S. Low-Cost Fabrication Method for Thin, Flexible, and Transparent Touch Screen Sensors. *Adv. Mater. Technol.* **2000441**, 1–6 (2020).

76. Chronakis, I. S., Grapenson, S. & Jakob, A. Conductive polypyrrole nanofibers via electrospinning: Electrical and morphological properties. *Polymer (Guildf).* **47**, 1597–1603 (2006).

77. Elschner, A. The spectral sensitivity of PEDOT:PSS films. *Sol. Energy Mater. Sol. Cells* **95**, 1333–1338 (2011).

78. Inoue, A., Yuk, H., Lu, B. & Zhao, X. Strong adhesion of wet conducting polymers on diverse substrates. *Sci. Adv.* **6**, 1–11 (2020).

79. Golabchi, A., Woeppel, K. M., Li, X., Lagenaur, C. F. & Cui, X. T. Neuroadhesive protein coating improves the chronic performance of neuroelectronics in mouse brain. *Biosens. Bioelectron.* **155**, 112096 (2020).

80. Golabchi, A., Wu, B., Cao, B., Bettinger, C. J. & Cui, X. T. Zwitterionic polymer/polydopamine coating reduce acute inflammatory tissue responses to neural implants. *Biomaterials* **225**, 119519 (2019).

81. Ji, G. *et al.* Fully Coated Semitransparent Organic Solar Cells with a Doctor-Blade-Coated Composite Anode Buffer Layer of Phosphomolybdic Acid and PEDOT:PSS and a Spray-Coated Silver Nanowire Top Electrode. *ACS Appl. Mater. Interfaces* **10**, 943–954 (2018).

82. Rutledge, S. A. & Helmy, A. S. Etch-free patterning of poly(3,4-ethylenedioxythiophene)-poly(styrenesulfonate) for optoelectronics. *ACS Appl. Mater. Interfaces* **7**, 3940–3948 (2015).

83. Defranco, J. A., Schmidt, B. S., Lipson, M. & Malliaras, G. G. Photolithographic patterning of organic electronic materials. *Org. Electron.* **7**, 22–28 (2006).

84. Laermer, F., Franssila, S., Sainiemi, L. & Kolari, K. Deep Reactive Ion Etching. *Handb.*

Silicon Based MEMS Mater. Technol. Second Ed. 444–469 (2015). doi:10.1016/B978-0-323-29965-7.00021-X

85. Duffy, P. *et al.* Synthetic bioresorbable poly-α-hydroxyesters as peripheral nerve guidance conduits; A review of material properties, design strategies and their efficacy to date. *Biomater. Sci.* **7**, 4912–4943 (2019).

86. Mapili, G., Lu, Y., Chen, S. & Roy, K. Laser-layered microfabrication of spatially patterned functionalized tissue-engineering scaffolds. *J. Biomed. Mater. Res. - Part B Appl. Biomater.* **75**, 414–424 (2005).

87. Zhang, F., Nyberg, T. & Inganäs, O. Conducting Polymer Nanowires and Nanodots Made with Soft Lithography. *Nano Lett.* **2**, 1373–1377 (2002).

88. Ludwig, K. A., Uram, J. D., Yang, J., Martin, D. C. & Kipke, D. R. Chronic neural recordings using silicon microelectrode arrays electrochemically deposited with a poly(3,4-ethylenedioxythiophene) (PEDOT) film * Related content Poly(3,4-ethylenedioxythiophene). *J. Neural Eng.* **3**, 59 (2006).

89. Li, D. & Guo, L. J. Micron-scale organic thin film transistors with conducting polymer electrodes patterned by polymer inking and stamping. *Appl. Phys. Lett.* **88**, (2006).

90. Bihar, E. *et al.* Fully Printed Electrodes on Stretchable Textiles for Long-Term Electrophysiology. *Adv. Mater. Technol.* **2**, (2017).

91. Sekitani, T. *et al.* Stretchable active-matrix organic light-emitting diode display using printable elastic conductors. *Nat. Mater.* **8**, 494–499 (2009).

92. Lim, B. J. & Mirkin, C. A. Electrostatically Driven Dip-Pen Nanolithography. 1474–1477 (2010).

93. Iandolo, D. *et al.* Development and Characterization of Organic Electronic Scaffolds for Bone Tissue Engineering. *Adv. Healthc. Mater.* **5**, 1505–1512 (2016).

94. Hebner, T. R., Wu, C. C., Marcy, D., Lu, M. H. & Sturm, J. C. Ink-jet printing of doped polymers for organic light emitting devices. *Appl. Phys. Lett.* **72**, 519–521 (1998).

95. Bharathan, J. & Yang, Y. Polymer electroluminescent devices processed by inkjet printing: I. Polymer light-emitting logo. *Appl. Phys. Lett.* **72**, 2660–2662 (1998).

96. Bao, Z. Materials and fabrication needs for low-cost organic transistor circuits. *Adv. Mater.* **12**, 227–230 (2000).

97. Didier, C., Kundu, A. & Rajaraman, S. Capabilities and limitations of 3D printed microserpentines and integrated 3D electrodes for stretchable and conformable biosensor applications. *Microsystems Nanoeng.* **6**, (2020).

98. Voss, F. K. *et al.* SI - Additive manufacturing of hydrogel-based materials for next-generation implantable medical devices. *Sci. Robot.* 16 (2017). doi:10.1126/science.1252826

99. Adly, N. *et al.* Printed microelectrode arrays on soft materials: from PDMS to hydrogels. *npj Flex. Electron.* **2**, 1–9 (2018).

100. Gilshtein, E. *et al.* Inkjet-Printed Conductive ITO Patterns for Transparent Security Systems. *Adv. Mater. Technol.* (2020). doi:10.1002/admt.202000369

101. Park, K. S. *et al.* Inkjet-Assisted Nanotransfer Printing for Large-Scale Integrated Nanopatterns of Various Single-Crystal Organic Materials. *Adv. Mater.* **28**, 2874–2880 (2016).

102. Krämer, S., Fuierer, R. R. & Gorman, C. B. Scanning probe lithography using self-assembled monolayers. *Chem. Rev.* **103**, 4367–4418 (2003).

103. Wise, K. D. Silicon microsystems for neuroscience and neural prostheses. *IEEE Engineering in Medicine and Biology Magazine* **24**, 22–29 (2005).

104. Campbell, P. K., Jones, K. E., Huber, R. J., Horch, K. W. & Normann, R. A. A Silicon-Based, Three-Dimensional Neural Interface: Manufacturing Processes for an Intracortical Electrode Array. *IEEE Trans. Biomed. Eng.* **38**, 758–768 (1991).

105. Obien, M. E. J., Deligkaris, K., Bullmann, T., Bakkum, D. J. & Frey, U. Revealing neuronal function through microelectrode array recordings. *Frontiers in Neuroscience* **9**, 423 (2015).

106. Rivnay, J., Wang, H., Fenno, L., Deisseroth, K. & Malliaras, G. G. Next-generation probes, particles, and proteins for neural interfacing. *Science Advances* **3**, e1601649 (2017).

107. Biran, R., Martin, D. C. & Tresco, P. A. Neuronal cell loss accompanies the brain tissue response to chronically implanted silicon microelectrode arrays. *Exp. Neurol.* **195**, 115–126 (2005).

108. Canales, A. *et al.* Multifunctional fibers for simultaneous optical, electrical and chemical interrogation of neural circuits in vivo. *Nat. Biotechnol.* **33**, 277–284 (2015).

109. Williamson, A. *et al.* Localized Neuron Stimulation with Organic Electrochemical Transistors on Delaminating Depth Probes. *Adv. Mater.* **27**, 4405–4410 (2015).

110. Jorfi, M., Skousen, J. L., Weder, C. & Capadona, J. R. Progress towards biocompatible intracortical microelectrodes for neural interfacing applications. *Journal of Neural Engineering* **12**, 011001 (2015).

111. Ferro, M. D. *et al.* NeuroRoots, a bio-inspired, seamless Brain Machine Interface device for long-term recording. *bioRxiv* 1–18 (2018). doi:10.1101/460949

112. Kuruvilla, A. & Flink, R. Intraoperative electrocorticography in epilepsy surgery: Useful or not? *Seizure* **12**, 577–584 (2003).

113. Khodagholy, D. *et al.* Highly Conformable Conducting Polymer Electrodes for In Vivo Recordings. *Adv. Mater.* **23**, H268–H272 (2011).

114. Khodagholy, D. *et al.* NeuroGrid: Recording action potentials from the surface of the brain. *Nat. Neurosci.* **18**, 310–315 (2015).

115. Jastrzebska-Perfect, P. *et al.* Mixed-conducting particulate composites for soft electronics. *Sci. Adv.* **6**, 6767–6791 (2020).

116. Yuk, H. *et al.* 3D printing of conducting polymers. *Nat. Commun.* **11**, 1604 (2020).

117. Kalmykov, A. *et al.* Organ-on-e-chip: Three-dimensional self-rolled biosensor array for electrical interrogations of human electrogenic spheroids. *Sci. Adv.* **5**, eaax0729 (2019).

118. Gifford, R. Continuous glucose monitoring: 40 years, what we've learned and what's

next. *ChemPhysChem* **14**, 2032–2044 (2013).

119. Kros, B. A., Hövell, S. W. F. M. Van, Sommerdijk, N. A. J. M. & Nolte, R. J. M. Poly(3,4-ethylenedioxythiophene)-Based Glucose Biosensors**. 1555–1557 (2010).

120. Wang, J. Y., Chen, L. C. & Ho, K. C. Synthesis of redox polymer nanobeads and nanocomposites for glucose biosensors. *ACS Appl. Mater. Interfaces* **5**, 7852–7861 (2013).

121. Bihar, E. *et al.* A fully inkjet-printed disposable glucose sensor on paper. *npj Flex. Electron.* **2**, 1–8 (2018).

122. Wei, F. *et al.* Serum creatinine detection by a conducting-polymer-based electrochemical sensor to identify allograft dysfunction. *Anal. Chem.* **84**, 7933–7937 (2012).

123. Belaidi, F. S. *et al.* PEDOT-modified integrated microelectrodes for the detection of ascorbic acid, dopamine and uric acid. *Sensors Actuators, B Chem.* **214**, 1–9 (2015).

124. Blau, A. *et al.* Flexible, all-polymer microelectrode arrays for the capture of cardiac and neuronal signals. *Biomaterials* **32**, 1778–1786 (2011).

125. Koutsouras, D. A. *et al.* Probing the Impedance of a Biological Tissue with PEDOT:PSS-Coated Metal Electrodes: Effect of Electrode Size on Sensing Efficiency. *Adv. Healthc. Mater.* 1901215 (2019). doi:10.1002/adhm.201901215

126. Pine, J. Recording action potentials from cultured neurons with extracellular microcircuit electrodes. *J. Neurosci. Methods* **2**, 19–31 (1980).

127. Richardson-Burns, S. M. *et al.* Polymerization of the conducting polymer poly(3,4-ethylenedioxythiophene) (PEDOT) around living neural cells. *Biomaterials* **28**, 1539–1552 (2007).

128. Pas, J. *et al.* Neurospheres on Patterned PEDOT:PSS Microelectrode Arrays Enhance Electrophysiology Recordings. *Adv. Biosyst.* **2**, 1–11 (2018).

129. Tomaskovic-Crook, E. *et al.* Human Neural Tissues from Neural Stem Cells Using Conductive Biogel and Printed Polymer Microelectrode Arrays for 3D Electrical Stimulation. *Adv. Healthc. Mater.* **8**, 1–10 (2019).

130. Benson, K., Cramer, S. & Galla, H. J. Impedance-based cell monitoring: Barrier properties and beyond. *Fluids and Barriers of the CNS* **10**, 5 (2013).

131. Ingels, F., Beck, B., Oth, M. & Augustijns, P. Effect of simulated intestinal fluid on drug permeability estimation across Caco-2 monolayers. *Int. J. Pharm.* **274**, 221–232 (2004).

132. Lo, C. M., Keese, C. R. & Giaever, I. Impedance analysis of MDCK cells measured by electric cell-substrate impedance sensing. *Biophys. J.* **69**, 2800–2807 (1995).

133. Jimison, L. H. *et al.* Measurement of barrier tissue integrity with an organic electrochemical transistor. *Adv. Mater.* **24**, 5919–5923 (2012).

134. Tria, S. A. *et al.* Dynamic monitoring of salmonella typhimurium infection of polarized epithelia using organic transistors. *Adv. Healthc. Mater.* **3**, 1053–1060 (2014).

135. Pappa, A.-M. *et al.* Optical and Electronic Ion Channel Monitoring from Native Human Membranes. *ACS Nano* acsnano.0c01330 (2020). doi:10.1021/acsnano.0c01330

136. Liu, H. Y. *et al.* Self-Assembly of Mammalian-Cell Membranes on Bioelectronic

Devices with Functional Transmembrane Proteins. *Langmuir* **36**, 7325–7331 (2020).

137. Andersson, P. *et al.* Active matrix displays based on all-organic electrochemical smart pixels printed on paper. *Adv. Mater.* **14**, 1460–1464 (2002).

138. Someya, T. *et al.* A large-area, flexible pressure sensor matrix with organic field-effect transistors for artificial skin applications. *Proc. Natl. Acad. Sci. U. S. A.* **101**, 9966–9970 (2004).

139. Inal, S. *et al.* Conducting Polymer Scaffolds for Hosting and Monitoring 3D Cell Culture. *Adv. Biosyst.* **1**, 1700052 (2017).

Chapter 2
12-well plate & Micro Electrodes Arrays

Introduction

Cell study and bioelectronic systems

Cell culture is a major tool to study biology. It provides models to experiment on, study cells behavior to drugs or interactions among themselves, and perform toxicology assays for pharmacological development. It allows experiments on specific topics such as cancer, aging, or bacterial and viral infections. Nevertheless, there is the weak rate of success of drugs assays based on simple cell culture systems from *in vitro* to *in vivo* model. Often, cell culture would hardly be representative of the original biological model it tries to mimic. *In vivo*, cells interact with other cells, fluids, air or even evolve under mechanical constraints. These biological models lack of predictivity and might result in misleading conclusions[1] obtained from over simplified *in vitro* cell culture experiments.

As shown in Figure 12, the *in vitro* models are evolving and getting more complex to get closer to the *in vivo* system[2]. Several parameters such as physical constraints, cell culture heterogeneity [3] can be added in the biological model. Mixing different cells cultures and integrating microfluidics systems also improve the similarity of the *in vitro* model to the *in vivo* one. Those enhanced cell cultures require a complementary monitoring tool. Optical screening through microscope could hardly monitor events occurring inside 3D structure[1], or simultaneous biomarkers spreads in large areas or multiple cell culture. As an example, the confocal microscopes: they can perform visualization of 3D biological structure but might lose temporal resolution of a rapid and prompt biological event occurring in multi distanced areas. Whereas electrical recording can perform real time monitoring of the event occurring in different location. To overcome this limitation, bioelectronic devices offers a complementary

monitoring to the visual control. It extracts electrophysiological information from the electrical signals of the biological model studied. As such, combining MEAs to optical tools offers a multiparametric monitoring.

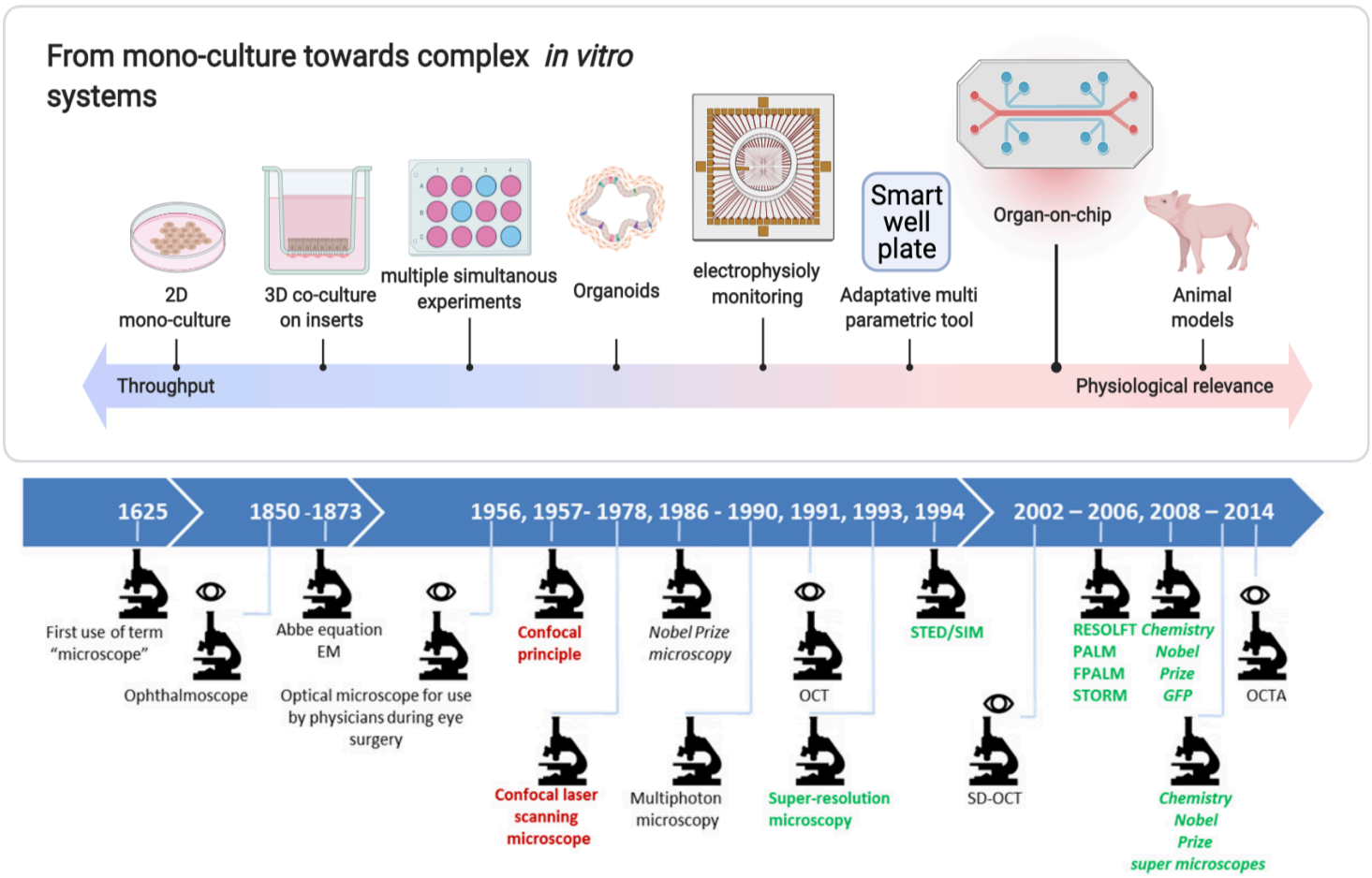

Figure 12: scheme showing the evolution of biological set up and experiment towards in vivo relevance. From Mono-culture models in petri dishes to organ-on-chip multiparametric systems. *In vitro* optical monitoring evolution. Resolution of the microscopes allows sub cellular monitoring of the *in vitro* systems studied. Different technique and options emerged as the fluorescent microscopes. The integration of electrophysiology into the biological equipment panel adds complementary data recording and stimulation from optical results.

To meet the requirements and expectations of researchers and manufacturers from the bioelectronics field, a survey has been conducted[4–7], and lead to the development of an innovative technology platform. With this instrument, adapted to technical demands and standards of traditional laboratories, different biological models can be more accurately validated. Multi parametric, dynamic and long-term monitoring are upgrading the

physiological data recording relevance. Design, packaging and technological compatibility were key aspects that have shaped the thinking during the development of this platform.

The work presented in this chapter follows the IONOSENSE ERC initiated by Pr. Roisin Owens: this proof of concept is based on the perspective of improving sensitivity and reliability of drug and toxicity assays performed in laboratories. From this project, two main statements were observed: Firstly, the *in vitro* experiment done are based on over-simplified biological models compared to the *in vivo* structures they intend to represent. As mentioned previously, those models are barely accurate, and it would be the root of the low success rate of drugs assays from *in vitro* to *in vivo* testing[8] . Secondly, traditional monitoring systems established for 2D biological models, such as visual monitoring via microscope, are not fitted for complex biological *in vitro* models as seen in chapter 5. Furthermore, current MEAs used to monitor the *in vitro* experiment lack of sensitivity towards some biomarkers. In this regards, organic electronic based devices have already been used to improve sensitivity to ionic flux and interfacing with biological tissues. More specifically, the organic electrochemical transistors (OECTs) have the particularity to detect and amplify the electrophysiological signals from biological events, with a better signal-to-noise ration than electrodes[9]. When a biological activity, characterized by an ion flux, occurs near the OECT, the ions penetrate the channel's conducting polymer, thus modifying its conductivity inducing a change in the drain current. The transconductance is determined by the volume of the conducting polymer, hence the size of the channel[10]. An amplifier can be obtained by tuning the OECT geometries, and achieving high transconductance at zero hate bias[11].They are able to detect ionic flux and its propagation occurring from an action potential[12], measure cell barrier functionality and integrity during toxicology assay[13], and can be functionalize to detect different metabolite in blood samples[14].

I have developed an *in vitro* instrument for biological assays based on the 12-well plate device. This tool is a standardized and easy to handle consumable, widely used in biological experiments for analytical research in *in vitro* model and diagnostic testing. Coupling the well plate device with bioelectronics technology is the key to improve and evolve the diagnostic and drug toxicity testing. Companies like Multichannel Systems have developed consumables and hardware such as their MEA2100-technology and Multi-well system. Applied biophysics have developed their ECIS, and Mimetas their OrganoPlate systems family.

To achieve this concept, transparent Organic Micro Electrode Arrays (OMEAs) were integrated into the 12-well plate device structure. In this configuration, the biological models can be evaluated in any standard biological laboratory equipment. Visual and electrophysiological studies can be performed simultaneously. Thus, this "smart" 12-well plate allows a multi parametric and simultaneous monitoring of the biological model studied.

In this section, I will describe the assembly of the "smart' 12-well plate detailing its different pieces: firstly, the plate/lid structure design and the material choices, then define the creation of the Printed Board Circuit (PCB). Afterwards, I will detail the design and fabrication of the OMEAs according to the restrictions and expectations from the *in vitro* experiment. Finally, in the last section, I will develop the assembly through material and electronic hardware used for both electrical connections and sealing, and the integration of the tool into standards biological plan and experiment.

2.1 Integration and advantages of Organic Micro Electrode Arrays in standard biological equipment

As described briefly in chapter 1, MEAs are adaptive tools and a solution that can be integrated in *in vitro* experiments and facilitate electrophysiological monitoring of more complex and elaborated structures such as co-cultures of biological models. As they are fabricated on glass or other transparent substrate, they allow optical and electronic characterizations simultaneously. Furthermore, the materials used for their fabrication process allows sterilization through ethanol, UV or autoclave[15] steam. MEAs translate ionic flux from the biological event to electrical impulses in its conductive tracks. Electrical data are extracted from the chip via a combination of hardware: a PCB gathering the chips connections, a National instrument system (NI system) performs the power transfer measurements, two Digital multimeter NI-PXI-4071 measured source and drain currents, and a NI-PXI 6289 for the drain gate voltage, wires, pogo pins.

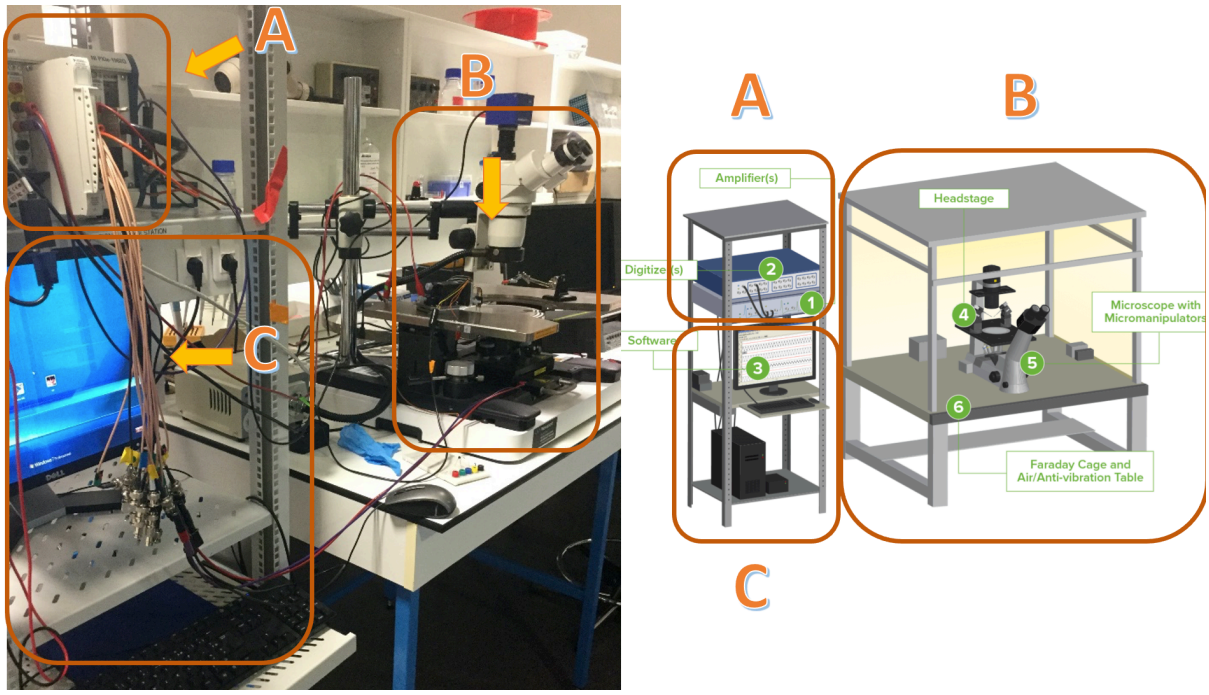

Figure 13: Electrical hardware and set up to extract electrophysiological & optical data. A) shows the amplifiers and the digital multimeter monitoring the biological set up in area B). In the latest, the *in vitro* culture on MEA is placed under a microscope surrounded by a faraday cage (not mandatory) and contact electrical hardware. C) is the software and hardware control set up from which the data are extracted.

As seen in Figure 13, these setups can be bulky and troublesome for users, as they are time consuming, non-intuitive for biologists and might damage MEAs chips or the biological matter over repetitive measurements. The chips and their monitoring hardware must be redesigned and reshaped to facilitate *in vitro* experiments in laboratory.

2.1.1 Single MEA chip VS multiple MEAs chips on a well plate

Regarding user-friendly handling and ease of use, a parallel can be made between petri-dishes or multiple well plates, and single unit or multi-unit recording chips. Figure 14 represents the analogy of single VS multiple test experimentation in biological assays protocol. Reproducibility is expected between the cell cultures, as well as for MEAs chips. Biological experiments should be conducted simultaneously and be repeatable. The multi-well plate tool answers those challenges by providing a single device on which multiple sets of experiments can be conducted simultaneously that are easy to use during experiments, ensuring reproducibility and stability of the trial. To maintain these advantages, and providing optical monitoring and electrical characterization simultaneously, I have designed MEAs in a 12-well plate format.

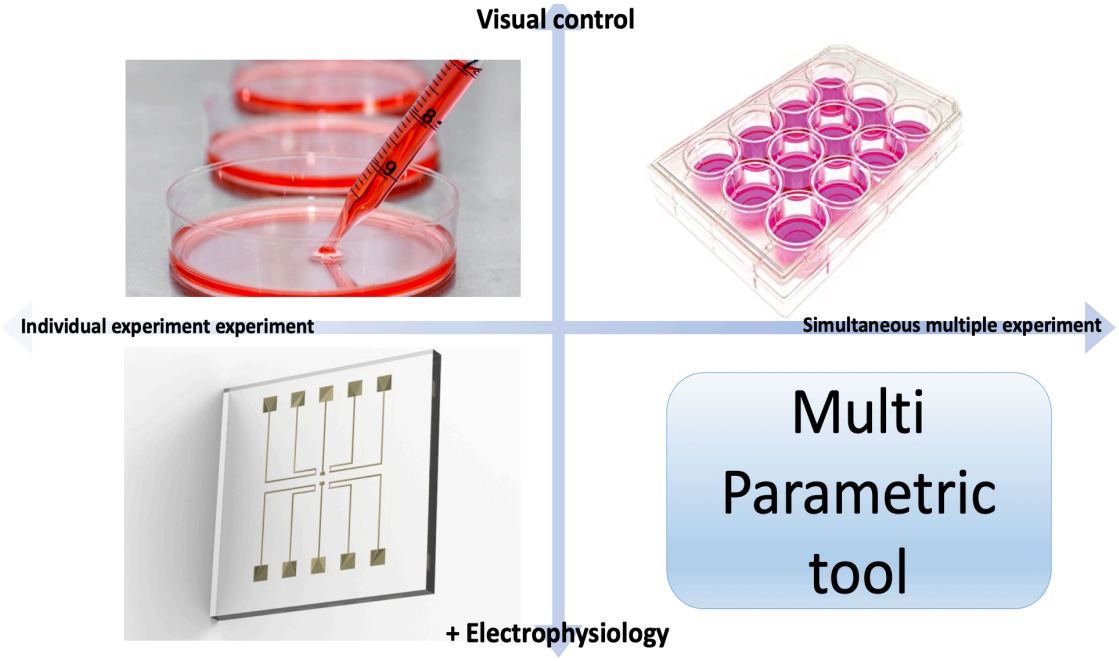

Figure 14: Single unit VS multi-well experiments. Petri dishes are used to perform one protocol on a large sample. Multi well plates perform simultaneously several analysis protocols in wells containing the same biological model. MEA initially performed biological experiment with single unit chip. Combining the multi well plate and the MEA chips creates a dynamic, simultaneous and multiparametric tool for biological experiments.

An additional asset derived from mimicking the design of this standard tool is that this "smart" well plate fits with biological equipment: incubator, hoods, microscope, autoclave

etc. The concept of lab on chip is initiated in the development concept of the 12-well plate. The assembly of biology, biochemistry and electronics are part of the exercise to develop these new diagnostic tools. Microfluidics, thermodynamic and mechanics are additional parameters added to create lab on chips. Here we are focusing on the electronic devices (MEA) layout and their integration in a biological structure (12-well plate), that can undergo thermal and chemical treatment.

Traditionally, MEAs are single unit chips, on which a well is attached, containing the biological element for the *in vitro* experiments. Various models have been investigated in the Bioelectronic laboratory through this set up: epithelial barrier formation over MEAs through cell culture insert (Transwells)[13], action potential detection from neurons cultured directly on top of MEAs[16], or wound healing assays[17]. They also were used to monitor 3D spheroids of co-culture cells in microfluidic chip[18].

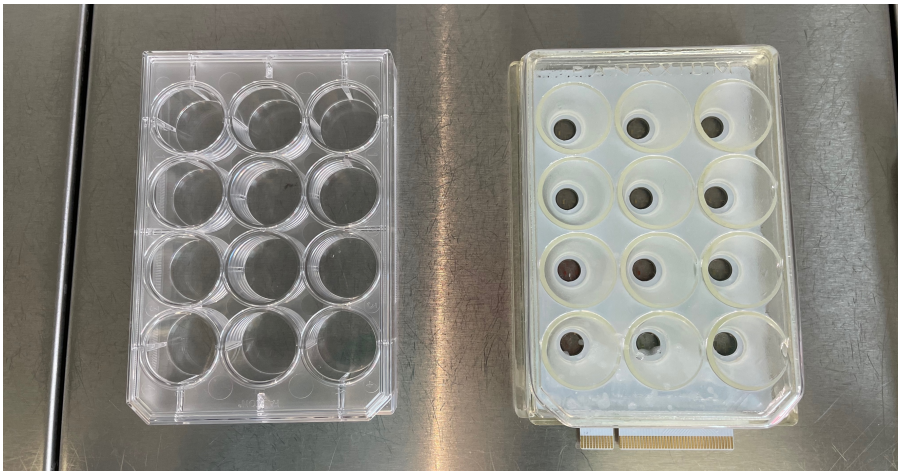

Figure 15: Comparison 12 well plate standard and our smart well plate. Dimensions and spacing of the wells are identical, as well as external geometry. Only the PCI connector add an extrusion to the prototype. The material from the prototype is becoming yellow as it ages. A different choice of material would be necessary

As we are moving toward multi parametric and simultaneous recording system for several individual MEAs chip, their layout must be adapted to new requirements.

2.1.2 Reproducibility and simultaneous recording

To increase repeatability and facilitate simultaneous recording through the multiple experiments and chips, I have fabricated several MEAs chips in a same batch, and on the same carrier: a wafer containing 12 MEAs. I have reevaluated and modified the fabrication protocol (described in the chapter 3) to increase their performance and their electrical characteristic's repeatability after previous work initiated on fabrication processes[19]. A different microfabrication approach has been developed to pattern organic materials for MEAs. Etching technique replaces the peel off steps used to pattern PEDOT:PSS. The aim is to increase repeatability of the device's electrical properties and topology for an industrial OMEAs processing approach.

By arranging the OMEAs in a 12 well plate format, the biological experiment is also treated equally from chip to chip. Regarding the biological experimental setup for electrical monitoring, measures were previously performed outside of the incubator or the microscope, as the hardware is bulky and non-sterile. This would create a harsh environment for the cell culture inside the wells, as temperature is decreasing, and sterility highly compromised during the electrical monitoring. To address this issue, a specific packaging was designed: from connection solutions to extraction of the electrical signal. Firstly, we replaced and reorganized all the connective pads from the different OMEAs chips: by gathering them in a PCI slot, we can connect easily to the hardware, via a printed circuit board (PCB). Secondly, I have designed a packaging system for the smart 12-well plate to remain in the incubator or the microscope during the biological experiment. As a result, the electrical characterization and monitoring can be performed inside an incubator or the biological hood during the time of the biological experiment. The smart 12-well plate and its biological matter remain in its sterile environment as shown later in this chapter in Figure 24. Similarly, while the optical monitoring is performed under microscope, electrical recording can be performed as the packaging allows placement and extraction of the data from a microscope chamber simultaneously.

2.2 “Smart” 12 well plate

2.2.1 Architecture and geometry

Microscopes, incubators, and other traditional biological laboratory equipment match standardized structures (ANSI/SALS microplates standard) to facilitate the combination of consumables and equipment. Fulfilling the same objectives when designing the smart well plate, we have based its structure upon the standard 12 well plate external dimensions and geometry. Figure 14 shows a comparison between the two architectures: single petri-dish and 12-well plate assimilated to single and multiple chips for *in vitro* experiment. External length, width and height were kept the same as shown in Figure 16. The placement of wells / MEAs are identical to the 12-well plate spatial arrangement.

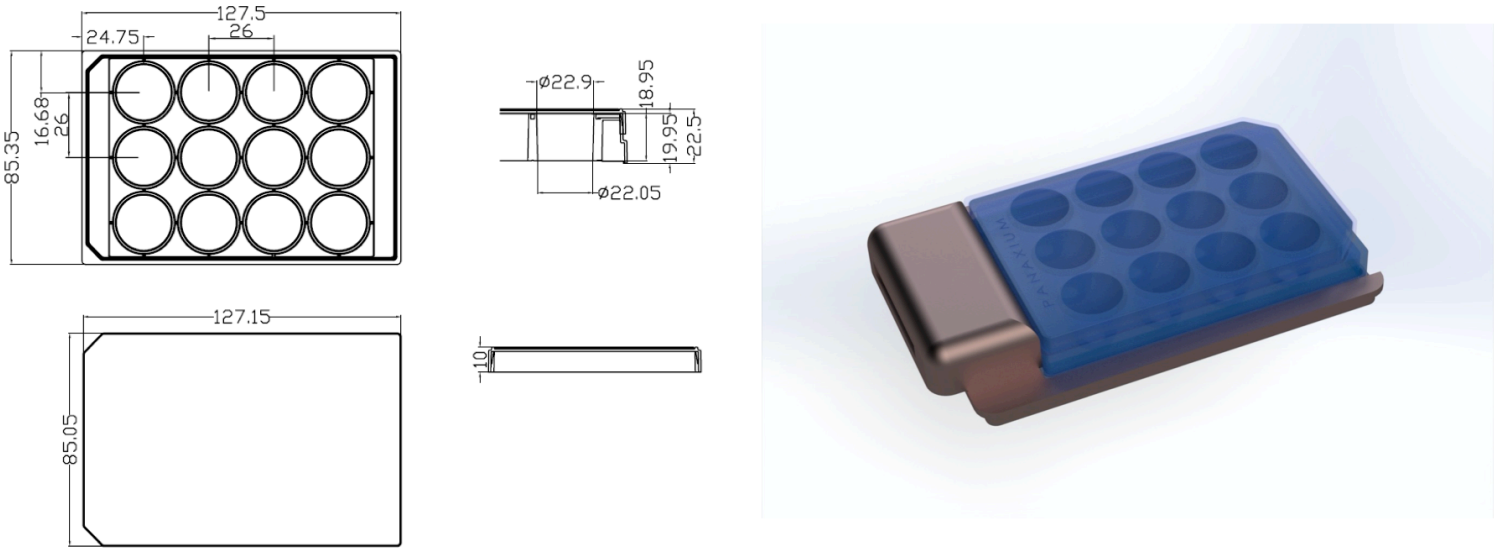

Figure 16: Geometry and dimensions of the 12 well plate. Standard dimensions are applied to the smart well plate in blue. External geometry of the biological container part (blue) follows the same structure as the 12 well plate. The cap is identical in size and structure. To fit the PCB and the chips, a third section in added beneath the cell container shown in Figure 17 e).

To include the PCB gathering the 12 MEAs, the cell container shelf shown has been sectioned in two distinct parts. The top one forming the wells (Figure 17 b)), and the bottom part holding the PCB n°1 (part c)) in place while having an aperture for the MEAs (part d)) to show through (part e)). A rectangular opening is created at the end of the bottom part to provide easy access to the PCB PCI slot connectors (part c)). From parts g) and PCB n°2 h) of, a flat cable extracts the data from biological instrument to the electronic software recording. f) is the holder maintaining the smart well plate inside the microscope plateau.

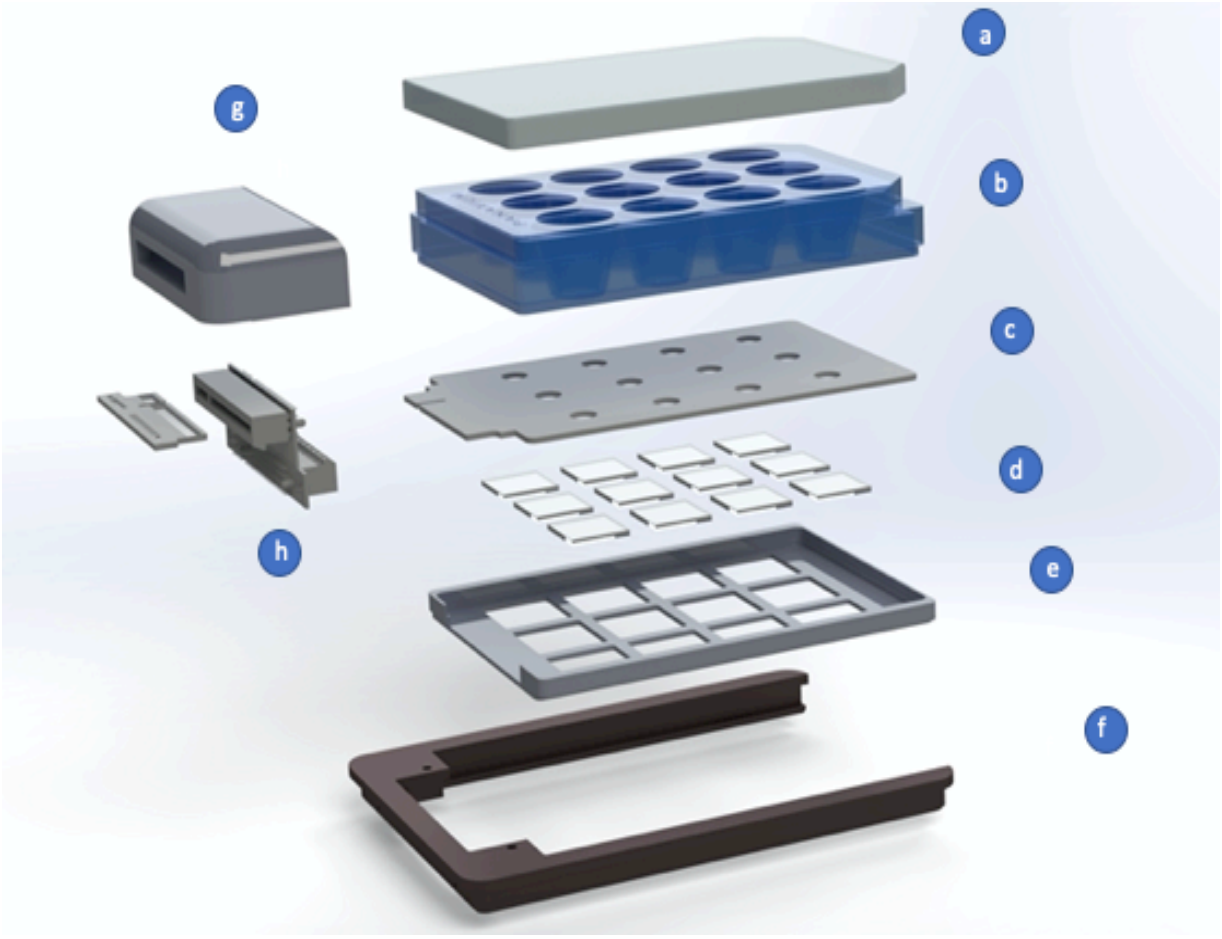

Figure 17: Solidwork rending of the smart well plate. Exploded view of the structures displays the different components. From top to bottom: the lid, cell restrictive environment top part. The PCB and its MEA supported by the bottom part of the smart well plate. And the holder with its additive PCB and cap as g) and h).

2.2.2 Choice of material

A transparent plastic, polyurethane, was chosen per the biological experiment requirements. The transparency of the material is mandatory as the visual control of the cell, volume and colors of media are important during experiments. Unfortunately, the cost of a biocompatible and transparent material was too high to be considered. To circumvent this issue, we decided to cover the overall 3D structure with PaC, which is biocompatible. The instruments has to undergo sterilization before going under any other laboratory tools, such as the incubator and the hood. Considering that the melting point of polyurethane is 98°C, it doesn't suit the autoclave sterilization process, which requires temperature of 120°C. Deformations of the 3D printed circuit also occurred during the steam cycle for sterilization, rendering the tool inoperable. Therefore, the ethanol bath solution is the best approach to fulfill sterilization requirements. We did not consider UV sterilization because organic materials are known to be sensitive to UV[20] and the performance of the MEAs would be deteriorated. The "smart" well plate could be sterilized with ethylene oxide. Unfortunately, this option was not available in the laboratory.

2.2.3 PCB designs and fabrication

Well plates dedicated to biological experiments use a specific standardized design. To fit into standards equipment found in biological laboratory, a Printed Board Circuit (PCB) was sketched to dispose the MEAs correspondingly to a 12-well plate pattern. The printed board circuit assembling MEAs is designed using Dip trace software. On side A, the restrictive environment is attached with PDMS. On side B, MEAs are electrically connected to the PCB. The conductive trace designed on this PCB gather all the connection pads of the 12 MEAs on a single edge, similar to a PCI slot. This enables easy access to the recorded data. The whole set up is maintained inside a microscope thanks to an aluminum holder. We have designed its structure to allow good optical focusing on the MEAs bottom part, and a solid holding of the tool to ensure security of the set up. By plugging the PCI slot into a flat cable extracting the data from the experimental area, it is possible to monitor optically & electronically biological events all together.

The first design draft integrated 12 MEAs in a 12-well plate design is shown in Figure 18. The space available by the surface of the PCB was the limiting factor to draw the conductive lines between the chip and the external PCI connector. Consequently, the number of connective pads available at each of the 12 MEAs was reduced to a maximum of 8 pads. The lines conducting data to the PCI end were drawn on both the top and bottom side of the PCB. Therefore, a total of 96 external PCI slots are spread equally on both ends.

The initial PCB design underwent modifications to achieve a higher number of sensing sites on the MEAs. As the external geometry itself cannot be expended due to standard dimensions, an extra conductive layer was added inside the PCB to allow more electric lines and contact pads to be drawn, hence increasing the number of sensing sites achievable. Inscription and numeration were directly printed on the PCB as illustrated in Figure 18.

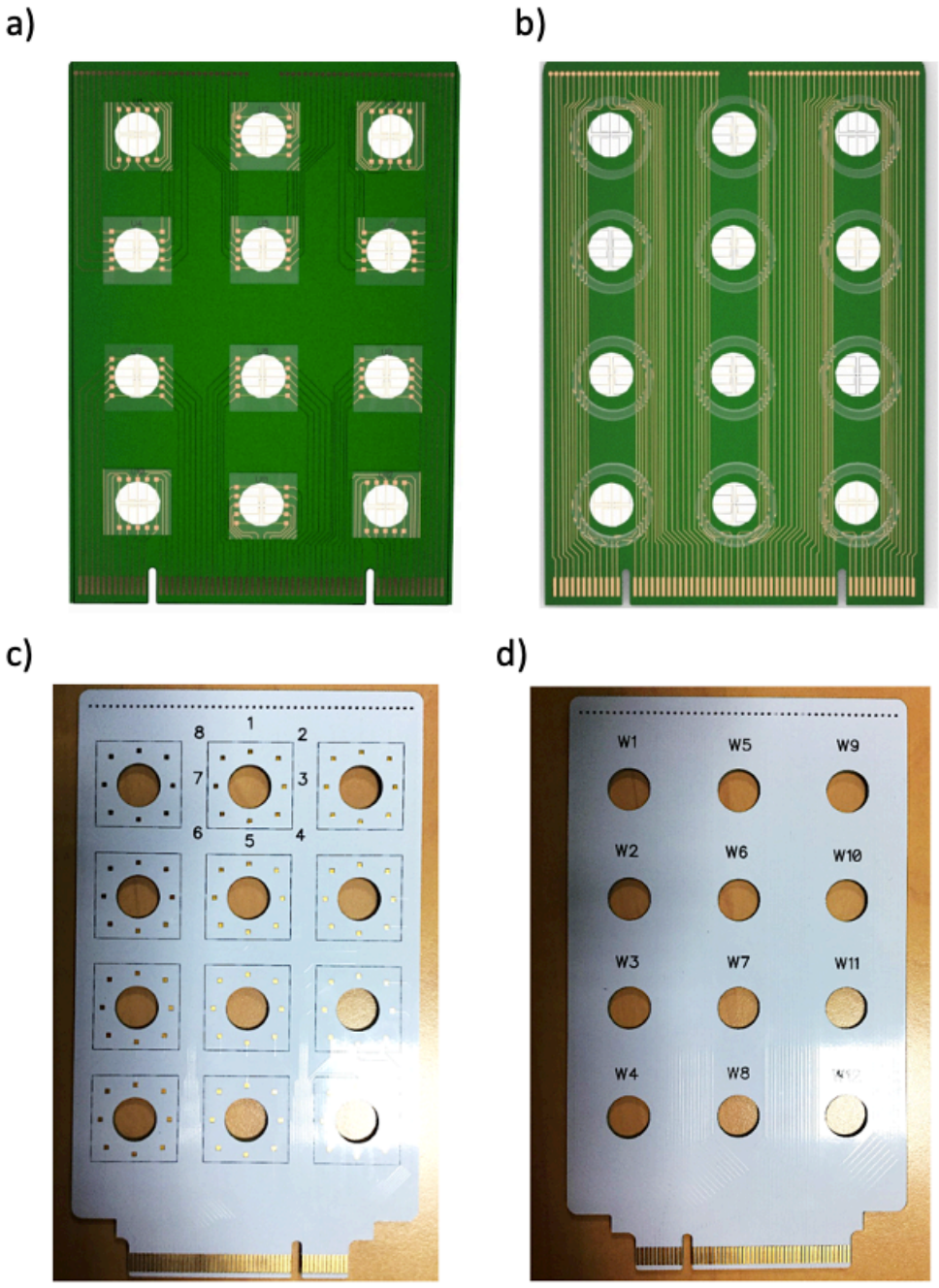

Figure 18: From Solidworks rending to final design PCBs n°1. a) and b) display the First PCB layout and design using solid works software. The spacing between wells exactly fit the 12 well plate standards seen in Figure 16. MEAs chip are electrically bonded to the PCB upon the bottom face a). Each one have 8 connections pads maximum. On the top face b), single glass wells could have been added individually, stucked to the PCB with a PDMS creating. c) and d) are pictures of the final PCB prototype. Well and pads numbering have been added to visually facilitate the user handling. Chips are now connected via 8 pads dispatched in circle as seen in c). A third layer of conductive tracks have been added inside the PCB. It allows to increase the spacing between the connecting pads and eased the bonding between the MEA chips and the PCB.

A second functional PCB was design for geometry and microscope lens focus purpose. In Figure 19 a), the PCI (peripheral component interconnect) slot needed to be elevated to reach the microscope plateau thanks to the PCB n°2 seen Figure 19 b). The PCB n°3 reorganized the electrical connection from the PCB n°2, allowing easy measurement connecting small banana slots and cables to harmonized with the NI system seen in Figure 19 d).

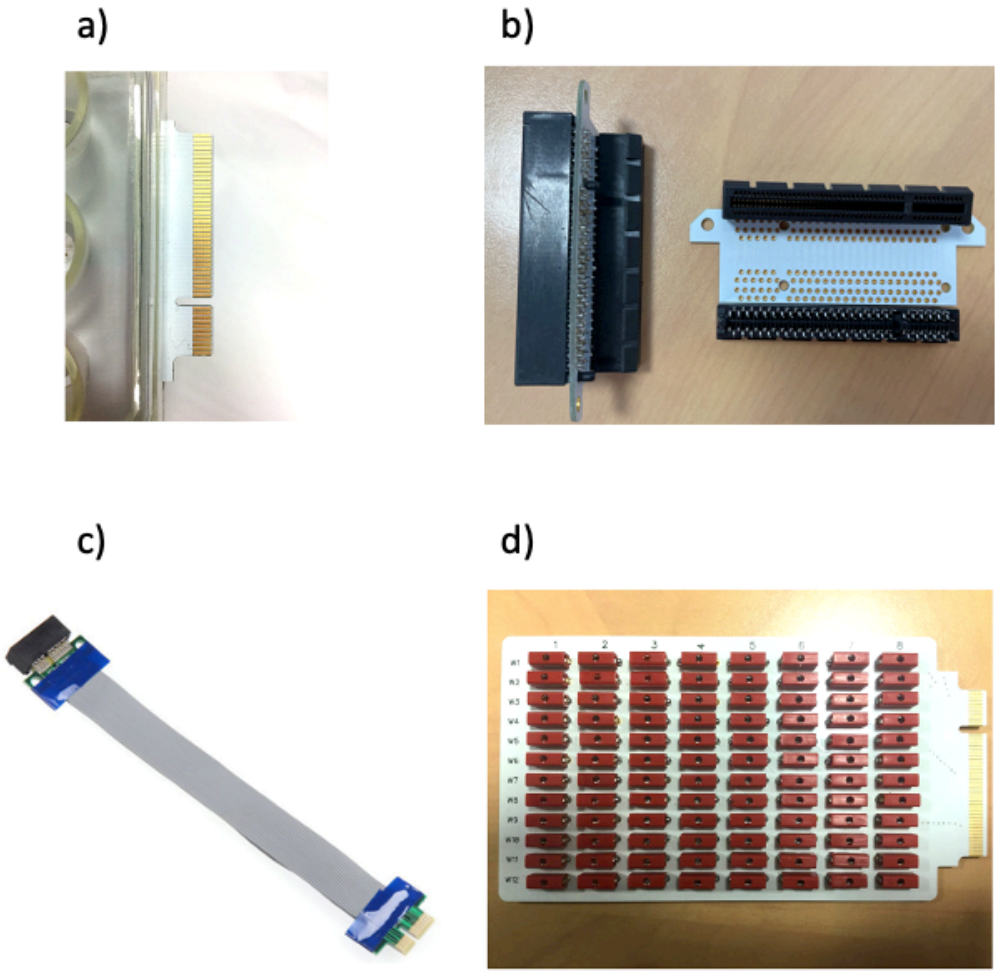

Figure 19: Connector and PCB card design for data extraction from biological equipment. a) is is showing the PCB n°1 PCI connectors chosen to gather all the conductive tracks from the MEA chips to the PCB n°2. b) displays PCB n°3, reorganizing the wells slots and pads from the chips in rows and column.

2.2.4 OMEAs design and fabrication protocol

The first OMEAs design integrated a choice of electrodes, OECTs or both at simultaneously in a single chip. They were made using glass slides as an easy and affordable substrate. The fabrication protocol used is based on the organic etching technique, which is more suited for the microfabrication industrialization. The conductive tracks were made of gold deposited via thermal deposition and patterned through lift-off technique. PaC deposited via CVD encapsulates the device. Organic material was patterned through holes made in the PaC. To do so, a patterned photoresist was used as a hard mask for the etching technique. Then, the organic material was spin coated on the device and patterned using etching technics over specified photoresist. The fabrication protocol will be detailed in chapter 3. Different patterns were designed depending on the biological experiment to be studied: action potential detection, lipids bilayer formation and MDCK II barrier growth and disruption. Electrodes of 10, 25, 50 and 100 micrometers were designed. Figure 20 shows different designs of electrodes and OECTs chip for the smart well plate.

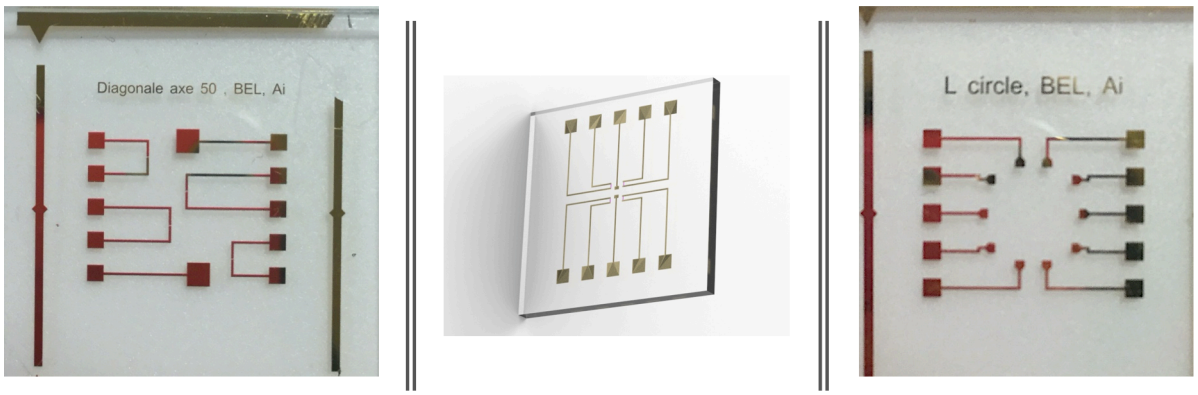

Figure 20: Different design of electrodes and OECTs for the chips. Multiple spacing and sizes of electrodes and OECTs were elaborated in order to fit different types of biological experimentations.

2.3 Assembly

2.3.1 Electrical connection

The first attempt to create electrical connections between the PCB and the OMEAs was to use copper tape. It would be easily cut with laser but challenging to put in place precisely. The second attempt involved silver paste deposition by hand using a needle to drop the material on the PCB pads. This technique failed due to the gap existing on the PCB gold pads (500um), avoiding nanoparticles to form proper electrical contact.

The final solution adopted to create the electrical continuity between the PCB and OMEAs was obtained through a combination of adequate anisotropic conductive paste (ACP) and a semi-automated bonding machine. This technique allowed constant deposition of ACP material, reproducible and precise alignment of the OMEAs and PCB's connection pad

2.3.2 Sealing and biocompatibility (PDMS)

To prevent potential leakage of media or any other liquid from the wells, we have used PDMS as sealing material. The deposition was made manually on the bottom ring of the glass well and centered on the PCB holes. While hardening on top of a hot plate at 80°C for two hours, the polymer glides into the PCB hole, reaching the OMEAs close surface and performs adequate sealing. It also provides biocompatibility, and the joint prevents the biological matter from being in contact with the toxic material from the PCB. This material can also undergo autoclaving and ethanol sterilization mainly used in *in vitro* experiments. Its curing and thermal range of applications are also compatible with the PCB and OMEAs material and do not degrade any of the assembled components. PDMS is also perfectly compatible with biological experimental protocols, and widely used in microfluidic systems[21], 3D structures for pressure sensors[22], cell restrictive environment[23] and more generally for lab-on-chip devices[24–27] .

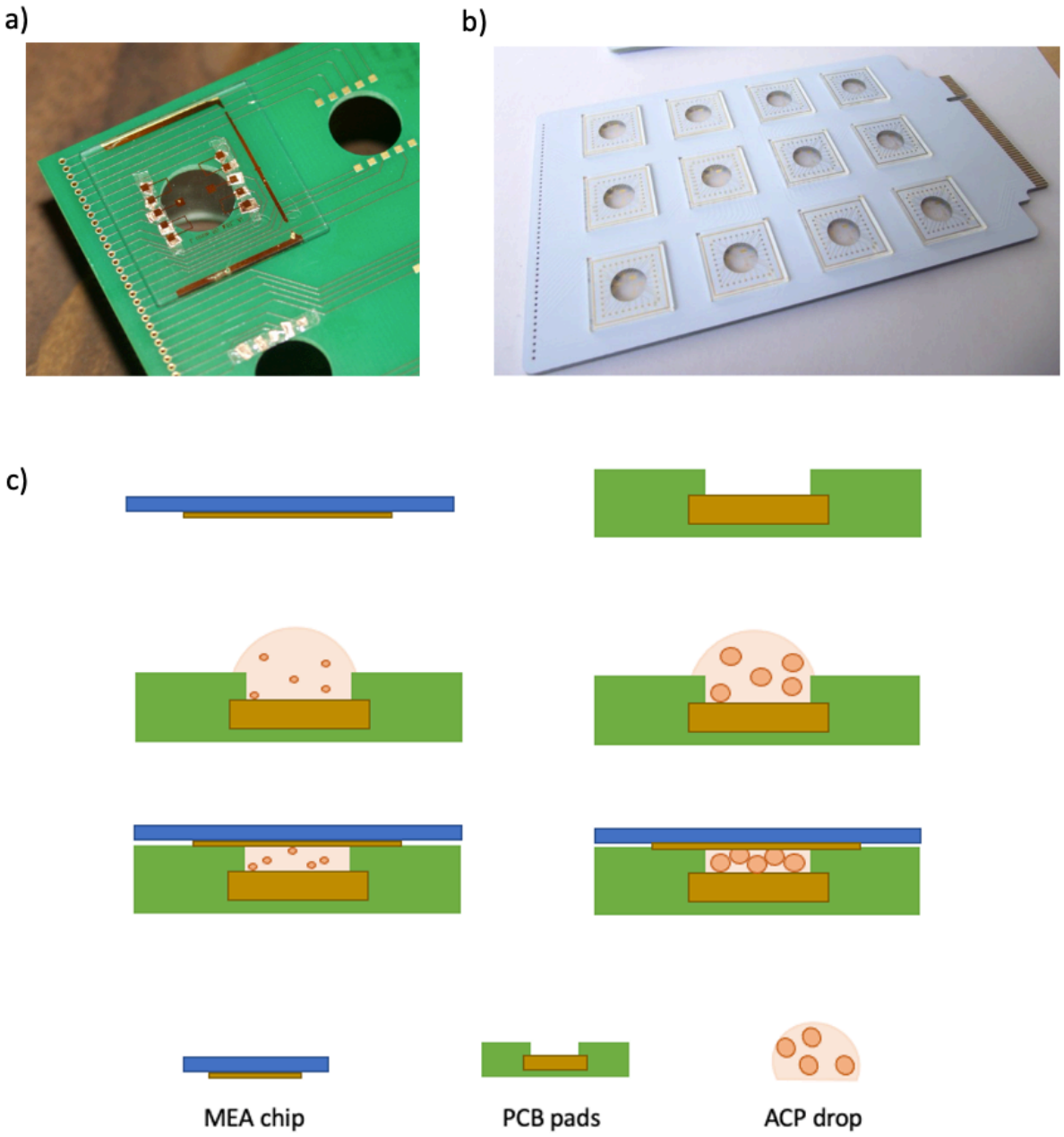

Figure 21: MEAs chips electrical connection to the PCB. a) Pictures of the different attempts to electrically bond the chips and the PCB pads together. Silver paste and copper scotch tape were tries as seen in a) but has poor electrical conductivity. Indeed, the topology of the connective pads of the PCB doesn't allow these technical solutions as the gap from the pads is too deep as seen on b). c) Final solution adopted using ACP and a bonding machine was successful. 14 Ohms resistance maximum was measured using a multimeter between an electrode on the MEA chips to the PCI slot corresponding

2.3.3 Electronic hardware and set up

Compatibility with an optical microscope was a key aspect during the design of the platform, as the plate should be able to fit onto the stage of a standard microscope as seen Figure 24 a) b) c). We developed a specific holder fitted to the plateau of the microscope depicted in Figure 22. This holder had three main objectives:

- Maintaining the 12-well plate assembly inside the microscope and placing the OMEAs at focus length of the bottom lens
- Integrating the functional PCB inside the holder and allowing the flat cables to connect at its extremity in a stable way
- Enabling easy exchanges between different 12 well plates once the measurement done.

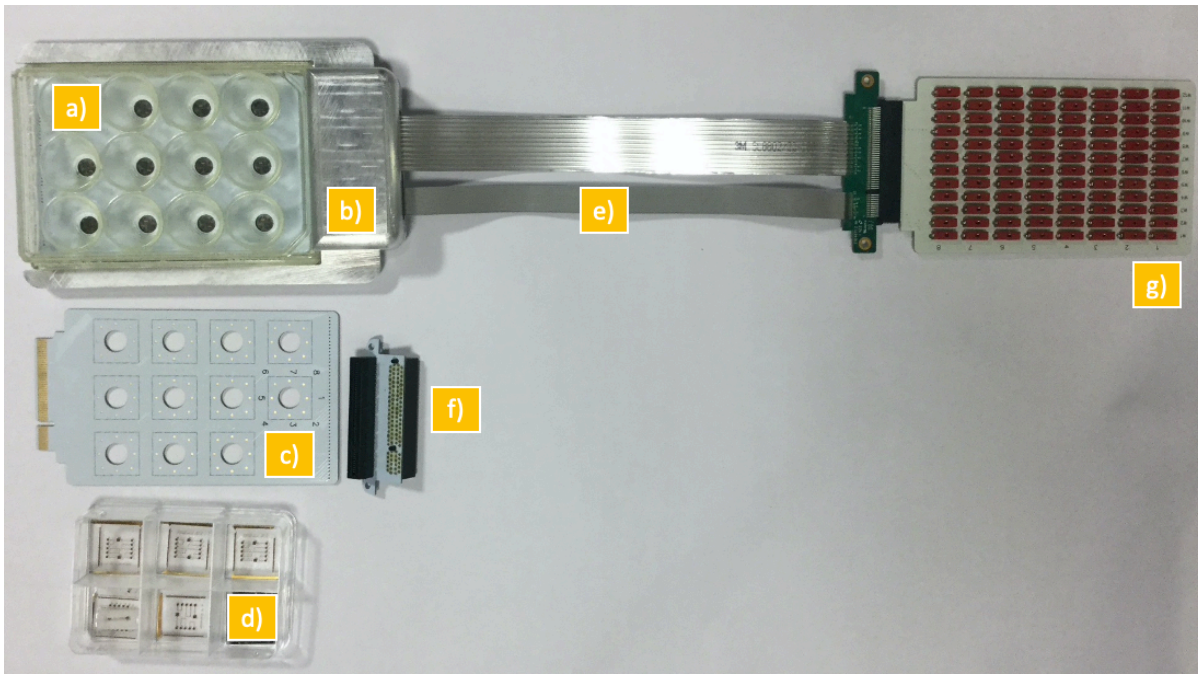

Figure 22: assembly of the several pieces of the smart well plate. a) is the smart well plate pieces assembled together onto the holder b) . The PCB n°1, c) and its MEAs chips d) are exposed separately. H) displays the PCB n°2 and its PCI slot assembled inside the holder. e) is the flat PCI express gathering the information from the PCB n°1 to the PCB n°3 g).

A prototype made of aluminum was extruded and assembled with the functional PCB and the PCI connectors. Flat wires extract the data from the 12 well plate within the microscope to the third banana connectors PCB as shown in Figure 23.

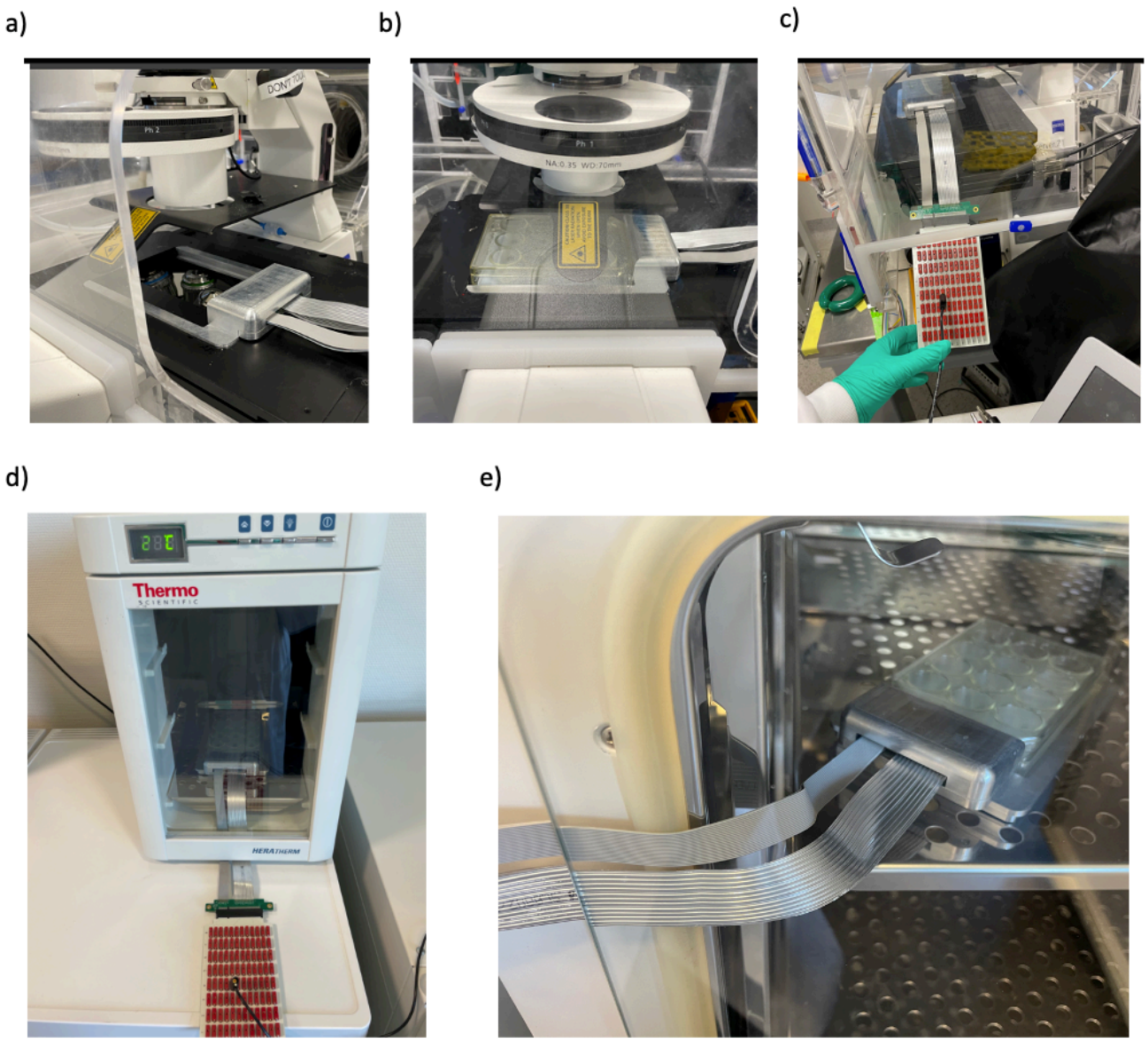

Figure 23: Smart well plates in use. The Holder is fitting inside the microscope plates as shown in a). The smart well plate is then inserted inside the holder b) and the focus is made on the MEA chips beneath. Finally, the data are gathered in the PCB n°3 outside the microscope thanks to the flat cables.

Biological experiment and dynamic/real time monitoring often imply incubation in physiological conditions (5% CO_2, temperature at 37°C) for days. The 12-well plate instrument can also be used without the holder and placed into an incubator (Figure 23 d) and c)), connected to the flat wire directly to the banana PCB, linked to the NI system.

2.4 Conclusions

A smart 12 well plate integrating MEAs was developed. Electrical conductivity from the MEAs to the third “banana” PCB was shown to be effective as resistivity recorded from a multimer indicated approximatively 30 ohms of resistivity. The tool can be used both inside microscopes, incubators, and biological hoods as show in Figure 24. By maintaining transparency and multi-channels recording, this equipment could allow simultaneous electrical and optical monitoring.

a)

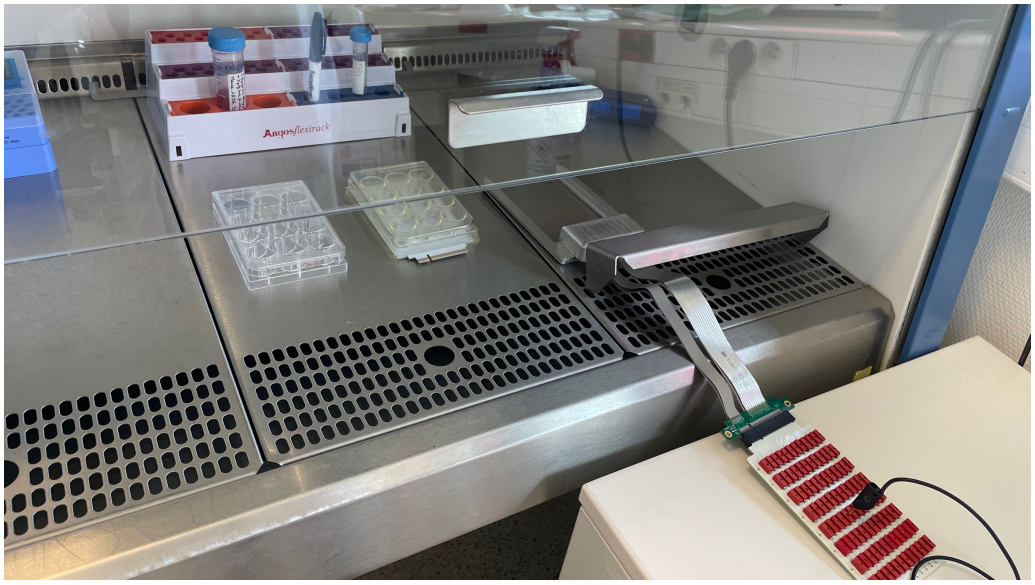

d)

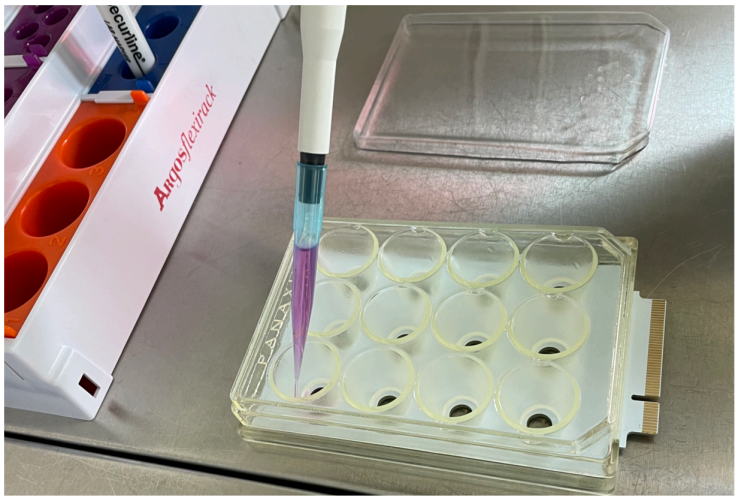

e)

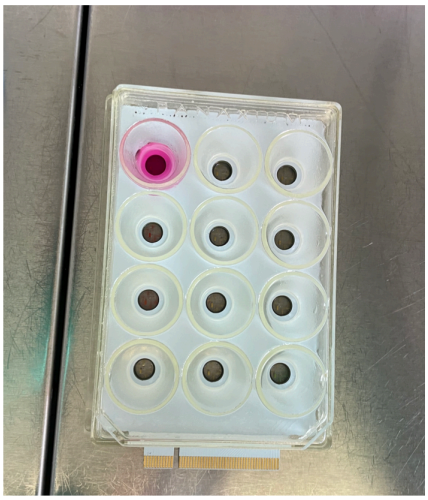

Figure 24: Smart well plate system in use for experiment inside a biological hood. a) The smart well plate, alongside its holder, are placed inside the cabinet. A flat wire connects the inside part of the system to the outer part of the hood to a plugging PCB. d) and e) shows media poured into a well. the transparency of the system allows to visually monitor the media colors.

Unfortunately, the plastic used to prototype the 12 wells would not offer sterilization in an autoclave with a temperature of 110°C. Autoclaving devices at this temperature are often mandatory when experimenting with extremely sensitive cells. Plastic deformation would occur during the sterilization program and deform the structure. As such, the device could not be used for most of the biological applications carried in the laboratory. The cost of a biocompatible, transparent and autoclavable material was too high to be considered. To finalize this part of the project, further modifications are investigated:

1. Use of a different polymer for the cell restrictive environment. Some polymers used as dental prosthetics are now available and more affordable. They are transparent and fully biocompatible. Only autoclaving sterilization would still not be an option as those polymers melting point are below 120°C.

2. Investigation of a different manufacturing processes for cell restrictive / biological container than additive manufacturing. Plastic injection could allow a wider choice of biocompatible and transparent material, with a higher melting temperature. By doing so, a completely new prototype design would have to be created, as this technique requires a mold for injections, and some angles and shape would not fit the fluidic mechanics of the injection

3. As PDMS can be removed from the different parts of the smart 12 well plate, a solution to remove MEAs and their electronic paste from the PCB should be reflected on. The idea of a reusable set up to reduce cost and environmental impact would greatly advantage the tool industrialization

4. To completely free the smart well plate from any bulky cable wiring, a wireless antenna could be implemented on the PCB or on the holder. This would further enhance the user-friendly use of the tool.

Bibliography

1. Edmondson, R., Broglie, J. J., Adcock, A. F. & Yang, L. Three-dimensional cell culture systems and their applications in drug discovery and cell-based biosensors. *Assay Drug Dev. Technol.* **12**, 207–218 (2014).

2. Pampaloni, F., Reynaud, E. G. & Stelzer, E. H. K. The third dimension bridges the gap between cell culture and live tissue. *Nat. Rev. Mol. Cell Biol.* **8**, 839–845 (2007).

3. Schmitz, A., Fischer, S. C., Mattheyer, C., Pampaloni, F. & Stelzer, E. H. K. Multiscale image analysis reveals structural heterogeneity of the cell microenvironment in homotypic spheroids. *Sci. Rep.* **7**, 1–13 (2017).

4. Country, B., States, U. & Kingdom, U. Global Bio Electronics Market. (2022).

5. Roots Analysis. 3D Cell Culture Market, 2015 - 2025. 1–241 (2015).

6. Indu, A. N. *et al.* The Neurodevice 2013 Report. (2013).

7. Walker, G. M. *et al.* A Framework for BIOELECTRONICS Discovery and Innovation. *Natl. Inst. Stand. Technol.* 1–38 (2009).

8. Horvath, P. *et al.* Screening out irrelevant cell-based models of disease. *Nat. Rev. Drug Discov.* **15**, 751–769 (2016).

9. Khodagholy, D. *et al.* In vivo recordings of brain activity using organic transistors. *Nat. Commun.* **4**, (2013).

10. Rivnay, J. *et al.* High-performance transistors for bioelectronics through tuning of channel thickness. *Sci. Adv.* **1**, 1–6 (2015).

11. Rivnay, J. *et al.* Organic electrochemical transistors with maximum transconductance at zero gate bias. *Adv. Mater.* **25**, 7010–7014 (2013).

12. Khodagholy, D. *et al.* NeuroGrid: Recording action potentials from the surface of the brain. *Nat. Neurosci.* **18**, 310–315 (2015).

13. Jimison, L. H. *et al.* Measurement of barrier tissue integrity with an organic electrochemical transistor. *Adv. Mater.* **24**, 5919–5923 (2012).

14. Braendlein, M. *et al.* Lactate Detection in Tumor Cell Cultures Using Organic Transistor

Circuits. *Adv. Mater.* **29**, (2017).

15. Uguz, I. *et al.* Autoclave Sterilization of PEDOT:PSS Electrophysiology Devices. *Adv. Healthc. Mater.* **5**, 3094–3098 (2016).

16. Pas, J. *et al.* Neurospheres on Patterned PEDOT:PSS Microelectrode Arrays Enhance Electrophysiology Recordings. *Adv. Biosyst.* **2**, (2018).

17. Curto, V. F. *et al.* Organic transistor platform with integrated microfluidics for in-line multi-parametric *in vitro* cell monitoring. *Microsystems Nanoeng.* **3**, 1–12 (2017).

18. Curto, V. F., Ferro, M. P., Mariani, F., Scavetta, E. & Owens, R. M. A planar impedance sensor for 3D spheroids. *Lab Chip* **18**, 933–943 (2018).

19. Ferro, M. (12) United States Patent. **2**, (2016).

20. Rutledge, S. A. & Helmy, A. S. Etch-free patterning of poly(3,4-ethylenedioxythiophene)-poly(styrenesulfonate) for optoelectronics. *ACS Appl. Mater. Interfaces* **7**, 3940–3948 (2015).

21. Zhang, L. *et al.* Parylene C-mediated-PDMS: An approach for functionalization of PDMS microfluidic devices. *17th Int. Conf. Miniaturized Syst. Chem. Life Sci. MicroTAS 2013* **3**, 1427–1429 (2013).

22. Kou, H. *et al.* Wireless wide-range pressure sensor based on graphene/PDMS sponge for tactile monitoring. *Sci. Rep.* **9**, 1–7 (2019).

23. Antfolk, M. & Jensen, K. B. A bioengineering perspective on modelling the intestinal epithelial physiology *in vitro*. *Nat. Commun.* **11**, (2020).

24. Sackmann, E. K., Fulton, A. L. & Beebe, D. J. The present and future role of microfluidics in biomedical research. *Nature* **507**, 181–189 (2014).

25. Bhatia, S. N. & Ingber, D. E. Microfluidic organs-on-chips. *Nat. Biotechnol.* **32**, 760–772 (2014).

26. Zhang, B., Korolj, A., Lai, B. F. L. & Radisic, M. Advances in organ-on-a-chip engineering. *Nat. Rev. Mater.* **3**, 257–278 (2018).

27. Comina, G., Suska, A. & Filippini, D. PDMS lab-on-a-chip fabrication using 3D printed

templates. *Lab Chip* **14**, 424–430 (2014).

Chapter 3
Microfabrication and design for Organic electrochemical transistors

Introduction

Merging electronics and biology

The transistor is a semi-conducting device used in electronic systems[1]. It enables modulation of signals when used as a switch, or can be used as an amplifier[2]. Developed in 1947 at Bell laboratories, the transistor has been widely used as an essential electronic component in the evolution of communication[3] and computing systems[4]. During the last decades, coupling electronic devices with medicine[5] paved the way for innovative diagnostics and therapies for medical applications. The field of bioelectronic based on electrophysiology provides new methods and monitoring for biological studies[6]. The Organic electrochemical transistor (OECT) is an alternative for electrodes, broadly used in medical studies, as described in chapter 1. Using the transistor function of amplification makes the OECT the perfect candidate to monitor biological events. Initially developed by Mark Wrightson's group in the 80's[7], the OECT is a three-terminal system (drain, source, gate). A semi-conductor or a conductor made from a conjugated polymer is used as the channel and connects the source and drain. The whole system is immersed in an electrolyte, where the gate regulates the drain current by doping or de-doping the polymer. OECTs have been used in many broad applications for *in vitro* and *in vivo* experiment[8,9]. From detection of analytes[10,11] (glucose, lactate sensing), to neuron action potential recording[12] and epithelial cell membrane integrity[13]. As briefly described in Chapters 2, OECTs designs may vary in number, spacing, size, and sometimes shape[14]. Nevertheless, the recording method and hardware remain identical.

3.1 OECTs electronic structure & matrix configuration

In previous OECTs designs, each transistor was individually monitored, and their recording was performed one after the other. Some biological events can occur simultaneously in multiple areas. Data recorded with individually monitored OECTs, one at a time, aren't representative of the biological events recorded. The detection of biomarkers is often missed, or the signal spreads too fast to be tracked. For example, reporting epileptiform activities such as seizure[15], or tissue barrier disruption[16], requires real-time monitoring on several locations.

To achieve an optimum electrophysiological recording, the sensitive area should be dense and filled with multiple OECTs, all of them recording simultaneously. Unfortunately, the electrical connections and the hardware system required to perform such measurements are heavy and unhandy.

To record from a single OECT, three contactors and three cables are necessary. One for source, drain, and the gate. For n OECTs individually monitored, the number of contact and cables is n × 3. The numerous wires, pogo-pins, contactors, and NI system coupling create a messy and bulky environment. This limits the number of OECTs that can be recorded from. To overcome those limitations, a passive matrix circuitry type is considered, as described in Figure 25.

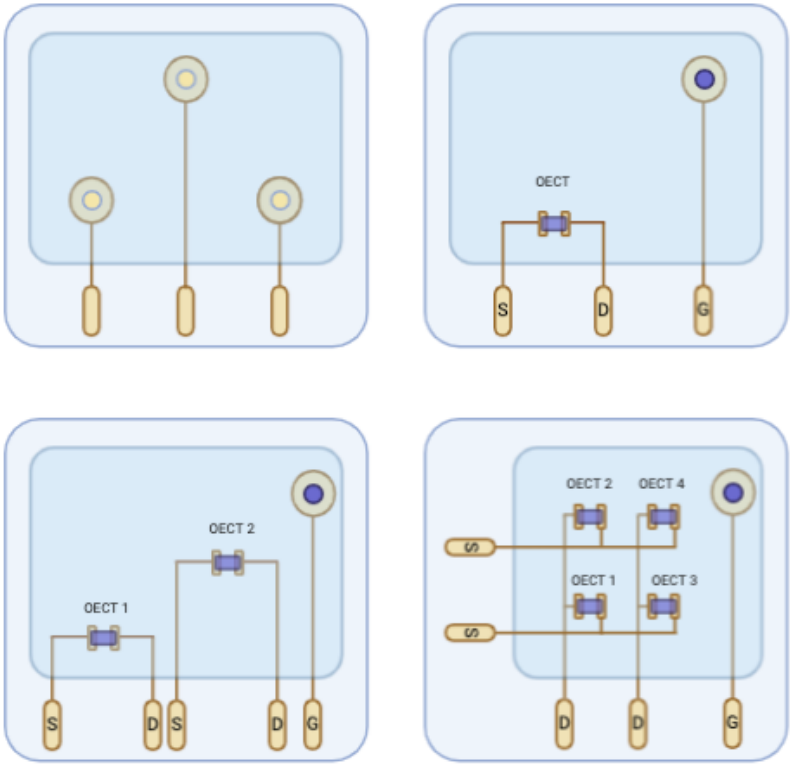

Figure 25: Design sketches for connection pads. The number of contactors required is shown for multiple electrodes and transistors individually monitored. The matrix design circuitry decreases the number of pads required.

In mathematics, a matrix refers to an arrangement in rows and columns of elements. In electronic circuitry, it indicates a method to arrange and control different components. Matrix circuitry, also referred to as gate arrays for transistors[17], arose during the computer era as a mean to enhance Complementary Metal Oxide semiconductor (CMOS) architecture. By organizing the electrical components, the commands efficiency and their energy consuming is optimized. The development of LED displays for screens has accelerated the integration of organic materials in electronic[18] (passive matrix display of organic LEDs). Its translation to the field of bioelectronics came alongside photovoltaic technology rising in the late 20's. Many approaches in the bioelectronic field have reached functional passive and active matrices devices[19],[20]. In the case of a passive matrix configuration, each transistor is controlled by an intersection of row and column in the matrix grid. An active-matrix display includes a capacitor prior to the component targeted. It allows to switch transistors much more rapidly.

An arrangement of rows and columns composes the OECTS matrix, organizing each source and drain of the transistors. In this regard, the design reduces the number of conductive lines and pins for connections. It leads to an increase in the density of recording sites and enables fast multiplexing. Coupled with a simple clocking Arduino system, automatic scanning of the area is possible, following the transistor's speed capacity. The final assembly would then reduce the complexity of the hardware of the experiment.

As a first step, a passive type of matrix is investigated to validate the project interests. I have designed a preliminary test device to calibrate the fabrication protocol and validate the stacking part in the matrix display. I have characterized and optimized every microfabrication steps prior to the design of a matrix of 16 OECTs + electrode device. In parallel, I have initiated the optimization of the fabrication protocol using Orthogonal Inc specific resists. Several steps were replaced or modified to enhance and facilitate device productions to translate the research protocols into an industrial one. In this chapter, I will describe in the first section the different implementations and attempts in the fabrication protocols. Then, I will detail the OECTs matrix development through test structures and firsts designs. Finally, the matrix OECTs characterization will conclude on the efficiency of the design.

3.2 Microfabrication protocols optimization

In collaboration with Orthogonal Inc, I have investigated new photolithographic products and techniques to improve and industrialize the fabrication protocol. Optimization attempts based upon the BEL protocol (in supplementary figures) have been made for the double layer resist for lift-off techniques, the dielectric resist patterning for insulation, and the organic friendly resist for etching sensitive material. Indeed, their chemical products are fluorinated (containing fluorine). There are of interest since as fluorosolvents and fluoropolymers, they are non-reactive and non-contaminating for our organic materials. Their chemical stability is improved: they are inert to other material compound by integrating a fluor atom in their chemical structure. This is of interest when looking for industrial protocols to process PEDOT:PSS patterning and other sensitive materials.

Going through the list of Orthogonal Inc photoresists, I will first explain the attempts to improve the metal lift-off step by studying **SL1, Neg1** double layer, and the e-beam deposition tool. Then, I will develop our first protocol using **OSCOR 5001** to pattern PEDOT:PSS via etching technique. Finally, I will describe the fabrication step involving the resist **DE1** as our device surface insulator.

Step	BEL Fabrication protocol	Optimizations	Key points
Metal patterning	S1813 lift off	Double stack SL1/Neg1	• Remove residues and sonicating step • Increase undercut to facilitate lift off and remove "ear rabbits"
Metal deposition	Thermal BOC Edward	E-Beam Alliance concept	• Automatize process • Increase directionality of the deposition (anisotropic deposition)
Organic Patterning	PaC sacrificial layer peel-off	Etching over OSCOR 5001 patterned photoresist	• Increase organic patterning definition • Process industrialized
Insulation	PaC	DE1 resist	• Replace PaC insulation • Reduces number of steps for the insulating layer

Table 1: Optimization attempts done from the Bel Protocol

3.2.1 Lift-off technique for Conductive Tracks (CT): SL1 + Neg 1 double stack

An alternative process described in Table 2 for gold lift-off has been investigated. I have developed the double-stack resist protocol. to replace the former **S1813** resist, I have used two different chemical resists from Orthogonal Inc: the **SL1+Neg1**. A double stack is a process involving two types of resists, spin coated one on top of the other: beneath, a non-sensitive to UV light resist, that usually is easily dissolvable to ease the lift of the second resist. The second one on top is photo patternable that define the design features. This allows to create a large and high undercut to improve the lift of the metal deposition. In parallel, it eliminates the need for sonication to completely lift the resist residues from the substrate that could occur during the S1813 step and prevent from "ear rabbits" effect. "Ear rabbits" is the name given by the gold residues formed by deposition of the metal on the resist edges profile. They stuck to the gold lines after lift of the resist and might leads to lines and encapsulation defects.

The double-stack has three main advantages for users:

1. easy lift of the resists thanks to the first layer of SL1.
2. tuning properties according to the feature's sizes and metal thickness. The thickness of the resist layer can be adjusted with the spin coating parameters. By doing so, the shape of the undercut can be perfectly controlled over the different photolithographic step
3. Fluorinated chemicals : Organic friendly

Scanning electronic microscope (SEM) was performed to evaluate the resist patterning step. SEM pictures are shown in Figure 26.

The undercut geometry depends mainly on the dipping time into the development bath. SL1 is a non-UV sensitive resist, spin-coated first on the substrate, and hard-baked. Following this step, the Neg1, a UV-sensitive resist, is also spin-coated over SL1 and soft-baked. The stack is then exposed through the photolithographic technique: the patterns are transposed from the mask to the Neg1 layer. After a first development bath in AZ 300 MIF, the openings are done on the unexposed Neg1 areas that dissolve. Then, the SL1 is dipped into Developer 100 bath, which dissolves the resist through the opening made on Neg1, in an isotropic manner. It is worth noticing that control over SL1 dissolution rate is complex. Creating a controlled

undercut requires precise control in every section of the photolithography step: the thickness of the resist, the temperature and time of the pre and post-baking steps and the development bath. All of those parameters are evolving and changing according to features geometries and sizes. This is challenging to obtain a similar undercut over different feature sizes.

Step	Tool	Parameters
SL1 spincoating	Manual Spin coater	60 sec : 1000 rpm : acc 0
SL1 soft baking	Hot plate	90°C : 1 min
Neg1 spincoating	Manual spin coater	60 sec : 3500 rpm : acc 1
Neg1 soft baking	Hot plate	110°C : 1 min
Photolithography	Photo aligner	UV line 365nm : 70mJ/cm²
Post exposure bake	Hot plate	110°C : 1 min
Development Neg1	Crystallizer bath	1 min in AZ 300 MIF bath then rinse 1 min in water
Development SL1	Wet etcher	Puddle developed SL1 using Developer 100 for 30 seconds, Spray rinsed for 5 seconds during drying spin cycle Repeated Puddle for 10 more seconds with an additional 5 second spray rinse during drying spin cycle

Table 2: resist double stack for easier and fast lift off using Orthogonal SL1 Neg1

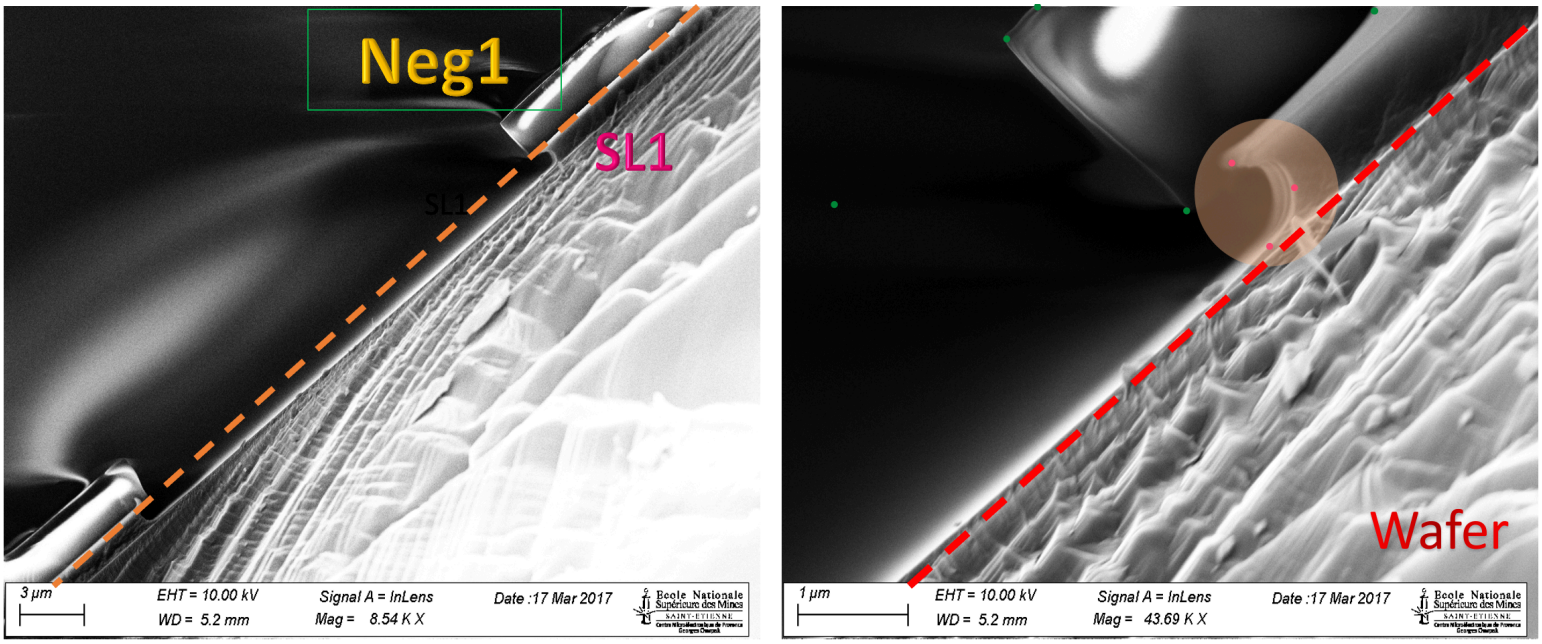

Figure 26. SL1+Neg1 double stack SEM pictures. The resists are separated by the orange line on the left picture. The double layer is resting on a sliced silicon wafer, bounded by the red line on the right picture. From the parameters detailed in the Table 2 , further optimization has been made on the layer thickness to reach higher definition of features. SL1 thickness is 900nm, and the Neg1 is 1.2um thick. The undercut depth reaches 700nm in a U shape as highlighted in the orange disc.

3.2.2 E-beam metal deposition (Gold deposition over Alliance e-beam and BOC Edward)

In the standard fabrication protocol elaborated in the laboratory of BEL, chromium is used as an adhesive layer evaporated between Parylene C and gold. The option of using titanium instead of chromium, which is less biocompatible, was evaluated. The alliance concept tool deposits metal by e-beam and is fully automated. As this machine allows a more directional deposition of materials, it has facilitated the lift-off of metal as resists side walls were not covered. Unfortunately, gold deposition by e-beam was not effective. As depicted in

Figure 27, holes and craters appeared on the surface of the metal and aged poorly. As such, this material type of deposition and tool were not considered any further. Furthermore, as isotropic deposition will be required later for the second layer of metal deposition, e-beam technique was left aside.

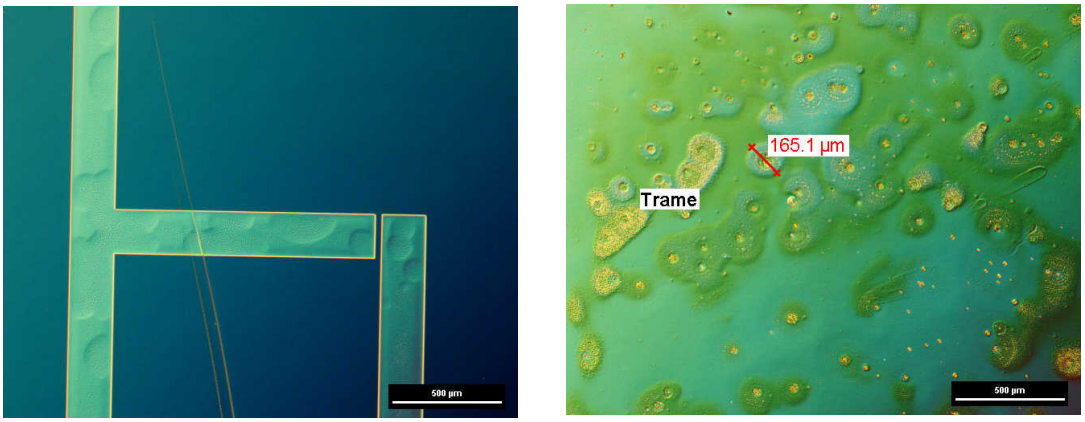

Figure 27. Titanium and gold deposition on PaC after lift-off. Using laser beam to heat the gold to perform sublimation for deposition appeared to be difficult in our equipment. Visible crater on metal appeared as soon as e-beam deposition is done. Aging of the devices deteriorate their appearance.

3.2.3 Etching organic material using OSCOR 5001

The development of organic patterning was based on previous development using Orthogonal Inc resist for etching technique. OSCOR 5001 was investigated in collaboration with the Panaxium team as a mask resist to etch away exceeding organic material. A protocol has been elaborated and results were obtained through etching and patterning over a layer of PEDOT:PSS spin-coated and cured. Table 3 details the fabrication protocol established.

Step	Tool	Parameters
OSCOR 5001 spin coating	Spin coater	35 sec : 1200 rpm : acc 3
OSCOR 5001 soft baking	Hot plate	65°C : 1min
Photolithography	Photo aligner	63mJ/cm²
OSCOR 5001 post exposure bake	Hot plate	90°C : 1min
Development Developer 100	Wet etcher	**2 times**: Puddle DEV 100 and wait 40 sec Then spin at 3000rpm acc2 for 30 sec
Etching	RIE	9.10^5mTorr, 50sccm O2, 5sccm CHF3, 150W, 1 min 30 sec
Stripping 903 stripper	Spin coater	**3 times**: Puddle **Stripper 903** and wait 1min. Then spin at 4000rpm acc:1 for 10sec

Table 3: PEDOT:PSS patterning protocol using etching technique over OSCOR 5001 patterned resist

Excellent features definitions have been obtained, up to 2μm diameter PEDOT:PSS disc. Unfortunately, lifting the resist after the RIE step appeared to be tricky and residues remained on the substrate as seen in Figure 28 c) and d). The stripping required mechanical strength through spin coating. Spraying vigorously over the device could not completely remove the OSCOR 5001 residues from the device.

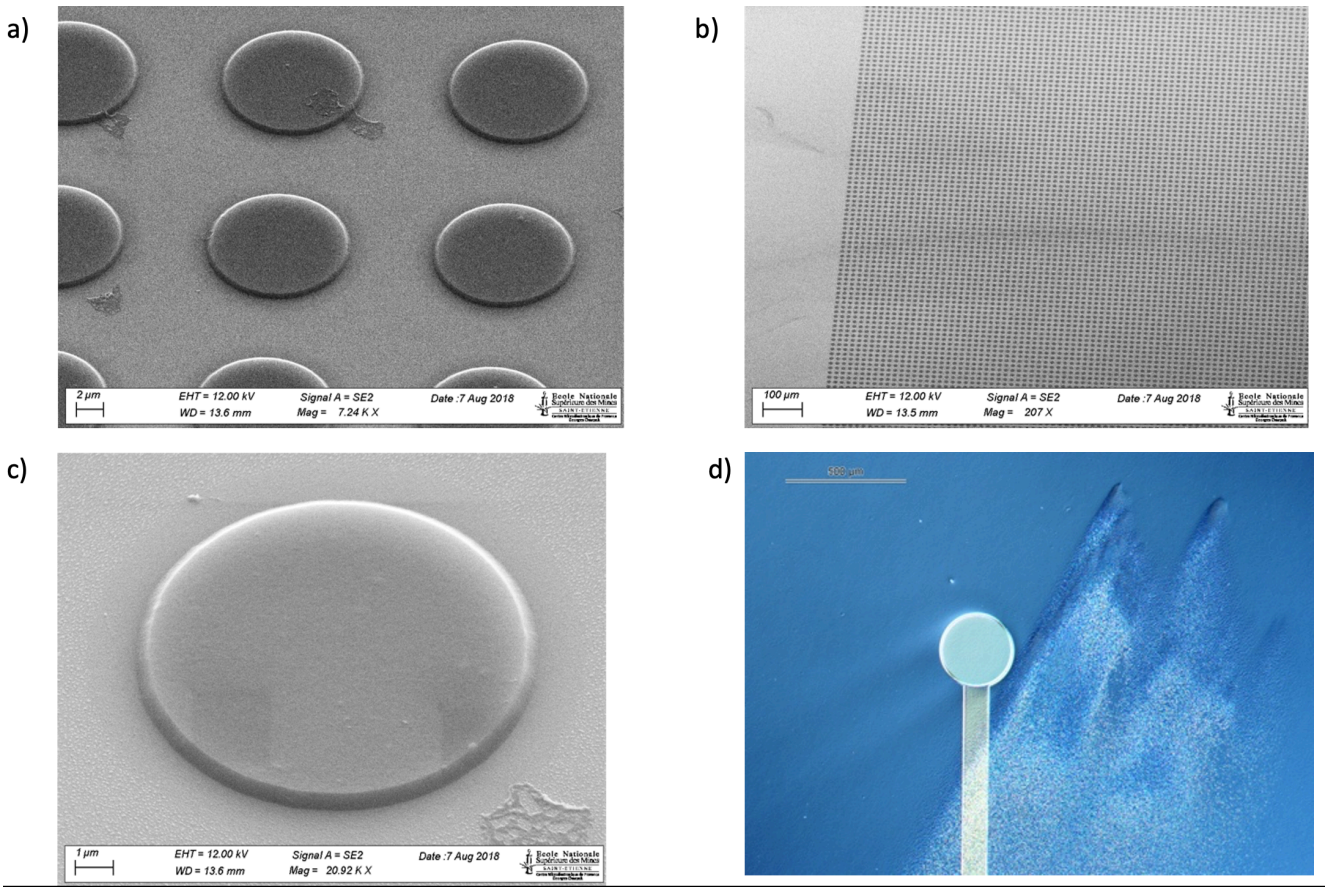

Figure 28: PEDOT:PSS patterning using etching protocol and the OSCOR 5001 resist. a) b) and c) are SEM pictures upon different magnitude and zoom of a same pattern of a 10 μm diam PEDOT:PSS discs. Some residues are remaining. c) and d) show the residues post etching and stripping step.

3.2.4 DE1 encapsulation

In the BEL fabrication protocol, the encapsulation and organic patterning are performed in the same step. Two layers of PaC are deposited on the device, separated by a thin soap layer. The first layer being the encapsulation and the second the sacrificial layer used to pattern the organic material. Photolithography is performed on the stack, and openings are created with RIE etching. Once the organics are spin-coated and hard-baked on the device, the PaC sacrificial layer is peeled off. As such, encapsulation and organic patterning are done. Less time-consuming steps in fabrication were considered to replace the PaC double stack and the peel-off technique. A new resist from Orthogonal Inc, the DE1, was developed as a dielectric layer compatible with organic materials. Its patterning protocol is detailed in Table 4.

Step	Tool	Parameters
DE1 spin coating	Spin coater	60 sec : 2500 rpm : acc 2
DE1 soft baking	Hot plate	1 min 80°C
Photolithography	Photo aligner	120mJ/cm^2
Development Dev 100	Crystallizer Bath	1 min 30 sec 70°C

Table 4: DE1 resist protocol over PEDOT:PSS organic material

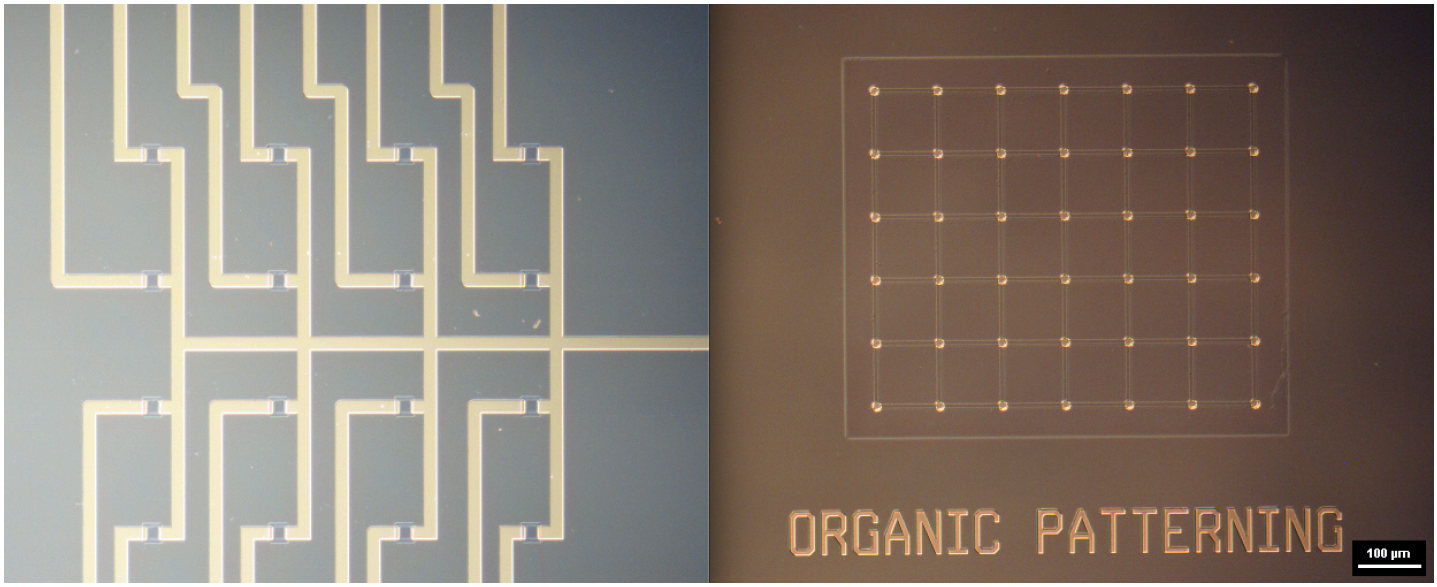

Figure 29: Organic patterning and DE1 encapsulation. On the left, a microscope pictures displays OECTs patterned with the etching process and the insulate with DE1 resist.

3.3 Conclusion and transition to the final fabrication process

Device's designs, a wide range of feature sizes can be drafted: from micrometer to millimeter scale geometries. As such, the double-stack SL1 + Neg1 was replaced by a negative resist: AznLOF2070. Its undercut provides more homogeneity as it is controlled over baking temperature and exposition rate.

Because many issues with our e-beam machine appeared, and as a more isotropic deposition of metal will be preferred (described in this chapter part II), I decided to use the same thermal deposition tool as the BEL protocol: the BOC Edward. It has a smaller chamber and the distance between the devices and the source of metal is short, allowing a more isotropic deposition of the metal.

To overcome the difficulty of resist residues by removing the OSCOR5001, Panaxium fabrication team has integrated a protective layer made of Polyvinyl alcohol (PVA) above the PEDOT:PSS layer. OSCOR 5001 is deposited and patterned on top of the PVA, which is not soluble in the developer of OSCOR 5001. After etching the non-protected PVA/PEDOT:PSS

stack, OSCOR 5001 is stripped and then PVA is stripped in water. This method leads to a much lower contamination of the PEDOT:PSS surface by residues of OSCOR 5001.

Finally, the development team decided to move from the DE1 resist as an insulator to PaC. The reason being that the resist isn't, yet, FDA approved for *in vivo* biocompatibility, where the PaC is. This decision relies on the industrial approach to facilitate the commercialization of devices with material already approved for biocompatibility.

Once the material and steps were set by the fabrication team, I adapted their fabrication protocol to a new multi-layered device design. Extracting each block of the etch process, and putting them back together in a different order, I elaborated a new process. The aim is to obtain a matrix layout to organize OECTs and minimize the contact pads. I have first created a test design to elaborate and control each step of the multi-layer assembly, then moved to a simplified version of an OECT matrix.

3.4 OECT Matrix configuration: Test, design & fabrication process changes

3.4.1 Transposition to our standard fabrication protocol. Details of the microfabrication process adaptation from protocol. Scheme and microscope pictures

When elaborating a protocol in microelectronics, each step is characterized and optimized according to the equipment available. Both characterization and process tools are of importance to achieve functional devices. Furthermore, as the various machines available are used numerous studies and have passed the state of "brand new and perfectly functional", independent variability was to be expected. A manufacturing tolerance must be considered in the protocol. The first challenge is to ensure good conductivity and insulation between the two layers of conductive tracks where it is required. The metal overlaying part shown in Figure 30 will be investigated and described in this section. Indeed, in the matrix circuit, some node of conductive material needs to be connected through the insulation layer. And other nodes need to be perfectly insulated to avoid crosstalk between the lines. Monitoring each step of the protocol is a crucial aspect of structure optimization.

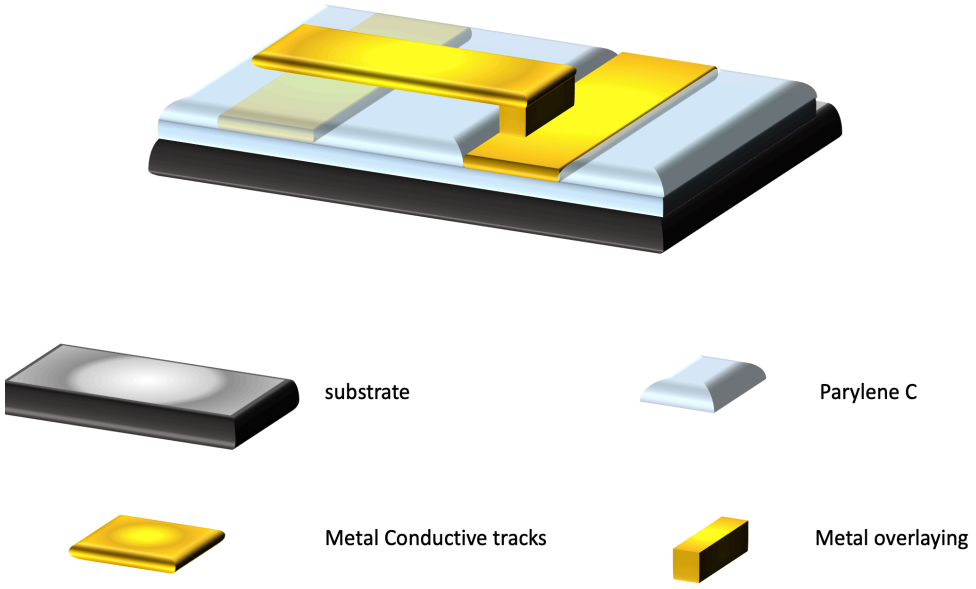

Figure 30. Double layering of metal over Parylene C. Electrical insulation and contact between lines. Metal overlaying critical step during fabrication process

3.4.2 Test Design for transistors and double layering fabrication protocol

To investigate the different structures of the matrix device and their layering, a specific set of masks was designed. The aim is three-fold: optimize the base, the inter insulating and the PaC encapsulating layer. Etching, patterning, and additive layering steps are paramount to the device fabrication protocol. Deposition and patterning of the organic material and the conductive tracks overlaying the PaC steps shown in Figure 30 are investigated in this first test design.

As seen in Figure 31, the design is divided into four distinct parts: left, right, center, and external areas detailed below. These test features allow the characterization of the layers and process step by step. Mechanical profilometry, microscope and optical reflectometry are used to control material thickness and feature sizes. Using such test features allows non-destructive monitoring of the fabrication protocol, avoiding characterization directly in sensitive areas of the device.

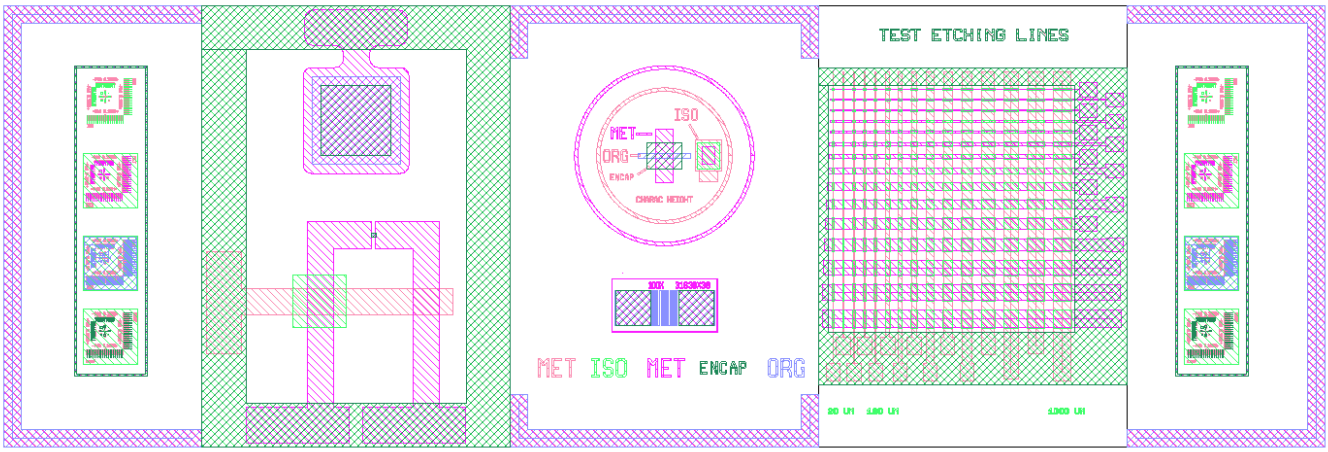

Figure 31: test design for multi layering fabrication protocol. External sections are used to place alignment mark for layer superposition during photolithography steps. The center part contains a circle with test figures to characterize each layers of material, the features definitions, and the material conductivity. Finally, the section. on the left contain a large OECT to test its electrical behavior on a multilayer structure. The right section contains rows and columns of gold layer, with PaC opening in between. It is used to test the etching limits and PaC wall angle minimum to perform a metal overlaying connection.

Transistor test design

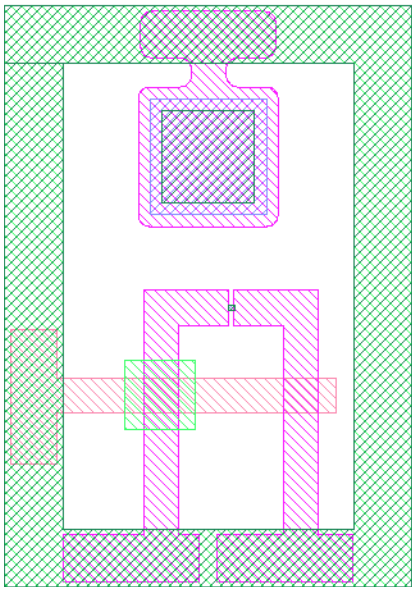

Figure 32. test design OECT matrix

Figure 32 depicts the left part including a millimeter-sized gate, a transistor, and a transversal line crossing the source and drain of the OECT. First, a layer of the Cr/Au, is deposited to create the transversal line. Then, a 450nm PaC insulating layer is deposited and patterned to create a hole over the conductive line. Both drain, source and gate are created on the second layer of metal and coated with an PaC encapsulation layer of 1µm. The second layer of PaC is patterned to obtain the channel and gate opening for the organic material deposition. PEDOT:PSS patterns are obtained using both protocols: the BEL and Etch fabrication processes, for comparative study. This crossing underneath the line serves two purposes: checking the contact or the insulation over two lines separated by the insulating layer of PaC.

Double layering connections and etching features

The right area shown in Figure 33 consists of features to characterize the various etching steps and the feasibility of metal overlays depending on the PaC wall profile. Fifteen conductive lines, ranging from 10 to 1000 μm large from the top layer overstep 15 other similar metallic lines, separated by a patterned layer of PaC with holes to enable contacts. Depending on the size of the patterns and the thickness of the PaC insulating layer, the etching edges profile differs from another. The etching protocol recipe mainly impacts the profile according to those parameters. If the edges are too straight/vertical, the gold deposition from the second metal layer won't create a smooth bond with the first layer (sketch). A minimal angle of 70 degrees is required to perform a bond between the two layers of metals, crossing over the insulating PaC layer.

a)

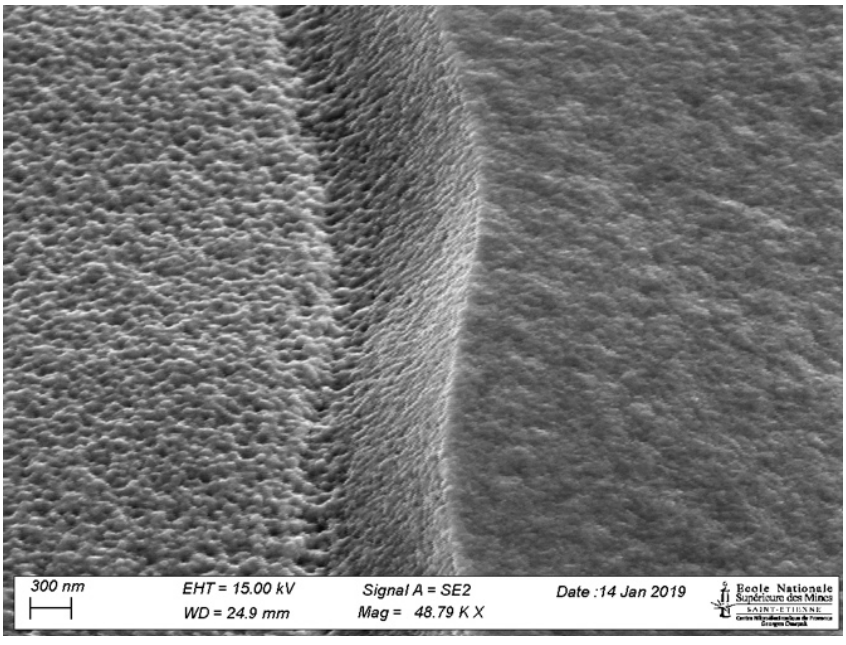

b)

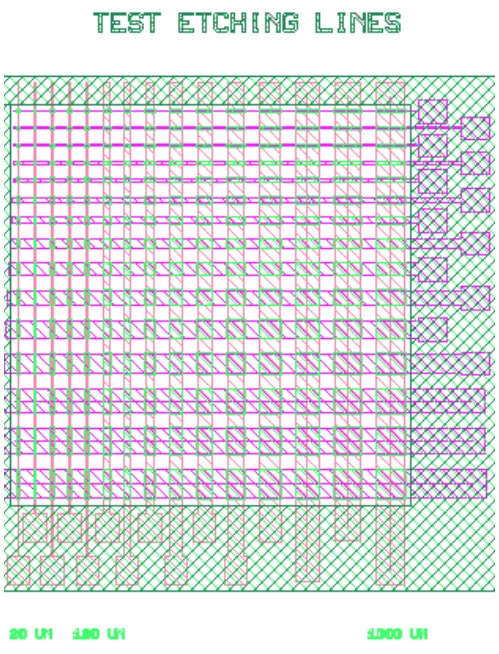

Figure 33. metal overlaying PaC. a) SEM pictures of gold deposition overlaying a Parylene C step. b) test figure used to characterize conductivity of the metal overlay

Fabrication steps controls

In process characterization and alignment mark

The last parts, center + external are illustrated in Figure 34, and include specific test structures, allowing some characterization tests during the fabrication process. Thickness, conductivity of the different materials, and design / geometric tolerances of patterns. Alignment marks are found on the external part in the form of two verniers. The Verniers are specific structures used to precisely align a mask during photolithography exposure step over previous structures patterned on the substrate.

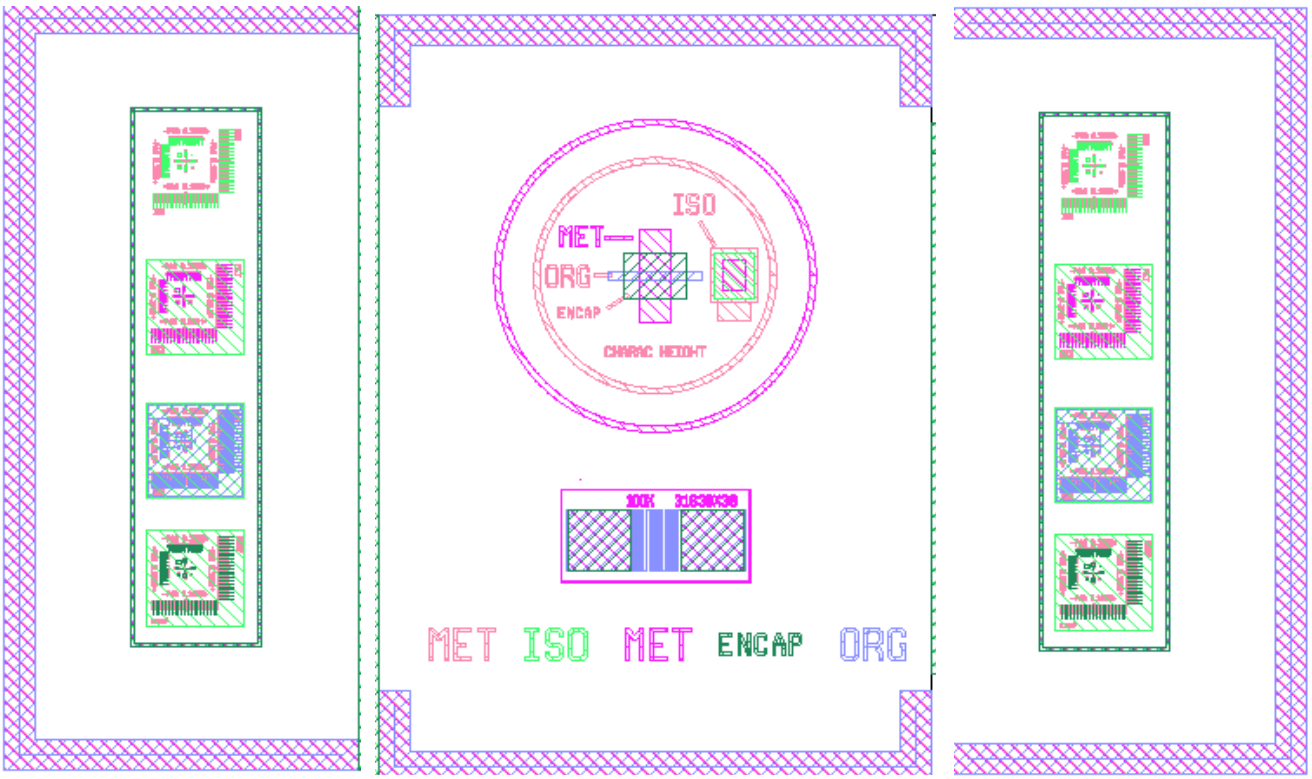

Figure 34.. External and center parts of the test design for matrix devices. The Serpentine for the organic conductivity measurement

Characterization of each fabrication step is an essential key to obtain reproducibility between each single device and in between batches. As the machine used has inconstant behavior, modifications in the design were done: line resistivity and thickness are measured using the circle figure at the center of the design. For a bigger device than a glass slide, this type of figure should also be added at the extremity of the design to extract average values of characterization all over the device.

Step 1: Conductive Track metal deposition.

Thickness and critical dimension are measured with the MET Figure 35 using a mechanical profilometer and a calibrated microscope. The thickness obtained during the first metal deposition is around 150nm for the chromium and gold, 5 nm of chromium and 145nm of gold. The target is centered on the design and is used as a base for future characterization test figures.

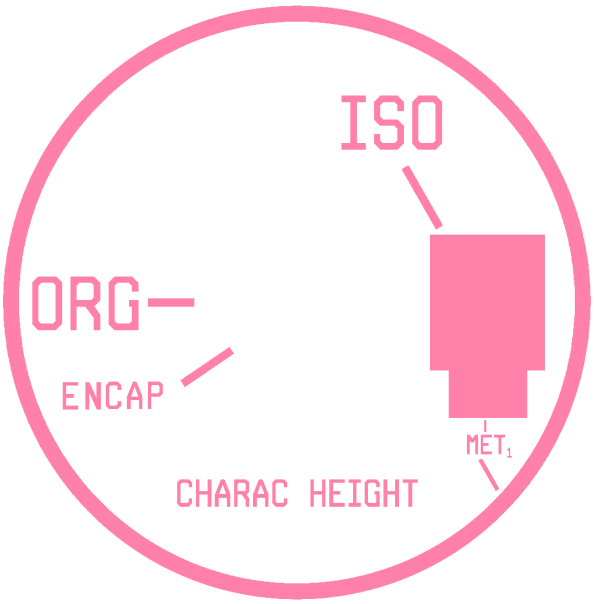

Figure 35. first layer of target test figures

Step 2: the insulating layer deposition and patterning.

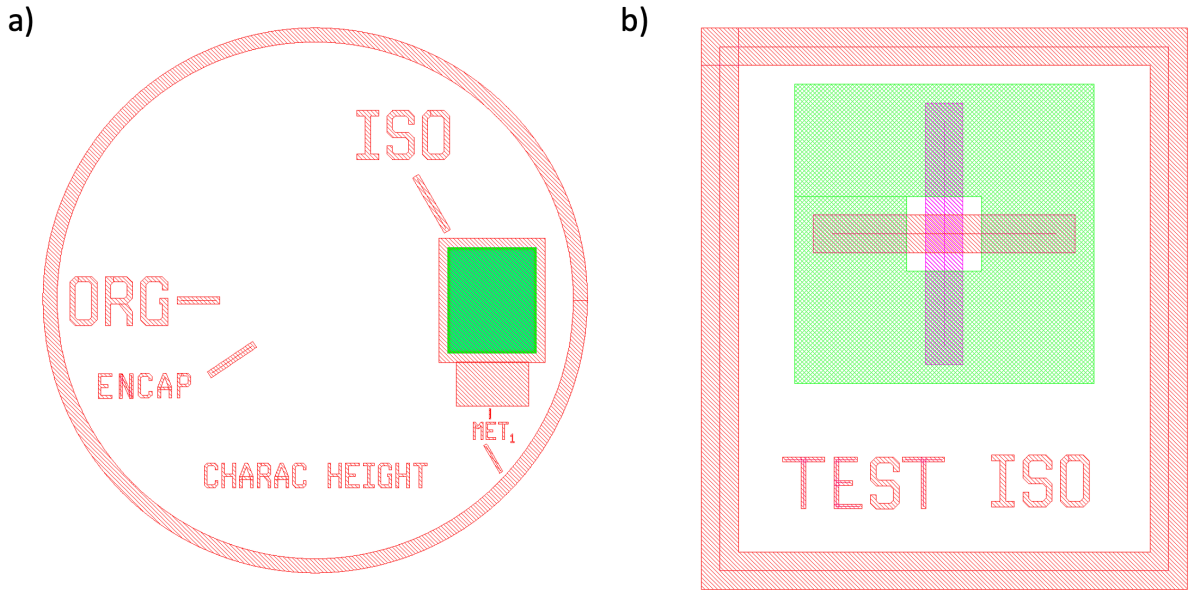

Figure 36. a) Central target for PaC insulation patterning. b) test figure for insulation patterning between two metal deposition and for overlaying metal conductivity

Figure 36 a) shows the central target with opening features for the insulating PaC layer. It is measured using a mechanical profilometer. The green areas represent where the PaC is etched. Its thickness is approximately 500 nm.

A multimeter is used for conductivity control at the center of the square. If the resistivity is 0 Ohm, then the PaC has been correctly etched. Figure 36 b) represent the test design for insulation of PaC control and the overlaying metal conductivity measure. A multimeter is used to monitor resistivity in between two extended metal lines. When connecting one extremity of the first horizontal metal line to the second vertical layer of metal, no conductivity should be observed, owing to the PaC square separation. Then, by connecting the second vertical metal layer with the vertical line, conductivity should be recorded. This shows that the second metal deposition overlay the PaC encapsulating square and provide good electrical contact between the CT.

The last two fabrication steps of metal and parylene deposition are repeated once more, the same characterization is done once more, but over the ENCAP and MET figure. Representing the second PaC layer deposition and the last metal patterning represented in Figure 37

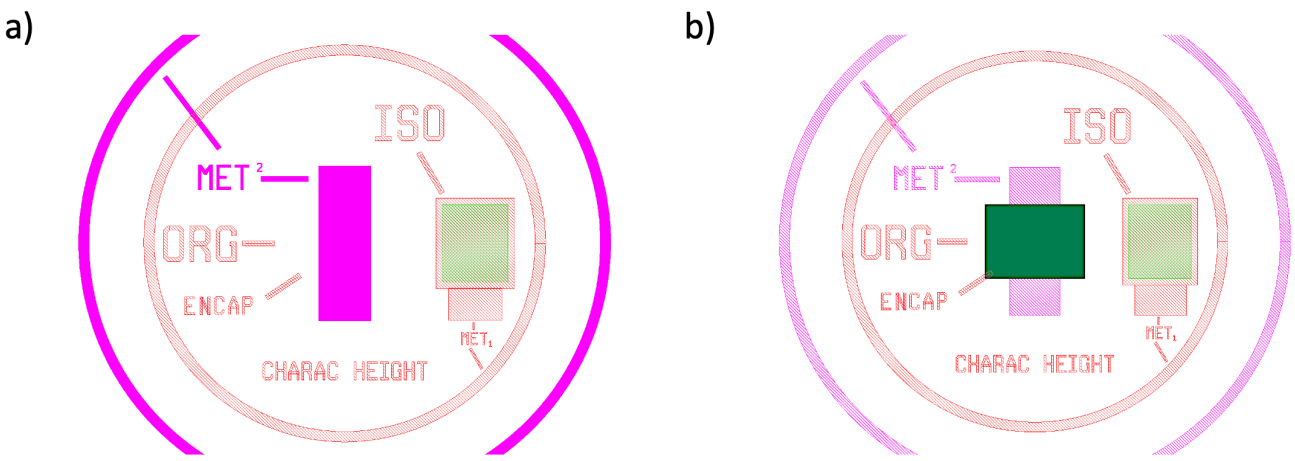

Figure 37. Central target. a) deposition of the second metal layer. Designed are depicted in purple color. b) Opening of the second layer of PaC test figure. The light and dark green rectangle represent PaC step features

Step 3: the organic material deposition and characterization

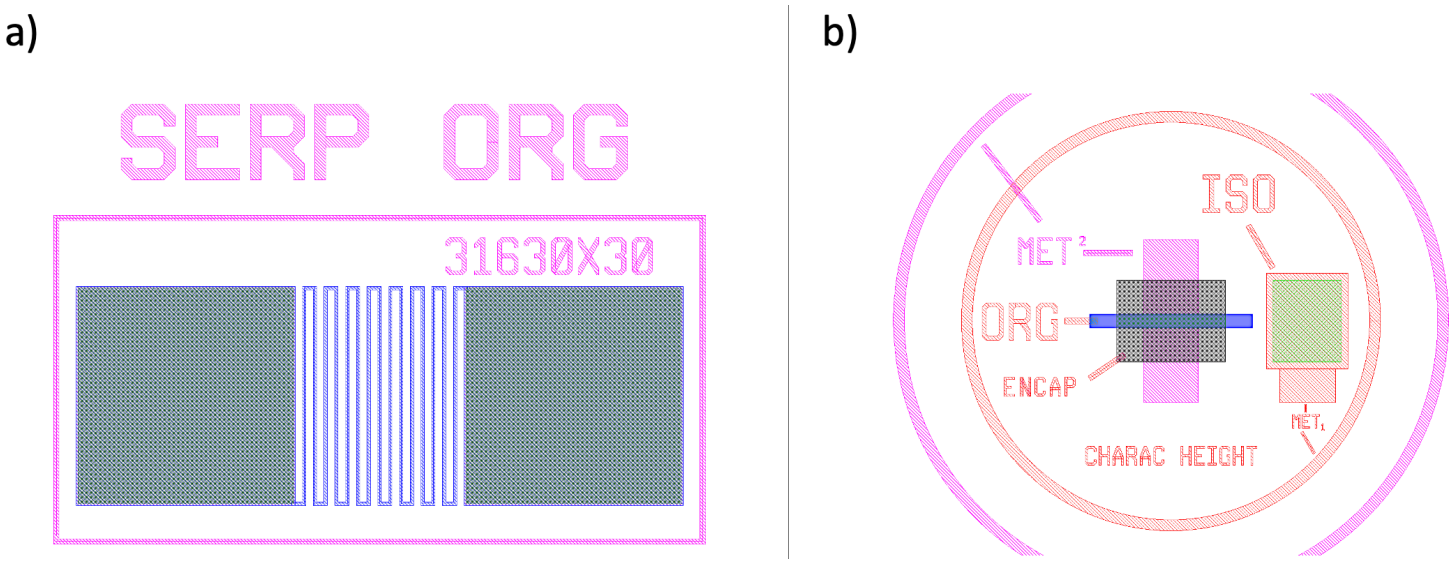

Figure 38. a) Serpentine used to characterize the organic material conductivity. The conductivity of the material is estimated using a multimeter and the formula of line resistivity. b) central target with the Organic material feature step in navy blue. The rectangle represents the area where the PEDOT:PSS will remain on the device.

Figure 38 a) shows the serpentine used to measure the conductivity of the organic material at the end of the fabrication process. By applying a voltage in between the two square pads, resistivity is extracted using a Keithley source. Then the organic material line conductivity is calculated by Ohm's law $U = RI$. The ORG structure on the central target in b) allows thickness measurement of the PEDOT:PSS deposition over the gold metallic layer number 2.

3.4.3 Test design conclusion

As a result of the design test batch, three parameters were validated.

1. The Pac insulation layer should be as thin as possible. It must allow contact between the two metallic layers but also ensure good insulation over the metallic layer crossing of the matrix. In my design, approximatively 450 nm PaC thick was decided.
2. The profile of the etched PaC for opening must have a maximum angle of 70° for the metal overlay to create electrical contact
3. The gold deposition could only be performed in one specific thermal evaporator in our cleanroom. The BOC Edward machine model used, having a small chamber and a short samples/crucibles distance, allows, to some extent, an isotropic deposition of metals shown in Figure 39.

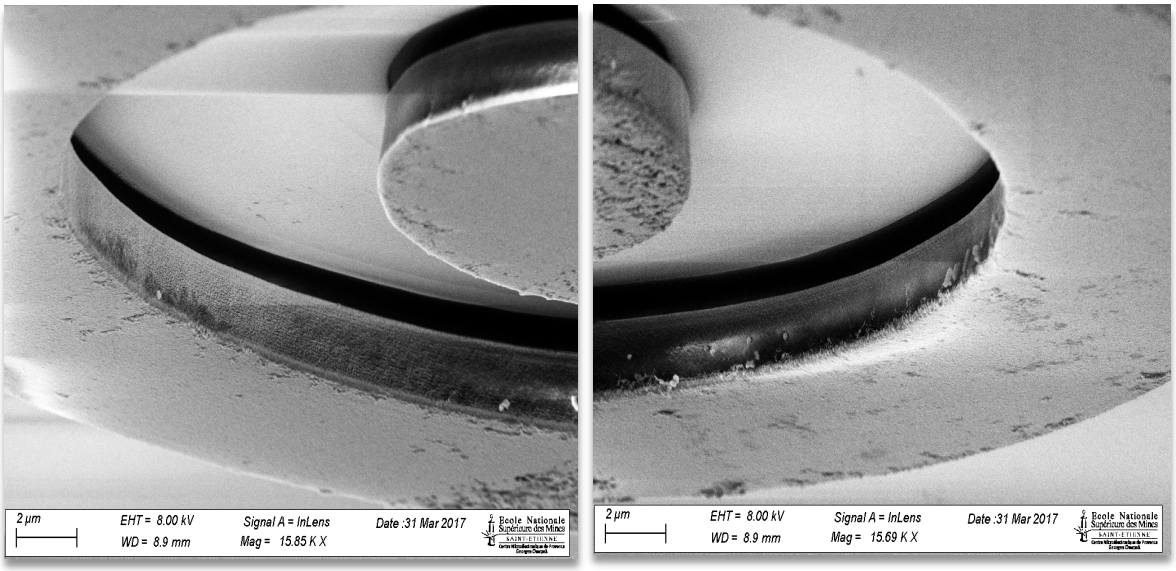

Figure 39. metal deposition over resist structure patterned on a wafer in the BOC Edward thermal deposition machine. The SEM pictures shows the double-stack layer SL1+Neg1 upside down, covered with gold deposited using the BOC Edward. The edges and walls of the features are covered with gold, showing an isotropic deposition during the evaporation process.

To conclude the test design, two fabrication protocols were selected: the BEL one using the peel-off technique and the Etching technique to pattern organic material layers. A base process is then used for both, and the process splits in two different ways to pattern PEDOT:PSS, the first being an etching technique using OSCOR resist, and the second one the BEL peel-off technique as depicted in Figure 40.

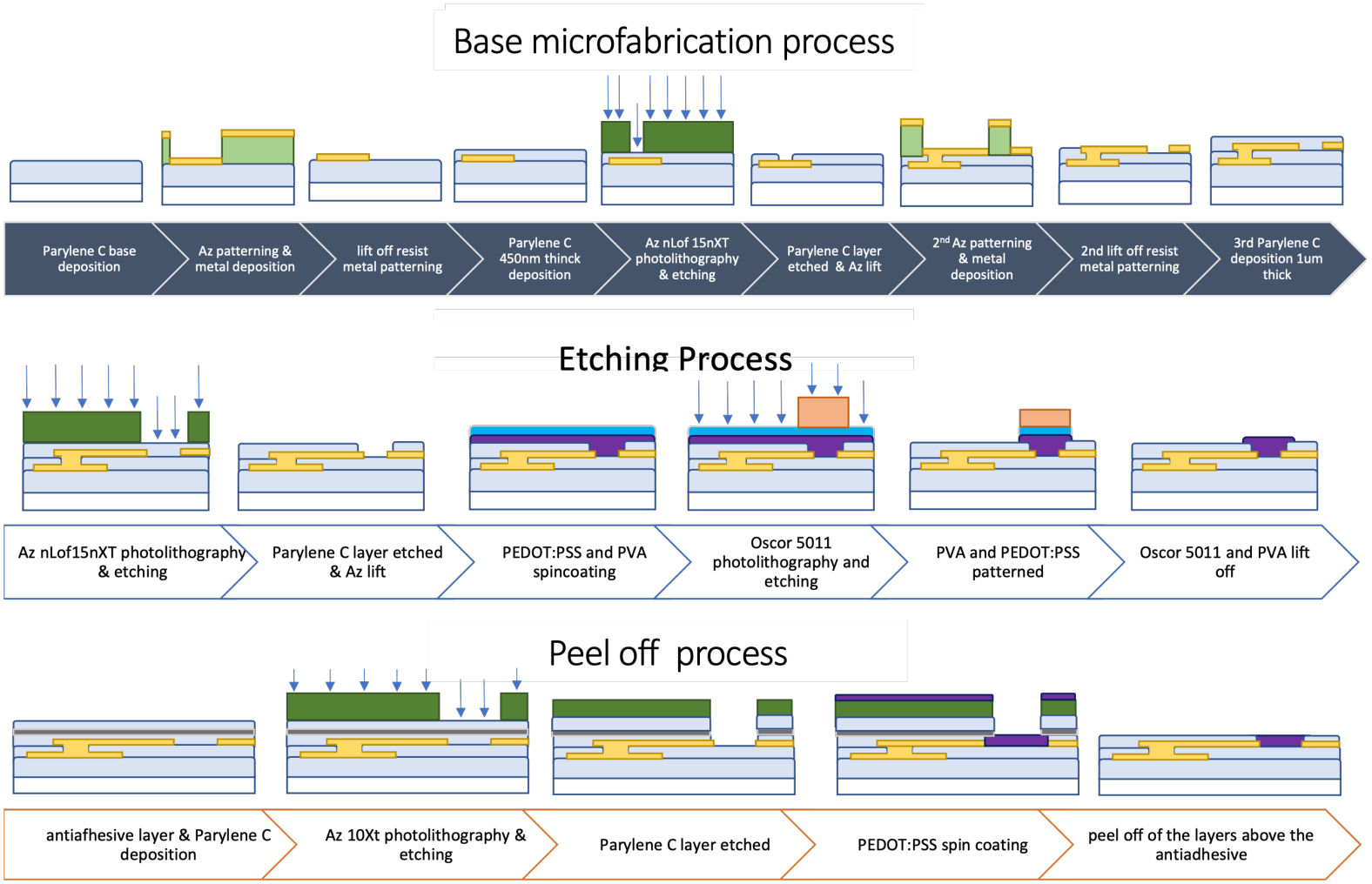

Figure 40. Fabrication protocols. Base process made from the etch fabrication protocol. Organic patterning is then split in two different lines: etching technic and BEL peel off step

3.5 1st design of 16 transistors and 2nd design (60 transistors) and results from characterization

3.5.1 First matrix design: electrical characterization

Once the fabrication process parameters are settled, a first device was designed and fabricated using the etching protocol shown in Figure 41. 16 OECTs of 40×28 µm constitute a matrix architecture. Eight control pads are dispatched in row and column, monitoring the drains and sources of the OECTs. 16 independent pads are devoted to the 16 electrodes of 1 mm contacts.

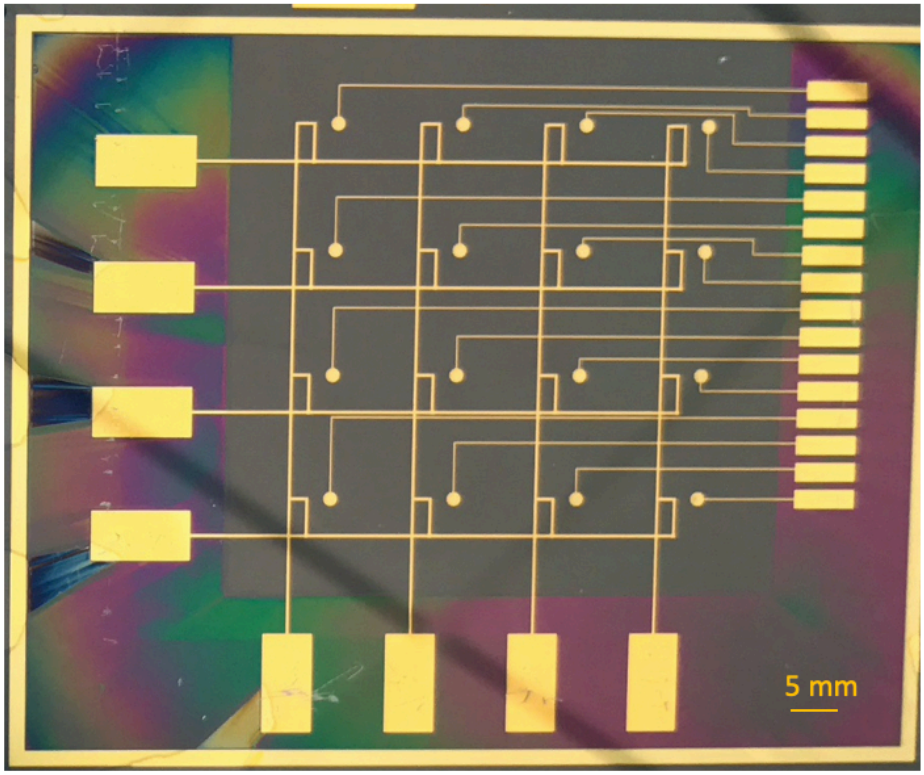

Figure 41. Matrix device made of 16 OECTs and 16 independent electrodes.

Following the batch production, we performed electrical characterization. A PDMS well is attached to the surface of the devices and filled with PBS. A silver/silver chloride (Ag/AgCl) pellet is dipped into the electrolyte and used as the gate for the OECTs.

To characterize an OECT, three main parameters are evaluated: its drain current modulation under variation of the collector voltage, providing its maximum transconductance, its cut-off frequency, and its time response. In the first experiment, only the transconductance and the cut-off frequency were of interest.

The matrix devices of 16 and 60 transistors were characterized using a NI system and a digital multimeter (DMM) with a built-in Labview software. The electrodes were characterized through electrochemical impedance spectroscopy (EIS) using an Autolab potentiostat (PGSTAT128N).

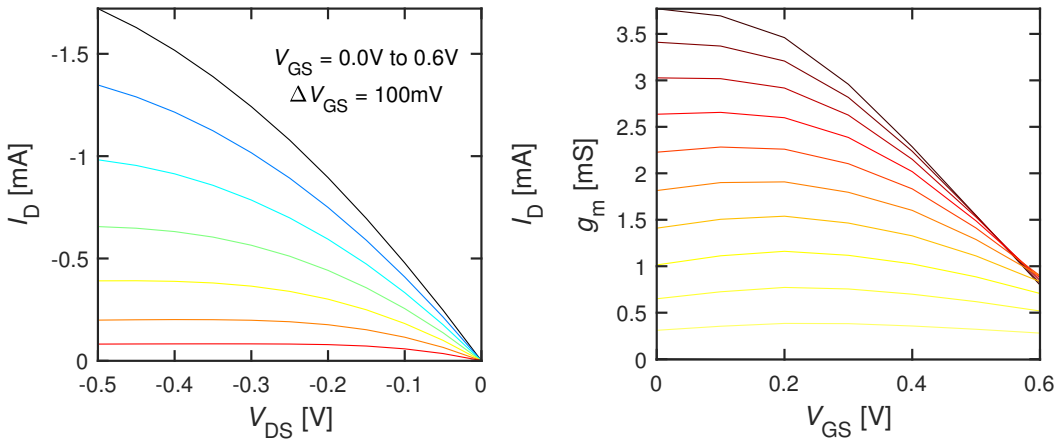

Figure 42. IV curve and transconductance curves extracted from the Matlab program written for data treatment. This result is extracted from one transistor of the matrix. The IV curve is obtained by fixing the gate voltage and changing the drain voltage from 0 to 6V. We the applied a drain bias V_D = 0.6 V, and changed the gate voltage from 0 to 0.6 V to obtained to transconductance curve.

EIS impedance for electrodes and cut-off frequencies, IV curve and bandwidth for OECTs were extracted. All measurements were made with NI system and customized Labview software. Data were treated using a Matlab program (shown in supplementary figure).

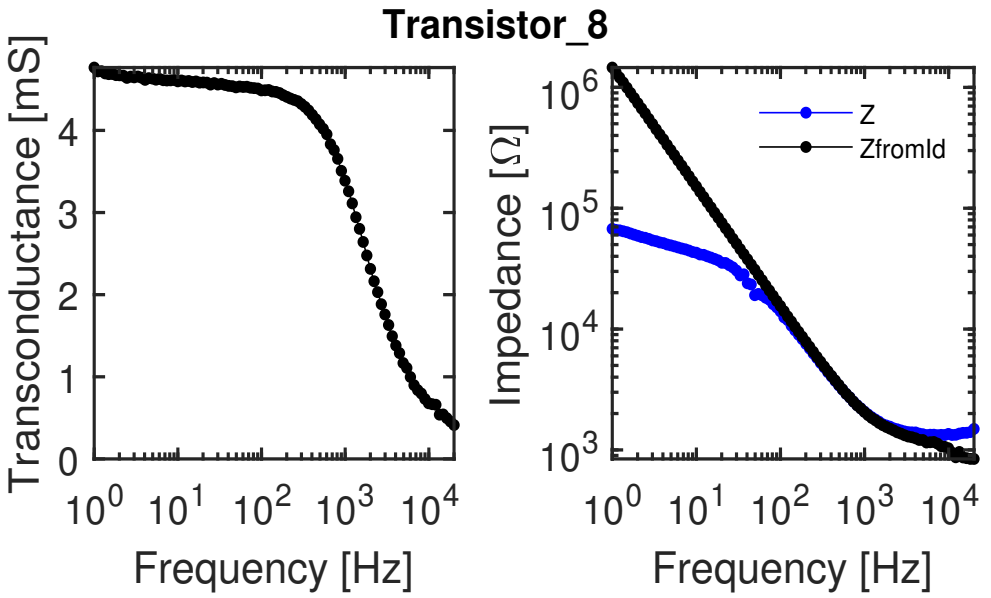

Figure 43. Bandwidth, impedance, and phases data from OECT n°8 characterization. The drain current is fixed at 0 V. A sinusoidal voltage is applied at the gate at different frequencies ranging from 1 to 1 kHz.

From the IV curve extracted from OECT n°8 characterization seen in Figure 42, we can confirm the gating effect and the transitive aspect of the transistors elaborated. From the bandwidth curve of the same transistor shown in Figure 43, the maximum transconductance shown is at V_{ds}0 V and is 5 mS, and the cut-off frequency reaches 10^3 Hz. Those values suggest an excellent behavior of the OECTs.

Unfortunately, as the machines used for the micro-fabrication are not performing constantly due to the PaC layer and the PEDOT:PSS etching step. Initially, the pad areas are fully etched. The idea is to remove any excess material in between pads to ensure good bonding with the connecting systems. By doing so, the CT were cut at the etched and non-etched junction of the design. As such, many devices were lost.

A second issue appeared through the PEDOT:PSS etch. Again, the same inhomogeneity in the RIE machine led to a PEDOT:PSS residue all over the device. Currently, this residue is much reduced but did not completely during the etching step.

3.5.2 Second designs: results and characterization

A second device was designed to increase the number and density of OECTs. 60 transistors are spread on a 1cm diameter disc surface. At the center, an electrode of 1mm diameter is used as a coplanar gate for the transistors. Cell culture will done upon those devices for further applications described in chapter 4. This design corrects the etching marge of error that was detected in the previous design. To overcome this potential issue during etching steps, the opening of the pads is now only restricted to a smaller diameter circle area inside the gold pads. By doing so, the full CT length is not going under the etching procedure. The etching step is terminated on top of the gold pad. It is worth noticing specific RIE tools should be dedicated to the step etching landing on gold (or other metals) for regular and industrialized process lines, as it produces particles that aggregate in the chamber and pollute the machine.

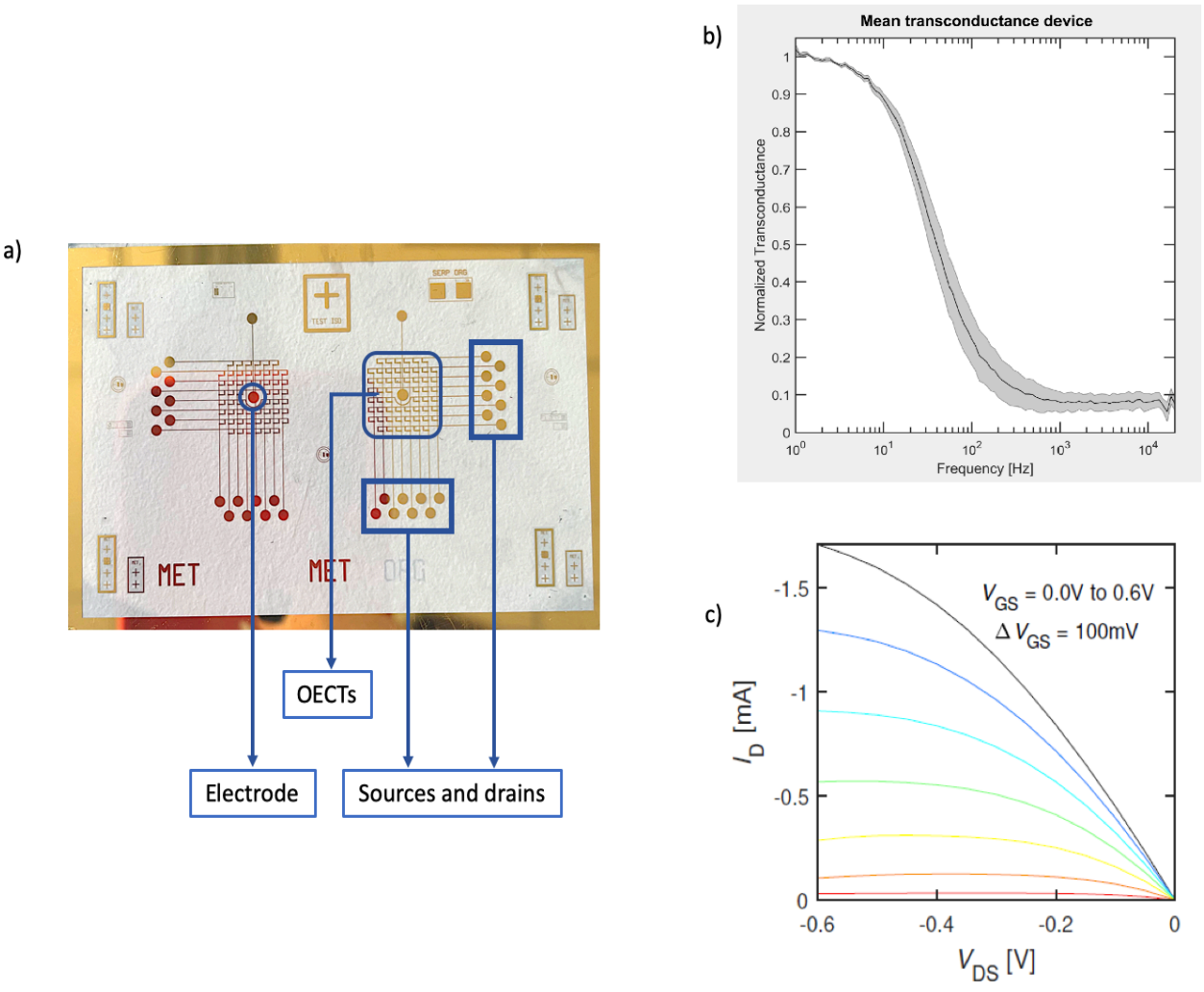

Figure 44. a) Matrix device made on glass slide. 60 transistors and 1 central electrode are displayed in this configuration. C) electrical characterization of a single OECT. Bandwidth and IV curve results. D) normalized mean transconductance of the 60 transistors over one matrix

A first electrical characterization is operated. Compared to the 16 electrodes matrix designs, those transistors show degraded electrical characteristics compared to the previous design, as seen in Figure 44. This might be due to the CT resistivity increasing because of their width being reduced from 200 to 60 µm. The cut-off frequency of the bandwidth is around 100 Hz, and the maximum transconductance is 4mS. The gain from the transconductance is not extremely high, but the cutoff frequency value enables detection of some biological markers, or cells tissues formation (cf. chapter 4). Cross talking between OECT was investigated as well. To do so, we connected one source and drain of one transistor only and

measured its conductivity. We reiterate the same operation but connect all the other sources and drains to the ground. By obtaining the same conductivity, we made sure the transistor was not connected to the others by crosstalk. By keeping the same connections where all source and drain were connected, we performed a measurement on line 1-A, where no transistor should be found. The absence of conductivity proved that the transistors were not cross-talking.

To perform those measurements, the devices were previously soaked in deionized water overnight. It is worth mentioning that every characterization step was performed in phosphate-buffered saline solution (pH = 7.4). This parameter is of great importance since degradation of the transistors will be observed during their application for *in vitro* experiments, detailed in the next chapter.

3.6 Conclusions

The OECT fabrication protocol and configuration were successfully revisited. Two processes were developed and translated into applications detailed in Chapters 4 and 5. One to pattern the PEDOT:PSS using an etching technique, and the other to replace PaC as insulation layer by the photo patternable resist DE1. Patterning organic material via etching instead of peel-off makes the protocol more suitable for industrial processes, repeatable, and scalable. DE1 resist allows thin layer and smooth edges of the features. These properties are more compatible with cells than harsh geometries and surfaces, described in the next chapter.

The matrix OECTs configuration and protocols were demonstrated. Its *in vitro* application are detailed in chapter 5. By arranging drains and sources in rows and columns, OECTs density can be increased, and their monitoring hardware simplified.

Coupling the matrix devices with an Arduino system to record simultaneously from multiple OECTs should be investigated in future development.

Bibliography

1. Adler, M. S., Owyang, K. W., Jayant Baliga, B. & Kokosa, R. A. The Evolution of Power Device Technology. *IEEE Trans. Electron Devices* **31**, 1570–1591 (1984).
2. Tanenbaum, M., Valdes, L. B., Buehler, E. & Hannay, N. B. Silicon n-p-n grown junction transistors. *J. Appl. Phys.* **26**, 686–692 (1955).
3. Lynn, L. H. The commercialization of the transistor radio in Japan: The functioning of an innovation community. *IEEE Trans. Eng. Manag.* **45**, 220–229 (1998).
4. Str, D. I. & By, B. U. T. E. D. application in television, radio and electronics.
5. Gillum, R. F. From papyrus to the electronic tablet: A brief history of the clinical medical record with lessons for the digital age. *Am. J. Med.* **126**, 853–857 (2013).
6. Lee, S., Ozlu, B., Eom, T., Martin, D. C. & Shim, B. S. Electrically conducting polymers for bio-interfacing electronics: From neural and cardiac interfaces to bone and artificial tissue biomaterials. *Biosens. Bioelectron.* **170**, 112620 (2020).
7. Baztán, M., Recalde, S. & Hernández, M. Advances in super-resolution imaging : applications in biology and medicine. 18–26 (2014).
8. Rivnay, J. *et al.* Organic electrochemical transistors. *Nature Reviews Materials* vol. 3 (2018).
9. Khodagholy, D. *et al.* In vivo recordings of brain activity using organic transistors. *Nat. Commun.* **4**, (2013).
10. Braendlein, M. *et al.* Lactate Detection in Tumor Cell Cultures Using Organic Transistor Circuits. *Adv. Mater.* **29**, (2017).
11. Pappa, A. M. *et al.* Organic Transistor Arrays Integrated with Finger-Powered Microfluidics for Multianalyte Saliva Testing. *Adv. Healthc. Mater.* **5**, 2295–2302 (2016).
12. Khodagholy, D. *et al.* NeuroGrid: Recording action potentials from the surface of the brain. *Nat. Neurosci.* **18**, 310–315 (2015).
13. Rivnay, J. *et al.* Organic electrochemical transistors for cell-based impedance sensing. *Appl. Phys. Lett.* **106**, (2015).
14. Donahue, M. J. *et al.* High-Performance Vertical Organic Electrochemical Transistors. *Adv. Mater.* **30**, 1–5 (2018).
15. Khodagholy, D. Conducting Polymer Devices for Bioelectronics. *Hal* (2012).
16. Jimison, L. H. *et al.* Measurement of barrier tissue integrity with an organic electrochemical transistor. *Adv. Mater.* **24**, 5919–5923 (2012).
17. Gamal, A. El *et al.* An Architecture for Electrically Configurable Gate Arrays. *IEEE J. Solid-State Circuits* **24**, 394–398 (1989).
18. Wang, Y., Alonso, J. M. & Ruan, X. A Review of LED Drivers and Related Technologies. *IEEE Trans. Ind. Electron.* **64**, 5754–5765 (2017).

19. Lee, W. *et al.* Transparent, conformable, active multielectrode array using organic electrochemical transistors. *Proc. Natl. Acad. Sci. U. S. A.* **114**, 10554–10559 (2017).

20. Someya, T. *et al. A large-area, flexible pressure sensor matrix with organic field-effect transistors for artificial skin applications*. www.pnas.orgcgidoi10.1073pnas.0401918101 (2004).

Chapter 4
Self-assembly of mammalian cell membranes on bioelectronics devices with functional transmembrane proteins

This chapter is based on the publication:

Self-Assembly of Mammalian-Cell Membranes on Bioelectronic Devices with Functional Transmembrane Proteins *Liu, H. Y. et al Langmuir* ***36****, 7325–7331 (2020)*

Introduction

Throughout the three years of PhDs study, I have elaborated and partially developed, three different types of fabrication processes for bioelectronic devices. As described in the previous chapter, each one of them had to be evaluated through 3 steps: surface topography, electrical characterization in PBS, and *in vitro* experiment. Topography and electrical characterization are discussed in previous chapter and provide the electrical properties of the device before any application. In this chapter, I test the behavior of the devices with biological matter. The bioelectronic devices' purpose is to interface with biology. The language transduced is the ionic flux from biological matter, to an electron flow in the electronic circuit. Ionic flow is the essence of any biological event, taking place through their membrane and the proteins embedded in its lipid bilayer. Our organic-based device aims to detect such fluctuations and transduces this signal by interfacing the ions flux and converting it to electronic current[1] (i.e., electrophysiology)

4.1 Cell study

In biology, cell study, or cytology, revolves around understanding of the single cell's structure and function. A cell is described through three main parts draft in Figure 45:

- the nucleus, containing the DNA
- the cytoplasm. All the cellular contents present between the nucleus and the plasma membrane
- the plasma membrane that forms the outer flexible surface of the cell. It separates the internal environment of the cell from the external environment.

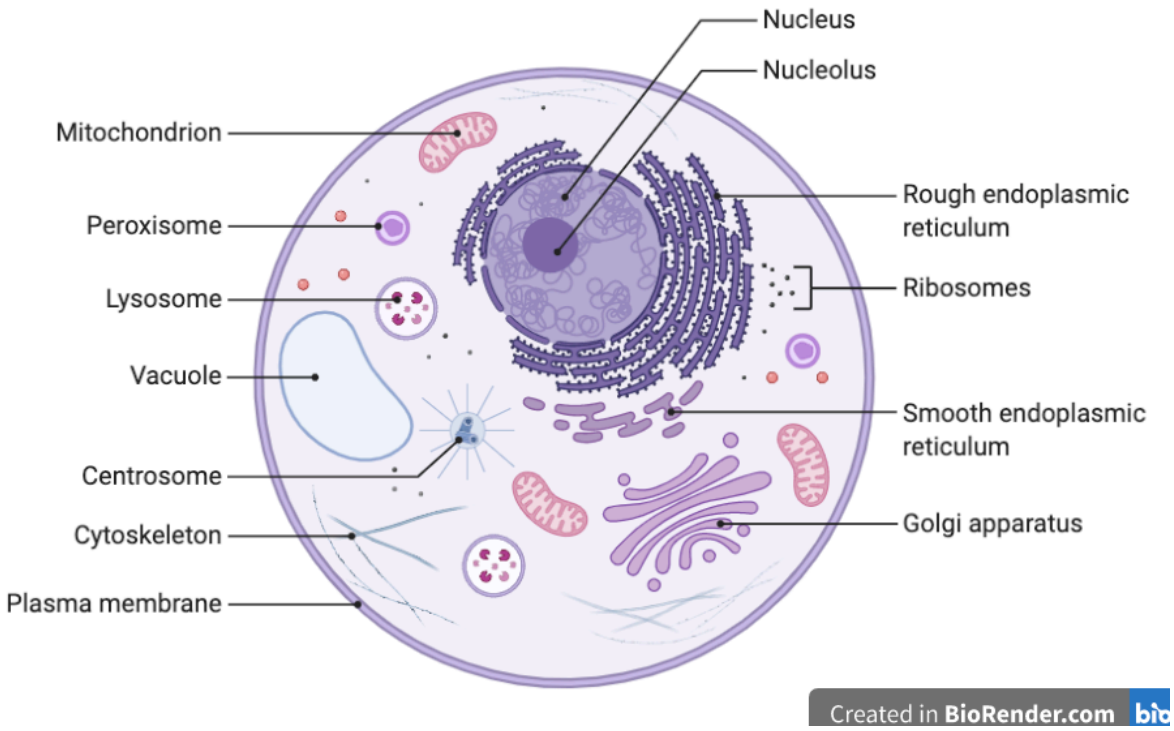

Figure 45: scheme of cell structure

As technology and techniques have improved over the last centuries, more in-depth and detailed answers to the cell's mechanism is discovered. For centuries, optical monitoring has been the primary technique used to understand cell's structure and behavior. Nowadays, the most advanced optic technologies allow insight into individual microsystems inside the cells. Nevertheless, optical monitoring through a microscope operates over thin layers of tissues, or 2D *in vitro* technology. Those planar and single-type cell model-based experiments are irrelevant regarding the complexity of the *in vivo* system they try to reproduce. To reduce the gap between *in vitro* models *and* the *in vivo* environment studied, complexity is included in the *in vitro* model: microfluidics systems, 3D co-cultures or scaffolds are being implemented in the cell experiment to emulate the whole biological systems. Those elaborated structures are hardly compatible with optical monitoring. To compensate these limitations, new tools and technique have arisen, namely bioelectronics to measure electrophysiology.

Electrophysiology is the biological field that studies the electrical and electrochemical properties of living organisms[2] at the tissue or molecular scales[3]. It extracts voltage or electric current from cells such as neurons, or organs like the heart. The generic tool used to perform electrical stimulation (E-Stim) and recording is the electrode4, in various configurations and shapes. Their operation mode varies from intracellular to extracellular actions.

At the macro scale and extracellular level, electrodes can record and stimulate entire organs or a large population of cells. Electroencephalogram (EEG), electrocardiogram (ECG) and electromyogram (EMG) record the electrical activity of areas of the brain, the heart, and the muscles to evaluate their proper functioning. In stimulation types therapies, the muscular rehabilitation after an injury uses E-stim to prevent muscle loss[5]. Also, defibrillators for emergency or implantable (ICD) uses electric stimulation to prevent or correct arrhythmia or perform defibrillation[6]. Pacemaker technology is an application of electrophysiology therapy at the macro scale.

At micro scale, electrodes can be used to record the ionic flows and membrane potentials of cells. Patch-clamp is a well-established procedure that uses micro-sized glass electrodes filled with conductive solution. It records the electrical activity of an insulated section of the cell membrane by sucking a patch inside its glass needle. It is referred as an intracellular technique because it measures the electrical gradient inside the cell. In contrast, MEAs are used to record ionic flux externally to the cell. Electrodes are placed near or in contact with

the cells, and monitor ion flows outside the membrane. Electroporation is another technique able to open ionic channels from the membrane by applying pulses, creating an electric field. To some extent, it creates holes in the lipid bilayer and porates the cell[7], momentarily or permanently. Its main application target cancerogenic cells from skin or subcutaneous tissues. Cochlear implants are an example of therapy using stimulation at the cellular levels, transducing external sounds to electrical impulse via electrodes placed along the nerve in the cochlea.

As mentioned above, the cell is structured by its plasma membrane. Its basic framework is the lipid bilayer. Two types of proteins are present in the membrane: The peripheral ones, where proteins are attached to the polar heads of the lipids, and the transmembrane proteins that are firmly embedded in the bilayer, protruding inside and outside the cell membrane. In this chapter, we will focus on the latter type: Transmembrane proteins (TMPs). The transmembrane proteins serve different purposes and functions: receptor, enzyme, linkers, cell-identity markers, ion channels and carriers. It is worth noticing that the membrane is a fluid structure, meaning lipids and proteins can move and rotate in their own half of the bilayer. This specificity is extremely important as it allows multiple function of the cell, such as their interaction on the membrane, the TMPs assembly, the self-healing mechanism, and the movement of some components of the membrane for growth, division, cellular junction

In this chapter, we study TMPs as part membrane permeability actuators by creating electrical gradient across the lipid bilayer. Ions channels and carrier allow selective permeability of the membrane by helping a specific molecule or ions to pass through the bilayer. By doing so, the plasma membrane has an influence on the ions and molecule concentrations inside and outside the cell. Usually, the inner part is more negatively charged, and the outer part positively charged. This electrical gradient occurring at the membrane is called membrane potential. This phenomenon is monitored by electrophysiology, by detecting the electrical gradient near the cells as shown in Figure 46.

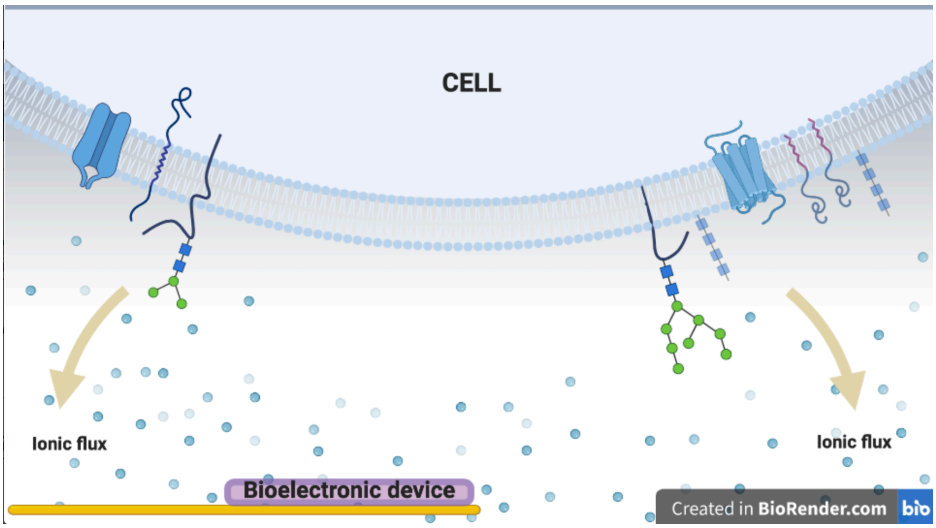

Figure 46: Electrophysiology: when electronics merge with biology. Example of ionic flux expressing by cells' membrane through transmembrane proteins. Detection of ion flux with a bioelectronic device

Bioelectronic devices technology

When interfacing biology, organic materials possess the particular propriety to conduct both ionic and electrical carriers[8]. Furthermore, they offer an improved mechanical matching with the organic tissues[9]. They are soft and compatible with flexible substrates[10], reducing the inflammation and body response to the device[11]. As such, bioelectronic devices are the ideal tool to transduce biological event from living organism into electrical data[12]. In this chapter, I will describe the efficiency of OMEAs to monitor the lipids barrier and the TMPs. The electrodes interface *in vitro* this new model established to study the cell's membrane and some of its proteins embedded.

This work was done in Collaboration between the group of Pr. R Owens in Cambridge, and the group of Pr Susan. Daniel from Cornell. I have provided one type of bioelectronic devices including electrodes covered by PEDOT:PSS and DE1 to perform the electrophysiological recording of the biological model.

This work was published in Langmuir in 2020[13]. All figures reproduced with permission.

Biological experiment

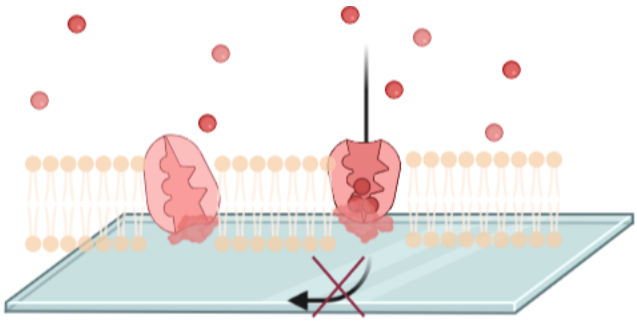

Figure 47: SLBs on rigid and. insulating substrates. Ions cannot pass through TMPs and protruded proteins are poorly embedded in the lipid bilayer.

Cell membrane and TMPs are complexes biological systems challenging to study or recreate *in vitro*. As mentioned above, membrane fluidity and fragility prevent any harsh experiment study that could damage the bilayer structure as depicted in Figure 47. This explains why previous work done to study TMPs is usually based on whole cell-based assay models. Patch-clamping is the most common technique used to monitor parts of plasma membranes proteins, but this method is laborious and the patches fragile. Attempts to recreate models of cell membrane *in vitro* hardly reproduce the biological properties of the TMPs. Another model known as supported lipids bilayers (SLB) is a technique where the recreated membrane is improved compared to patch clamp and allows optical monitoring thanks to the transparent 2D support surface. Unfortunately, as they are created from TMPs inclusion into purified lipids, they unsuccessfully reproduce the orientation of the proteins embedded in the lipids[14]. Besides, SLBs are formed on glass substrates. Being an electrical insulator, they preclude any measurement of ion flows across the ion channels. Glass is a rigid substrate and the protruded proteins carrying the ions across the membranes are compressed, and are nit functional. Thus, preventing the protein subunit assembly and ability to interact with other cells makes biological model inaccurate as shown in Figure 47.

In this study, innovative methods were developed to create SLBs[15]. Recreation *in vitro* of the lipid membrane has been achieved over transparent bioelectronic devices, thus enabling dual electrical and optical monitoring of TMP function in its native membrane environment. This bilayer is supported by a soft conductive organic material, PEDOT:PSS. Used as a negatively charged hydrated cushion under the lipid's bilayer, PEDOT:PSS acts as the inner part of the cell to the bilayer, and allows absorption of ions from the outer part, and helps positioning of the TMPs on the lipids membrane. As the recreation of SLBs on a softer substrate than glass is more complex, a protocol to extract native membranes from cells and transfer them to the PEDOT:PSS surface was developed[16]. Then, we investigated the proteins functional properties and orientation of our model using a protease assay.

To conclude, we used our model to study the ATP-gated P2X2 ion channel, a therapeutic target for multiple pain modalities including neuropathic, inflammatory, and chronic pain states.

Here we describe a platform adapted and tuned to a biologically complex model. Its surface has friendly properties to lipids bilayers such as smooth, hydrated, and soft structures. Plus, by providing transparency with the OECT, the device allows simultaneous optical tracking of single protein motions to characterize protein diffusion; and sensing of TMP function using electrical impedance spectroscopy (EIS). This monitoring technique measures the impedance of the biological system over a range of frequencies. To do so, an equivalent circuit of the SLBs is elaborated (Figure 50 e). From there, The Nyquist plot is drowned, representing the real and imaginary part of the impedance. Each point of the curves is obtained from one frequency. The Shape of the curve is characteristic of the different element present in the model measured.

The conducting polymer (PEDOT:PSS) is used to support the SLB. Our platform maintains the compositional complexity of the native plasma membrane, the membrane fluidity of the lipids and proteins, the native protein orientation in the membrane. It can directly monitor ion channel activity across it as drawn in Figure 48. Protocols for assembling complex biological SLBs over the topographic and highly negatively charged surface of the hydrated polymer were adjusted, as the surface of PEDOT:PSS makes the self-assembly process that is easy on glass, significantly more difficult.

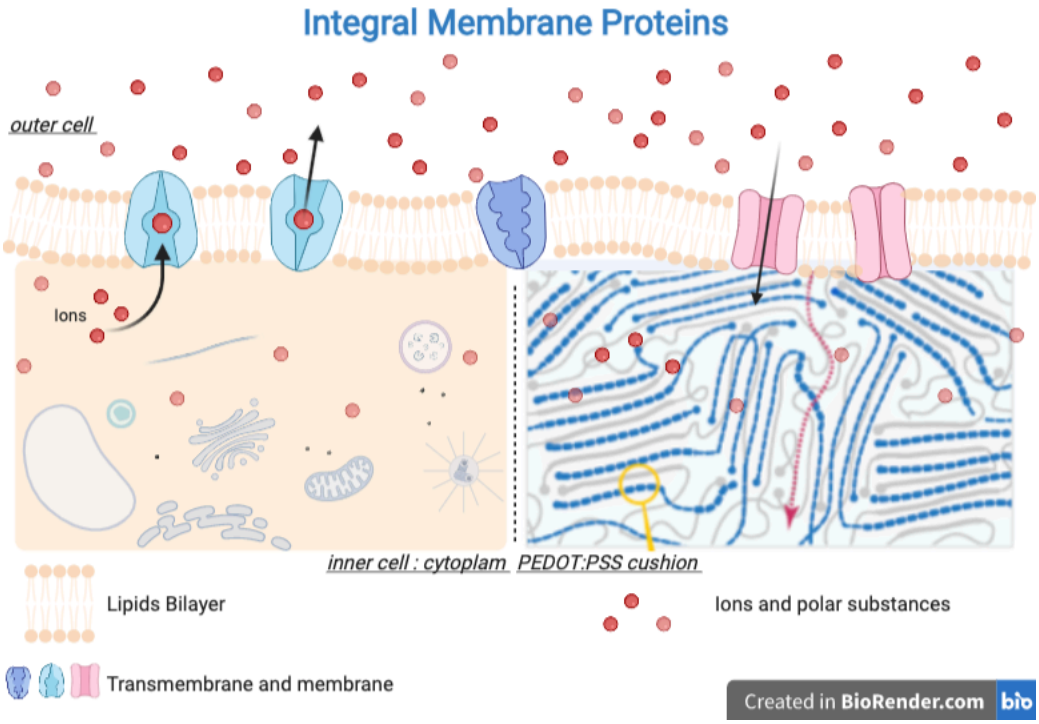

Figure 48: Electrophysiological model studied from the Lipids Bilayer and its TMPs experiment.

4.2 Lipids bilayers and TMPs experiment

Cells and plasmids

BHK cells were purchased from the American Type Culture Collection (ATCC) and grown in Dulbecco's modified Eagle medium (DMEM) (CellGro) supplemented with 10% fetal bovine serum (Gibco), 100 U/ml penicillin and 10 µg/ml streptomycin (CellGro), 1% HEPES buffer (CellGro). The plasmids used in this work have been reported in previous literature[17]. The pYFP-GPI-N1 or pINR3-Neon-THR-P2X2 were used for transfection of BHK cells to express a glycophosphatidylinositol (GPI) anchored yellow fluorescent (YFP) protein or neon green fused transmembrane P2X2 receptor. The pYFP-GPI-N1 plasmid and the pINR3-Neon- THR-P2X2 plasmid were gifts from the Baird/Holowka and the Kawate research groups at Cornell University, respectively. Preparation of plasma cell membrane vesicles (blebs): This procedure has been reported in previous literature[16], but salient details are provided here. In brief, 9 × 105 BHK cells were seeded in 10 cm culture dishes (Corning) and grew for 24 hours in a 37 °C, 5% CO2 incubator. 18µL of Turbofect transfection reagent (ThermoScientific) and 6µg of DNA plasmid were used to transfect the BHK cells and incubated for 24 hours. Then, cells were washed with GPMV buffer (2 mM CaCl2, 10 mM HEPES, 150 mM NaCl at pH 7.4). 4 ml of GPMV buffer with 25 mM formaldehyde (FA) and 2 mM dithiothreitol (DTT) (0.075%FA) were incubated with the cells to induce the formation of plasma cell membrane vesicles (blebs) for 2 hours at 37 °C. The solution containing the cell membrane blebs were settled on ice for 15 min to separate cell debris from the more buoyant cell membrane blebs, which were then collected from the supernatant. Characterization of blebs were reported in previous literature.

Preparation of liposomes :

The process of forming the liposomes has been described in previous literature[16,17]. Liposomes of desired compositions were made from the following components: 1,2- dioleoyl-sn-glycero-3-phosphocholine (DOPC) and 1,2-dioleoyl-3-trimethylammonium-propane (DOTAP), purchased from Avanti Polar Lipids. The desired ratio of lipids was mixed in

chloroform and dried by nitrogen stream. Then, the lipid films were stored under the vacuum for three hours to evaporate chloroform. PBS buffer were added to the dried lipid film to concentration of 2 mg/ml. Once rehydrated, the solution was extruded through a 50 nm membrane (GE Health) 15 times. Characterization of these vesicles is provided in Supporting Figure S1

Formation of SLBs

To assemble a planar cell membrane bilayer on a support, the 100 µl of cell membrane bleb solution at approximately 5 × 108 blebs/ml were added into the well and incubated for 15 mins. After incubation, the well was rinsed with PBS buffer. Then, 100 µl of liposomes at 2 mg/ml was added into the well and incubated for 30 mins. Next, the well was washed with PBS buffer. 100 µl Polyethylene glycol 8000 (PEG8k, 30% w/v) in PBS buffer was added into the well and incubated for 15 mins more. The well was rinsed with PBS buffer to remove PEG8k after bilayer formation. For supported bilayers made from lipids-only, the procedure is the same as above without the step that introduces the blebs.

Device fabrication: The fabrication protocol relies on a 4-stack layer step. First, 3 µm thick Parylene C layer is added through chemical vapor deposition on top of the wafer. Then, Cr/Au 150nm thick electrodes are patterned using photolithography with AZnLof 2070 as the lift off resist. PEDOT:PSS solution, Clevios PH1000 containing 5 vol% ethylene glycol and 1 vol% (3-glycidyloxypropyl) trimethyoxysilane, is spin-coated at 1500 rpm for 90 seconds, baked on a hotplate at 130 ºC for one hour and dry-etched using orthogonal resist 5011 as protective mask. Finally, a dielectric resist, DE1 from Orthogonal Inc, is spin-coated and patterned on top as the encapsulation layer via photolithography. The devices pictures and set up are shown in Figure 49.

Modelling of EIS measurement :

The measured impedance spectra were fitted to a model using the EC-lab software. The equivalent circuit used to extract the electrical properties of the membrane consist of a resistor and a capacitor in series, accounting for the electrolyte and the PEDOT:PSS film respectively, along with a parallel resistor-capacitor component also connected in series

accounting for the membrane. (Figure 50 e) The PEDOT: PSS electrode is represented by a capacitive element due to its purely capacitive behavior as suggested in recent studies. A parallel resistor and capacitor component represent the membrane (SLB) system. The parallel resistor and capacitor circuit represents the cell membrane. It is typically used in literature to account for passive membrane or transmembrane ion transport in biological layers (i.e., cell membranes, cell monolayers).

4.3 Result & discussion

4.3.1 Lipids and TMP platform

EIS was used to record the presence of the membrane and electrically monitor the assembly process of the SLB. The resistance of the film increases as every step is added on top of the devices: blebs, then liposomes. EIS monitored the for long term membrane formation, disruption, and healing. It shows the increase of resistance during the formation stage, and its decrease when ethanol is added as proof of disruption of the membrane

To form the native SLB, a multi-step process was carried out. First, cells were transfected with the membrane protein of interest and chemically induced to bleb off small vesicles from the plasma membrane, resulting in proteoliposomes containing the native lipids of the cell membrane and the expressed proteins. These proteoliposomes, commonly referred to as “blebs”, were then adsorbed onto the PEDOT:PSS surface, followed by the addition of a small amount of positively charged liposomes. These liposomes (Figure S1), act as nucleation sites for planar bilayer formation, more easily rupturing to form an SLB on the negatively charged PEDOT:PSS surface and simultaneously inducing rupture of the neighboring absorbed blebs. Although only a small fraction of positively charged lipids are used in this step, it is essential to note that these lipids are not naturally present in cell membranes, but used here to facilitate the SLB assembly process. Eventually, the patches of SLBs heal together to form a continuous layer. To further ensure complete rupture of any remaining blebs or liposomes, we add a buffer spiked with polyethylene glycol (PEG) to create osmotic stress to drive the completion of this assembly process.

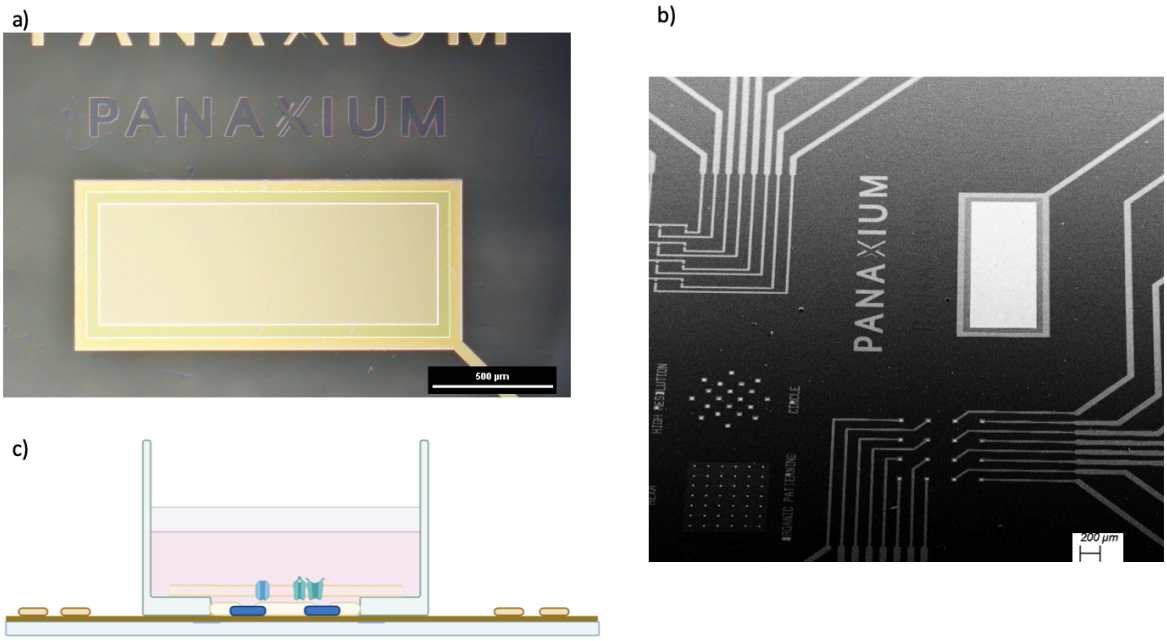

Figure 49: Device used for the *in vitro* monitoring of the TMPs function. a) microscope image of the electrode used. b) SEM picture of the sensitive area of the device. c) experimental scheme of the lipid bilayer deposition over the device

The membrane formation and the continuity of the healed patches were optically verified using a photobleaching experiment (Figure 50 b). A membrane intercalating fluorophore, R18, was used to label the blebs before rupture. A ~20-micron diameter spot was bleached in the plane of the fluorescently-labeled bilayer and its recovery was monitored over time. Fluorescence of the bilayer approaches full recovery after 300 seconds, with a diffusion coefficient of 0.91 ± 0.03 $\mu m^2/s$ and mobile fraction 99.5 ± 0.05%. The mobility confirms that the lipids within the membrane plane are mobile and that the membrane probe, initially confined to the ~100 nm bleb membrane surface, is now free to move within the SLB over at least the 20 microns scale.

EIS was used to confirm the presence of the membrane and monitor each stage of the self-assembly process electrically (Figure 50 c). At first, we see the intrinsic features of the PEDOT:PSS surface alone in the bathing buffer solution. Next, the addition of the blebs results in a shift toward higher resistance. With the addition of liposomes, the shift is greater, until

finally, after PEG8k solution was added and rinsed out, we see the highest complex impedance values for this system. Impedance values of the native membrane were compared against a liposome-only membrane (Figure 50 d) and resistance and capacitance values were calculated (after modeling the equivalent circuits for each of the bilayers using the model in Figure 50 e) Rb, native = 0.14 kΩ.cm2, Cb, native = 0.17µF/cm2 and Rb, lipid = 0.78 kΩ.cm2, Cb, lipid = 0.18µF/cm2. The substantially lower membrane resistance value of the native SLB, compared to the liposome only SLB, is attributed to the molecular complexity of the native membrane, that is the presence of ion channels or other "leaky" elements, or a poorer ability to pack as tightly as the pure lipids. Another possibility could be the difference in membrane self-assembly quality between native SLB and liposome only SLB. This comparison highlights the sensitivity of the device in detecting the difference in membrane composition or quality. We show the time-resolved evolution of the membrane formation using continuous EIS monitoring (Figure 50 f&g). In both cases, it was observed that the PEG-induced osmotic shock results in a marked increase in the resistance after further promoting the "healing" the bilayer. We verified that increase in resistance is not due to the presence of any remaining PEG in the solution after rinsing Finally, we investigate our ability to monitor disruption of the assembled cell membrane using ethanol, known to have a strong effect on the permeability of membranes. The EIS measurements show a decrease in membrane resistance with increasing concentration of ethanol, supporting our conclusion that the device is sensitive enough to quantitatively detect disruption of the membrane layer by ethanol.

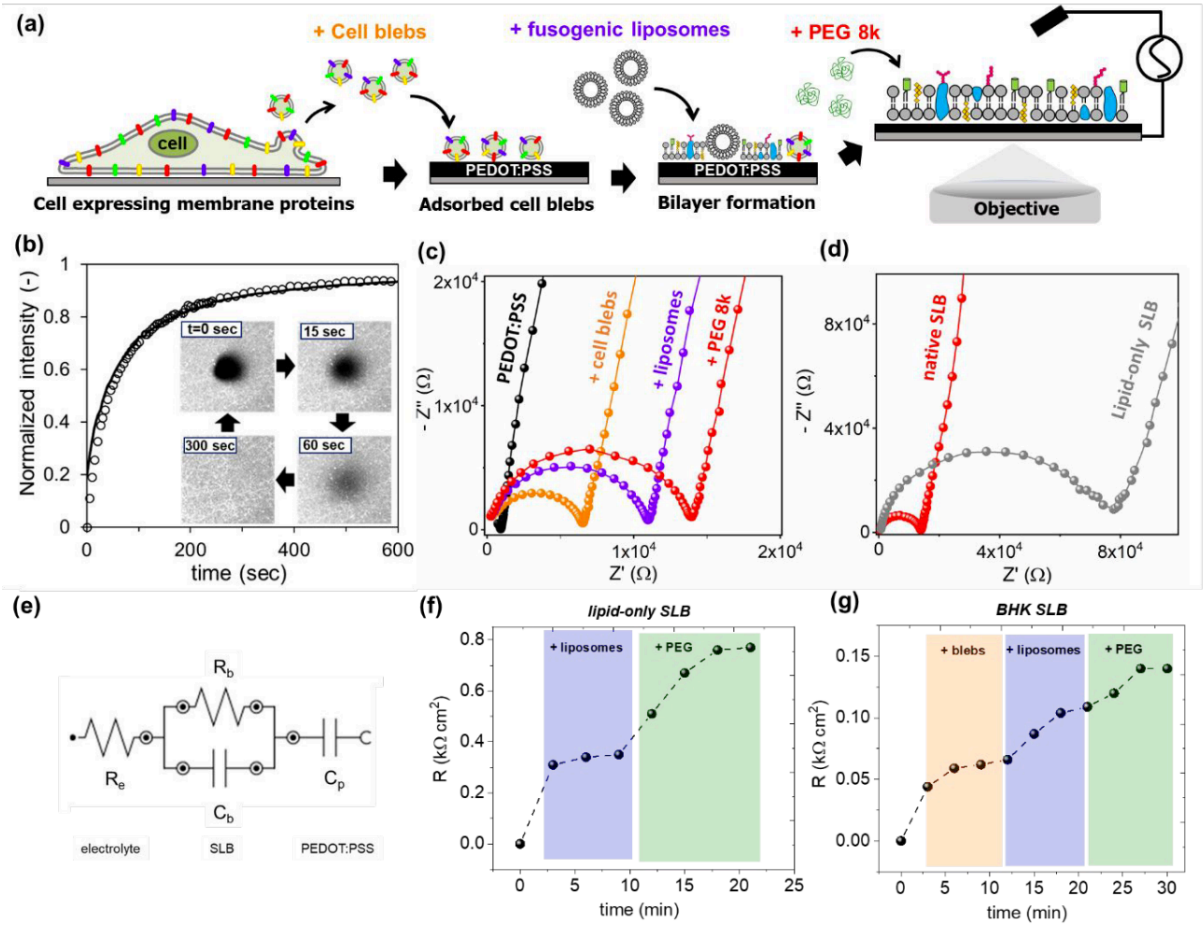

Figure 50: Combined optical and electrical monitoring of Baby Hamster Kidney cell SLB formation. (a) Cell bleb rupture and bilayer self-assembly on a PEDOT:PSS film after the addition of positively charged liposomes and soluble PEG (8k). (b) A photobleached spot in an R18-labeled SLB illustrates the fluidity of the membrane over the micron scale, with the corresponding recovery curve used to calculate the diffusion coefficient. (c) Nyquist plots showing the formation of the native planar cell membrane at each stage in (a); after addition of cell blebs (orange), after addition of the liposomes (purple); and after addition of PEG (red). (d) Comparative Nyquist plot of the native SLB (red) and a liposome-only SLB (grey). (e) The equivalent circuit used to model the EIS data. (f) Time resolved changes in resistance as the SLB forms on the polymer surface. (g) Resistance changes for the supported native membrane formation over time.

Membrane protein mobility and correct orientation is crucial for TMP function. In particular, for ion channels, protein units move and undergo conformational changes necessary for opening and closing; and orientation is critical for the proper directionality of ion flux. To show the power of our platform in sensing TMP function, we studied the ATP-gated P2X2 ion channel, a therapeutic target for multiple pain modalities including neuropathic, inflammatory, and chronic pain states. Protein ion channels in cell membranes are key elements in pain signaling with around 80 ion channels having strong links to pain

sensation.34 However, only a few of these channels are understood well enough to be successfully drugged for pain management. The effective treatment of pain remains a challenge that has been exacerbated by the opioid crisis, stressing the urgent need to better understand the underlying causes of pain and find new targets to manage it with minimal side effects. In the case of P2X2, many questions persist about its function, including how lipid regulation may influence ion flux, the process by which monomer units may come together to yield an ATP-sensitive gating events, and more. Thus, having a platform that provides a native environment of lipids and proteins from the plasma membrane surface with the ability to study these interactions and factors would greatly enhance such studies.

As a proof of concept, we use our platform bearing baby hamster kidney (BHK) membranes expressing P2X2 ion channels to measure the ion channel response under different conditions. P2X2 ion channels are ATP gated; open in the presence of ATP and closed in its absence (Figure 51 a). Figure 51 b shows the impedance profile changes in response to ATP treatment. The plots show the impedance value for the bare electrode in black, the value for the membrane prior to treatment with ATP in red, and then a shift to lower impedance values once ATP is added to the solution in blue. The relative difference in the resistances between +ATP and –ATP after fitting the impedance data with the model is captured in Figure 51 c in the first set of bars. In a control experiment, carried out on a different electrode with a membrane not expressing P2X2, the relative change in resistance +/- ATP is much less, as shown in the second set of bars. In this bar chart, we have normalized the resistances to the values without ATP on each device for comparison, noting that the electrodes themselves have some variation that makes it difficult to compare absolute values across the two devices. However, within a device, there is a clear distinction when ATP is added or not, especially when P2X2 is expressed in the membrane. The significant decrease in the membrane resistance observed for the first case, is likely due to P2X2 activation and opening, allowing small positive ions, like Na+ or Ca2+ present in our buffer, to pass across the membrane. Dual modality monitoring using our platform thus confirms that the P2X2 protein is mobile, correctly oriented, and functioning as an ion channel in response to native gating ligands.

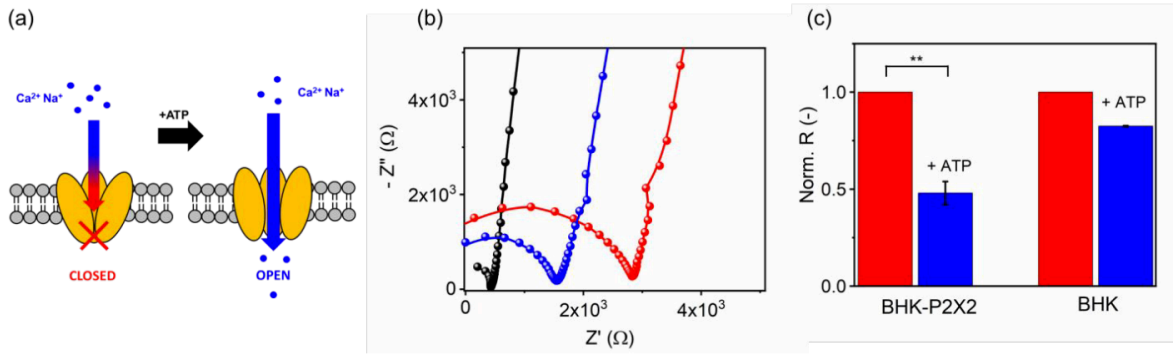

Figure 51 : Ion channel function study using the native membrane on an organic electronic transducer. (a) Schematic of PX2X ATP-gated ion channel. (b) Nyquist plot of the electrode prior to (black) and after (red) the P2X2-rich membrane formation as well as after treatment with ATP (blue). (c) Calculated membrane resistance of the P2X2-rich membrane before (red) and after (blue) ATP (10 µM) treatment showing a clear decrease in the resistance of the membrane in response to ATP and the corresponding values of the BHK membrane not expressing any P2X2 (patterned histograms) (n = 3, p = 0.009).

4.3.2 Conclusion

A bioelectronic platform for *in vitro* assays that combines native cell membrane materials with organic electronic devices was developed. This model allows both optical and electrical monitoring. Made of materials compatible with membranes, it has the capacity to study TMP functions. The specific fabrication process used to pattern PEDOT:PSS and DE1 as insulation layer provides an extremely smooth surface for the lipids bilayer to form. Indeed, rough and inhomogeneous surfaces and sharp edges might cause the lipids barrier to disrupt, which is avoided using this specific device. A second work using the same devices was published in ACS Nano in May 202018. The TREK-1 ion-channel were expressed from the HEK cell line and imbedded in a similar lipid bilayer spread on top of the device. The PEDOT:PSS coated electrodes performed EIS measurements to monitor quantitatively of ligand-mediated TREK-1 interaction with arachidonic acid and spadin, that activate and suppress respectively the TREK-1 channel (see in Appendix)

This union of bioelectronic device with native mammalian-cell material is the first instance truly biomimetic membrane-functionalized. This platform overcomes several major challenges of current similar biological model. It overcomes: 1) the inability of non-native, reconstituted supported bilayers to replicate complex compositions representative of the plasma membrane surface, by using plasma membrane “biopsies” in the form of blebbed proteoliposomes that express the ion channel target. 2) the material mismatch between membranes and traditional sensor surfaces, by employing a hydrated polymer surface that preserves TMP mobility. 3) Limitations of traditional ion channel measurement platforms (e.g., patch clamp or black lipid membrane devices) for scale up processing in large array formats. Finally, 4) limitations in multi-modal information collection.

The bioelectronic chip enables direct electronic read-out of specific interactions taking place at the cell membrane related to key physiological events, while also allowing for conventional optical characterization. The ability to electrically discriminate between membrane compositions, the ability to readout small molecule interactions with these

membranes, and, for the first time, the ability to readout the activity of mammalian ion channels expressed within those membranes when subjected to changes in stimuli that alters their response, was shown. As ion channels and other TMPs represent an important class of targets for drugs to combat disease, the ability to scale up these devices, through lithography for the electronic components and self-assembly for the biological components, will be greatly beneficial. Rapid screening for active drugs against ion channels is a critical need for pain management, neurological disorders, etc. More fundamentally, many basic questions remain unanswered regarding how lipid-protein or protein-protein interactions lead to biophysical changes in TMP function and activity. Here, we offer a platform that can begin to get at the heart of these questions by using molecular biology tools to tailor the membrane compositions examined with these devices, opening a technology that is unmatched by any current platform for these kinds of studies.

Bibliography

1. Rivnay, J., Owens, R. M. & Malliaras, G. G. The rise of organic bioelectronics. *Chemistry of Materials* vol. 26 679–685 (2014).

2. Murbach, J. M. *et al.* In situ electrochemical polymerization of poly(3,4-ethylenedioxythiophene) (PEDOT) for peripheral nerve interfaces. *MRS Commun.* **8**, 1043–1049 (2018).

3. Barone, D. G. & Malliaras, G. G. Epidermal electrophysiology at scale. *Nature biomedical engineering* vol. 3 165–166 (2019).

4. Guide, T. A. *THE AXON GUIDE A Guide to Electrophysiology & Biophysics Laboratory Techniques*.

5. Dehail, P., Duclos, C. & Barat, M. Electrical stimulation and muscle strengthening. *Annales de Readaptation et de Medecine Physique* (2008) doi:10.1016/j.annrmp.2008.05.001.

6. J.E., T., J.D., G. 2nd. & G.H., B. The implantable pace-maker-cardioverter-defibrillator: radiographic aspects. *Radiographics* (1994).

7. Gehl, J. Electroporation: Theory and methods, perspectives for drug delivery, gene therapy and research. *Acta Physiol. Scand.* **177**, 437–447 (2003).

8. Zeglio, E., Rutz, A. L., Winkler, T. E., Malliaras, G. G. & Herland, A. Conjugated Polymers for Assessing and Controlling Biological Functions. *Advanced Materials* vol. 31 (2019).

9. Iandolo, D. *et al.* Development and Characterization of Organic Electronic Scaffolds for Bone Tissue Engineering. *Adv. Healthc. Mater.* **5**, 1505–1512 (2016).

10. Lacour, S. P. *et al.* Flexible and stretchable micro-electrodes for *in vitro* and in vivo neural interfaces. *Medical and Biological Engineering and Computing* vol. 48 945–954 (2010).

11. Lee, W. *et al.* Nonthrombogenic, stretchable, active multielectrode array for electroanatomical mapping. *Sci. Adv.* **4**, (2018).

12. Zhang, Y. *et al.* Supported Lipid Bilayer Assembly on PEDOT:PSS Films and Transistors.

Adv. Funct. Mater. **26**, 7304–7313 (2016).

13. Liu, H. Y. *et al.* Self-Assembly of Mammalian-Cell Membranes on Bioelectronic Devices with Functional Transmembrane Proteins. *Langmuir* **36**, 7325–7331 (2020).

14. Liu, H. Y., Chen, W. L., Ober, C. K. & Daniel, S. Biologically Complex Planar Cell Plasma Membranes Supported on Polyelectrolyte Cushions Enhance Transmembrane Protein Mobility and Retain Native Orientation. *Langmuir* (2018) doi:10.1021/acs.langmuir.7b02945.

15. Richards, M. J. *et al.* Membrane Protein Mobility and Orientation Preserved in Supported Bilayers Created Directly from Cell Plasma Membrane Blebs. *Langmuir* (2016) doi:10.1021/acs.langmuir.5b03415.

16. Liu, H. Y. *et al.* Supported Planar Mammalian Membranes as Models of in Vivo Cell Surface Architectures. *ACS Appl. Mater. Interfaces* (2017) doi:10.1021/acsami.7b07500.

17. Liu, H. Y., Chen, W. L., Ober, C. K. & Daniel, S. Biologically Complex Planar Cell Plasma Membranes Supported on Polyelectrolyte Cushions Enhance Transmembrane Protein Mobility and Retain Native Orientation. *Langmuir* **34**, 1061–1072 (2018).

18. Pappa, A.-M. *et al.* Optical and Electronic Ion Channel Monitoring from Native Human Membranes. *ACS Nano* acsnano.0c01330 (2020) doi:10.1021/acsnano.0c01330.

Chapter 5
Epithelial VS electrogenic cell application

Introduction

Merging biology and electronics promises tremendous development of novel therapy and diagnostic through bioelectronic devices[1]. Organ-on-chip models are now becoming more common in drug and toxicology assays[2]. As an example, the study of tissues interface *in vitro*[3] can be performed by Electrical impedance sensing (EIS), in addition to the optical methods traditionally used. Electrodes on transparent substrates and microscopes combined allows simultaneous recording of the biological events. OECTs are bringing advantages to this study on multiple aspects: they are biocompatible and mechanically matching the living tissues, but they are also transparent and amplify the signals locally[4].

What are electrogenic and non-electrogenic cells?

Electrogenic refers to the creation of a net flow of charge. In the biological field, this flow designates the ion flux inside and in between cells. Embedded in the cell membrane, ion channels, known as electrogenic pumps/channels, are creating this net flow of charges. We will define an electrogenic cell as a cell able to produce electrical activity via ion pumps. Non-electrogenic cells doesn't create electrical activity (via action potentials). Epithelial cell and muscle cell are respectively examples of non-electrogenic and electrogenic cells. While the first acts as an impermeable barrier, the second reacts to and produces electrical signals.

In this work, I investigate the use of bioelectronic devices *in vitro.* On one hand, biocompatibility and long-term electrical stability were performed on control devices immersed in cell culture media. On the other hand, electrical monitoring was performed to evaluate the two categories of cells. Firstly, I have monitored the growth of an epithelial cell barrier using OECTs. Placed in between the gate and the channel of the transistor, the cells

grow directly on the surface of the PEDOT:PSS. The barrier integrity is modeled as a resistance increasing as much as the cells close tight. Then, I have measured action potential from a nerve bundle placed over bioelectronic devices. Electrodes successfully detected the ion flux propagation from one axon of the bundle to the other.

Following characterization in PBS of the two matrix designs described in chapter 3, I have implemented, using the OECT matrix, a biological tissues model to validate the proper functioning of the device. The aim is to confirm the design and the fabrication protocol of the matrix structure. This experiment is based on previous work done by Ramuz et. al[5]: Madin-Darby canine kidney (MDCK) II cells were cultivated directly on the channels of transistors. An identical biological set up is applied on top of 2nd generation matrix system, comparing two organic patterning protocols: the etching and peel off technique. In the first section of this chapter, I demonstrate the efficiency and robustness of the peel-off protocol over the etching protocol, as the last one couldn't survive during the long-term biological experiment.

Finally, a second experiment using electrogenic cells was performed on the same matrix design, with the etching protocols to pattern the organic material. As previously suspected, the devices performances failed, and no measurement could be obtained neither from the OECTs, or the electrode. A second device made with a peel off technique and electrodes successfully recorded action potentials from the nerve bundle.

5.1 Non-electrogenic cells: epithelial barrier growth and disruption detection

Epithelial cells form tissues that allows organs and the whole body to interact with both its internal and external environment. They are held together by cell junctions. I will focus on tight junctions and gap junctions in this chapter. Tight junctions are occurring when transmembrane proteins (TMPs) strands fusing together between two cell membranes. An epithelial layer is the combination of epithelial cell held together by cells junction arranged in layers, more or less dense and tightly packed, as shown in Figure 52.

MDCK II are cells that can form an epithelial barrier *in vitro*. They form a confluent and dense cell layer in a couple of days[6]. The ionic permeability of the formed tissue decreases as the cell-junctions increase. To determine the barrier integrity, trans-epithelial electrical resistance (TEER) is characterized using electrochemical impedance measurements[7]. Cells were seeded on top of OECTs devices and an Ag/AgCl pellet was used on the media surface as gate. As the cells grow and form a barrier, its TEER increases, and the ionic current gets limited between the gate and the OECT channel as depicted in Figure 52. The drain current and resulting transconductance show a lower cut-off frequency as the epithelial barrier is forming over the transistor channel.

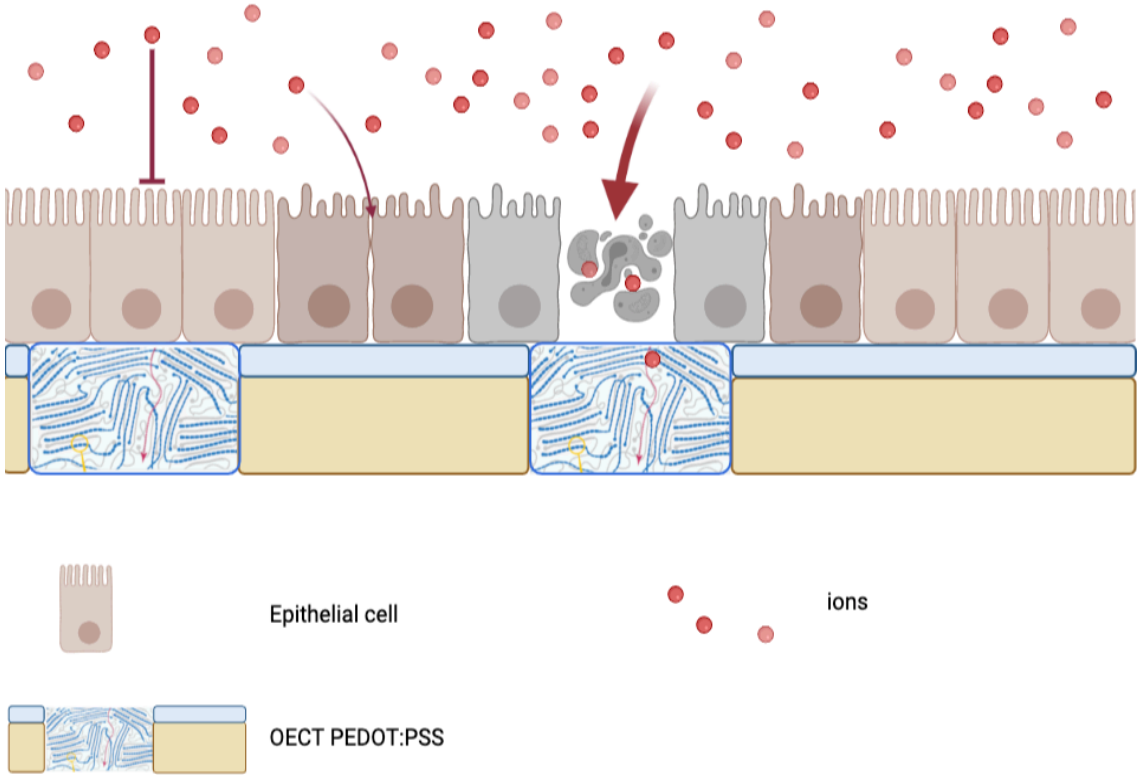

Figure 52: Electrophysiological model to study non electrogenic cell barrier. MDCK II cells are directly seeded on OECTs. When a voltage is applied to the gate in the upper media of the model, an ion flux in created toward the transistors. If the epithelial barrier integrity is not compromise, the ions cannot reach the OECTs. If the barrier is damaged, then ions penetrate the OECTs and modulate its transconductance.

Following the decision detailed in chapter 3 to dismiss the use of DE1 as insulating layer of the device, the new process involving PaC and organic etching were used. Two types of devices were then crafted following BEL and the etch technique processes, to compare efficiency of the new fabrication technique for long term *in vitro* experiment.

5.2 Electrogenic cells: Nerve-on-chip

The brain gives, processes, and receives information from and to the body: sensory and motor signals. They need to travel a long distance and rapidly. This is possible thanks to the nerve. Their structures support a fast propagation of the signals and protect the neuron fibers[8]. Nevertheless, little is known on the mechanism of nerve disruptions diseases, or degeneration and reparation of the neurons, despite the many tragic outcomes that might come from it[9]. Electrophysiology on the peripheral nerve system (PNS) is a field developed since 1952[10] to study the propagation of action potentials (AP), and understand the functions and properties of the neurons and their structure. Recently, bioelectronic studies have spread the use of electrodes and MEAs to understand and treat PNS disorders[1], *in vitro*[11] or *in vivo*[12]. Organic materials newly investigated[12] in the fabrication of MEAs allow a better interface with the PNS.

Neurons can integrate and propagate electrical signals. In the peripheral nervous system (PNS), nerve structure gathers bundles of axon in the connective tissue named endoneurium. Assembled in fascicles, they are wrapped in a protective sheath called perineurium. Themselves can be grouped in the epineurium, the outermost layer of the nerve structure in the PNS. Nerve from the PNS serve two function:

1. sensory conduct from receptors to central nervous system (CNS), or in between organs called afferent nerve
2. motor function, called efferent nerves, guiding signals from the CNS to muscles

The electrical signals conveyed through the body are based on electrochemical impulses called action potentials (AP). Their speed can reach 120m/s alongside axons. To achieve such speeds, the peripheral nerve axons possess a myelin sheath, made from Schwann cells. Similar to oligodendrites in the brain, they provide support and protection to the axons. Additionally, they insulate the axon fibers by sections, resulting in the transmembrane current only occurs at the node of Ranvier, creating the saltatory conduction. Instead of travelling all along the unmyelinated axon, the action potentials jump from node to node, where sodium channels are grouped, accelerating the impulse propagation. To study these signals and diagnose disorders in the PNS, physical examination can be performed. Otherwise, more in-depth

imaging technique such as magnetic resonance neurography or ultrasonography allows studies of structure of the nerve[13]. Electrophysiology assays of the PNS recording the compound action potentials (CAP)[14], or a single AP propagation, from the nerve *in vitro* or *in vivo*, are a new method to study the function of the nerve. However, as described above, the structure of nerves of the PNS is extremely complex and difficult to reproduce *in vitro*. Co-culture of dorsal root ganglion and Schwann cells are usually standard and efficient models. For *in vitro* assays, monitoring is generally optical and achieved through microscopes.

In this work, a nerve-on-a-chip platform was constructed as shown schematically in Figure 53, and a biological experiment to follow the propagation of an AP from a myelinated axon using an OMEA was developed. Similar to the *in vitro* and *in vivo* work previously published on OECTs for AP detection of epilepsy on the cortex[15,16], this model was designed to prove the same property of OECT to detect and amplify the signal from a motor neuron of the peripheral nervous system.

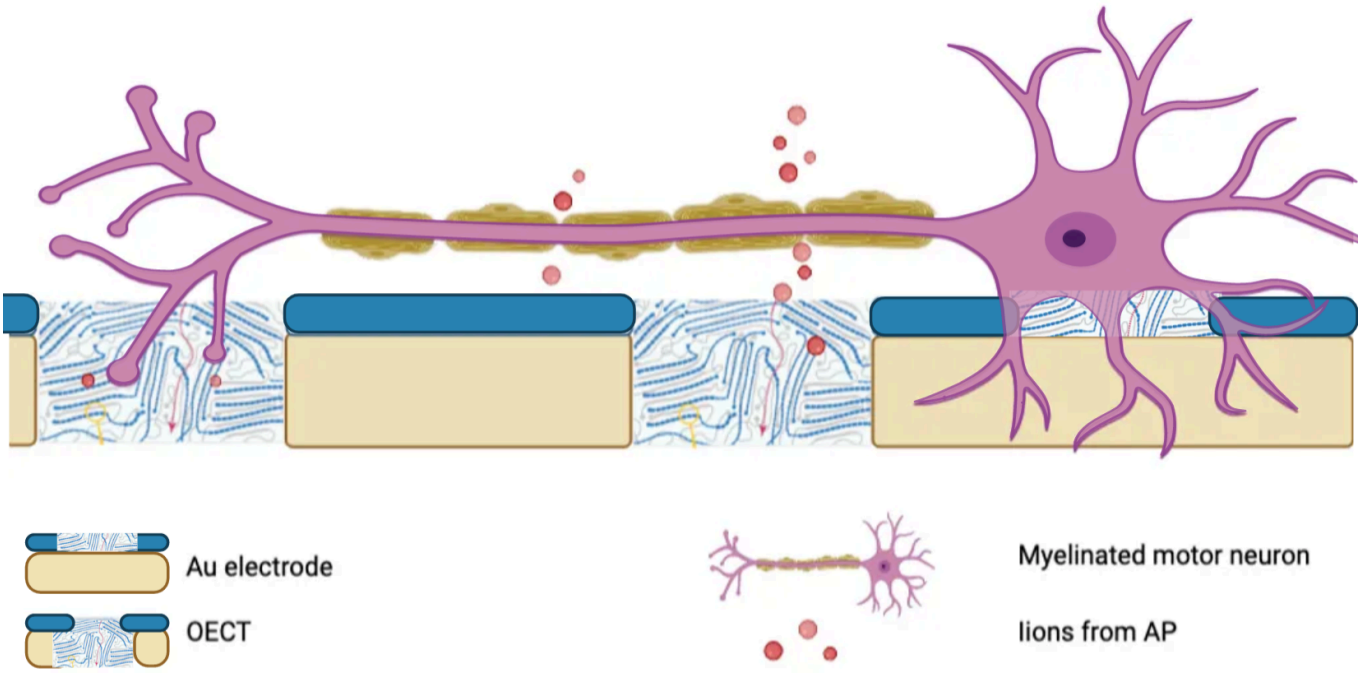

Figure 53: Electrophysiological simplified model to study action potential propagation. OECTs are placed beneath myelinated axons and a 1.5mm diameter electrode is placed under the bulb of the motor neurons. The OECT should be able to monitor the propagation of the AP alongside the axon, by detecting the ion flux gradient impacting the PEDOT:PSS channel conductivity.

We have adjusted our experiment from the biological model published by Dr. Sharma, A. D. *et a*[17]. The previous experiment on MDCK II indicates a good behavior of the matrix stack, the same protocol using the etching technique for organic was reiterated, with Panaxium's team fabricating the device batch in CR. Once more the inefficiency of the etching procedure for organic patterning and obtained results from a different OMEAs made of electrodes with peel-off technique for PEDOT: PSS dispositions was demonstrated.

Here, a nerve-on-chip model is used to follow the propagation of an AP from a myelinated axon *in vitro*. A co-culture of human motor neuron and Schwann cells are seeded to form a spheroid. Then, they are inserted into a PDMS mold to functionalize into axons and myelin sheath. This 3D biological model was deposited onto an OMEA in a matrix design as shown Figure 54. OECTs are integrated to follow AP alongside the growing nerve. This nerve-on-chip structure allows simultaneous optical and electrical monitoring of the biological structure. Indeed, made on glass or Parylene substrate, the OMEAs provide transparency over OECTs.

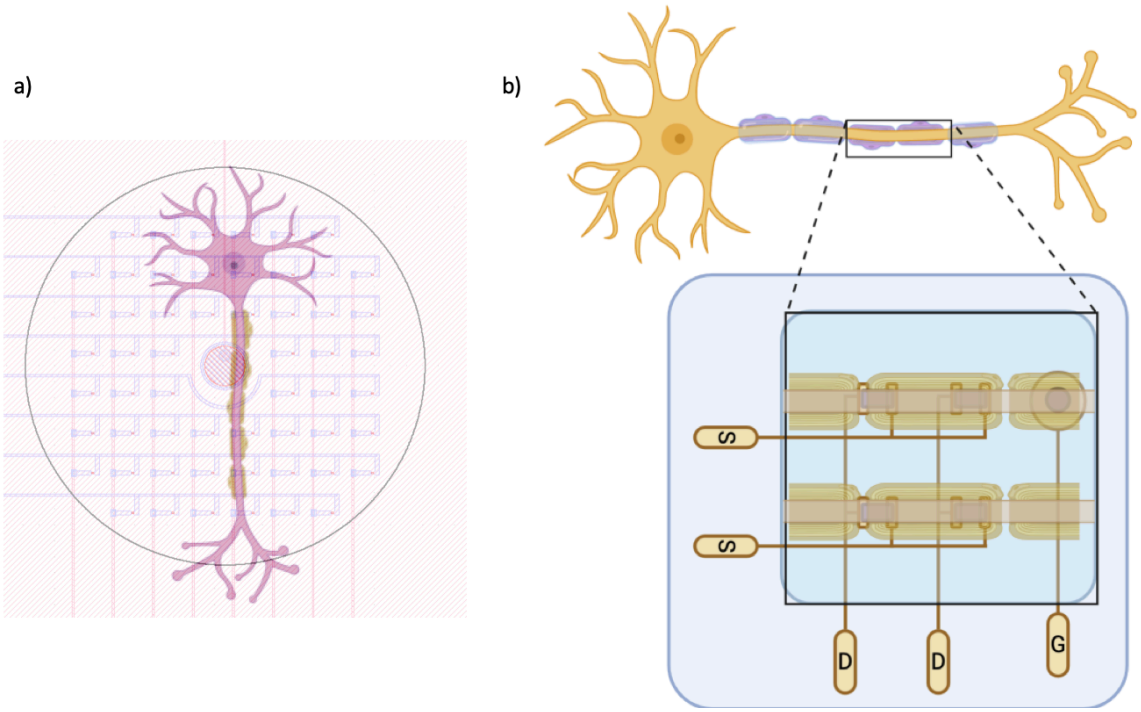

Figure 54: Scheme of the biological experiment. a) myelinated nerve growth over matrix device. b) section of myelinated fibers covering the OECTs and electrode from the device

5.3 Material and methods

5.3.1 Epithelial barrier experiment: MDCK II

To confirm the new matrix multi-stack protocol, and the etching process for organic patterning, the experiment follows previous publication and methodologies developed and usually applied at the BEL and BEST laboratories[18].

Device fabrication, measurement set up and biological model

Industrial Process: etching technique

The fabrication protocol relies on a four stacks layer step. First, a layer of 3μm thick Parylene C was added via chemical vapor deposition on top of the wafer. Then, 150nm thick Cr/Au electrodes were patterned using photolithography with AZnLof 2070 as the lift-off resist. Another layer of Parylene C 2μm thickness was added with silane A74 to improve adhesion. The openings were made through reactive ions etching (CF4 & O2) over Az 15nXt patterned as protecting layer. PEDOT:PSS solution, Clevios PH1000 containing 5 vol% ethylene glycol and 1 vol% (3-glycidyloxypropyl) trimethyoxysilane was spin-coated at 1500 rpm for 90 seconds, baked on a hotplate at 130 ºC for 1 hour and dry etched using orthogonal resist 5011 as protective mask.

Laboratory process: Peel-off technique

Like the industrial protocol, up until the second deposition of Cr/Au layer patterning, a second and third layer of PaC was deposited over the device, separated by a thin layer of 2% soap solution. The two layers were then patterned using Az10Xt under photolithographic patterning. Then, the same PEDOT:PSS solution was spin-coated and soft baked for one minute at 110°C on a hot plate. Finally, the sacrificial third layer of PaC was peeled-off, and the device hard-baked in the oven at 110°C for 30 minutes.

Glass wells were stuck on the matrix with PDMS, and sterilization was done in ethanol bath under the biological hood. To maintain a sterile environment as much as possible, electrical cables were cleaned and inserted into the in the hood and not moved, as well as

pogo pins holder and the Ag/AgCl gate. The NI system was placed next to the hood to facilitate recording of the device. Electrical characterization was performed once more in the set up to ensure their electrical behavior before seeding cells

MDCK II cells seeding

Madin-Darby canine kidney cells II were cultured in DMEM low glucose media supplemented with 10% of fetal bovine serum, 430 mg/mL glutamine, 50 U/mL of penicillin, 50 µg/mL of streptomycin and 50 µg/mL of gentamicin. These products were purchased from Invitrogen. The cells were incubated in a humidified atmosphere at 37 °C and 5% CO_2. MDCK II cells were seeded at 5×10^4 cell/cm^2 in each well and growing for three days to obtain an epithelial monolayer. The media was replaced every two days.

5.3.2 Nerve-on-chip

Human Schwann cell (hSCs) culture

Container Preparation

A solution of 0,01% poly-L-ornithine (A-004-M, Sigma) in sterile water was mixed and used to cover the surface of a cell culture flasks. After one hour of incubation at 37°C, the solution was removed, and the flask was washed four times with sterile water. Then, 7.5mL of 10ug/mL laminin solution in PBS was added into the flask and stored at 4°C overnight. Specific medium was prepared by mixing 500 mL of Schwann cell basal medium, 25mL of Fetal bovine serum, 5mL of Schwann cell growth supplement and 5mL of penicillin/streptomycin solution (Kit P60123, Innoprot). The laminin was removed, and 15 mL of culture medium equilibrate at 37°C is added to the container before plating.

hSCs plating

The frozen hSCs (cat# 10HR-188, iXCells Biotechnologies) vial from Fujifilm was thrown in the water bath two minutes at 37°C to defrost and added to flask. The culture was left undisturbed in incubation at 37°C for minimum 16 hours. Then, medium media was changed every 24 hours until cell passage.

Passaging cell

When 80% of confluence was reached, media was removed, and cells were rinsed with 10mL of PBS. Then, 3mL of Trypsin EDTA were added and cells were incubated at 37°C for 3 minutes. When detached, 8mL of hSCs medium was added, and the total volume was transferred to a 50mL falcon tube. The tube was centrifuged at 200g 5 minutes at room temperature (22°C). The supernatant was discarded, and the pellet was resuspended in 1mL of hSCs culture medium. Cells are then added in a new flask coated with 10mL of fresh medium.

Human Motor Neuron (hMNs) culture

Medium preparation

The medium for hMNs was mixed from a kit sold by Fujifilm: 100mL of iCell Base medium (#C1050) + 2mL of iCell Neural supplement A (#M1032) + 1mL of Nervous supplement B (M1031). The medium was warmed at room temperature and 1mL was added in a 50mL falcon tube.

hMNs thawing

1mL of hMNs medium is added in a 50 mL Falcon tube. The hMNs frozen vial was warmed 2 minutes 30 seconds in water bath at 37°C, and the totality transferred to the 50mL falcon tube containing medium, dropwise with a swirling motion to minimize osmotic shock. The vial was rinsed with 1mL of hMNs medium and transferred to the falcon tube. The total volume was then adjusted to 10mL by slowly adding hMNs medium dropwise while swirling. The solution was transferred to a 15mL falcon tube and centrifuged at 200g for 5minutes at room temperature. The supernatant was removed, and the pellet resuspended in 1mL of hMNs medium.

Spheroid's elaboration

Well plate + agarose

To create spheroids, a solution of 1% (w/v) agarose (Sigma Aldrich) in deionized water was prepared and autoclaved. After heating the solution for one minute in a microwave, 75 uL were added to each well of a 96 well plate. It forms a meniscus on the bottom of the well. After 10 minutes at room temperature, the cool downed agarose forms a non-adherent round bottom well.

Co-culture assembly

75 000 Cells of hSCs and 75 000 hMNs cells were mixed and added in each well filled with 200 uL hMNs media. Cells were incubated at 37°C and half of the media is changed every 48 hours. Spheroids were forming around the 3rd day of co-culture in the well plate.

Cell restrictive mold / environment

Using Solidworks CAD, a specific PDMS mold was created to contain cells and was inspired from the original publication. Initially, a solid plastic reproduction mold was extruded. Then, PDMS 1:10 was mixed, and centrifuged at 3000rpm for two minutes. Once the bubbles are cleared, the preparation was poured into the mold and cured on a hot plate at 60°C for four hours. The PDMS mold was then extracted from the reproductive mold.

5.4 Results

5.4.1 MDCK II barrier formation over OECTs

The characterization done in the biological hood confirms the pre-measurement carried out in the electrical lab. The 60 OECTs incorporated in the matrix design were performed identically as two weeks before. Then, media and cells were seeded, and a second measurement was done the same day.

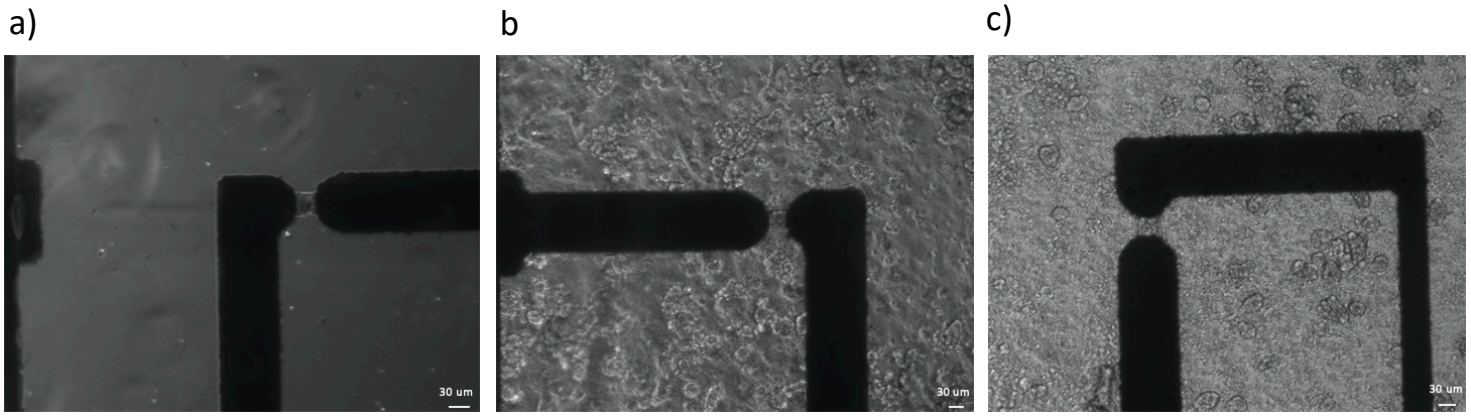

Figure 55 : MDCK II seeding over OECTs matrix device microscope pictures. a) device control before cell seeding. b) device using peel off technique day 5 post seeding c) device using etching technique day 3 post seeding. The epithelial barrier was fully developed and pack at day 5.

Two days after seeding, pictures b in Figure 55, OECTs and matrix devices made using etching protocol for organics start to deteriorate. As shown in Figure 56, some area where MDCK II are forming a dense epithelial barrier are detected by the OECTs located beneath, decreasing their cut-off frequency.

Transistors perform almost identically, without noticeable changes in their electrical behavior as expressed by the bandwidth seen in Figure 56 b1) and c1). It is worth noticing that the contact pads are being scratched (shown in supplementary figure). The metal is ripped off the surface as much as the pogo pings are placed and removed upon them alongside the multiple measurements.

Three days into post seeding, OECTs from the etching process did not show any sign of conductivity in their channel, thus being unable to perform electrical characterization of the epithelial barrier formation. The conductivity between source and drain ids decreasing, and more noise appears during recording as seen in Figure 57 f). The OECTs made from peel off technique are still performing well as seen Figure 56 C2) and Figure 57 c). The decrease of cut-off frequencies during day 2 and 4 shows the monitoring of the MDCK II barrier development over the channels.

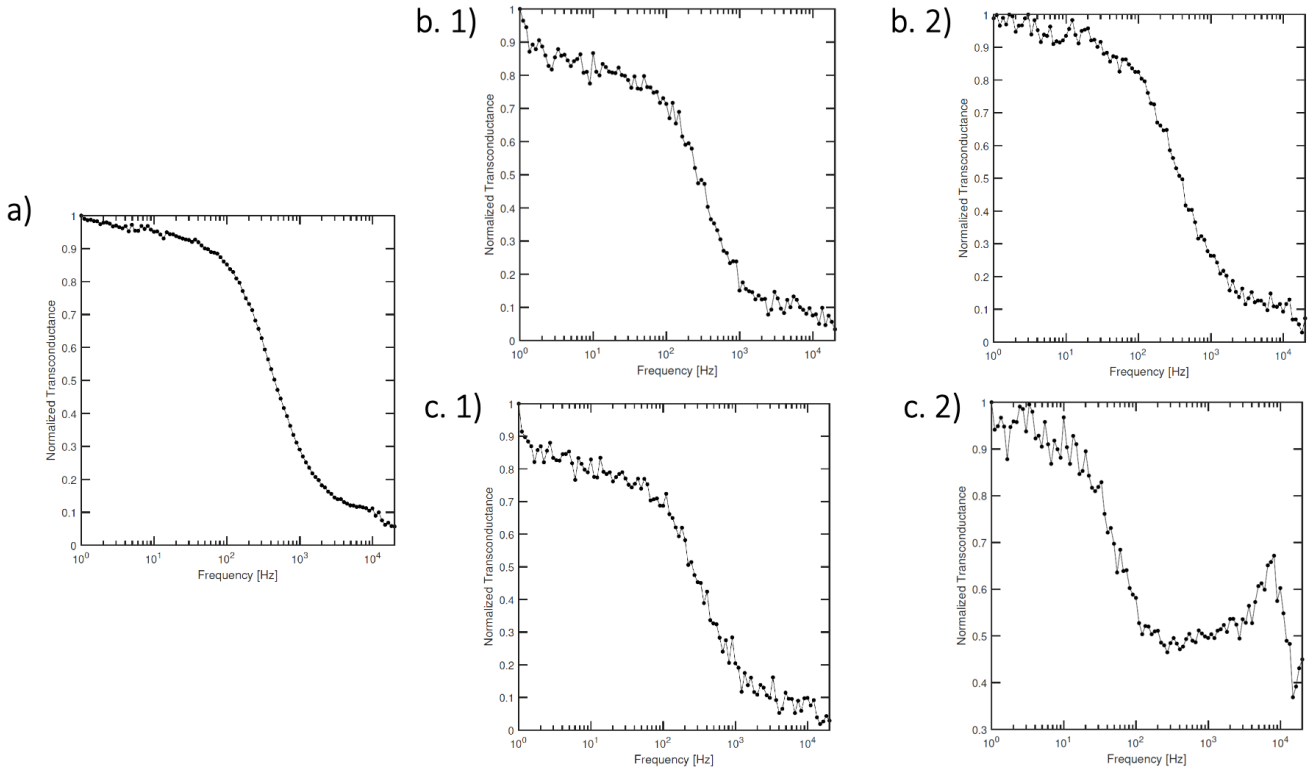

Figure 56 : Comparison of two OECTs from the same matrix made using the peel off technique. a) shows the OECT cut off frequency characterized in media at day 0. b1) OECT A and c1) OECT B cut off frequencies at day 1 after cell seeding. At day 4, b2) displays the cut off frequency of the OECT A, that is not covered by cells, and C2) displays the decreased cut off frequency of the OECT B covered by epithelial cell. The bandwidths differences show that the presence or not of the cell barrier coverage is detected by the matrix of OECTs.

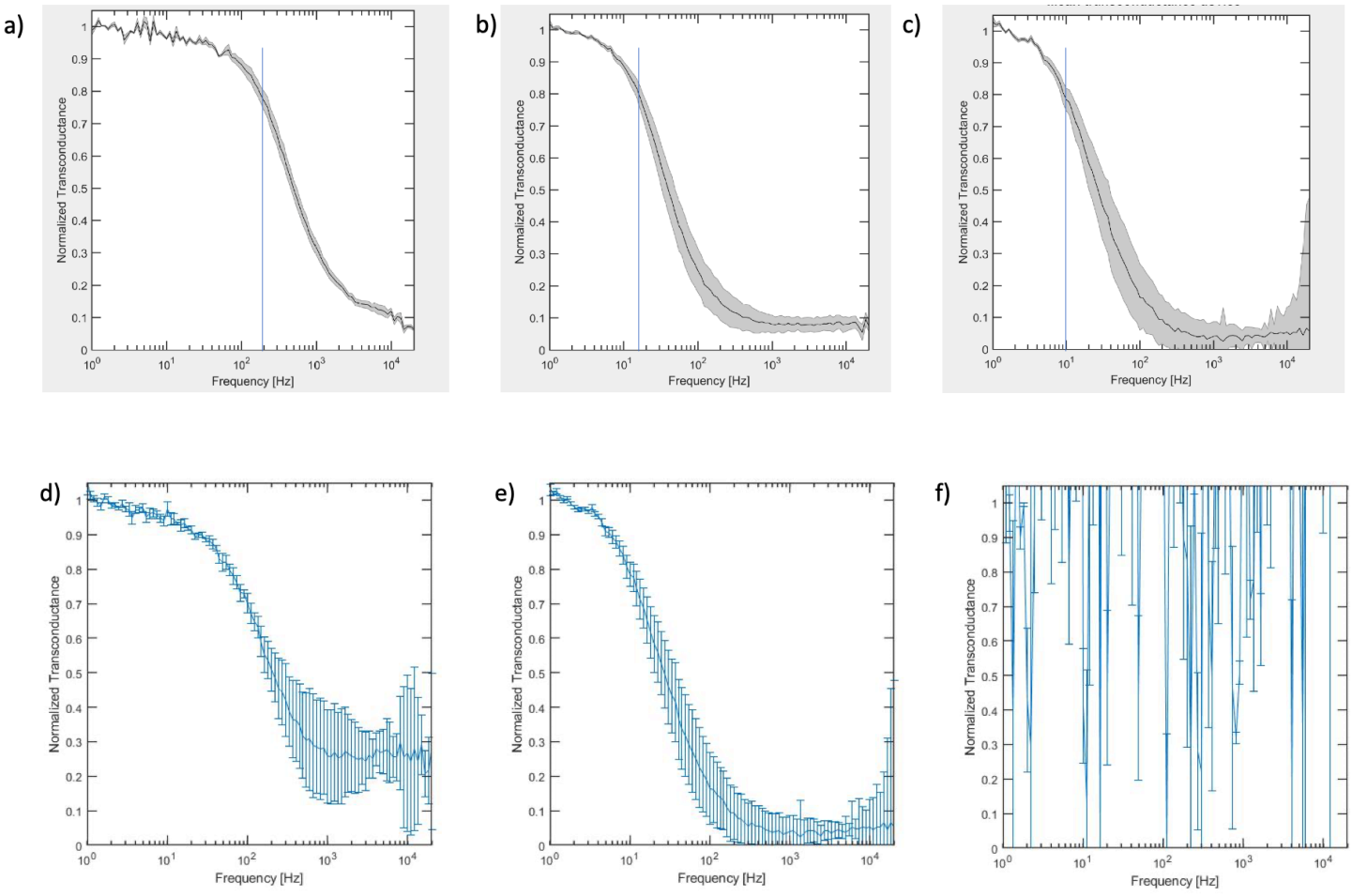

Figure 57: Mean and Normalized transconductance curve from devices used. a) evolution of the mean transconductance of the 60 OECTs from a peel off device over time. The cut-off frequency decreasing is significant of the epithelial barrier forming over the matrix b) 2 days c) 4days. Results from characterization and comparison between processes. d) control devices from the experience compared to devices e) peel-off and f) etching bandwidths.

5.4.2 Nerve on chip

Device fabrication

The device design and protocol chosen for this experiment is the matrix made of 60 transistors and 1 central electrode. The fabrication protocol is based on the multilayer stack developed for matrix designs, and the organic is etched following the etching protocol described in Figure 58 b. For this experiment, the batch was produced and characterized thanks to the Panaxium team. To fit the 3D cell structure size and geometry, the design had to incorporate a dense number of transistors and recording site. The device contains 60 electrodes in a 1cm diameter disc, as shown in Figure 58 c. The aim of the experiment is to follow the propagation of an AP alongside the myelinated motor neuron. The cells fibers are directed in the PDMS mold and should grow a tube shape. OECTs should be align beneath and track the propagation. The central electrode would be use as the AP trigger and stimulate at the bulb/spheroid structure.

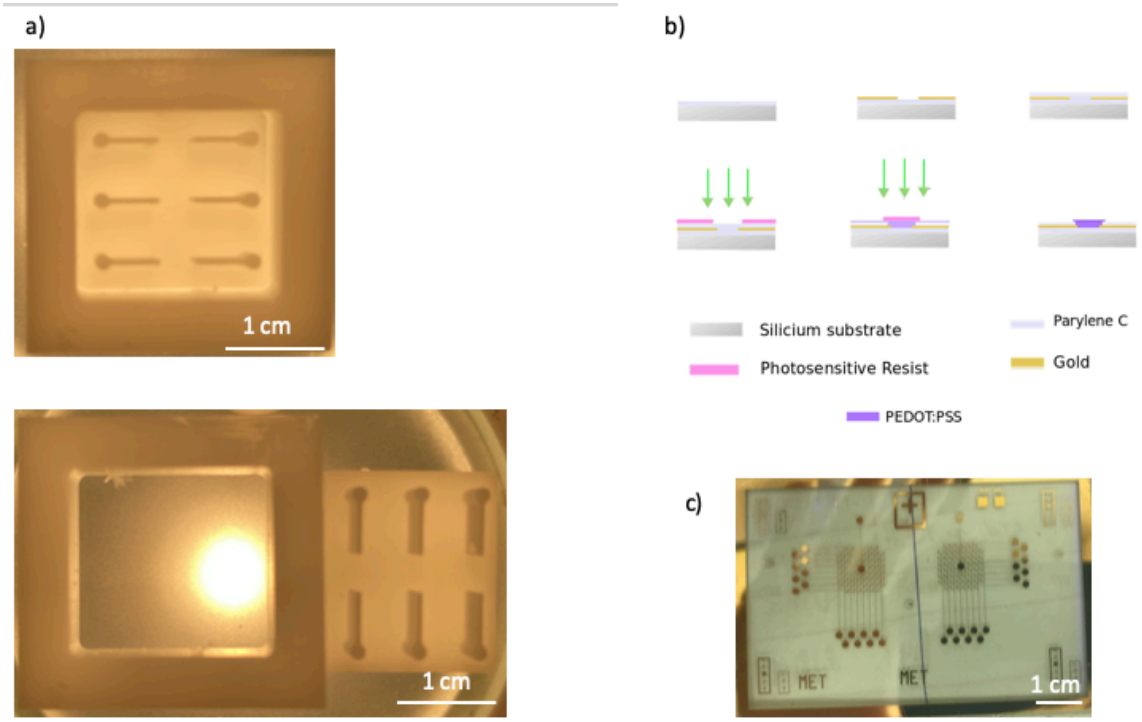

Figure 58: different structures used for the NoC. a) The primary mold is used to create the PDMS structure that holds the cells growth in Matrigel and Media. b) Scheme of a simplified fabrication protocol to pattern the organic material using the etching technique. c) Picture of the bioelectronic OECT matrix device used as a substrate for the NOC experiment.

Structure assembly

Cell restrictive environment to MEA assembly and sterilization

The PDMS molds were stuck on the matrix device using a thin layer of fresh PDMS. They were aligned on the OECTs and central electrode as seen in Figure 59 a. Glass wells were attached around the mold and on top of the device. They were fixed using again fresh PDMS as depicted in Figure 59 b. The assembly was then washed three times for 10 minutes with 2% antibiotic/antimycotic wash buffer (10 000u/mL penicillin + 10 000 μg/mL strep + 25 μg/mL Fungizone Gibco).

Matrigel and spheroids seeding

Once the spheroids were formed, they were implanted in the PDMS mold, at the bulb section. The Matrigel stored at -20°C was defrosted slowly in an ice bucket. When reaching 0°C, the Matrigel starts to liquify, and can be inserted into the mold over the spheroids. The devices were then incubated for 5 minutes at 37°C to let the Matrigel polymerize. Thereafter, 200 μL of media was added to the well for the motor neuron to develop.

During the first week, cells are cultured in Pre-myelination co-culture medium, allowing the motor neuron to develop and the neurites to grow alongside the mold. The pre-myelination media comprises a mix of hNs Medium with 10% Hyclone FBS and 1%Antibiotic/Antimycotic wash buffer (12389802, Fisher Scientific). The medium is changed every 48 hours.

Then for three weeks, the medium was replaced by myelination co-culture medium. It allows the SCs to differentiate and aggregate on around the MN already developed as seen in Figure 59c. The myelination co-culture medium is a mix of 10% Hyclone FBS (12389802, Fisher Scientific), 10ng/mL of rat-b-NGF (#7815-NG-025, R&D systems), and 50ug/mL of L-ascorbic acid (A92902, Sigma). Half of the myelination medium changed every 48 hours.

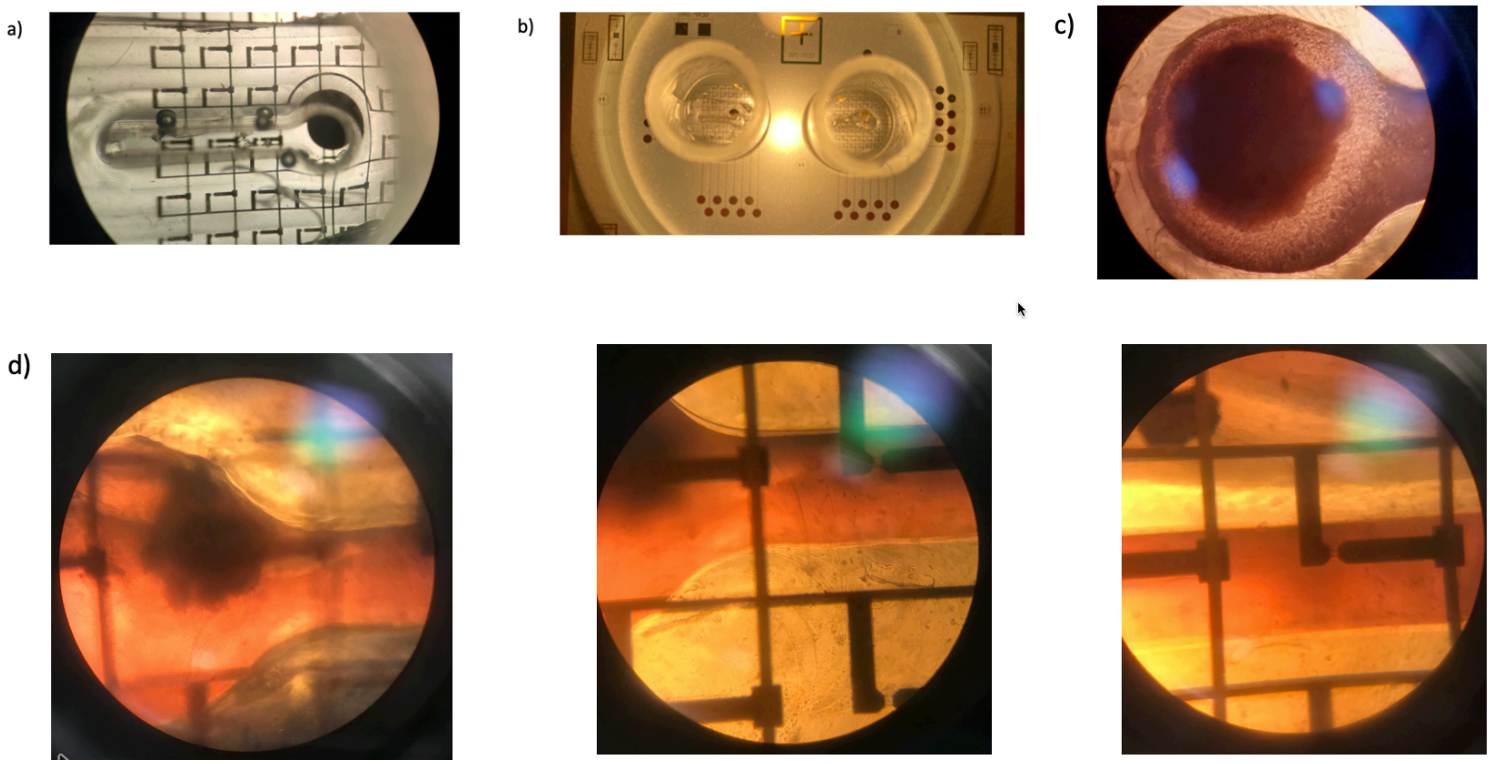

Figure 59: Assembly of the Nerve-on-chip. a) PDMS mold aligned to the matrix for the electrode to be in the bulb section and the OECTs in the axon's growth axe. b) complete device. Two parts are used, one for the NoC and the other for the control. c) Microscope pictures of the spheroids seeded in the bulb section embedded in Matrigel in control sample cultivated in Transwell. d) Developped nerve bundle on top of the matrix devices after 3 weeks of culture in Matrigel and Media

As shown in Figure 60, the biological co-culture developed inside the PDMS Matrigel. The presence of a Transwell or a bioelectronic device beneath didn't seemed to interfere with the cell biological development. The motor neuron as well as the Schwann cell migrated inside the tube section and began to differentiate.

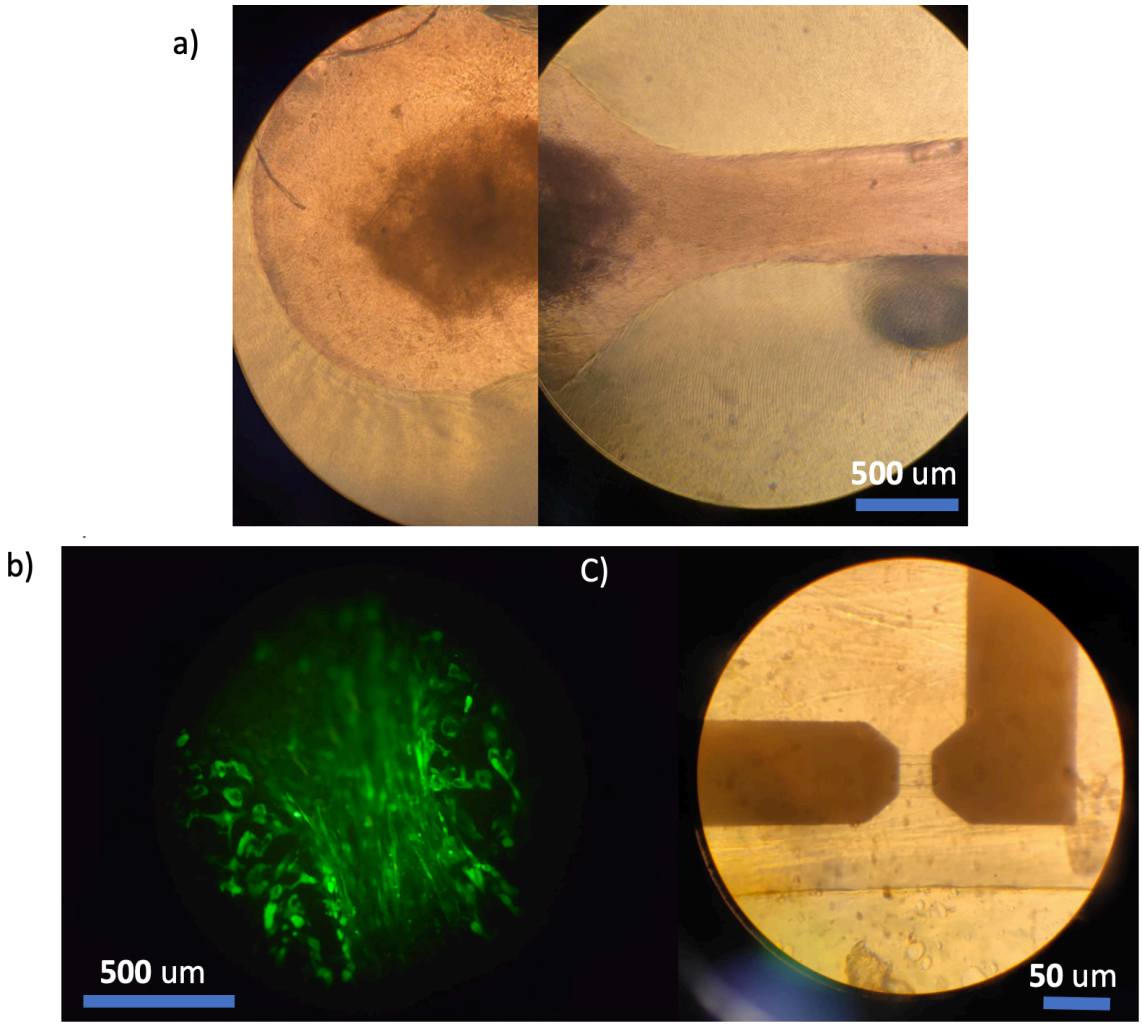

Figure 60 : Nerve-on-chip cells culture growth 20 days after the spheroid seeding. a) Control cell model. The PDMS mold and its spheroids are placed inside a Transwell. The bulb developed multiple neurites that spreads inside the tube section of the mold. b) Fluorescent microscope image of the coculture bundle at day 12. Schwann cells starts to migrate alongside the axons. c) Microscope pictures of a neurite growing on top of the OECT channel.

No electrical recording was performed using the matrix device. The drain current dropped in a similar way than the MDCK II experiment. This issue questions the performance of the etched devices to monitor long-term biological experiment. To validate the biological model, we have decided to use external MEA to record and stimulate the nerve. These electrodes were produced following the BEL fabrication protocol involving peel-off technique patterning for the PEDOT:PSS. The device contains 10 electrodes of 50 µm diameter spaced by 150 µm in a rectangular geometry shown in the Figure 61.

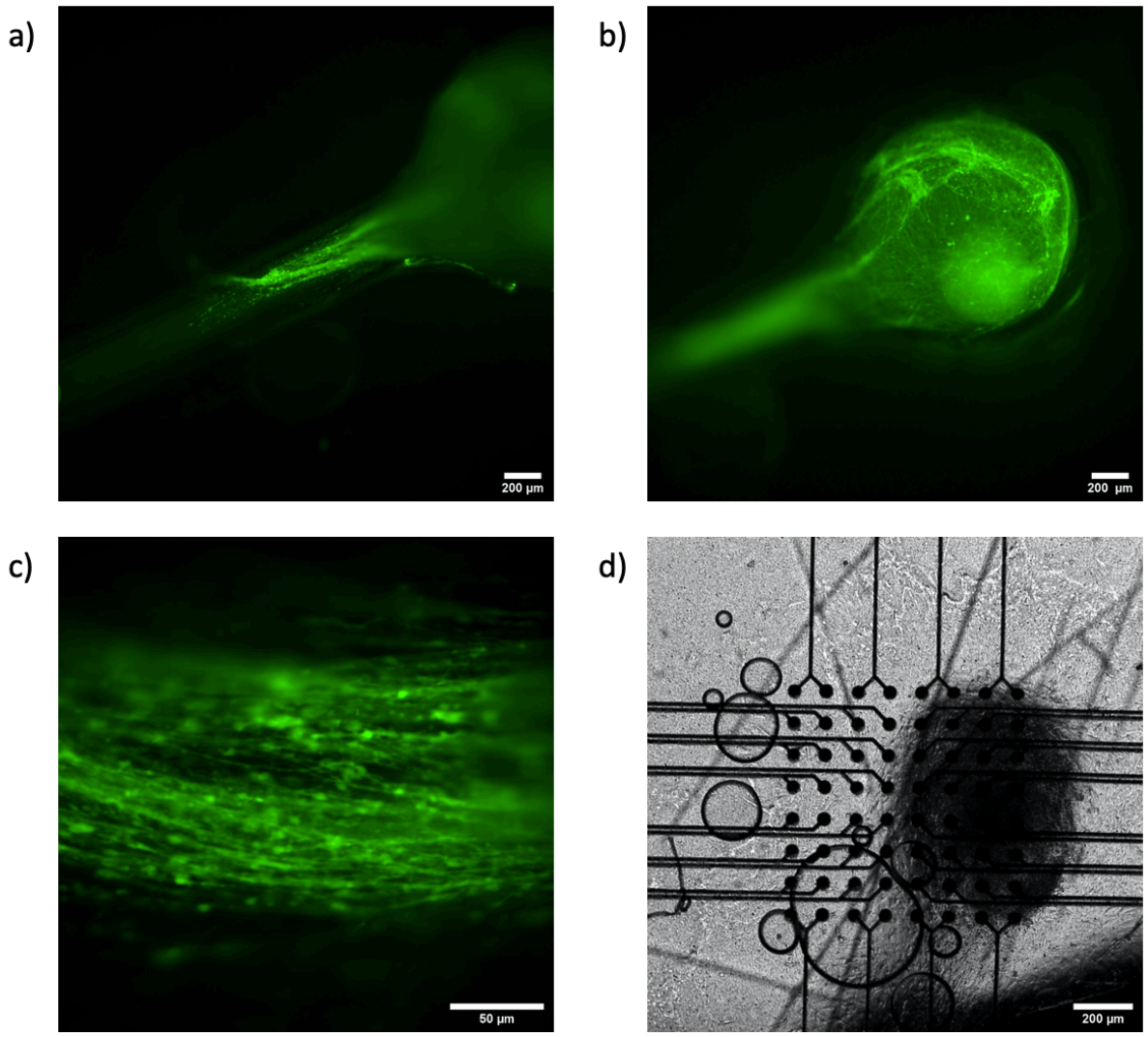

Figure 61. NoC images obtained from a fluorescence microscope. Calceïne AM (viability marker) was added to the biological marker for the microscope to detect the 3D structures. a), b) and c) are pictures from a control biological model inside the PDMS mold. At diffent scale, the 3D structures of the nerve bundles show the differentiation of the Motor neuron into axons, and the Schwann cell migration. d) is a pictures of the control NoC deposited on the OMEAs

In the Figure 62, we used the following parameters: one electrode (B10) was used to stimulate the bundle with 5 μA for 100μs. The recording was performed using the 9 other electrodes.

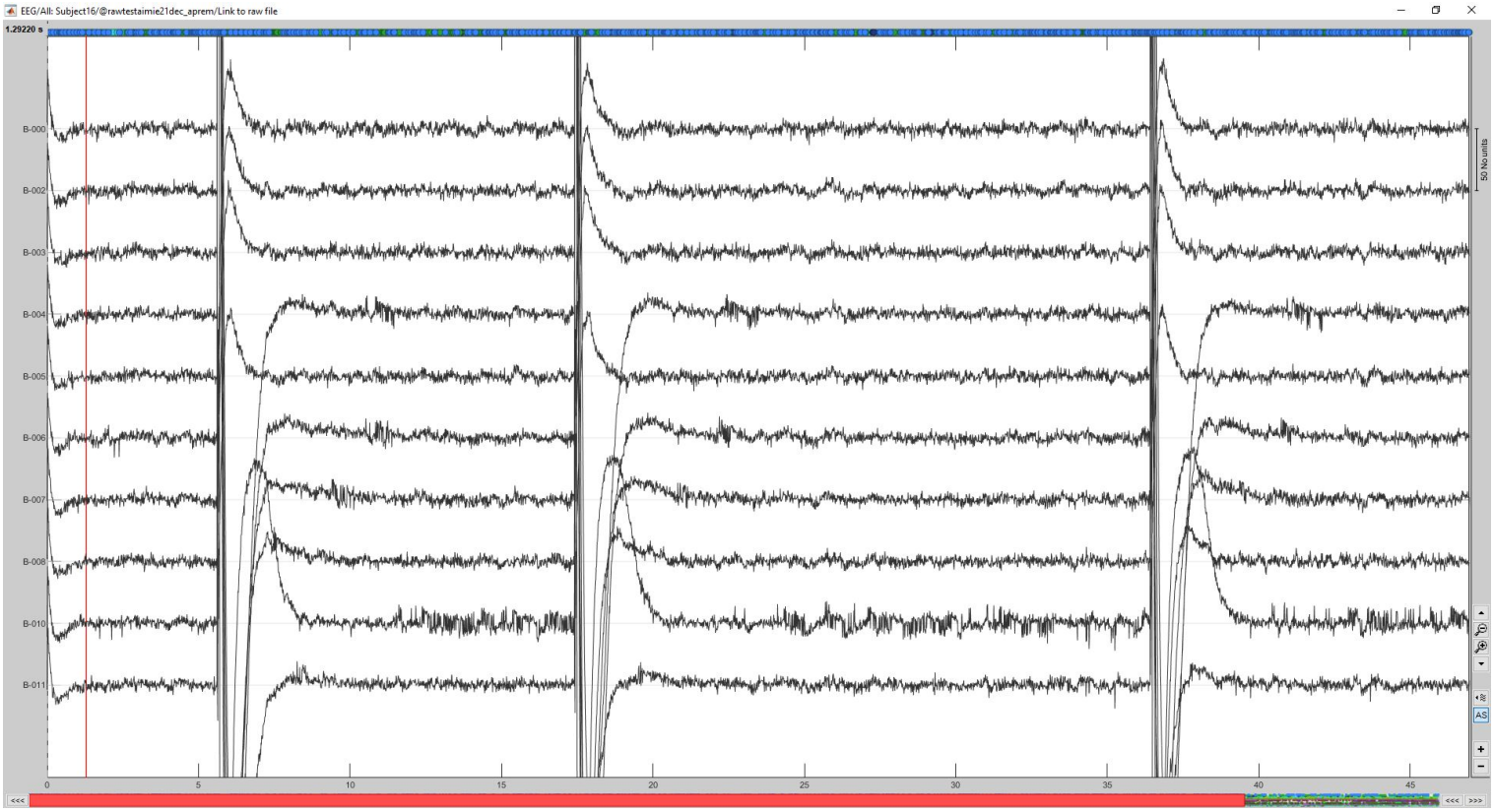

Figure 62: Brainstorm software plotting the electrodes stimulation and recording simultaneously.

Three stimulation were manually triggered from the electrode B10. Artefacts are seen on the 10 channels depicted in the Figure 62. A pattern is expressed sequentially with an offset on each electrode monitoring channel. This could be the expression of the signals input travelling from B10 electrode through the nerve bundle, to the other electrodes.

5.5 Conclusion

The epithelial barrier experiment was repeated two times: firstly, in Cambridge BEST laboratory, and secondly at the BEL laboratory from Gardanne. The devices used where made from the same batch at the Centre de Microélectronique de Provence's clean room. The results obtained delivered two conclusions:

1. The matrix multi-layer fabrication protocol is effective, and performs well over a week-long *in vitro* experiment
2. The etching technique to pattern organic shows a defect in the device lifetime for long term monitoring

The nerve-on-chip experiment confirms this hypothesis. The OECT matrix devices used for the experiment were produced using the etching fabrication protocol. They failed similarly to the one used in the MDCK II experiment made using the same process. Nevertheless, the biological model was a success. Thanks to the extra MEAs used to process the stimulation and the recording, we have shown that the nerve bundle was producing electrophysiological activity upon stimulation.

OECTs have previously shown promising results as a tool to study epithelial barrier formation and disruption. When cells are directly seeded over its surface, it has delivered two main advantages: its transparency for optical monitoring, and its simultaneous electrical recording of barrier formation and disruption. To map the whole forming barrier and its potential local disruption, the matrix disposition allows a higher density of OECTs recording sites. We have demonstrated the efficiency of the microfabricated structure overlaying multi-stack of PaC and metallic lines layers. Plus, we had shown that adding an organic layer patterning over the multi-stack was possible when the peel-off technique was used. Unfortunately, the etching step to pattern PEDOT:PSS over the multi-stack requires further investigation to improve the lifetime of the device.

Considering the multiple fabrication issues during etching steps, such as the presence of PEDOT:PSS residues, unusual behavior from the machines was initially suspected. From the fabrication step, the Az 15 nXt resist residues from the etching step of the PaC were firstly

shown and corrected during an isolated test. Secondly, PEDOT:PSS residues over the surface devices were popping irregularly depending on the batches fabricated in the cleanroom.

Bibliography

1. Chen, R., Canales, A. & Anikeeva, P. Neural recording and modulation technologies. *Nat. Rev. Mater.* **2**, 1–16 (2017).
2. Zhang, B., Korolj, A., Lai, B. F. L. & Radisic, M. Advances in organ-on-a-chip engineering. *Nat. Rev. Mater.* **3**, 257–278 (2018).
3. Antfolk, M. & Jensen, K. B. A bioengineering perspective on modelling the intestinal epithelial physiology *in vitro*. *Nat. Commun.* **11**, (2020).
4. Rivnay, J. *et al.* Organic electrochemical transistors. *Nature Reviews Materials* vol. 3 (2018).
5. Ramuz, M. *et al.* Combined Optical and Electronic Sensing of Epithelial Cells Using Planar Organic Transistors. *Adv. Mater.* **26**, 7083–7090 (2014).
6. Rivnay, J. *et al.* Organic electrochemical transistors for cell-based impedance sensing. *Appl. Phys. Lett.* **106**, (2015).
7. Ramuz, M. *et al.* Optimization of a planar all-polymer transistor for characterization of barrier tissue. *ChemPhysChem* **16**, 1210–1216 (2015).
8. Mahar, M. & Cavalli, V. Intrinsic mechanisms of neuronal axon regeneration. *Nat. Rev. Neurosci.* **19**, 323–337 (2018).
9. Holmes, D. Repairing the neural highway. *Nature* **552**, S50–S51 (2017).
10. Grayson, D. R. Laboratory of molecular neurobiology (1988-1994). *Pharmacol. Res.* **64**, 339–343 (2011).
11. Gribi, S., du Bois de Dunilac, S., Ghezzi, D. & Lacour, S. P. A microfabricated nerve-on-a-chip platform for rapid assessment of neural conduction in explanted peripheral nerve fibers. *Nat. Commun.* **9**, 1–10 (2018).
12. Murbach, J. M. *et al.* In situ electrochemical polymerization of poly(3,4-ethylenedioxythiophene) (PEDOT) for peripheral nerve interfaces. *MRS Commun.* **8**, 1043–1049 (2018).
13. Gasparotti, R., Padua, L., Briani, C. & Lauria, G. New technologies for the assessment of neuropathies. *Nat. Rev. Neurol.* **13**, 203–216 (2017).
14. González-González, M. A. *et al.* Thin Film Multi-Electrode Softening Cuffs for Selective Neuromodulation. *Sci. Rep.* **8**, 1–15 (2018).
15. Khodagholy, D. *et al.* High transconductance organic electrochemical transistors. *Nat. Commun.* **4**, 1–6 (2013).
16. Khodagholy, D. *et al.* NeuroGrid: Recording action potentials from the surface of the brain. *Nat. Neurosci.* **18**, 310–315 (2015).
17. Sharma, A. D. *et al.* Engineering a 3D functional human peripheral nerve *in vitro* using the Nerve-on-a-Chip platform. *Sci. Rep.* **9**, 1–12 (2019).
18. Strakosas, X., Bongo, M. & Owens, R. M. The organic electrochemical transistor for biological applications. *J. Appl. Polym. Sci.* **132**, 1–14 (2015).

Conclusion

In vitro testing is essential to treatment development and innovation in pharmacology. To improve their predictivity and accuracy, involved biological models are developed into more complex structures, thus becoming closer to the *in vivo* system they intend to reproduce. However, the foremost blocking parameters to the understanding of biology relies on the limited technique of observations and analysis available for *in vitro* experiments. Indeed, most monitoring protocols are optically based, which limits the survey coverage to the optical scope, camera sensitivity and frame rate. Biomarkers can occur simultaneously at different locations, for example during epileptic activity, or be too fast for the microscope's camera. Spatial temporality of the biological might even be lost during the monitoring of the experiment.

The work presented in this manuscript aimed to develop a multiparametric platform to monitor *in vitro* experiments. Electrophysiological monitoring was implemented into standard biological experiment to complement the optical method. Chapter 1 reviewed the OMEAs state-of-the-art. It explains why conducting polymers are of interest to interface with biology. Their fabrication protocol, purposes, and applications are detailed. It then concludes on the importance of electrophysiology in biological study.

Chapter 2 focused on the OMEAs chips insertion into a 12-well plate format. To fit easily into biological experiment protocols or standard equipment, a "smart well plate" based on standard biological tool was designed and prototyped. Using CAD software, the 12-well plate's skeleton structure was sketched, modified to include OMEAs. Twelve chips are inserted in the wells, all connected via a PCB gathering the electrophysiological data to an external port. The transparency and geometry of the system allow standard microscopy imaging. Plus, the holder and cables integrated in the tool conception grant continuous monitoring of the experiment inside hoods, incubators, microscope. Thus, the full system enables to perform multiparametric monitoring of the *in vitro* assay, including simultaneous and continuous recording of optical and electrophysiological data.

In chapter 3, optimization of the OMEAs fabrication step and electrical architecture was described. Microfabrication's steps from the established and stabilized laboratory protocol were modified to industrialize OMEAs and OECTs production. New methods to process organic material were developed. The dry etching method was studied to pattern the PEDOT:PSS. The DE1, a new photoresist, was used over patterned organic layers to perform encapsulation of the device. Then, the OECTs electrical connections were reorganized into an electrical matrix architecture. Each microfabrication steps of the multi-layered device were tested using a dedicated design. Following the validation of the multi-stack device protocol, a first 16-OECTs matrix device is fabricated and characterized in PBS solution, and iterate in a second 60-OECTs design.

Chapter 4 is focused on Optical and Electronic Ion Channel Monitoring from Native Human Membranes. This work was published as an article in ACS Langmuir. Transmembrane proteins embedded in a lipid bilayer were deposited on the OMEAs developed using the new etching pattern protocol for the organic material, and the DE1 resist encapsulating on top. Being extremely fragile and difficult to study *in vitro*, this new biological model was successfully monitored by the bioelectronic device. The monitoring using a gold electrode covered with PEDOT:PSS to sense the ATP gating using electrical impedance spectroscopy was performed. This showed the performance of the OMEAs to record biological event from a complex and fragile biological model.

Finally, two applications of the OECT matrix devices are detailed in the Chapter 5. First, the matrix was used as a substrate to monitor endothelial cell growth *in vitro*. MDCK II cells were seeded directly on top of the OECTs, used to map the formation of the epithelial cell barrier. Two types of fabrication process were used and compared to patterned PEDOT:PSS : the peel-off process from BEL laboratory, and the etching protocol. With both processes, the transistors characterization in PBS shows satisfying electrical behavior. Cut-off frequencies of the OECTs were monitor as the indicator for the MDCK II cells growth. Indeed, the peel-off device cutoff frequencies showed a significant decrease over time, validating the cell coverage and density over the transistor's channel. Unfortunately, only the peel-off processed devices succeeded to perform monitoring of the endothelial cell barrier formation *in vitro*. The etched devices conductivity was lost 2 days post cell-seeding. This first experiment shown that the matrix architecture was performing to monitor an endothelial cell barrier formation.

In a second experiment, the OECT-matrix device was used to monitor the bioelectrical activity of a developed 3D nerve-on-chip model. In this assay, only the etched-type matrix device was used. To create the 3D model, a spheroid of Schwann cell and motor neuron co-culture was seeded in a PDMS well containing Matrigel. The Spheroids developed myelinated neurites, growing over OECTs channels. As the devices failed to record activity from the biological model, we used different OMEAs to validate the nerve biological integrity. Spontaneous activity and induced activity from stimulation were recorded. This shown that the nerve structure biological model produced compound action potentials spontaneously or induced by stimulation.

Outlook

Organic electronic and conjugated polymers have shown promising results as a multiparametric device to monitor *in vitro* experiment. Integrated in a standard biological tool, they provide electrophysiological data that complete the optical monitoring results for drug and toxicity assessments. The pharmacology industry could greatly profit from the use of bioelectronic devices. Further development is required for the etch process to pattern organic when the devices are used in long-term *in vitro* experiment. Industrialization of the microfabrication protocols are necessary to increase the stability and repeatability of the bioelectronic devices. As briefly mentioned in the chapter 1, additive manufacturing is pushing boundaries of the electronic manufacturing field. Applications involving hybrid processing of organic material are bridging the gap with photolithographic technique and reach micrometer resolution of organic features printing.

As *in vitro* biological models evolve toward 3D structures and autonomous organ-on-chips, planar and rigid bioelectronic devices will reach their limits. 2D OMEAs designs won't be sufficient anymore to monitor biological events from these models. New fabrications methods and structures are emerging such as the PEDOT:PSS scaffold, or conductive hydrogels.

APPENDIX

1 CHAPTER 3 :

Matlab Program for OECTs characterization

This script will plot the output curve, transfer curve, drain conductance and transconductance based on an IV curve. At the end it will export the output curve into a .txt file to be used for origin.

```
        clear; close all;
        set(0,'DefaultFigurePosition',[40,100,700,630]); %(figure size for
         export)
        % load usefull functions
addpath(genpath('D:\Aimie\usefull_functions'));
        % location of data
        folder = 'D:\Aimie\Data\measurment BEST Cambridge\Aimie p\MEASURMENT
         30 01 2020 DEVICE 1\30 01 20 CHARAC\DEVICE G';
filename = 'IV *.tdm';
        % check if there are some files?
        files = dir(fullfile(folder,filename));
        if isempty(files)
fprintf('\nThere are no files with that specifications:\n%s%s\n \n',...
                folder,filename);
return end
```

```
        % order files chronologically

temps = [files(:).datenum]; [~,temps] = sort(temps); files =
{files(temps).name}.'; clear temps;

        % create output folder

        if not(isfolder(fullfile(folder,'output')));

         mkdir(folder,'output'); end

output_folder = fullfile(folder,'output\');

for i_file = 1:length(files)
%           get           IV           curve           from           data
IV = IV_file2var(fullfile(folder,files{i_file}));

    % round Vg and Vd

IV(:,1) = round(IV(:,1)*1e3)/1e3; IV(:,2) = round(IV(:,2)*1e3)/1e3; Vg_hat =
unique(IV(:,2));

    % remove hysteresis

IV_nohys = IV_removehys(IV);

% plot

[gm,gd] = get_gm_gd(IV_nohys);
hFig = figure;
hAx_out = subplot(2,2,1);
hAx_trans = subplot(2,2,2);
hAx_gd = subplot(2,2,3);
hAx_gm = subplot(2,2,4); plotIV_output(IV_nohys,1e3,hAx_out);
plotIV_transfer(IV_nohys,1e3,hAx_trans);
plotIV_gd(IV_nohys(:,1),IV_nohys(:,2),gd,1e3,hAx_gd);
plotIV_gm(IV_nohys(:,1),IV_nohys(:,2),gm,1e3,hAx_gm);

    % remove sweep information from transconductance and
 drainconductance

hTxt = findobj(hAx_gd,'Type','text'); delete(hTxt); hTxt =
findobj(hAx_gm,'Type','text'); delete(hTxt);
```

- `%      % global axis if needed`

```
    %  ylim(hAx_out,[-3.5,0]);
    %  ylim(hAx_trans,[-3.5,0]);
    %  ylim(hAx_gd,[0,6.5]);
    %  ylim(hAx_gm,[0,3.5]);
    %  xlim(hAx_out,[-0.8,0]); xlim(hAx_gd,[-0.8,0]);
        % save data to txt file

    [~,mySave,~] = fileparts(files{i_file});

    output = IV_fororigin(IV_nohys,fullfile(output_folder,
    [mySave,'_output.txt']));

    transfer = transfer_fororigin(IV_nohys,fullfile(output_folder,
    [mySave,'_transfer.txt']));

    % export figure to .pdf
    % add title
    annotation('textbox', [0 0.89 1 0.1], ...

    'String', mySave,... 'Interpreter','none',... 'FontSize',12,...
    'FontWeight','bold',... 'EdgeColor', 'none', ...
    'HorizontalAlignment', 'center');

    export_fig(fullfile(output_folder,mySave),'-pdf','-nocrop','-
    transparent',hFig);

  close(hFig);

end



clear; close all; warning('off','all');

% load usefull functions

addpath(genpath('C:\Users\Panaxium_wk2\Documents\MATLAB\Marcel
\usefull_functions')); addpath(genpath(strcat(pwd,'\FitSine')));

% set default figure position to other screen

set(0,'DefaultFigurePosition',[100,100,500,500]);
```

```
% location of data

folder     =     'C:\Users\Panaxium_wk2\Documents\MATLAB\Aimie\Data\Matrice
data\Wafer ok';

filename = '20190412_150539.tdms';

% options

stitching                                    =                                    0;
plotfit = 0; fitpoints_per_period = 100;

%%%%%%%%%%%%%%%%%%%%%%%%%%%%%%%%%%%%%%%%%%%%

%%%%%%%%%%%%   ALLOCATING   %%%%%%%%%%%%

%%%%%%%%%%%%%%%%%%%%%%%%%%%%%%%%%%%%%%%%%%%%

% check if there are some files?

files = dir(fullfile(folder,filename));

if isempty(files)

fprintf('\nThere are no files with that specifications:\n%s%s\n \n',...

        folder,filename);

return end

% create output folder

if not(isfolder(fullfile(folder,'output')));

 mkdir(folder,'output'); end

output_folder = strcat(fullfile(folder,'output'));

% order files chronologically

temps    =    [files(:).datenum];    [~,temps]    =    sort(temps);    files    =
{files(temps).name}.'; clear temps;

% allocate lists for measurement

gm_mean = zeros(length(files),1);

frequencies
```

```
% allocate lists for experimental data

All_VgAmp   =   cell(length(files),1);   All_VgPhi   =   cell(length(files),1);
All_VgOff = cell(length(files),1);

% transconductance at low

% gate voltage amplitude

% gate voltage phase shift

% gate voltage offset

All_IdAmp   =   cell(length(files),1);   All_IdPhi   =   cell(length(files),1);
All_IdOff   =   cell(length(files),1);   All_IgAmp   =   cell(length(files),1);
All_IgPhi   =   cell(length(files),1);   All_IgOff   =   cell(length(files),1);
All_export = cell(length(files),1);

% loop through files

for i_file=1:size(files,1)

% drain current amplitude

% drain current phase shift

% drain current offset

% gate current amplitude

% gate current phase shift

% gate current offset

% export data

    %%%%%%%%%%%%%%%%%%%%%%%%%%%%%%%%%%%%%%%%%%%

    %%%%%%%%%%%%   ALLOCATING   %%%%%%%%%%%%%

    %%%%%%%%%%%%%%%%%%%%%%%%%%%%%%%%%%%%%%%%%%%

    % open new figure

hFig = figure(i_file); set(hFig,'Units','centimeters'); % initialize subplot
windows

ax_gm ax_Z ax_IdPhi ax_IgPhi ax_all

    % open figure for check fitting
```

```
if                                                                  plotfit
hFig_fit                                =                           figure;
ax_fitVg = subplot(3,1,1); % gate voltage ax_fitId = subplot(3,1,2); % drain
current     ax_fitIg     =     subplot(3,1,3);     %     gate     current
hFit = {1,hFig_fit,ax_fitVg,ax_fitId,ax_fitIg};

else

        hFit = cell(1,5);

end

    % load data into cache

[~,MATfile.ConvertedData,MATfile.ConvertVer,...
MATfile.ChanNames,MATfile.GroupNames,MATfile.ci]            =           ...
evalc('convertTDMS(0,fullfile(folder,char(files(i_file))))');

%          get          number          of          frequency          sweep
% NumFreq=MATfile.ConvertedData.NumOfSegments-1;

NumFreq = (length(MATfile.ConvertedData.Data.MeasuredData)-4)/4;

=                              subplot(2,2,1);                              %
=                              subplot(2,2,2);                              %
=                              subplot(2,2,3);                              %
=                              subplot(2,2,4);                              %
= [ax_gm,ax_Z,ax_IdPhi,ax_IgPhi];

% allocate lists

f=zeros(NumFreq,1);

VgA=zeros(NumFreq,1);

VgAErr=zeros(NumFreq,1);

VgPhi=zeros(NumFreq,1);

VgPhiErr=zeros(NumFreq,1);

VgOffset=zeros(NumFreq,1);

IdA=zeros(NumFreq,1);

% gate voltage

% drain current
```

```
transconductance

impedance

drain phase shift

gate phase shift

f_final = str2double(f_temp{1});

% fit gate voltage

chan                =                (ii-1)*4                +                3;
DataWave=MATfile.ConvertedData.Data.MeasuredData(chan).Data;
Lw=length(DataWave); %wave length

dt = Nc/(f(ii)*(Lw-1));

IdAErr=zeros(NumFreq,1);

IdPhi=zeros(NumFreq,1);

IdPhiErr=zeros(NumFreq,1);

IdOffset=zeros(NumFreq,1);

IgA=zeros(NumFreq,1);

IgAErr=zeros(NumFreq,1);

IgPhi=zeros(NumFreq,1);

IgPhiErr=zeros(NumFreq,1);

IgOffset=zeros(NumFreq,1);

% gate current

   %%%%%%%%%%%%%%%%%%%%%%%%%%%%%%%%%%%%%%%%%%%

   %%%%%%%%%%%%%%%   FITTING   %%%%%%%%%%%%%%%

   %%%%%%%%%%%%%%%%%%%%%%%%%%%%%%%%%%%%%%%%%%%

   % cycle through each frequency to fit the sine

   for ii=1:1:NumFreq

       % get frequency

chan                =                (ii-1)*4                +                2;
f_temp   =   MATfile.ConvertedData.Data.MeasuredData(1,chan).Name;   f_temp   =
```

```
strsplit(f_temp);
f(ii)                          =                          str2double(f_temp{1});
f_temp =

MATfile.ConvertedData.Data.MeasuredData(1,end-3).Name;        f_temp        =
strsplit(f_temp);

dt = MATfile.ConvertedData.Data.MeasuredData(chan).Property(3).Value;

time                           =                          linspace(0,Lw*dt,Lw);
period                           =                          round(Lw*dt*f(ii));
ds = round(Lw/(fitpoints_per_period*period)); if ds==0;

ds=1;                                                                    end
Datads=downsample(DataWave,ds);
timeds=downsample(time,ds)';
clear                                                                DataWave
clear                                                                    time
lb=round(0.2*length(timeds));
ub=length(timeds)-lb;
[VgA(ii),VgPhi(ii),VgOffset(ii),VgAErr(ii),VgPhiErr(ii)]= ...

            FitSine(timeds(lb:ub),Datads(lb:ub),f(ii),

{hFit{1},hFit{3}});

%

% fit drain current

chan                =                (ii-1)*4                +                4;
DataWave=MATfile.ConvertedData.Data.MeasuredData(chan).Data;
Lw=length(DataWave); %wave length

dt = Nc/(f(ii)*(Lw-1));

dt = MATfile.ConvertedData.Data.MeasuredData(chan).Property(3).Value;

time=linspace(0,Lw*dt,Lw);
period                           =                          round(Lw*dt*f(ii));
ds = round(Lw/(fitpoints_per_period*period)); if ds==0;

ds=1;                                                                    end
Datads=downsample(DataWave,ds);
```

```
timeds=downsample(time,ds)';
clear                                                    DataWave
clear                                                        time
lb=round(0.2*length(timeds));
ub=length(timeds)-lb;
[IdA(ii),IdPhi(ii),IdOffset(ii),IdAErr(ii),IdPhiErr(ii)]= ...

            FitSine(timeds(lb:ub),Datads(lb:ub),f(ii),

{hFit{1},hFit{4}});

%

% fit gate current

chan               =               (ii-1)*4               +               5;
DataWave=MATfile.ConvertedData.Data.MeasuredData(chan).Data;
Lw=length(DataWave); %wave length

dt = Nc/(f(ii)*(Lw-1));

dt = MATfile.ConvertedData.Data.MeasuredData(chan).Property(3).Value;

time=linspace(0,Lw*dt,Lw);
period                          =                          round(Lw*dt*f(ii));
ds = round(Lw/(fitpoints_per_period*period)); if ds==0;

ds=1;                                                                end
Datads=downsample(DataWave,ds);
timeds=downsample(time,ds)';
clear                  time;                  clear                  DataWave;
lb=round(0.2*length(timeds));
ub=length(timeds)-lb;
[IgA(ii),IgPhi(ii),IgOffset(ii),IgAErr(ii),IgPhiErr(ii)]= ...

            FitSine(timeds(lb:ub),Datads(lb:ub),f(ii),

{hFit{1},hFit{5}});

if hFit{1} pause(0.5);

        end

    end; clear ii;

    %%%%%%%%%%%%%%%%%%%%%%%%%%%%%%%%%%%%%%%%%%%%%
```

```
    %%%%%%%%%%%%%%   PLOTTING   %%%%%%%%%%%%%

    %%%%%%%%%%%%%%%%%%%%%%%%%%%%%%%%%%%%%%%%%

    % plot transconductance

gm=IdA./VgA;              gmErr=gm.*sqrt((IdAErr./IdA).^2+(VgAErr./VgA).^2);
hold(ax_gm,'on')
plot(ax_gm,f,gm/1e-3,...

'Marker','o',... 'MarkerSize',3,...

'Color','k',...

'MarkerFaceColor','k');
% errorbar(myplot('gm'),f,gm/1e-3,gmErr,'bo'); % store transconductance at
low frequencies gm_mean(i_file) = mean(gm(1:10));

%              plot              drain              phase              shift
% Idphishift=mod(-VgPhi+IdPhi,180);

Idphishift=mod(180-VgPhi+IdPhi,360);
IdphishiftErr=sqrt(IdPhiErr.^2+VgPhiErr.^2);            hold(ax_IdPhi,'on')
plot(ax_IdPhi,f,Idphishift,...

'Marker','o',... 'MarkerSize',3,... 'Color','k',... 'MarkerFaceColor','k');

    %errorbar(myplot('IdPhi'),f,Idphishift,IdphishiftErr,'b<');

    % plot impedance

Z=VgA./IgA; ZErr=Z.*sqrt((IgAErr./IgA).^2+(VgAErr./VgA).^2); hold(ax_Z,'on')
plot(ax_Z,f,Z,...

'Marker','o',... 'MarkerSize',3,... 'Color','b',... 'MarkerFaceColor','b');

    %errorbar(myplot('Z'),f,Z,ZErr,'ko');

%              plot              gate              phase              shift
% Igphishift=mod(-VgPhi+IgPhi,90);

Igphishift=mod(180-VgPhi+IgPhi,360)-180;
IgphishiftErr=sqrt(IgPhiErr.^2+VgPhiErr.^2);            hold(ax_IgPhi,'on')
plot(ax_IgPhi,f,Igphishift,...

'Marker','o',... 'MarkerSize',3,... 'Color','b',... 'MarkerFaceColor','b');
```

```
    %errorbar(myplot('IgPhi'),f,Igphishift,IgphishiftErr,'k<');
    %%%%%%%%%%%%%%%%%%%%%%%%%%%%%%%%%%%%%%%%%%%%
    %%%%%%%%%%%%%   Stitching    %%%%%%%%%%%%
    %%%%%%%%%%%%%%%%%%%%%%%%%%%%%%%%%%%%%%%%%%%%
taue=1; IgfromIdA=IdA.*f*2*pi*taue; IgfromIdAErr=IgA.*(IdAErr./IdA);

ZfromId=VgA./IgfromIdA;
[~,stitch_LB] = min(abs(f-500)); [~,stitch_UB] = min(abs(f-1000));

taueEst=mean(ZfromId(stitch_LB:stitch_UB)./ Z(stitch_LB:stitch_UB));

    ZfromId=ZfromId/taueEst;

ZfromIdErr=ZfromId.*sqrt((VgAErr./VgA).^2+(IgfromIdAErr./ IgfromIdA).^2);

IgfromIdphishift=Idphishift-90;                    IgfromIdphiErr=IdPhiErr;
IgfromIdphishiftErr=sqrt(IgfromIdphiErr.^2+VgPhiErr.^2);

    % plot impedance

hold(ax_Z,'on') plot(ax_Z,f,ZfromId,...

'Marker','o',... 'MarkerSize',3,... 'Color','k',... 'MarkerFaceColor','k');

    %errorbar(myplot('IdPhi'),f,Idphishift,IdphishiftErr,'b<');
    % plot gate phase shift

hold(ax_IgPhi,'on') plot(ax_IgPhi,f,IgfromIdphishift,...

'Marker','o',... 'MarkerSize',3,... 'Color','k',... 'MarkerFaceColor','k');

    %errorbar(myplot('IdPhi'),f,Idphishift,IdphishiftErr,'b<');

if                                                          stitching
stitch_f        =round(0.5*(stitch_UB+stitch_LB));        stitch_Z        =
[ZfromId(1:stitch_f);Z(stitch_f+1:end)]; stitch_IgPhi =

[IgfromIdphishift(1:stitch_f);Igphishift(stitch_f+1:end)]; hold(ax_Z,'on')

plot(ax_Z,f,stitch_Z,... 'Marker','o',...

'MarkerSize',6,... 'Color','r',... 'MarkerFaceColor','none');
```

```
hold(ax_IgPhi,'on') plot(ax_IgPhi,f,stitch_IgPhi,...

'Marker','o',...              'MarkerSize',6,...              'Color','r',...
'MarkerFaceColor','none');

        %errorbar(myplot('IdPhi'),f,Idphishift,IdphishiftErr,'b<');

end

    %%%%%%%%%%%%%%%%%%%%%%%%%%%%%%%%%%%%%%%%

    %%%%%%%%%%%%%%   Nyquist    %%%%%%%%%%%%%

    %%%%%%%%%%%%%%%%%%%%%%%%%%%%%%%%%%%%%%%%

    %     %now plot the Nyquists

  • %  Zr=Z.*cos(Igphishift*pi/180);
  • %  Zim=Z.*sin(Igphishift*pi/180); %
  • %  ZrfromId=ZfromId.*cos(IgfromIdphishift*pi/180);
  • %  ZimfromId=ZfromId.*sin(IgfromIdphishift*pi/180); %

    % figure;

  • %  plot(Zr,Zim,'c.');hold on;
  • %  plot(ZrfromId,ZimfromId,'b.');hold on;
  • %%%%%%%%%%%%%%%%%%%%%%%%%%%%%%%%%%%%%%%%
  • %%%%%%%%%%%%%%   FORMATTING   %%%%%%%%%%%%%
  • %%%%%%%%%%%%%%%%%%%%%%%%%%%%%%%%%%%%%%%%
  • % format transconductance

    figure(hFig);
    xlabel(ax_gm,'Frequency                          [Hz]','FontSize',12);
    ylabel(ax_gm,'Transconductance [mS]','FontSize',12);

      ○ %  ylim(plot_gm,[0 10]);
      ○ %  set(plot_gm,'YTick', linspace(0,0.8,5))
      ○ % format impedance

        xlabel(ax_Z,'Frequency                    [Hz]','FontSize',12);
        ylabel(ax_Z,'Impedance                [\Omega]','FontSize',12);
        set(ax_Z,'YScale','log','YTick',logspace(0,9,10));
        legend(ax_Z,{'Z','ZfromId','stitched'},...
```

```
        'Location','northeast','FontSize',8,'Box','off');

    % format drain phase shift

    xlabel(ax_IdPhi,'Frequency [Hz]','FontSize',12);
    ylabel(ax_IdPhi,'Drain Phase Shift [°]','FontSize',12);
    ylim(ax_IdPhi,[-10 190]);
    set(ax_IdPhi,'YTick', linspace(0,180,4));

    % format gate phase shift

    xlabel(ax_IgPhi,'Frequency [Hz]','FontSize',12);
    ylabel(ax_IgPhi,'Gate Phase Shift [°]','FontSize',12);
    ylim(ax_IgPhi,[-5 95]); set(ax_IgPhi,'YTick',linspace(0,90,4));

    % sync x-axis

    set(ax_all,'XScale','log','XTick',logspace(0,10,11));
    linkaxes(ax_all,'x');
    xlim([f(1) f(NumFreq)]);

    % global settings

    set(ax_all,'Box','on','LineWidth',1);
    set(ax_all,'FontSize',12,'Layer','top');
    set(ax_all,'TickLength',[0.025,0.025]);
    % set(myplot('IgPhi'),'TickLength',[0.01,0.01])

    % add title

[~,mySave,~] = fileparts(files{i_file}); annotation('textbox', [0 0.89 1
0.1], ...

'String', mySave,... 'Interpreter','none',... 'FontSize',12,...
'FontWeight','bold',... 'EdgeColor', 'none', ... 'HorizontalAlignment',
'center');

%%%%%%%%%%%%%%%%%%%%%%%%%%%%%%%%%%%%%%%%%%%%

%%%%%%%%%%%%%   Exporting    %%%%%%%%%%%%

%%%%%%%%%%%%%%%%%%%%%%%%%%%%%%%%%%%%%%%%%%%%

% export figure to .pdf
```

```
[~,mySave,~]                    =                    fileparts(files{i_file});
myPDF = fullfile(output_folder,mySave); export_fig(myPDF,'-pdf','-nocrop','-
transparent',hFig);

% store data for each measurement

All_VgAmp{i_file,1} = VgA; All_VgPhi{i_file,1} = VgPhi; All_VgOff{i_file,1}
=  VgOffset;  All_IdAmp{i_file,1}  =  IdA;  All_IdPhi{i_file,1}  =  IdPhi;
All_IdOff{i_file,1}     =     IdOffset;     All_IgAmp{i_file,1}     =     IgA;
All_IgPhi{i_file,1} = IgPhi; All_IgOff{i_file,1} = IgOffset;

% export data

All_export{i_file,1} =[f,... gm,gmErr,...

% gate voltage amplitude

% gate voltage phase shift

% gate votlage offset

% drain current amplitude

% drain current phase shift

% drain current offset

Z,ZErr,...     Idphishift,IdphishiftErr,...     Igphishift,IgphishiftErr,...
ZfromId,ZfromIdErr,... IgfromIdphishift,IgfromIdphishiftErr];

% get name of save-file

[~,mySave,~]                    =                    fileparts(files{i_file});
mySave    =    fullfile(output_folder,[mySave,'.txt']);    %    write    header
mySaveID = fopen(mySave,'w'); fprintf(mySaveID,strcat('freq',...

'                              gm                              gmErr',...
'                               Z                               ZErr',...
'                       Idphishift                      IdphishiftErr',...
'                       Igphishift                      IgphishiftErr',...
'                          ZfromId                         ZfromIdErr',...
' IgfromIdphishift IgfromIdphishiftErr'));

fprintf(mySaveID,'\nHz S S Ohm Ohm ° ° ° ° Ohm Ohm ° °\n'); fclose(mySaveID);
%      write      data      in      columns      seperated      by      blanks
dlmwrite(mySave,All_export{i_file,1},'precision',10,...
```

```
% gate

% gate

% gate

current amplitude

current phase shift

current offset

'delimiter',' ','newline','unix','-append'); end; clear i_file;

%                                   %                                   clear;
%                         clearvars('-except','R','gm_mean','f','device',...
%                                   'All_VgAmp','All_VgPhi','All_VgOff',...
%                                   'All_IdAmp','All_IdPhi','All_IdOff',...
%                                   'All_IgAmp','All_IgPhi','All_IgOff',...
%                                   'All_VrAmp','All_VrPhi','All_VrOff',...
% 'All_VeAmp','All_VePhi','All_VeOff','All_export')
```

BEL MICROFABRICATION PROTOCOL

#	Process	Material	Tool	Parameters
1	Initial Cleaning	Glass slides/Soap	Tissue	Low concentration soap
		Glass slides/Soap	Ultra-sonic bath	10 min - low concentration (~2%) s
		Acetone/IPA	Ultra-sonic bath	10 min - 80% Acetone/20% IPA
		IPA	Spray bottle	IPA rinse, dry with air gun
2	AZ nLof 2070 Deposition for	S1813/Developer	Spin coater	500rpm/10sec - dynamic resist disp
			Hot plate	1 min @ 110 °C
		EXPOSURE	Mask aligner	130 mJ/cm ^{2}
		Developer	Glassware	30 sec development
3	Plasma Cleaning		RIE	100 W/60 sec/50 sccm O_2
4	Metal Evaporation	Chromium/Gold	Manual Evaporator	5nm Cr/100nm Au
5	Lift-off	Acetone/IPA	Glassware	Soak overnight
			Ultra-sonic bath	15-20 min
		Acetone/IPA	Glassware	Submerge sample in acetone for 1
6	PaC Deposition		PE100	100W/90 sec/50 sccm O_2
		Parylene C/Silane/Al foil	PaC CVD tool	Load Al boat with 2.7 g PaC
7	Soap Deposition	Soap	Class 1000 spin coater	2% soap solution, 1000 rpm/30 se
8	PaC Deposition	Parylene C/Al foil	PaC CVD tool	Load Al boat with 3.5 g PaC
9	AZ 10xT Deposition for PaC E	AZ 10xT	Spin coater	500rpm/10sec - dynamic resist disp
			Hot plate	2 min @ 110 °C
			Mask aligner	280 mW/cm ^{2}
		AZ developer	Glassware	4-5 min development
		DIW		Submerge in DIW, rinse lightly at si
10	PaC Etch		RIE	15 min, 160 W/O2 50sccm/CHF3 5
11	PEDOT:PSS Deposition		PE100	100W/90 sec/50 sccm O2
		PEDOT:PSS	Ultra-sonic bath	10-15 min sonication
		PEDOT:PSS, filter 1.2 µm, sy	Class 1000 spin coater	3000 rpm 35 sec
12	PEDOT:PSS Soft Bake		Hot plate	60 sec @100 °C
13	Peel Off		Tweezers	Scratch edges of glass slide, peel u
14	PEDOT:PSS Hard Bake		Hot plate	60 min @130 °C
15	PEDOT:PSS Soak	DIW	Beaker	3x20 min

2 CHAPTER 4

Supporting Information

Self-assembly of mammalian cell membranes on bioelectronic devices with functional transmembrane proteins

Han-Yuan Liu[1†], Anna-Maria Pappa[2†], Aimie Pavia[4,5]Charalampos Pitsalidis[2], Quentin Thiburce[3], Alberto Salleo[3], Róisín M. Owens[2] and Susan Daniel[1*]*

[†] These authors contributed equally to this work.
** Corresponding authors*

[1]Robert F. Smith School of Chemical and Biomolecular Engineering, Olin Hall, Ithaca, NY 14853, USA
[2]Department of Chemical Engineering and Biotechnology, Philippa Fawcett Drive, CB30AS, Cambridge, UK
[3]Department of Materials Science and Engineering, Stanford University, 496 Lomita Mall, Stanford, CA 94305, USA
[4] Department of Flexible Electronics, Ecole Nationale Supérieure des Mines, CMP-EMSE, 13541 Gardanne, France
[5]Panaxium SAS, 13100 Aix-en-Provence, France

1. Liposome size and zeta-potential characterization

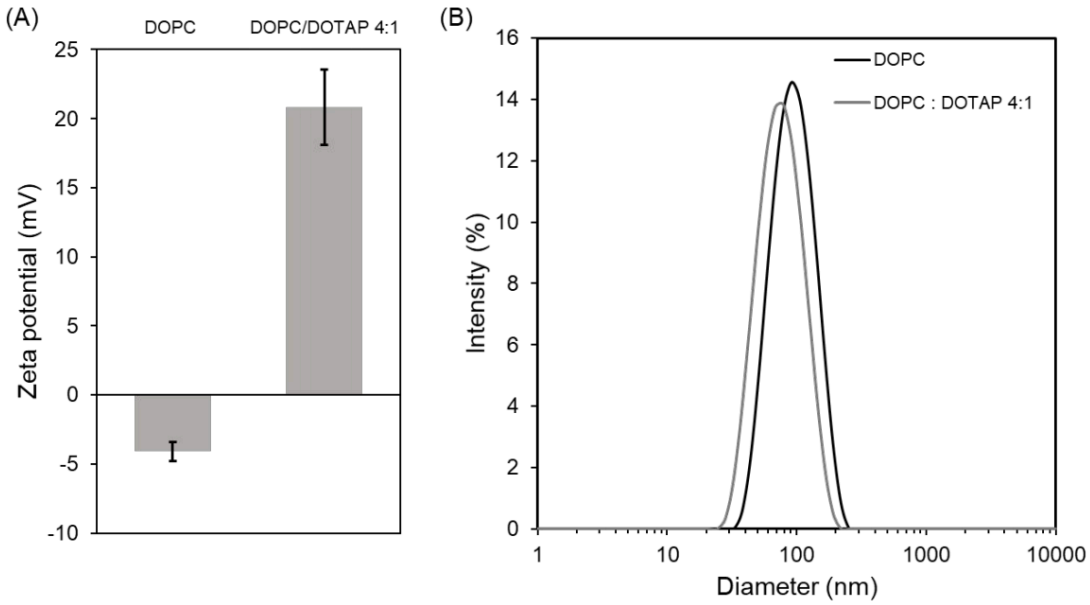

Figure S1. Liposome size and zeta-potential characterization by dynamic light scattering. (A) Zeta-potential values of DOPC only and the DOPC/DOTAP 4:1 liposome mixture. The zeta-potential of DOPC liposomes is found around -4mV while that of DOPC/DOTAP 4:1 is around +20mV. (B) Size characterization of both DOPC and DOPC/DOTAP 4:1 indicating that the size of both particles is around 100 nm.

2. **Effect of PEG addition on membrane quality: investigation of the membrane properties after a washing step that removes any surface bound PEG or excess of it.**

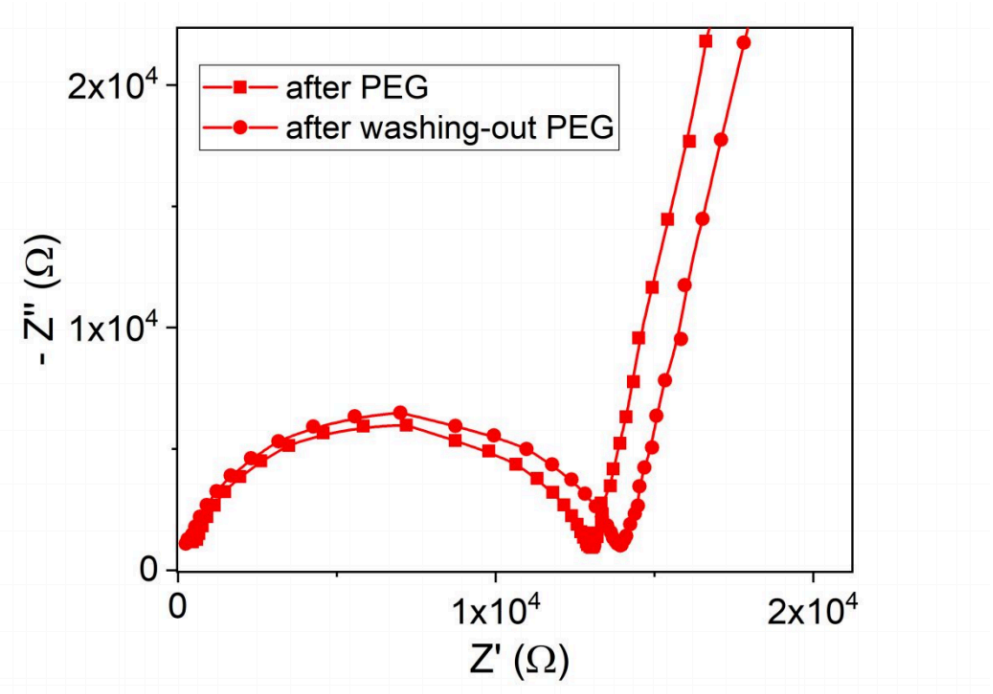

Figure S2. EIS measurements before (squares) and after (circles) removing PEG in the bulk solution when no bilayer or vesicles are present (control experiment). The result suggests that the increase in the membrane resistance after PEG addition in figure 3 is not due to the presence of PEG in the bulk solution, but in the formation of a defect-free SLB.

3. **Addition of a typically used SLB disruptor, EtOH, at different concentrations reveals concentration dependent changes in membrane resistance possibly attributed to different levels of interaction i.e., pore/hole formation and membrane disruption.**

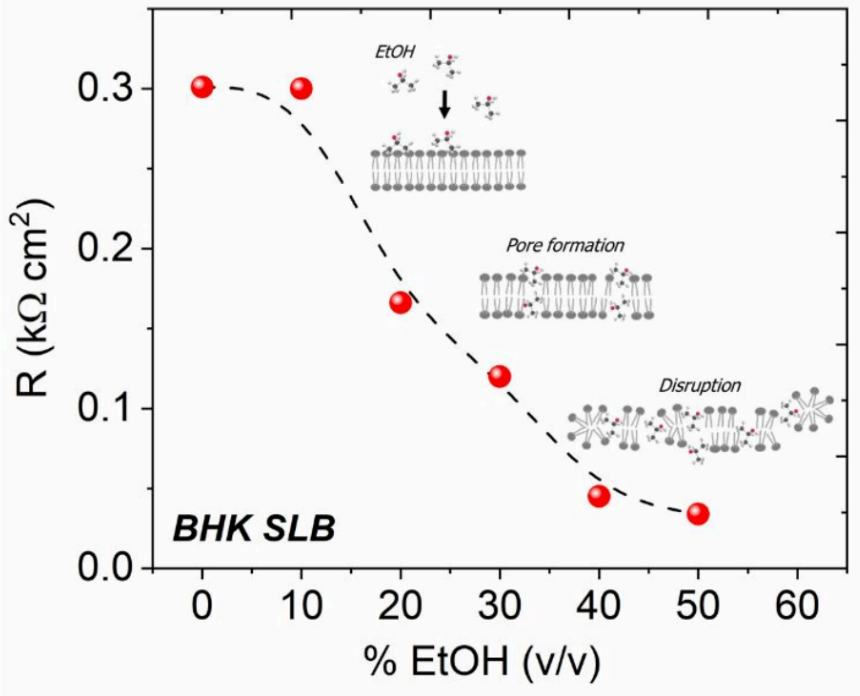

Figure S3. Membrane disruption by EtOH characterized by EIS monitoring. The resistance of BHK membrane decreases with increasing concentration of EtOH. This decrease can be initially attributed to pore formation and subsequently to membrane disruption as depicted in the inset cartoons.

4. Effect of ATP on BHK plasma membranes that lack overexpression of P2X2 channels.

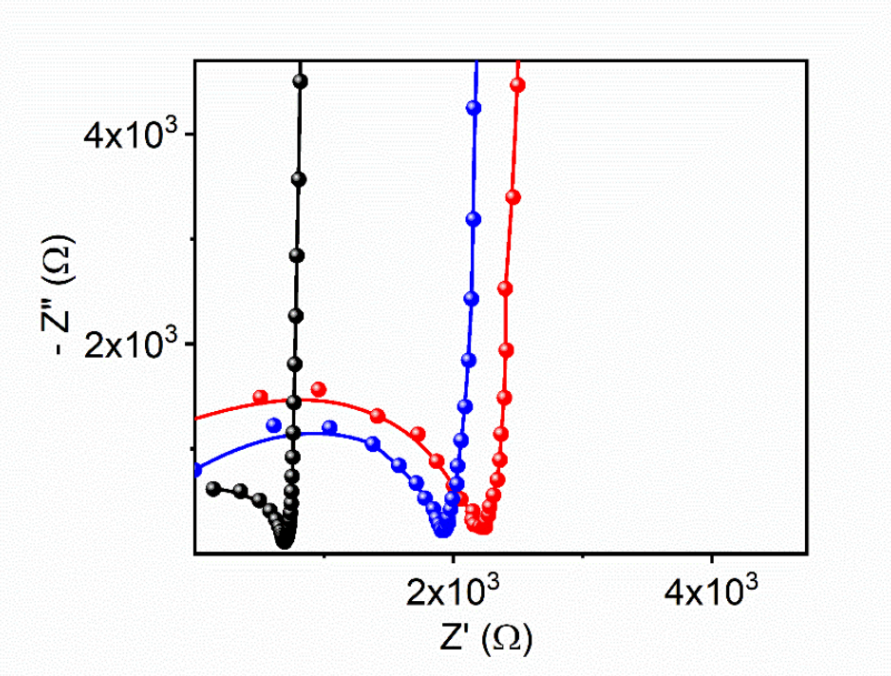

Figure S4. Nyquist plot of the BHK membrane before and after ATP treatment suggesting negligible changes in the resistance of the membrane after ATP addition compared to the changes in the BHK-P2X2 membranes.

5. Modelling of EIS data to extract membrane properties

As a representative example, we provide in **Table 1**, the extracted resistance (R) and capacitance (C) values after fitting, of all the components of the equivalent model for the experimental data presented in Fig. 3b, *i.e.*, PEDOT:PSS electrode, after BHK-P2X2 SLB formation and after addition of ATP. e = electrolyte; p = PEDOT:PSS; b = bilayer.

Table 1: Fitting results of the experimental set of Fig. 3b

	R_e/ Ω	C_p/ µF	R_b/ Ω	C_b/ nF
Bare electrode	443	2.18	-	-
+ SLB	213.5	2.23	2805	1.68
+ ATP	213.5	2.22	1578	2.73

3 CHAPTER 5

1. Brainstorm program used to analyze data from electrodes: detection of stimulation and spikes sorting

$$e^{\pi i} + 1 = 0$$

```
function varargout = brainstorm( varargin ) % BRAINSTORM Brainstorm startup
function.
%
% USAGE: brainstorm
```

- % brainstorm start
-
- % brainstorm nogui
- interface (for scripts)
-

```
%        brainstorm server
 server (completely headless)
: Start Brainstorm
: Start Brainstorm
: Start Brainstorm with hidden
: Start Brainstorm on a distant
%        brainstorm [script] [args] : Start Brainstorm in server mode
 and execute the input script
% brainstorm ... local database (in .brainstorm folder)
```

- % brainstorm stop
-

- % brainstorm reset
- preferences and database)
-
- % brainstorm digitize
- system
- % brainstorm update
- Brainstorm update
-

% brainstorm autopilot ...

following arguments

% brainstorm setpath

current path

% brainstorm startjava

dynamic classpath

- % brainstorm info
-
- % brainstorm license
- window
- % brainstorm tutorial name
-

: Start Brainstorm with a local

: Quit Brainstorm

: Re-inialize Brainstorm (delete

: Digitize points using a Polhemus : Download and install latest

: Call bst_autopilot with the

: Add Brainstorm subdirectories to : Add Brainstorm Java classes to : Open Brainstorm website

```
: Displays license agreement
                                    : Run the validation script
attached to a tutorial (ctf, neuromag, raw, resting, yokogawa
```

- % brainstorm tutorial all
-
- % brainstorm test
-
- % brainstorm deploy
-

```
: Run all the validation scripts
: Run a coverage test
: Create a zip file for
distribution (see bst_deploy for options)
% brainstorm deploy 1 : Compile the current version of
 Brainstorm with Matlab mcc compiler
%        brainstorm deploy 2        : Compile including SPM and
 FieldTrip functions used by Brainstorm
%        brainstorm workshop        : Download OpenMEEG and the SPM
 atlases, and run some small tests
%  res = brainstorm('status')       : Return brainstorm status
 (1=running, 0=stopped)
%

@=============================================================================
===
%   This   function   is   part   of   the   Brainstorm   software:   %
https://neuroimage.usc.edu/brainstorm
%
```

```
% Copyright (c)2000-2020 University of Southern California & McGill
University

% This software is distributed under the terms of the GNU General
 Public License

% as published by the Free Software Foundation. Further details on the GPLv3
```

- % license can be found at http://www.gnu.org/copyleft/gpl.html. %
- % FOR RESEARCH PURPOSES ONLY. THE SOFTWARE IS PROVIDED "AS IS," AND
- THE
- % UNIVERSITY OF SOUTHERN CALIFORNIA AND ITS COLLABORATORS DO NOT MAKE
- ANY
- % WARRANTY, EXPRESS OR IMPLIED, INCLUDING BUT NOT LIMITED TO
- WARRANTIES OF
- % MERCHANTABILITY AND FITNESS FOR A PARTICULAR PURPOSE, NOR DO THEY

  ASSUME ANY

- % LIABILITY OR RESPONSIBILITY FOR THE USE OF THIS SOFTWARE. %
- % For more information type "brainstorm license" at command prompt. %
- ========@
- %

```
% Authors: Francois Tadel, 2008-2021 % Make sure that "more" is off

more off

% Compiled version

isCompiled = exist('isdeployed', 'builtin') && isdeployed;

if isCompiled

    BrainstormHomeDir = fileparts(fileparts(which(mfilename)));

else

    % Assume we are in the Brainstorm folder
```

```
    BrainstormHomeDir = fileparts(which(mfilename));
    % Add path to the core subfolders, used in this function
corePath    =    fullfile(BrainstormHomeDir,    'toolbox',    'core');    if
~exist(corePath, 'dir')
error(['Unable to find ' corePath ' directory.']); end
    % Test if the folders are already in the path first
    p = path();
    if isempty(strfind(p, corePath))
addpath(corePath, '-BEGIN');
addpath(fullfile(BrainstormHomeDir, 'toolbox', 'io'), '- BEGIN');
addpath(fullfile(BrainstormHomeDir, 'toolbox', 'misc'), '- BEGIN');
end end
%                    Get                    JOGL                    version
%              If              JOGL1              is              available
if exist('javax.media.opengl.GLCanvas', 'class') &&
exist('com.sun.opengl.util.j2d.TextRenderer', 'class')
    JOGLVersion = 1;
% If JOGL2 is available
elseif exist('javax.media.opengl.awt.GLCanvas', 'class') JOGLVersion = 2;
% If JOGL2.3 is available
elseif exist('com.jogamp.opengl.awt.GLCanvas', 'class') JOGLVersion = 2.3;
% No JOGL available
else
    JOGLVersion = 0;
end
```

```
% Define jar file to remove from the Java classpath

switch (JOGLVersion)

end

end end

case 0, case 1, case 2, case 2.3,

jarfile = ''; disp('ERROR: JOGL not supported'); jarfile =
'brainstorm_jogl1.jar';
jarfile = 'brainstorm_jogl2.jar';
jarfile = 'brainstorm_jogl2.3.jar';

% Set dynamic JAVA CLASS PATH

if ~exist('org.brainstorm.tree.BstNode', 'class')
% Add Brainstorm JARs to classpath javaaddpath([BrainstormHomeDir
'/java/RiverLayout.jar']); javaaddpath([BrainstormHomeDir
'/java/brainstorm.jar']); javaaddpath([BrainstormHomeDir
'/java/vecmath.jar']);

    % Add JOGL package

if ~isempty(jarfile)
javaaddpath([BrainstormHomeDir '/java/' jarfile]);

end end

% Deployed: Remove one of the two JOGL packages from the Java
 classpath

if isCompiled
% Find the entry in the classpath if ~isempty(jarfile)

jarfileRemove =
setdiff({'brainstorm_jogl1.jar', 'brainstorm_jogl2.jar',
'brainstorm_jogl2.3.jar' jarfile);

for i = 1:length(jarfileRemove)
dynamicPath = javaclasspath('-dynamic'); iClass =

find(~cellfun(@(c)isempty(strfind(c,jarfileRemove{i})), dynamicPath));
```

```
if ~isempty(iClass) javarmpath(dynamicPath{iClass(1)});

end end

% Default action : start

if (nargin == 0)

    action = 'start';

    BrainstormDbDir = [];

else

    action = lower(varargin{1});

% Local start

    if ismember(action, {'start', 'nogui', 'server'}) && (nargin == 2)

 && strcmpi(varargin{2}, 'local')

        BrainstormDbDir = 'local';

    else

        BrainstormDbDir = [];

end end

res = 1;

switch action

case                                                    'start'

bst_set_path(BrainstormHomeDir);      bst_startup(BrainstormHomeDir,      1,

BrainstormDbDir);

case                                                    'nogui'

bst_set_path(BrainstormHomeDir);      bst_startup(BrainstormHomeDir,      0,

BrainstormDbDir);

case                                                  'server'

bst_set_path(BrainstormHomeDir);     bst_startup(BrainstormHomeDir,     -1,

BrainstormDbDir);

case                                                'autopilot'

if ~isappdata(0, 'BrainstormRunning')
```

```
bst_set_path(BrainstormHomeDir);

bst_startup(BrainstormHomeDir, 2, BrainstormDbDir);

end

res = bst_autopilot(varargin{2:end});

    case 'digitize'

        brainstorm nogui

panel_digitize('Start');
case {'status', 'isstarted', 'isrunning'}

        res = isappdata(0, 'BrainstormRunning');

    case {'exit', 'stop', 'quit'}

bst_exit();

case 'reset' bst_reset();

case                                                                    'setpath'
disp('Adding    all    Brainstorm    directories    to    local    path...');
bst_set_path(BrainstormHomeDir);

case 'startjava' disp('Starting Java...');

case  {'info',  'website'}  web('https://neuroimage.usc.edu/brainstorm/',  '-
browser');

case                                                                     'forum'
web('https://neuroimage.usc.edu/forums/', '-browser');

case                                                                    'license'
bst_set_path(BrainstormHomeDir);               bst_set('BrainstormHomeDir',
BrainstormHomeDir); bst_license();

case                                                                    'update'
%  Add  path  to  java_dialog  function  addpath(fullfile(BrainstormHomeDir,
'toolbox', 'gui')); % Update
```

```
bst_update(0);

case 'tutorial' bst_set_path(BrainstormHomeDir); tutonames = varargin{2};
%                                Tutorial                                folder
if (nargin < 3)

tutorial_dir = 'C:\Work\RawData\Tutorials'; else

tutorial_dir = varargin{3};

end

       % Run all the tutorial scripts

       if isequal(tutonames, 'all')

           tutonames =

{'ctf', 'raw', 'epilepsy', 'resting', 'neuromag', 'yokogawa', 'auditory'};

       elseif ischar(tutonames)

tutonames = {tutonames}; elseif ~iscell(tutonames)

error('Invalid call.'); end

       % Run all the requested validation scripts

       for i = 1:length(tutonames)

           disp([10 '===== TUTORIAL: ' upper(tutonames{i}) '

=====']);

           startTime = tic;

           if (length(varargin) == 4)

eval(['tutorial_' lower(tutonames{i}) '(''' tutorial_dir ''', ''' varargin{4}
''');']);

else

eval(['tutorial_' lower(tutonames{i}) '(''' tutorial_dir ''');']);

end

% Done
```

```
            stopTime = toc(startTime);
            if (stopTime > 60)
                disp(sprintf('BST> Done in %dmin\n',
round(stopTime/60)));
run
else
        disp(sprintf('BST> Done in %ds\n', round(stopTime)));
    end
    % Close report viewer if it is not the last tutorial to
if (i < length(tutonames)) bst_report('Close');
end end
case 'test' bst_set_path(BrainstormHomeDir); if (nargin < 2)
error(['You must specify an empty test folder.' 10 'Usage: brainstorm test
test_dir']);
end
test_dir = varargin{2}; test_all(test_dir);



case                                                    'workshop'
%  Runs  Brainstorm  normally  (asks  for  brainstorm_db)  if  ~isappdata(0,
'BrainstormRunning')
bst_set_path(BrainstormHomeDir);
bst_startup(BrainstormHomeDir, 1, BrainstormDbDir);
end
% Message
java_dialog('msgbox', 'Brainstorm will now download additional files needed
for the workshop.', 'Workshop');
```

```
        % Downloads OpenMEEG

bst_plugin('Install', 'openmeeg', 1); % Downloads the TMP.nii SPM atlas
bst_normalize_mni('install');
% Message

java_dialog('msgbox', ['Brainstorm will now test your display and open a 3D
figure:' 10 10 ...

' - You should see two surfaces: a brain surface and a transparent head.' 10
...

with your mouse, ' 10 ...

' - Make sure you can rotate the brain

' - Then close the figure.' 10

10],                                                    'Workshop');
%          Creates          an          empty          test          protocol
ProtocolName      =      'TestWorkshop';      gui_brainstorm('DeleteProtocol',
ProtocolName);  gui_brainstorm('CreateProtocol',  ProtocolName,  0,  0);  %
Display       the       default       anatomy       cortex       and       head
hFig = view_surface('@default_subject/

tess_cortex_pial_low.mat');
hFig = view_surface('@default_subject/tess_head.mat', [], [],

hFig);

waitfor(hFig);

% Delete test protocol

gui_brainstorm('DeleteProtocol',                              ProtocolName);
%                            Confirmation                             message
java_dialog('msgbox', 'You computer is ready for the

workshop.', 'Workshop');

   case 'deploy'

        % Close Brainstorm

        if isappdata(0, 'BrainstormRunning')
```

```
bst_exit();

end

       % Initialize path

bst_set_path(BrainstormHomeDir);

       % Get Matlab version

ReleaseName                    =                    bst_get('MatlabReleaseName');
%          Add          path          to          java_dialog          function
deployPath = fullfile(BrainstormHomeDir, 'deploy'); addpath(deployPath);

bst_set('BrainstormHomeDir', BrainstormHomeDir); % Remove .brainstorm from
the path rmpath(bst_get('UserMexDir'));



rmpath(bst_get('UserProcessDir'));                    %                    Update
if (nargin > 1)

bst_deploy_java(varargin{2:end});

else

bst_deploy_java();

end

otherwise

       % Check if trying to execute a script

if file_exist(action) ScriptFile = action;

elseif file_exist(fullfile(pwd, action)) ScriptFile = fullfile(pwd, action);

else

           ScriptFile = [];

end

       % Execute script
```

```
if                                                          ~isempty(ScriptFile)
% Start brainstorm in server mode (local database or not) if (length(varargin)
> 1) &&

any(cellfun(@(c)isequal(c,'local'), varargin(2:end)))

                brainstorm server local;

                params = setdiff(varargin(2:end), 'local');

            else

                brainstorm server;

params = [];

end

            % Execute script

if                                                              ~isempty(params)
panel_command('ExecuteScript', ScriptFile, params{:});

else

panel_command('ExecuteScript', ScriptFile); end

% Quit

    brainstorm stop;
% Display usage

else

disp(' ');

            disp('Usage : brainstorm start
Brainstorm');

            disp('        brainstorm nogui
Brainstorm with hidden interface (for scripts)');

                                                    : Start
Brainstorm on a distant server (completely headless)');

            disp('        brainstorm <script> <args> : Start
```

```
Brainstorm in server mode, execute the input script and quit');

disp(' brainstorm ... local : Start Brainstorm with a local database (in
.brainstorm folder)');

           disp('        brainstorm stop            : Quit
Brainstorm');

disp(' brainstorm update : Download and install latest Brainstorm update (see
bst_update)');

disp('        brainstorm server
: Start

: Start
```

```
disp('  brainstorm  reset  :  Re-initialize  Brainstorm  database  and
preferences');

           disp('        brainstorm digitize        : Digitize
electrodes positions and head shape using a Polhemus system');

           disp('        brainstorm setpath
subdirectories to current path');

           disp('        brainstorm startjava
Java classes to dynamic classpath');
: Add Brainstorm

: Add Brainstorm

: Open Brainstorm

: Open Brainstorm

: Display
website');

forum');
```

```
license');
disp('        brainstorm info
disp('        brainstorm forum
disp('        brainstorm license
           disp('        brainstorm tutorial name
validation script attached to a tutorial (ctf, neuromag, raw,
resting, yokogawa)');
           disp('        brainstorm tutorial all    : Run all the
validation scripts');
           disp('        brainstorm packagebin      : Create separate
zip files for all the currently available binary distributions');
                   disp('  res = brainstorm(''status'')
         brainstorm status (1=running, 0=stopped)');
                   disp(' ');
                end
end
        % Return value
        if (nargout >= 1)
            varargout{1} = res;
end end
```

===== SET PATH =====

```
: Return
function                                    bst_set_path(BrainstormHomeDir)
% Cancel add path in case of deployed application if bst_iscompiled()
return end
    % Brainstorm folder itself
```

```
addpath(BrainstormHomeDir, '-BEGIN'); % make sure the main brainstorm folder
is in the path

   % List of folders to add

   NEXTDIR = {'external','toolbox'}; % in reverse order of priority

   for i = 1:length(NEXTDIR)

       nextdir = fullfile(BrainstormHomeDir,NEXTDIR{i});

       % Reset the last warning to blank

lastwarn('');
% Check that directory exist if ~isdir(nextdir)

: Run the

-------------------------------

error(['Directory "' NEXTDIR{i} '" does not exist in Brainstorm path.' ...

'Please re-install Brainstorm.']);

end

        % Recursive search for subfolders in each main folder

        P = genpath(nextdir);

        % Add directory and subdirectories

addpath(P, '-BEGIN'); end

    % Adding user's mex path

userMexDir    =    bst_get('UserMexDir');    addpath(userMexDir,    '-BEGIN');
%    Adding    user's    custom    process    path    userProcessDir    =
bst_get('UserProcessDir'); addpath(userProcessDir, '-BEGIN');

end

BST>                          Starting                          Brainstorm:
BST>                                  ================================
BST>                          Version:                          27-Apr-2021
BST>          Compiling          main          interface          files...
BST>              Emptying              temporary              directory...
```

```
BST> Deleting old process reports...
BST> Loading configuration file...
BST> Checking internet connectivity... failed BST> Could not check for Brainstorm updates. BST> Initializing user interface...
BST> Starting OpenGL engine... hardware
BST> Reading process folder...
BST> Loading current protocol...
BST> ================================
```

Published with MATLAB® R2019a

Scientific contributions

Part of the work described in this thesis resulted in publications listed here below.

Optical and Electronic Ion Channel Monitoring from Native Human Membranes Anna-Maria Pappa, Han-Yuan Liu, Walther Traberg-Christensen, Quentin Thiburce, Achilleas Savva, Aimie Pavia, Alberto Salleo, Susan Daniel, and Róisín M. Owens (2020), *ACS Nano,* DOI: 10.1021/acsnano.0c01330

Self-assembly of mammalian cell membranes on bioelectronic devices with functional transmembrane proteins Han-Yuan Liu, Anna-Maria Pappa, Aimie Pavia, Charalampos Pitsalidis, Quentin Thiburce, Alberto Salleo, Róisín M. Owens, and Susan Daniel (2020), *Langmuir,* DOI: 10.1021/acs.langmuir.0c00804

École Nationale Supérieure des Mines
de Saint-Étienne

NNT : *2021LYSEM018*

Aimie PAVIA

Design and fabrication of organic electronic devices for in vitro diagnostics: from petri dish to multiparametric systems

Speciality : Bioelectronics

Keywords : Organic electronics, Conducting polymer, OECT, *in vitro*, Neuron cell, matrix

Abstract :

Drug and toxicity assays are necessary to develop advanced treatments as a way of improving diagnostics and treatment. However, the actual in vitro models are currently not on par regarding the *in vivo* system they attempt to mimic. Two research directions can be invested in to overcome this issue: 1) elaboration of more complex *in vitro* biological model and 2) improvement of the *in vitro* experiment monitoring. We propose a multi-parametric system approach integrating bioelectronic devices complementing optical monitoring. A review on Organic Microelectrodes introduces the field of organic materials. To include electrophysiology monitoring steps into usual biological experiments, the planar bioelectronic chips are assembled in the form of a standard cell biology tool: the 12-well plate. To overcome the number limitation of channels available for both input and output monitoring, Organic electrochemical transistor (OECT) designs were arranged and optimized in a matrix structure. The bioelectronic device's ability to monitor biological experiments *in vitro* is tested to monitor a) the transmembrane proteins in a lipids bilayer b) an epithelial barrier formation, and c) detect electrogenic cell activity. In conclusion, we have included bioelectronic devices into generic tools from the biological experiment is possible, and allows multiparametric monitoring of the *in vitro* experiment.

École Nationale Supérieure des Mines
de Saint-Étienne

NNT : *2021LYSEM018*

Aimie PAVIA

Design et fabrication de dispositifs organiques électroniques pour le diagnostic in vitro: du Petri dish vers un système multiparamétrique

Spécialité: Bioélectronique

Mots clefs : Électronique organique, Polymère conducteur, OECT, *in vitro*, Cellule neurale, matrix

Résumé :

Les études pharmacologiques sont primordiales dans le développement des traitements de pointe. Cependant, les tests in vitro faisant partie intégrante des essais précliniques ne sont pas prédictifs du système in vivo qu'ils tentent d'imiter. Deux axes de recherche sont investis pour répondre à cette problématique: 1) Élaborer un modèle biologique in vitro plus complexe. 2) Améliorer les méthodes de contrôle in vitro. Nous proposons un système de suivi multiparamétrique intégrant des dispositifs bioélectroniques, permettant la surveillance électrophysiologique complémentaire au contrôle visuel des expérimentations in vitro. Un état de l'art des microélectrodes organiques (OMEA) introduit le domaine des matériaux organiques. Puis, afin d'intégrer un suivi électrophysiologique dans des expériences biologiques usuelles, les OMEA sont assemblées sous la forme d'un outil utilisé en biologie cellulaire (la plaque 12-puits). Afin de contourner la restriction du nombre de canaux adressables par l'électronique, le design du transistor électrochimique organique (OECT) est adapté en architecture matricielle. Des étapes de fabrication des OECTs sont optimisées. La capacité des dispositifs bioélectroniques à monitorer des expériences biologiques in vitro est évaluée pour a) contrôler la viabilité d'une bicouche lipidique b) mesurer la formation d'une barrière cellulaire épithéliale, et c) détecter l'activité de cellules électrogéniques. Ces dispositifs bioélectroniques peuvent être intégrés dans les protocoles standards de la pharmacologie, et permettent un monitoring multiparamétrique de l'expérience in vitro.